Durability of Polyimide/Titanium Adhesive Bonds:

An Interphase Investigation

Rachel K. Giunta

Dissertation submitted to the Faculty of the
Virginia Polytechnic Institute and State University
in partial fulfillment of the requirements for the degree of

Doctor of Philosophy

in

Materials Science and Engineering

Ronald G. Kander, Chair
David A. Dillard
John G. Dillard
Terry L. St. Clair
Thomas C. Ward

October 18, 1999
Blacksburg, Virginia

Keywords: Polyimide, Interphase, PETI-5 Adhesive, Durability, Degradation, Aging, Notched Coating Adhesion Test, Dynamic Mechanical Thermal Analysis, Chromic Acid Anodization, Ti-6Al-4V, Pore Penetration

Durability of Polyimide/Titanium Adhesive Bonds:

An Interphase Investigation

Rachel K. Giunta

(ABSTRACT)

When bonded joints are subjected to harsh environmental conditions, the *interphase*, the three-dimensional region surrounding the adhesive/substrate interface, becomes critically important. Frequently, failure occurs in this region after adhesively bonded systems are subjected to elevated temperature oxidative aging. In a previous study, this was found to be the case with a polyimide adhesive bonded to chromic acid anodized (CAA) Ti-6Al-4V. The objective of the current research has been twofold: 1) to investigate the effect of thermal aging on the interphase region of polyimide/titanium adhesive joints, and 2) to evaluate the method used in the current study for durability characterization of other adhesive/substrate systems.

The method used in this research has been to characterize the effect of elevated temperature aging on the following systems: 1) Notched coating adhesion (NCA) specimens and 2) bulk samples of dispersed substrate particles in an adhesive matrix. The NCA test has the advantages of an accelerated aging geometry and a mode mix that leads to failure through the interphase, the region of interest. The bulk samples have the advantage of an increased interphase volume and allow for the application of bulk analysis techniques to the interphase, a region that is traditionally limited to surface analysis techniques.

The adhesive systems studied consisted of one of two polyimide adhesives, LaRC™ PETI-5 or Cytec Fiberite™ FM-5, bonded to CAA Ti-6Al-4V. The model filled system consisted of a PETI-5 matrix with amorphous titanium dioxide filler. Through the use of the NCA test, it was determined that bonded specimens made with FM-5 lose approximately 50% of their original fracture energy when aged in air at 177°C for 30 days. This aging temperature is well below the glass transition temperature of the

adhesive, 250°C. At the same time, the failure location moves from the anodized oxide layer to the adhesive that is directly adjacent to the substrate surface, the interphase region. Through surface analysis of this region, it is determined that the adhesive penetrates the pores of the CAA surface to a depth of 70 to 100 nm, promoting adhesion at the interface. With aging, the adhesive in the interphase region appears to be weakening, although analysis of the bulk adhesive after aging shows little change. This indicates that adhesive degradation is enhanced in the interphase compared to the bulk.

Analysis of the model filled system gave similar information. Specimens containing titanium dioxide filler had glass transition temperatures that were approximately 20°C lower than the neat polyimide samples. In addition, the filled samples contained a significant portion of low molecular weight extractable material that was not present in the neat specimens.

The tan delta spectra from dynamic mechanical thermal analysis of the filled specimens exhibited a shoulder on the high-temperature side of the glass transition peak. This shoulder is attributed to the glass transition of the interphase, a distinct phase of the polyimide which is constrained by adsorption onto the filler particle surfaces. As a function of aging time at 177° or 204°C, the shoulder decreases substantially in magnitude, which may relate to loss of adhesive strength between the polyimide and the filler particles.

From this research, it has been illustrated that information relating to the durability of adhesively bonded systems is gained using an interfacially debonding adhesive test and a model system of substrate particles dispersed in an adhesive matrix.

DEDICATION

to

my husband, Dr. Anthony Andrew Giunta

whose love, patience, and undying support has added joy to my life in countless ways

and to

my parents, Dr. Dennis Knudsen and Bonnie Knudsen

who understood my struggles and celebrated my victories in every step of this endeavor.

Acknowledgements

I would like to thank the following individuals and organizations for their assistance and support over the course of this research:

Dr. Ronald Kander, my advisor for his enthusiastic guidance and support throughout this research project.

Dr. Terry St. Clair who, in addition to serving on my committee, made it possible for me to carry out the final two years of my research in his organization, the Advanced Materials and Processing Branch at NASA Langley Research Center.

Dr. David Dillard, Dr. John Dillard, and Dr. Tom Ward for serving on my committee and supplying a wealth of knowledge in the area of polymer science and engineering.

The Center for Adhesive and Sealant Science and the Adhesive and Sealant Council Education Foundation, who provided financial support throughout this project as well as many valuable opportunities to attend meetings of the Adhesion Society and the Adhesive and Sealant Council.

Susette Sowers, Tammy Jo Hiner, Linda Haney, Katy Hatfield, and Kim Mills who took care of numerous administrative details, particularly during the two years I was not in Blacksburg.

Mia Siochi, NASA Langley, for being a terrific office mate and a source of valuable discussions. Your breadth of knowledge and work ethic have been an inspiration to me.

Jeffrey Hinkley, Cheol Park, and Lee Nicholson, NASA Langley, for discussions that have aided in many aspects of this research project.

Scott Wallace and Sean Britton, NASA Langley, for valuable assistance with manufacturing and testing of samples.

Michael Craven, SURP ′97 and Kristie Gholson, LARSS ′99, two summer students whose hard work and dedication contributed significantly to this research project.

Members of my research group at Virginia Tech: Jennifer McPeak, Julie Martin, Scott Steward, Julie Dvorkin, and Jeff Schultz, who have been great friends in addition to sharing their knowledge and skills.

Members of other research groups at Virginia Tech who have provided valuable assistance: Mitch Jackson, Brenda Jackson, Dave Porter, Mark Muggli, Rob Jensen, Michelle Jensen, Amy Eichstadt, Buo Chen, and Hari Parvatareddy. I look forward to continued contact with all of you at conferences and meetings.

Others at Virginia Tech whose contributions made this research possible: Steve McCartney and Frank Cromer.

Finally, I would like to thank my family: my father, who truly made me realize that this was a goal that I could accomplish; my mother, whose unwavering support helped me through many difficult moments; my sister, Sara, and her husband, Ron, for their encouraging words and for giving me a beautiful niece, Jenna; and my husband Tony, for his love and encouragement and for always believing in me.

Table of Contents

List of Figures

List of Tables

Chapter 1: Introduction

When bonded joints are subjected to harsh environmental conditions, failures tend to occur near the interface.[1-5] Therefore, the long-term durability of adhesive joints is critically dependent on the three-dimensional adhesive/substrate interphase. Although changes in adhesive performance after aging are measured routinely, the interaction of an adhesive with the substrate during aging is not well understood.[6] As depicted by Drzal *et al.*,[7] the interphase exists from the point in the substrate where the local properties begin to differ from the bulk, through the interface, and into the adhesive until the properties equal those in the bulk. Figure 1.1 is based on Drzal's schematic representation of the interphase as it applies to metal/adhesive bonds. The thickness of the interphase can vary greatly, with estimates ranging from a few nanometers to a few thousand nanometers.[7, 8] The thickness of the interphase, therefore, has traditionally limited its characterization to surface-sensitive techniques. In the current research, the study of the effect of elevated temperature aging on the interphase of adhesive joints pairs the analysis of the joints themselves with the analysis of a model system. The model system consists of dispersed particles of the substrate of interest in a polymer matrix. It can be shown that in the current system, approximately one third of the matrix volume is expected to behave as an interphase (see Section 3.2.2.3). Thus, characterization of the system using bulk analysis techniques should allow for mechanical, thermal, and chemical analysis of the interphase region.

Analysis of the adhesive-substrate interphase is essential in the study of the durability of high-performance adhesives. A current area of adhesive durability research is the development of critical technologies for elevated temperature aerospace applications. High performance polymeric adhesives are needed for bonding titanium in structural components of aircraft. These joints have been designed to withstand a temperature of 177ºC for 60,000 hours while maintaining desirable mechanical properties.[9] LaRC PETI-5,[10-18] a phenylethynyl-terminated polyimide adhesive, was developed for potential use in high-temperature aircraft applications. The structure of the PETI-5 precursor, which undergoes chain extension and crosslinking of the end groups during cure, is illustrated in Figure 1.2. Prior to cure, the molecular weight of PETI-5 used in the current study is 5,000 g/mol. After an elevated temperature cure, the lightly crosslinked, amorphous polyimide has a glass transition temperature of 260°C. FM-5, developed by Cytec Fiberite, Inc., Havre de Grace, MD, is a blended adhesive based on PETI-5. It has a slightly lower glass transition temperature, 250°C. Details regarding the blend components are proprietary. The potential for use of PETI-5 or FM-5 in the aerospace industry has prompted numerous investigations of the durability of these adhesive joints with Ti-6Al-4V,[14, 18, 19] an alloy of 90% titanium, 6% aluminum, and 4% vanadium.

In one such study, Parvatareddy *et al.*[19] investigated thermal aging of double cantilever beam (DCB) specimens of FM-5 adhesive bonded to chromic acid anodized (CAA) Ti-6Al-4V. Specimens were aged at 177°C or 204°C in air. The failure surfaces of DCB specimens, as received and aged for 12 months, are shown in Figure 1.3. Prior to specimen aging, the bonded samples fail cohesively, through the centerline of the adhesive. Following 12 months of aging at 177° or 204°C, there are two distinct failure modes. The central portions of the specimens continue to fail cohesively. However, the edges of the specimens, upon visual inspection, appear to have failed at the adhesive/substrate interface.

These failure regions were analyzed by x-ray photoelectron spectroscopy (XPS).[20] Titanium was detected on the metal failure surface but not on the adhesive failure surface, indicating that the failure did not occur in the metal oxide layer. Evidence of FM-5 adhesive (carbon, oxygen, and nitrogen at the known binding energies) was

detected on both failure surfaces. This indicates that the failure occurred through the adhesive interphase, close enough to the titanium substrate that the titanium could be detected within the sampling depth of the XPS, typically 5 to 10 nm. This type of failure occurred only around the edges of the bond. Therefore, it appears that degrading species, presumably oxygen, diffused through the edges of the bonded specimen during elevated temperature aging in air, and this degradation led to failure in the interphase.

The primary objective of the current research has been to investigate the effect of thermal aging on the interphase region of PETI-5 and FM-5 bonded to chromic acid anodized titanium substrates. From Parvatareddy's work,[19, 20] it appears that degradation is occurring when the adhesive is simultaneously exposed to the adherend, elevated temperatures, and air. While previous work has focused on changes in adhesive strength and bulk polymer properties as a function of aging time, the current study will focus on changes in the adhesive adjacent to the substrate surface as a result of elevated temperature aging. The polyimide/Ti-6Al-4V interphase was investigated using an interfacially debonding adhesive test and a model system of dispersed TiO_2 particles in a polyimide matrix. The adhesive joints, bulk polymer samples, and model filled samples were aged at elevated temperatures for up to 3 months in air. Adhesive samples were characterized using the notched coating adhesion (NCA) test[21] and several surface analysis techniques. Chemical, thermal, and mechanical changes in the bulk polymer and the filled model system were investigated using dynamic mechanical thermal analysis, differential scanning calorimetry, infrared spectroscopy, and extraction.

An additional objective of the present study is to evaluate the use of the NCA test and the model system described above for durability characterization of other adhesive-substrate systems. As is observed in the example of Parvatareddy's study, the interphase is subject to environmental attack in many adhesive systems, particularly when metal adherends are used.[22] Thus, there is a great need for methods of assessing the durability of this region of the adhesively bonded joint.

These objectives lead to the following thesis:

The effect of thermooxidative aging on the adhesive interphase region of a bonded joint can be demonstrated by characterizing the effect of aging on the following systems: 1) an adhesive joint that is constrained to fail through the interphase, and 2) a model system consisting of dispersed particles of a substrate material in an adhesive matrix.

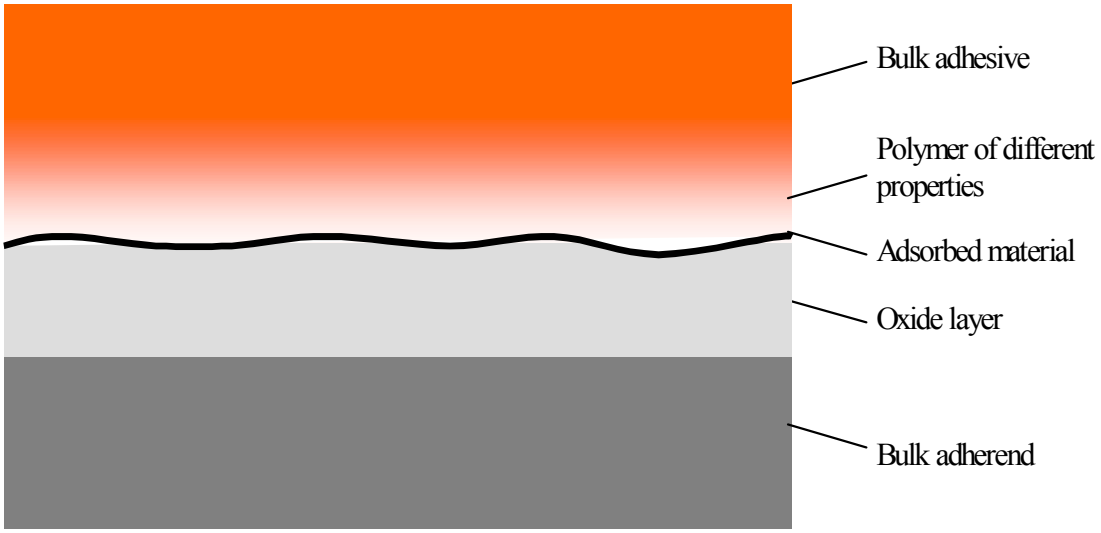

Figure 1.1: Schematic representation of the components of the three-dimensional interphase between adhesive and substrate, after Drzal et al.[7]

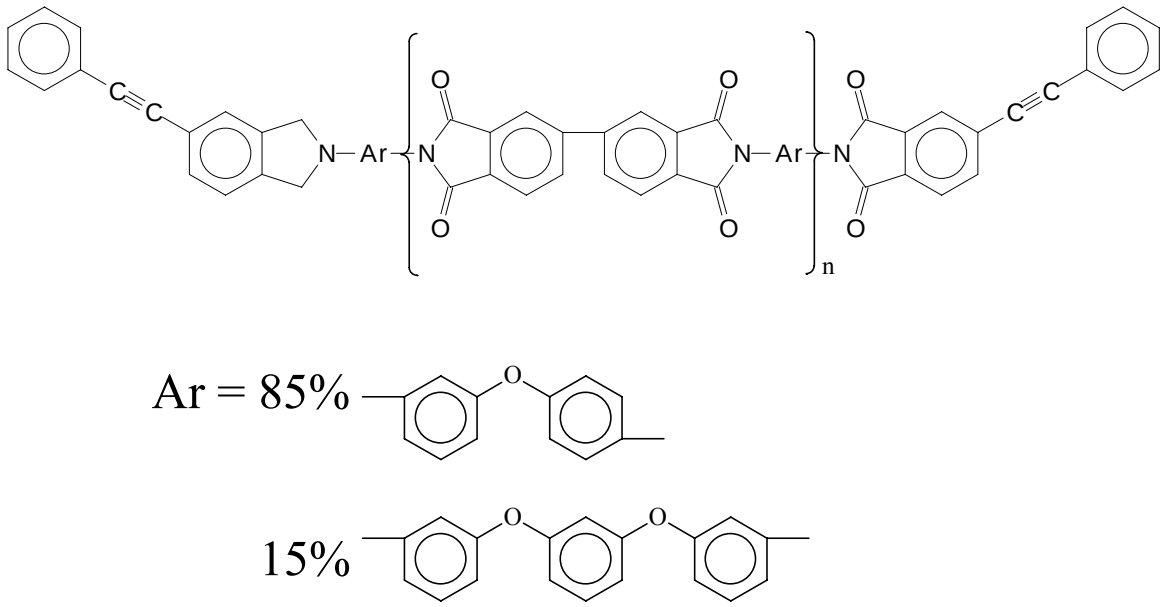

Figure 1.2: Structure of PETI-5 before cure. $<M_n>$ = 5,000 g/mol.

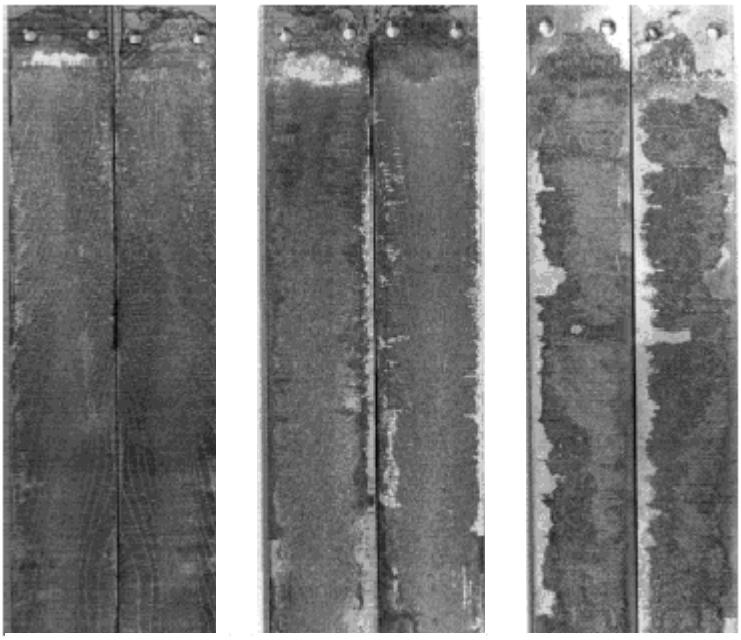

As received 12 months 177°C 12 months 204°C

Figure 1.3: Failure surfaces of double cantilever beam specimens of FM-5 adhesive bonded to chromic acid anodized Ti-6Al-4V, from Parvatareddy et al.[19] *Samples shown are as received, aged in air at 177°C for 12 months, and aged in air at 204°C for 12 months.*

Chapter 2: Background

2.1 Adhesion and Adhesives

The use of adhesives as a means of joining materials offers many advantages over conventional mechanical fasteners, such as rivets, bolts, and welds.[22] These advantages include:[23]

1) Ability to bond dissimilar materials and damage-sensitive materials;
2) Fabrication of complicated shapes;
3) Vibration response and enhanced damping control;
4) Weight reduction;
5) Joint sealing protection;
6) Smoother aerodynamic surfaces;
7) Improved fatigue strength.

These advantages have led to a great increase in the use of adhesives and, in particular, to the widespread application of structural adhesives. Kinloch defines structural adhesives as those which polymerize to form "high-modulus, high-strength adhesives between relatively rigid adherends, so that a load-bearing joint is constructed."[22]

Structural adhesives are frequently utilized in the aerospace industry for bonding aluminum and titanium alloys, and in other applications including construction and

general engineering. For a structural adhesive to be effective, it must be able to transmit loads from one adherend to another. Two requirements for this to occur include:[22]

1) Interfacial molecular contact between adhesive and adherend;

2) Forces acting across the adhesive/substrate interface to prevent them from separating under an applied load.

2.1.1 Interfacial Contact

To satisfy the requirement of intimate molecular contact, the adhesive must be able to wet the adherend during bonding. The thermodynamics of wetting are described by the Young equation,[24]

$$\gamma_{SV} = \gamma_{SL} + \gamma_{LV} \cos\theta \,, \qquad \textit{Equation 2.1}$$

where γ are the surface energies, and the subscripts *SV*, *SL*, and *LV* refer to the solid-vapor, solid-liquid, and liquid-vapor boundaries, respectively. This is represented schematically in Figure 2.1. The equilibrium contact angle, θ, must equal 0° for the liquid adhesive to spontaneously wet the surface and spread freely. Therefore, for spontaneous wetting to occur,

$$\gamma_{SV} \geq \gamma_{SL} + \gamma_{LV} \,. \qquad \textit{Equation 2.2}$$

When $\theta > 0°$, the spreading and wetting of a solid surface requires the application of pressure to the liquid adhesive.

As can be seen in Equation 2.2, wetting of a solid surface with a high surface free energy can be achieved more readily than wetting a low-energy solid surface. High-energy surfaces include metals, metal oxides, and ceramics, while low-energy surfaces include organic compounds, such as polymers. In the current study, the substrate surface of

interest, the oxide of a titanium alloy, is a high-energy surface for which wetting is expected to be thermodynamically favorable.

2.1.2 Theories of Adhesion

Intimate molecular contact between adhesive and substrate is a necessary, but not sufficient, condition for effective bonding. There must also be sufficiently strong forces acting across the interface to hold them together under an applied load. The nature of these forces is not fully understood, however there are several proposed theories of adhesion. Wake[25] and Kinloch[26] have reviewed the widely recognized theories of adhesion. These theories are divided into four categories: adsorption, diffusion, electrostatic, and mechanical interlocking.

2.1.2.1 Adsorption Theory

Adsorption is the most widely accepted of the adhesion theories.[26] Provided that contact between two surfaces is sufficiently intimate, the surfaces will adhere due to forces across the interface. The most common of the forces leading to adsorption are secondary or van der Waal's forces. These forces are responsible for the attraction of electrically neutral bodies to one another. Because van der Waal's forces always contribute to adhesive bonding,[25] secondary forces are an important consideration in the current work.

2.1.2.2 Diffusion Theory

Diffusion across an interface requires two mutually soluble materials, typically two polymeric materials that are joined well above their glass transition temperatures. Bonding in the current study involves a polyimide adhesive and a metallic substrate; therefore, diffusion between polymeric components is not expected to contribute to adhesion in this investigation.

2.1.2.3 Electrostatic Theory

According to the electrostatic theory of adhesion, electrons are transferred across the interface, upon contact of adhesive to substrate, to balance the respective Fermi levels.

This transfer creates a double layer of electrical charge at the interface. These forces contribute appreciably to adhesion only in a few special circumstances,[22] and are not expected to contribute significantly to adhesion in this study.

2.1.2.4 Mechanical Interlocking Theory

Mechanical adhesion, or *keying*, involves the flow of adhesive into interstices of the substrate surface. Subsequent solidification locks the adhesive into the well. According to Venables,[27] mechanical interlocking is critical for good initial bond strength and long-term durability of metal-polymer bonds. Because of the microporous nature of the substrate of interest in this study, chromic acid anodized titanium, mechanical interlocking is expected to contribute substantially to adhesion in this investigation.

2.2 The Interphase

Structural adhesive joints, when tested as made, typically fail cohesively through the centerline of the adhesive.[19, 22] However, in any study of adhesive joint durability, failure in the vicinity of the adhesive/substrate interface becomes an important consideration.[22] Sharpe[28] is credited with the first use of "interphase" to describe the boundary layers between adhesive and substrate. He emphasizes the importance of characterizing such boundary layers in analysis of the composite adhesive/substrate structure. More recently, Sancaktar[29] has stated that adequate analysis and understanding of the interphase "is critical for design of efficient bonded structures and composite materials."

Mechanisms of environmental degradation leading to failure in the interphase include:[22]

1) Displacement of adhesive on adherend (e.g. by water) due to the rupture of secondary bonds at the adhesive/adherend interface;

2) Mechanical weakening and failure of the oxide layer;

3) Failure in a boundary layer of adhesive close to the substrate surface (i.e. in the interphase) which has properties differing from the bulk adhesive.

Of these, failure in the adhesive boundary layer is of the greatest interest in the present study. This interest is generated by the change in failure location of FM-5 adhesive bonds after aging, illustrated in Figure 1.3. It is well accepted that the mechanical properties of an adhesive material near the interface differ from those in the bulk adhesive.[29] This boundary layer may well possess a different chemical and physical structure than the bulk adhesive, e.g. different molecular weight or crosslink density[6] or migration of plasticizers to the surface.[28]

Three contributions to an apparently weakened interphase include thermal stresses, conformational stresses, and chemical interactions or catalysis. One or more of these contributions can occur at a given interface. Thermal stresses arise from the difference in the coefficient of thermal expansion, α, between the substrate and the adhesive. As the adhesive bond cools from an elevated curing temperature, the thermal contraction of the adhesive is restricted by the substrate. The α of a metallic substrate can be an order of magnitude lower than that of many adhesives. Under this thermal load, the low-modulus adhesive strains much more than the high-modulus substrate. Because of the static stress, failure of the polymer chains near the substrate can occur at a lower applied load than the comparable bulk polymer chains. In addition, the stressed polymer chains are more prone to chemical degradation than the unstressed bulk polymer chains. As stated by Kinloch, "Such stresses render primary and secondary bonds more susceptible to environmental attack by lowering the free energy barrier for, and so increase the rate of, bond rupture."[22]

Polymer chains in an interphase are also stressed due to adsorption of polymer molecules on a substrate, either by primary or secondary bonding. This causes the polymer chains to be in a higher-energy conformation than would be attained in the bulk.[30] Again, susceptibility to degradation is enhanced by the imposed stress.

Since metals and metal oxides are common catalysts in organic reactions, it is possible for a metallic substrate to catalyze a chemical reaction of a polymeric material at an adhesive/substrate interface. Dillingham and Boerio report such a catalysis of an epoxy cure reaction by hydroxyl groups present on the aluminum oxide substrate surface.[31] If

thermal or conformational stresses exist, the polymer chains may be even more likely to undergo catalyzed degradation. Thus, the existence of an interface can significantly affect the properties of the adhesive in the interphase region.

2.2.1 Titanium Surface Treatments

The titanium alloy Ti-6Al-4V is used widely for aerospace applications of bonded structures. As discussed earlier, the adhesive/metal oxide interface is often susceptible to environmental attack. This is true in the case of titanium/adhesive bonded joints.[32] To improve the durability of the interphase, several surface treatments for Ti-6Al-4V have been developed.[27, 33] These surface treatments are categorized into three classes, based on the surface roughness obtained during the treatment. Class I treatments, which include phosphate fluoride etching,[34] produce no roughness and the poorest durability of the three classes. Class II treatments, including PasaJell and Turco etch, produce bonds with an intermediate level of durability. This class of adherends display macroroughness but little or no microroughness. Surface preparations producing oxide layers with a microrough surface, Class III treatments, produce the most durable bonds. This class of treatments includes chromic acid anodization (CAA) and sodium hydroxide anodization (SHA).[35] CAA was selected as the surface treatment for the adhesive bonds in the current study because of the durability of these bonds and the database of research on polyimide/CAA Ti-6Al-4V bonds.[19]

2.2.2 Polymer / Titanium Dioxide Interaction

The photocatalytic degradation of polymers by titanium dioxide has been studied extensively (e.g. refs 36-39). Interest in this area is a result of the use of titanium dioxide as a pigment in paints and other polymeric compounded materials. Most of the polymers studied, including polyethylene,[37] nylon,[38] and poly(vinyl chloride),[39] experienced enhanced UV degradation in the presence of titanium dioxide pigments. The effect of titanium dioxide on the thermal and thermooxidative stability of polymers has received less attention, although the limited available data[36, 40, 41] suggest a destabilizing effect in some polymers. Visser[40] found that titanium dioxide filler (as well as aluminum, tungsten, and calcium oxides) enhanced the degradation of polysiloxane elastomers under

cyclic stress at elevated temperatures, while zinc, tin, and copper oxides stabilized the elastomers. Elastomer degradation in the presence of titanium dioxide was characterized by weight loss and a significant increase in modulus during elevated temperature testing. Filler surface treatments did not influence the stability of the filled elastomers; thus, it was concluded that the stability of the filled elastomers was not a result of changes in the strength of polymer-filler adsorption. Rather, it is proposed that the destabilization is related to an intrinsic ability of certain inorganic oxides to catalyze polysiloxane degradation reactions. McDaniel and St. Clair[41] evaluated the thermooxidative stability of polyimide/titanium dioxide ceramers using dynamic thermogravimetric analysis. A decrease in the 5% weight loss temperature was observed when titanium dioxide loadings were greater than 20% by weight. Evidently, polyimide degradation was enhanced by the presence of titanium dioxide, as was observed with the polysiloxane elastomers.

2.2.3 Chemical Degradation of the Interphase

Parvatareddy's durability study[19] of FM-5/Ti-6Al-4V adhesive samples, discussed in Chapter 1, resulted in aged DCB specimens that exhibited a "picture frame" type failure, as seen in Figure 1.3. This is indicative of a degradation mechanism involving the diffusion of species, presumably oxygen, into the bond. The edges of the aged adhesive joints failed within the interphase region of the adhesive (or the adhesive boundary layer). Thus, a weakening of the adhesive interphase is occurring to the extent that it becomes the weak link in the bonded system.

From this previous study, it was unknown whether chemical changes (and subsequently, mechanical property changes) in the adhesive interphase region of this system during aging are the same as chemical changes in the bulk adhesive. Surface analysis by XPS indicates that the elemental composition on the failure surfaces of Parvatareddy's samples is the same as that of bulk FM-5.[20] However, one cannot conclude from these data that the chemical compositions are identical. Although peak resolution of XPS data can be used to identify the elements' chemical environments based on shifts in binding energies, only the percentage composition of the detected elements was reported.

Furthermore, spectroscopic techniques such as nuclear magnetic resonance or infrared spectroscopy are better suited than XPS for the detection of subtle chemical changes in organic polymers, since peak resolution of XPS data can be somewhat subjective. The lack of surface sensitivity, however, becomes a problem. Although IR techniques such as diffuse reflectance and attenuated total reflectance are considered "surface" techniques, typical penetration depths are approximately one micron. A 10-nm interphase region of an adhesive, therefore, only constitutes one percent of the analyzed volume of material. Saturation of the spectrum by the bulk adhesive prevents the identification of chemical changes in the interphase.

The current investigation includes the fabrication and analysis of an interphase-rich model system of dispersed titanium dioxide particles in a polyimide matrix. Detection of chemical changes in the interphase, due to the presence of titanium dioxide, is therefore possible by non-surface sensitive spectroscopic techniques.

2.3 Polymer Durability

Since the early 1960s, the subject of polymer durability has been of great interest and importance. This was brought about by the development of new fields of technology, such as high-speed aviation, rocketry, instrument engineering, and electronics[42] for which polymeric materials had great potential. Long-term stability to heat, light, atmospheric oxygen, and other agents, in many cases, became the limiting factor in the use of polymers in high-performance applications.

As polymeric materials with improved durability have been developed, the potential applications for polymeric materials have become more demanding. Polymer durability has remained a critical issue for reasons of safety, health, security, and protection of capital investment.[43]

The rigid conditions of thermal, mechanical, and oxidative stability for long durations, required by elevated temperature aircraft applications, have challenged scientists and engineers to develop polymers for composite matrices and adhesives with better stability than ever before. An additional challenge is the ability to determine if a material will be

able to withstand the service conditions for the lifetime of the aircraft. Several materials for potential use in elevated temperature aircraft applications have been developed[12, 44-47] and are currently being evaluated for this purpose. Prior to use, the long-term durability of these materials must be clearly demonstrated. This will require either real-time testing of materials beyond one lifetime of service[48] or development and validation of accelerated aging[49, 50] and/or lifetime prediction methods.[49-53]

A variety of approaches has been used to evaluate and/or predict polymer durability. Oxidative weight loss,[50, 52] microcracking behavior,[53] and extrapolation of mechanical properties after accelerated isothermal aging[49] have been investigated as accelerated aging and lifetime prediction methods for elevated temperature aerospace applications. While useful information can be gained from accelerated aging studies, one must treat these data very carefully, as complex degradation mechanisms and synergistic effects can cause accelerated / predicted results to vary considerably from real time aging behavior.

For example, investigators often use dynamic thermogravimetric analysis (TGA) to determine the relative thermooxidative stability of polymers. The temperature at which a specific amount of mass is lost (i.e. 2%, 5%) during a programmed temperature ramp is reported as a measure of a polymer's stability. In the case of polyimides and several other high-performance polymers, the 5% weight loss temperature is often in the range of 400 to 500ºC. The degradation mechanisms at this high temperature may be radically different from those in the relatively slow degradation that occurs at these materials' service temperatures, around or below 200ºC.[50] Additionally, weight loss data alone is not necessarily a prediction of a polymer's lifetime. The relationship between mechanical property retention and small degrees of polymer weight loss has not been established with any degree of certainty.[49]

Dynamic TGA experiments have been used with varying heating rates to create a simple lifetime estimate based on first order decomposition kinetics. This requires the assumption of time-temperature equivalence, and the predictive power of such experiments has not proven to be valid. The existence of multiple degradation

mechanisms occurring consecutively or concurrently is believed to have prevented the success of this method.[52]

A similar method[52] has been used as a preliminary screening of resin systems. In this method of evaluating a material's thermooxidative stability, the Arrhenius activation energy, E, is plotted as a function of the pre-exponential factor, k_0, from Equation 2.3,

$$k = k_0 \exp\left(\frac{-E}{RT}\right), \qquad \textit{Equation 2.3}$$

where k is the reaction rate, R is the gas constant, and T is the absolute temperature.

The activation energy for a single weight loss event can be determined, diminishing the effect of multiple degradation mechanisms. A "kinetic map" is used to display the data, with each material and each weight loss event appearing as a single data point. An example of such a kinetic map for several polyimides, an arylene ether, and a sulfone can be seen in Figure 2.2. From the Arrhenius equation, isothermal weight loss data can be calculated. For example, in Figure 2.2, lines have been drawn on the kinetic map corresponding to 1% weight loss after 100,000 hours at 150ºC and 200ºC. If the data point for a material lies to the left of a line, it is predicted to lose more than 1% of its weight at the given time and temperature, while a material to the right of the line is predicted to lose less than 1% of its weight.

Here, LaRC™ TPI and LaRC™ 8515 are predicted to survive 100,000 hours at 200ºC. The derivative TGA thermograms of 5260, a bismaleimide, showed two maxima, each corresponding to a weight loss event. Looking at the second maximum, 5260 (2), the material should be suitable for use at 150ºC. However, the low temperature process, 5260 (1), causes the polymer to lose more than 1% of its weight. While this kinetic mapping method reduces some of the assumptions required in other TGA durability studies, first order kinetics and the inherent assumption of weight loss corresponding to loss of mechanical properties are still required.

2.4 Durability of FM-5 Adhesive

Several researchers have studied the effects of long-term elevated temperature aging on Cytec Fiberite™ FM-5 adhesive. The results of these studies imply that physical and chemical aging occur simultaneously in the adhesive, and that chemical aging dominates at long aging times.

2.4.1 FM-5/Ti-6Al-4V Adhesive Joints

Parvatareddy *et al*.[19] have studied the effects of aging on the fracture energy of Ti-6Al-4V/FM-5 bonds. DCB specimens were aged at 150°, 177°, and 204ºC in air at ambient pressure and reduced pressures of 2 psi and 0.2 psi for up to 18 months. All aging temperatures were below the glass transition temperature of FM-5 adhesive, 250°C. Following aging, some specimens from each environment were rejuvenated for 2 hours at 300ºC. The purpose of the rejuvenation was to reverse any physical aging that had occurred. The critical strain energy release rate (G_c) of the samples was monitored as a function of aging time in the various environments. The specimens that were aged in ambient pressure air showed a 40% drop in fracture energy and the smallest recovery upon rejuvenation. For any given aging temperature, the 0.2 psi specimens had the lowest drop in fracture energy and the largest recovery upon rejuvenation. Thus, it was concluded that the primary aging mechanism in air at 204ºC and ambient pressure was chemical aging, and a combination of physical and chemical aging were occurring at reduced pressure. The relationship between air pressure and degree of chemical aging also illustrates that a component of the air aging atmosphere, i.e. oxygen, is causing the chemical degradation.

2.4.2 FM-5 Neat Resin

2.4.2.1 Tensile Properties

Xu, Parvatareddy, and Dillard[54] have studied the change in tensile properties of neat FM-5 adhesive upon aging. Specimens were aged for up to twelve months at 177ºC in air at ambient pressure and a reduced pressure of 2 psi. The effect of these aging conditions on

the failure stress and failure strain is given in Figure 2.3 and Figure 2.4, respectively. The drop in failure stress and failure strain is a result of embrittlement of the resin due to degradation. The significant increase in the amount of embrittlement occurring at ambient pressure compared to reduced pressure implies that exposure to air at elevated temperatures leads to chemical changes in the resin and subsequent embrittlement. Physical aging may also be contributing to the degradation.

2.4.2.2 Glass Transition Temperature

Parvatareddy *et al*.[19] found further evidence of physical and chemical aging of FM-5 indicated by changes in the T_g of the neat resin upon aging. Neat FM-5 resin was aged in air at 177ºC and 204ºC. To separate the effects of physical and chemical aging, samples were rejuvenated at 300ºC for two hours to reverse the effects of physical aging. Glass transition temperatures of samples aged at 204°C, as determined using DSC, are presented in Figure 2.5. The increase in glass transition temperature as a function of aging time is attributed to a combination of physical and chemical aging. The portion of this increase that is reversed upon rejuvenation is attributed to physical aging.

2.4.2.3 Weight Loss and Extraction

In addition, Parvatareddy *et al*.[19] measured a significant weight loss of neat FM-5 resin upon aging at 177°C in air. Also, the soluble portion of neat resin, as determined by extraction with N-methyl pyrrolidinone (NMP), increased during aging.[19] The gel fraction of FM-5 after extraction with NMP is presented as a function of aging time in Figure 2.6. The weight loss and the soluble fraction of resin were lower when aging was performed in a reduced pressure air atmosphere. It was inferred from these results that oxidative aging led to chain scission.

There is substantial evidence that aging FM-5 at elevated temperatures causes a combination of physical and chemical aging in the resin. A decrease in fracture energy and tensile strength, an increase in T_g, and formation of low molecular weight species have been presented. Additionally, a decrease in the extent of aging at a reduced oxygen

partial pressure illustrates that chemical aging of the adhesive is related to diffusion of the degrading species.

In the current study, the glass transition temperature of neat and filled specimens were studied as a function of aging time, and similar weight loss and extraction studies have been performed on neat resin and filled specimens. The changes in T_g, weight loss, and changes in soluble portion of the polymer during elevated temperature aging were used to characterize the effect of titanium dioxide on chemical aging of the polyimide. In addition, the extracted material was analyzed using gel permeation chromatography.

2.5 Notched Coating Adhesion Test

In the present work, adhesive performance was measured using the NCA test.[21, 55] Schematics of an NCA specimen and an NCA test are shown in Figure 2.7 and Figure 2.8, respectively. The NCA test is based on self-delamination theory,[56] the phenomenon of delamination of a sufficiently thick coating from a substrate, caused by residual stresses within the coating. In the NCA test, the stresses within the coating are increased by applying a load to the NCA specimen. A debond between the adhesive and the substrate is initiated by notching the adhesive coating. The specimen is pulled in tension until the initial adhesive debond propagates. The strain at which the debond propagation occurs, the critical strain, is used to calculate the critical strain energy release rate, G_c, of the system. This is a measure of the adhesive/substrate system's resistance to fracture. Assuming the steady-state condition, according to Dillard *et al*.,[55] Equation 2.4 is used to calculate G_c, where

$$G_c = \frac{h}{E}\left\{\left[\sigma_o^2 + \sigma_o E\varepsilon_c\right](1-\nu) + \frac{1}{2}(\varepsilon_c E)^2\right\} \qquad \textit{Equation 2.4}$$

and h is the adhesive thickness, E is the modulus of the adhesive, ν is Poisson's ratio of the adhesive, σ_o is the sum of all residual stresses within the adhesive, and ε_c is the critical strain to cause debond propagation.

There are two major advantages of the NCA test in this study. First, the "open-faced" adhesive geometry may allow aging to occur more quickly than in traditional adhesive bonds due to the shortened diffusion path. In a traditional adhesive bond geometry, the adhesive is sandwiched by two substrates, so diffusion of species in the environment can only occur through the edges of the adhesive bond. The diffusion path length, therefore, is half the width of the adhesive specimen, generally 6 to 12 mm. In an NCA specimen, the diffusion path length is the thickness of the adhesive, generally less than 1 mm. Since diffusion time is proportional to the square of the diffusion distance, the total time for a specimen to reach equilibrium with the environment may be decreased by up to two orders of magnitude. The second advantage of the NCA test is the incorporation of two modes, or mixed mode I and II, that drives the failure toward the interface. This allows surface characterization of the area of interest in this investigation, the interphase region, at all stages of the durability study.

2.6 Filled Polymer Systems

In the current study, the interphase region of an adhesive joint was modeled by dispersing particles of titanium dioxide in a PETI-5 matrix. The large surface to volume ratio of the filled system enables a substantial portion of the polymer to behave as an interphase. In addition, the bulk nature of the samples allows them to be characterized mechanically, thermally, and chemically using bulk analysis techniques, whereas the nanometer-scale thickness of the interphase traditionally limits the characterization to surface-sensitive techniques. Although previous researchers have studied filled polymer systems extensively, the objective of these investigations has primarily been to improve material properties by addition of filler, rather than to model an adhesive/substrate interphase.[8, 57-60]

There are several advantages to modeling the polymer/metal oxide interface using a system of dispersed oxide particles. Any chemical changes that occur within the polymer, due to the existence of the TiO_2 particles, are likely to be the same changes that occur at the polymer/metal oxide interface of adhesively bonded joints. Changes in the model system, however, will occur in a larger volume fraction of the polymer, as

compared to the interphase region of an adhesive joint, due to the greatly increased surface to volume ratio of the model system.

Another benefit of the model system is the presence of the TiO_2 particles in the system during the testing of the adhesive. Using multi-frequency dynamic mechanical thermal analysis (DMTA), fit to the Kohlrausch-Williams-Watts (KWW) equation,[61, 62] one can quantify the cooperativity of the system, or the breadth of the distribution of relaxation times. The measure of cooperative motion of a system is sensitive to changes at an interface. For example, adsorption of polymer chains on a filler particle is expected to cause an increase in the breadth of relaxation times, due to immobilization of adsorbed molecules.[30]

The filled model system used in this study consisted of a PETI-5 polyimide matrix with dispersed particles of titanium dioxide. Amorphous titanium dioxide, rather than a crystalline form, was used to emulate the titanium dioxide on the surface of chromic acid anodized Ti-6Al-4V.[27] Nagpal and Davis[63] and Mauritz and Jones[64] have made films of polymers filled with amorphous titanium dioxide, and the oxide has remained amorphous in the presence of polymer to at least 500°C. Since the specimens for the present study were processed at 371°C and aged at 177°C, it is believed that filler remained amorphous throughout the study.

2.7 Dynamic Mechanical Thermal Analysis

In DMTA, the modulus of the material of interest is measured as a function of temperature and/or the frequency of the applied sinusoidal stress. When polymeric materials are subjected to a sinusoidal stress, the strain response generally lags behind the applied stress by a phase angle, δ.[65] This is due to the viscoelastic nature of polymers; that is, polymers behave in a manner intermediate between that of an elastic solid and a viscous liquid.[66] If a shear force is applied to a perfectly elastic solid, all of the applied energy is recovered upon release of the force. In contrast, a shear force applied to a Newtonian fluid is not recoverable, with the energy being dissipated as heat from internal friction.[24] In the case of polymers, viscoelastic materials, a portion of the applied force is

recoverable (elastic) while the rest is lost (viscous). The phase angle, δ, characterizes the viscoelastic nature of a material. A perfectly elastic solid has a phase angle of 0°, while that of a viscous liquid is 90°.

The phase lag in a polymer results from the time necessary for molecular rearrangements to occur.[65] If the strain, ε, is expressed as

$$\varepsilon = \varepsilon_o \sin \omega t \qquad \textit{Equation 2.5}$$

where ε_o is the applied strain, ω is the frequency expressed in radians per second, and t is time, then the corresponding stress, σ is

$$\sigma = \sigma_o \sin(\omega t + \delta) \qquad \textit{Equation 2.6}$$

where σ_o is the applied stress.

Expanding the expression for σ gives

$$\sigma = \sigma_o \sin \omega t \cos \delta + \sigma_o \cos \omega t \sin \delta . \qquad \textit{Equation 2.7}$$

The stress, therefore, has two components, one proportional to cos δ, in phase with the strain, and one proportional to sin δ, out of phase with the strain. The stress-strain relationship can then be defined using two modulus terms, G' and G'', in the following expression:

$$\sigma = \varepsilon_o G' \sin \omega t + \varepsilon_o G'' \cos \omega t \qquad \textit{Equation 2.8}$$

where

$$G' = \frac{\sigma_o}{\varepsilon_o}\cos\delta \quad \text{and} \quad G'' = \frac{\sigma_o}{\varepsilon_o}\sin\delta \qquad \textit{Equation 2.9}$$

Hence,

$$\tan\delta = \frac{G''}{G'} \qquad \textit{Equation 2.10}$$

The storage modulus, G', is in phase with the strain, while the loss modulus, G'' is 90° out of phase with the strain. The terms "storage" and "loss" originate from the elastic and viscous contributions, respectively.[67]

Transitions in polymers, such as the glass transition, are characterized by changes in the polymer's molecular mobility that are time, temperature, and frequency dependent. These transitions cause changes in the G', G'' and tan δ values measured by DMTA. The two transitions of importance to the current study are the glass transition and the beta transition. The glass transition, by the standard nomenclature, is typically labeled the alpha transition. Sub-T_g transitions are then labeled beta, gamma, and so forth, with decreasing temperature. The glass transition is the most prominent in amorphous polymers. Molecularly, it corresponds to the onset of large-scale conformational rearrangements of the polymer chain backbone. The secondary transitions (beta, gamma, etc.) result from molecular motions that occur in the glassy state. These are typically attributed to rotations of side groups attached to the main chain or from limited motions within the chain backbone.[65]

2.7.1 Glass Transitions

DMTA has been performed on several filled polymer systems.[30, 58, 68-70] Bott, Taylor, and Ward[58] found, for a metal-filled polyisoimide, the tan δ peak at the glass transition was broader and higher in magnitude upon incorporation of the filler. This was explained as dissipation of mechanical energy due to frictional losses caused by polymer segments moving across the filler surfaces. Perrault and Duchesne[69] studied the effect of iron

oxide incorporation into polybutadiene. They found that the tan δ and loss modulus peak heights were inversely related to the quality of the solid-binder interface. This is consistent with the explanation by Bott regarding frictional losses with filler incorporation. Tan δ and loss modulus peaks in filled samples were approximately double those of non-filled systems. In addition, there was a general trend of increasing ratios of filled to non-filled peak heights as a function of aging up to 56 days at 60°C. The implication here is that the polymer/filler adhesion decreased during aging. Landel[30] applied time-temperature superposition to the dynamic mechanical spectra of a model filled system of polyisobutylene with small glass beads. Relaxation and retardation spectra were calculated for the pure polymer and the filled system. Landel interpreted a divergence of the spectra of filled samples from that of the pure polymer to be the result of immobilization of chains by adhesion to the glass filler particles. The effect was similar to the role of entanglements, causing a portion of the spectrum to be shifted toward longer relaxation times. The magnitude of this shift was predicted to increase with stronger polymer/filler adhesion.

Dynamic mechanical relaxation data can often be fitted using the Kohlrausch-Williams-Watts (KWW) function

$$\phi(t) = \exp\left(-\left(\frac{t}{\tau}\right)^{\beta}\right). \qquad \textit{Equation 2.11}$$

In this equation, t is time, τ is a characteristic relaxation time, and β is a parameter that characterizes the breadth of the relaxation time distribution. The β parameter is between 0 and 1, with β=1 indicating a single relaxation time and β=0 indicating an infinitely broad dispersion. From the above observations, in which tan δ peaks were broadened after incorporation of filler particles, one would expect a significant decrease in β upon incorporation of filler particles. Fitzgerald[71] *et al*. found this to be the case in the characterization of silicon dioxide/poly(vinyl acetate) microcomposites. Incorporation of 0 to 20% silicon dioxide led to significant decreases in β, as listed in Table 2.1. Here,

broadening was observed only on the high-temperature side of the loss modulus versus temperature curve; the onset of the T_g remained constant. It was concluded that the local polymer environment was "microheterogeneous," and that the chains interacting with SiO_2 have slower relaxation times than do those in a more mobile environment.

In the current study, analysis of dynamic mechanical data includes calculations of β values from KWW fits to the loss modulus data. In addition, tan δ and loss modulus peak heights were investigated as a function of aging time.

2.7.2 Beta Transitions

Beta transitions in polymers have frequently been associated with the polymer's mechanical properties,[72] particularly fracture toughness[73, 74] and impact resistance.[75, 76] Impact resistance of polycarbonate has been shown to be greatest at the temperature corresponding to the maximum of the beta transition tan δ peak at impact frequencies.[76] The magnitude of the beta transition of a series of poly(arylene ethersulfones) was found to increase with fracture toughness and decrease with the polymer's crosslink density.[74]

Several researchers have reported a beta transition in the dynamic mechanical or dielectric spectra of polyimides.[77-84] This transition is generally observed between 50° and 250°C.[81] Significant decreases in magnitude[80, 85] and increases in temperature[86] of the beta relaxation loss modulus have been observed after aging below the glass transition temperature. A decrease in the magnitude of the beta transition tan δ peak of polyimides during aging has also been associated with decreases in mechanical properties, including ductility.[85]

Because of the established relationships between beta transitions, mechanical properties, and aging, the effect of filler particle incorporation and elevated temperature aging on the beta transition is of great interest in the present work.

2.8 Infrared Spectroscopy

Diffuse reflectance infrared spectroscopy is a convenient and effective spectroscopic technique for materials that are neither soluble nor transparent. Polyimides have been well characterized with infrared spectroscopy, with characteristic sharp imide peaks at 1775 and 1720 cm^{-1}.[87] The carbon-carbon triple bond in the phenylethynyl group of PETI-5 is observed at 2213 cm^{-1}.[46] Wood[88] has characterized the cure of PETI-5 by following the magnitude of this peak as a function of cure time and temperature. In the present study, diffuse reflectance IR has been used to compare the cures of neat and TiO_2-filled PETI-5 and to investigate chemical changes due to elevated temperature aging.

2.9 X-Ray Photoelectron Spectroscopy

2.9.1 XPS Technique

When radiation of sufficient energy $h\nu$ impinges on a surface, electrons are ejected with energies E_n given by the equation

$$E_n = h\nu - I_n \qquad \textit{Equation 2.12}$$

Where I_n is the ionization potential to the nth ionized state of the atom on the surface.[89] When x-rays are used for the energy source, the technique is known as x-ray photoelectron spectroscopy, or XPS. Because the high-energy x-ray source causes inner core electrons to be ejected, the ionization potentials relate to orbitals that are almost purely atomic in character. Therefore, the binding energies determined by XPS are characteristic of the source atom, but are also slightly dependent on molecular environment. Detailed analysis of the absolute and relative binding energies and relative peak intensities corresponding to the direct photoionization of core levels can provide data on structure and bonding in systems.[90] Because the escape depth of the ejected electron is limited, typically to 5 to 10 nm, XPS is an excellent technique for analyzing the near-surface region of the sample of interest.[90]

2.9.2 Differential Charging in XPS

XPS is frequently utilized for the analysis of metal-to-adhesive failure surfaces. When these failures occur in the region near the polymer-metal interface, as they do in the current study, the resulting metal failure surface often consists of a metal substrate covered with either polymer islands or a polymer layer of varying thickness.[91] The corresponding adhesive failure surface can be represented by a polymer substrate covered with islands of metal or metal oxide. In these situations, where analysis surfaces exhibit inhomogeneous conductivity and electron affinity, XPS analysis is prone to differential charging.[92-95]

While performing XPS, the outgoing photoelectron leaves a positive charge on the sample surface. In an insulator, the spectrometer cannot conduct electrons to the sample surface to compensate for this charge. As a result, a positive charge is built up on the specimen under analysis. While uniform charging of a non-conductor shifts the whole spectrum, generally to higher binding energies, differential charging causes different components of a sample to shift by different amounts. Thus, the typical means of correcting for uniform charging, such as the use of adventitious carbon as a binding energy reference, supply erroneous binding energies for a portion of the sample components.[96]

For example, Pertsin *et al.*[91] performed XPS on a sample consisting of platinum clusters on a polydimethylphenyleneoxide film. While the C 1s photopeak is shifted by +1 eV from its normal position of 285.0 eV, the Pt 4f peak is shifted by 1.9 eV from its usual value of 71.1 eV. Thus, a difference in charging of 0.9 eV is present. While interpreting XPS data from inhomogeneous surfaces, it is important to be aware of the possibility of differential charging so that these effects are not misinterpreted as true chemical shifts.

Table 2.1: Variation in the KWW parameter, β, with microcomposite SiO_2 incorporation, after Fitzgerald, et al.[71]

% SiO_2 by weight	KWW β parameter
0	0.56
5	0.55
10	0.50
15	0.42
20	0.32

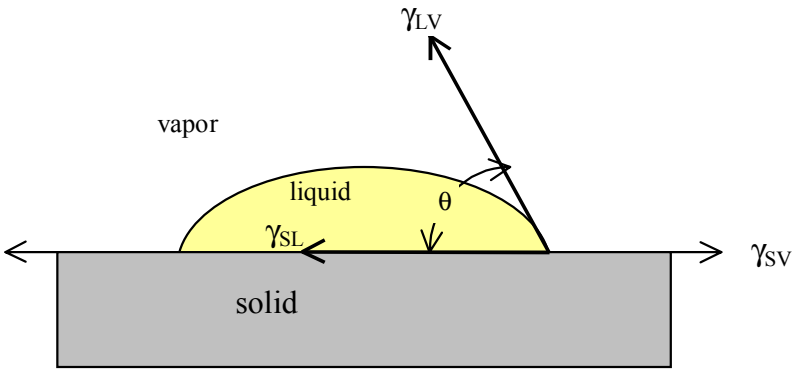

Figure 2.1: A liquid drop resting at equilibrium on a solid surface.[22]

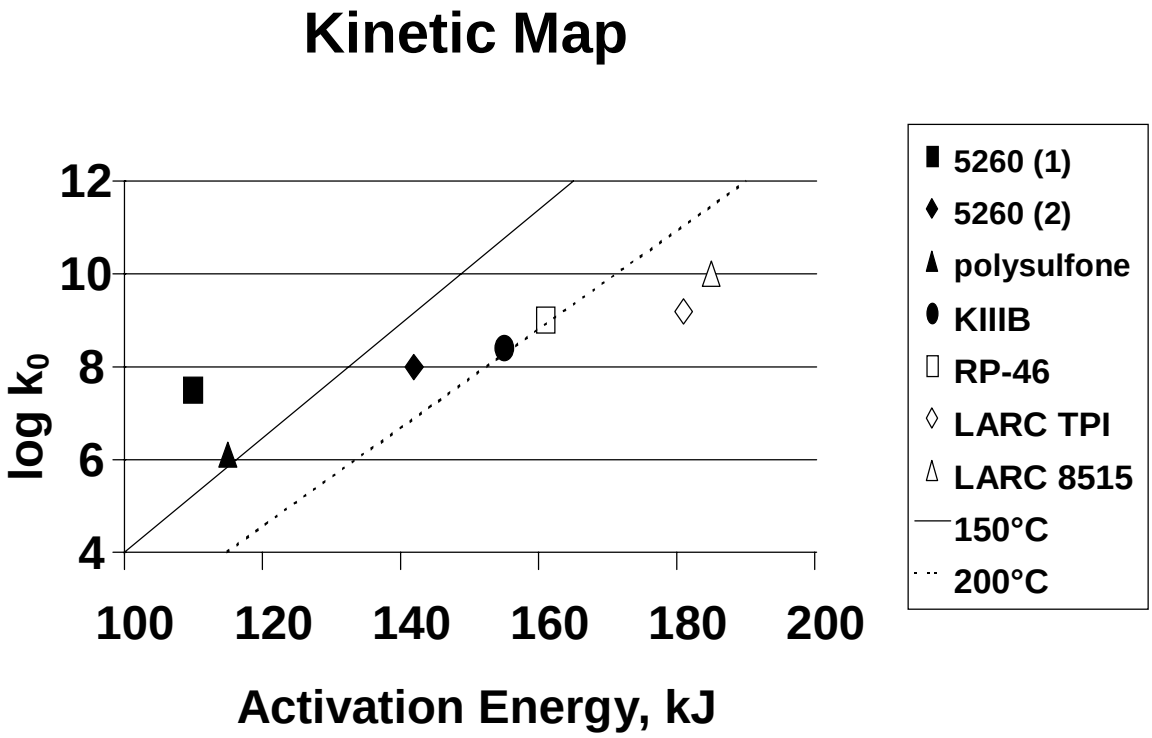

Figure 2.2: An example of a kinetic map for polymer lifetime prediction, after Kiefer et al.[52] *If the data point for a material lies to the left of a line, it is predicted to lose more than 1% of its weight at the given time and temperature, while a material to the right of the line is predicted to lose less than 1% of its weight.*

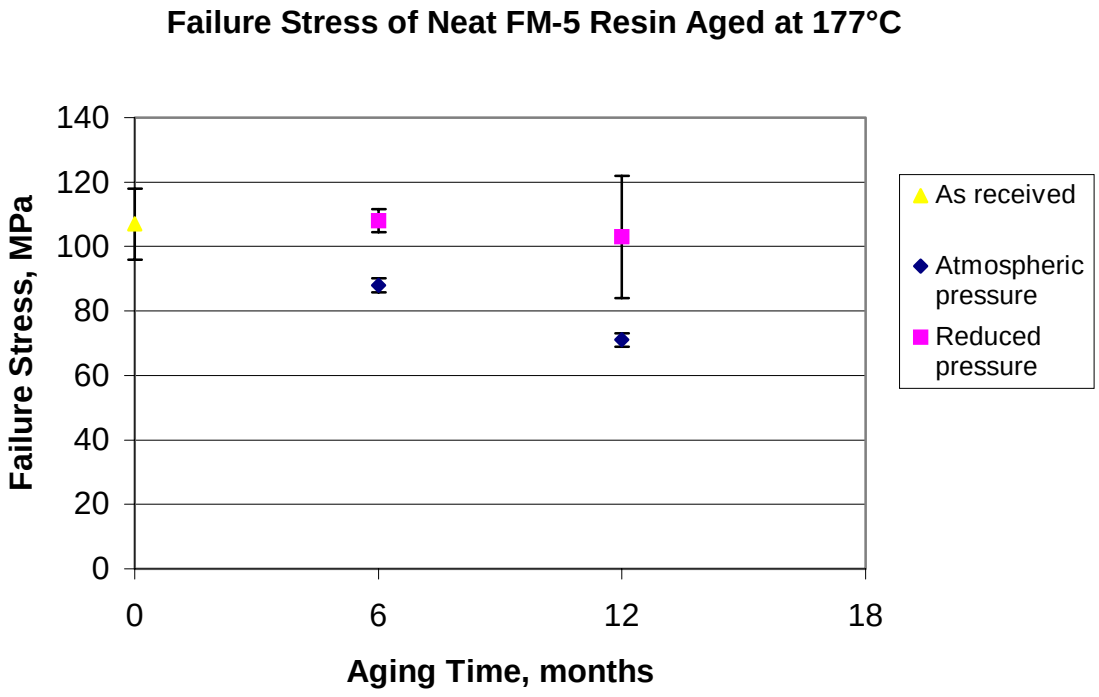

Figure 2.3: Tensile stress to failure of FM-5 neat resin as a function of aging time at 177°C, after Xu et al.[54] *Samples were aged in air at atmospheric pressure or a reduced pressure of 2 psi.*

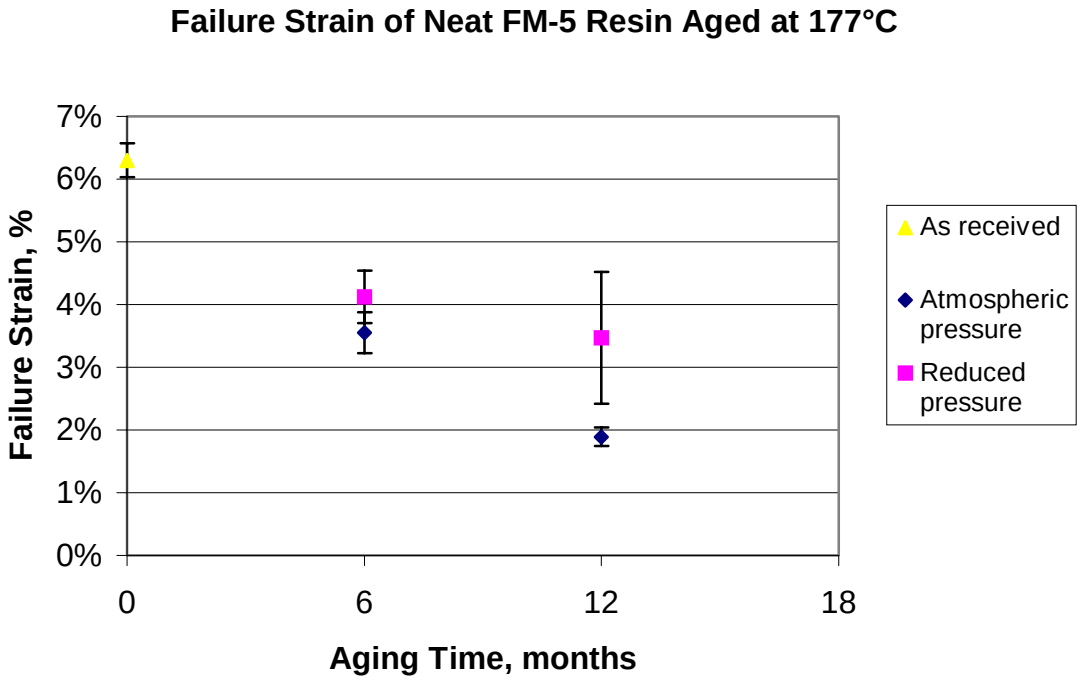

Figure 2.4: Tensile strain to failure of FM-5 neat resin as a function of aging time at 177°C, after Xu et al.[54] *Samples were aged in air at atmospheric pressure or a reduced pressure of 2 psi.*

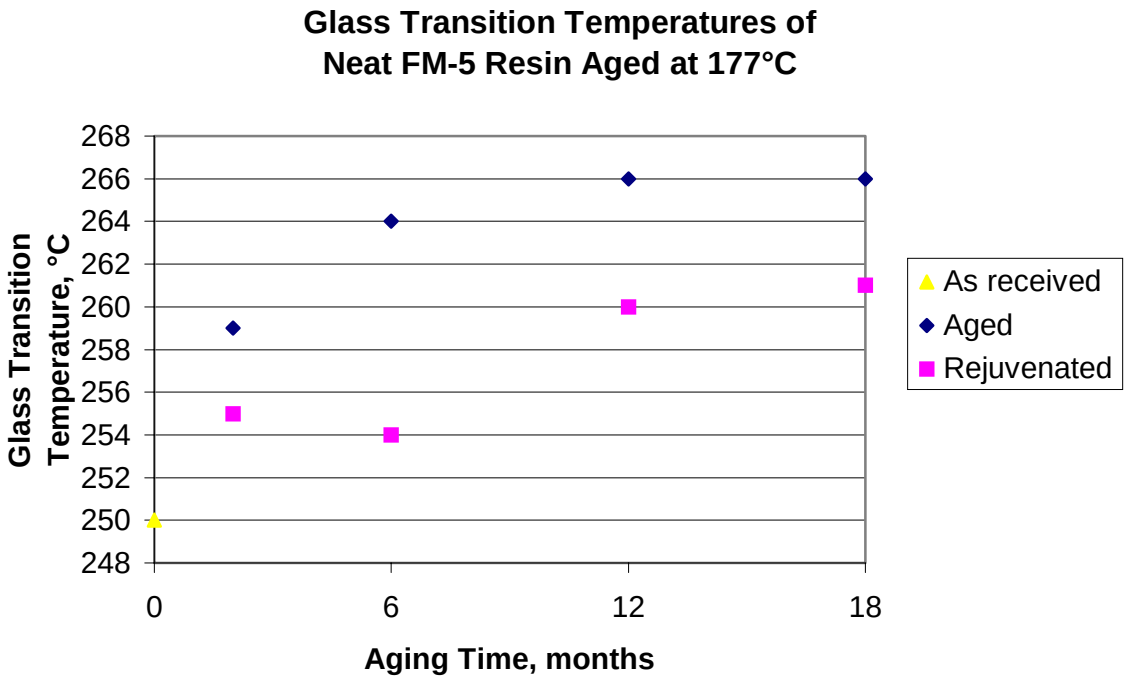

Figure 2.5: Glass transition temperatures of FM-5 neat resin as a function of aging time at 177°C, after Parvatareddy et al.[19, 20]. *Samples were aged in air at atmospheric pressure. Rejuvenated samples were held at 300°C for 2 hours to reverse the effects of physical aging.*

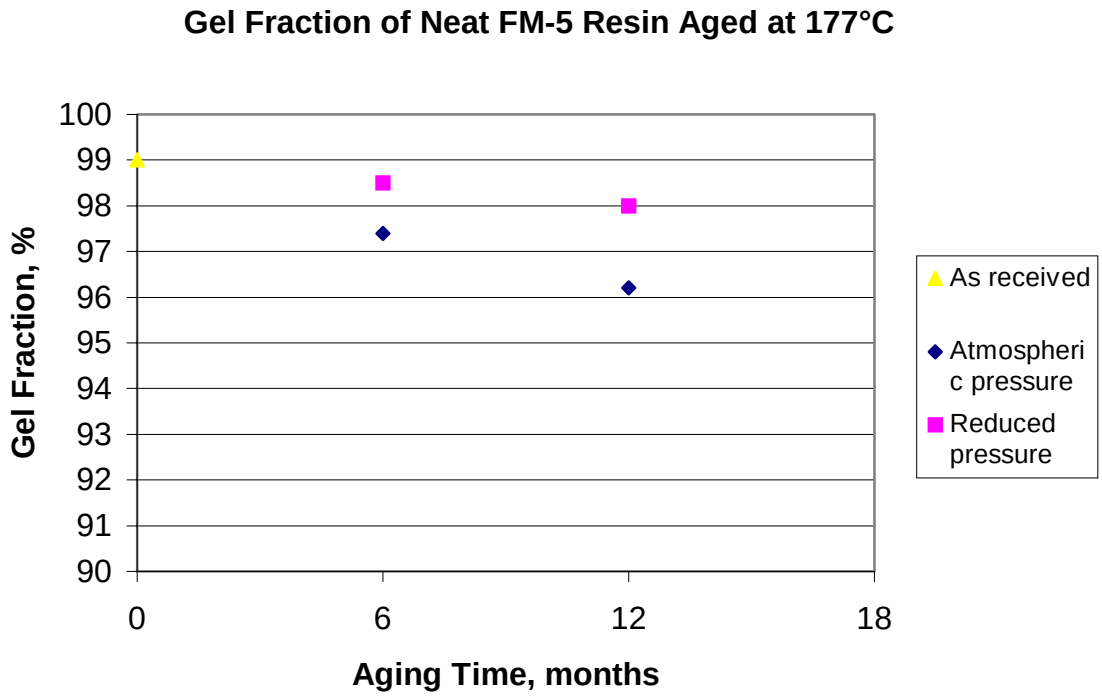

Figure 2.6: Gel fraction of FM-5 neat resin as a function of aging time at 177°C, using NMP as the extracting solvent, after Parvatareddy et al.[19] *Samples were aged in air at atmospheric pressure or a reduced pressure of 2 psi.*

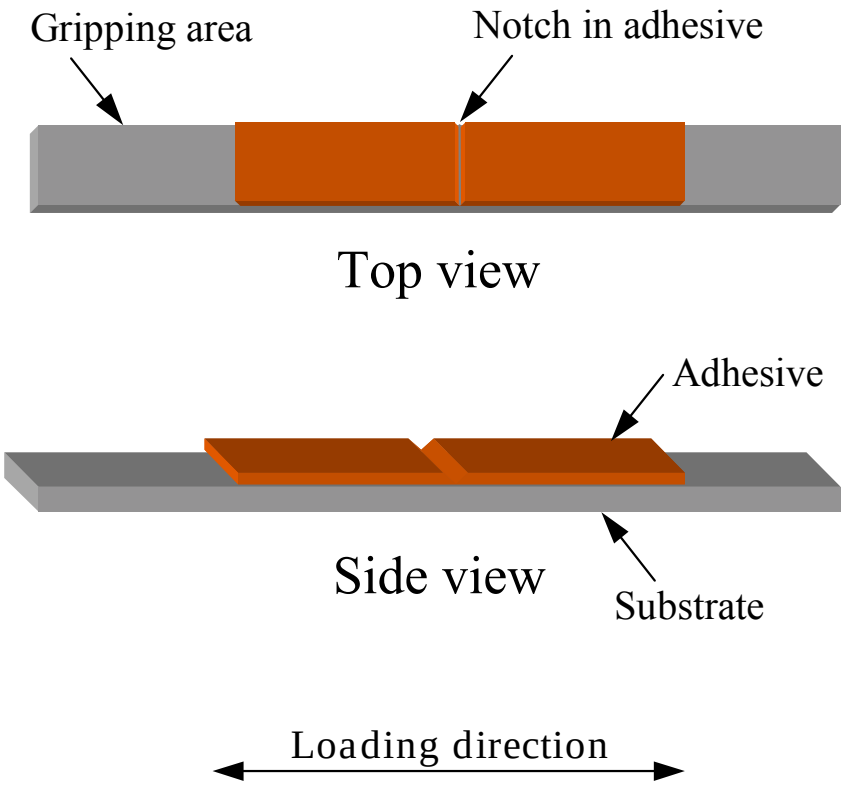

Figure 2.7: Schematic of a notched coating adhesion specimen.

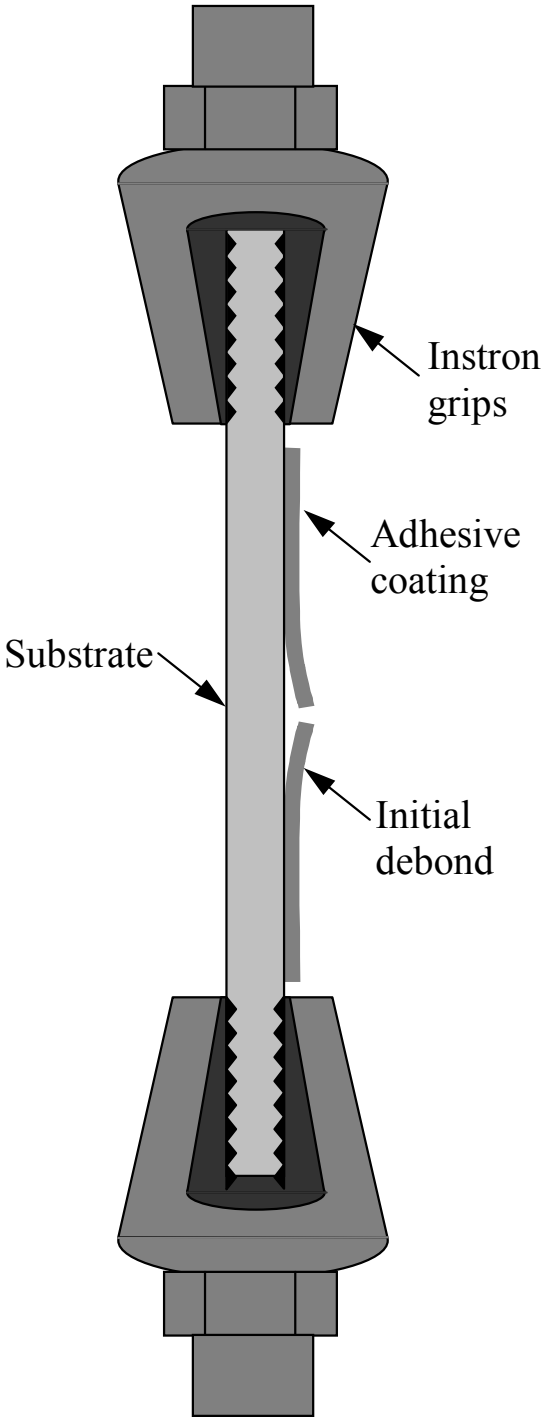

Figure 2.8: Notched coating adhesion specimen during testing.

Chapter 3: Experimental Techniques

3.1 Materials

3.1.1 Adhesives

The focus of this study involves the behavior of two polyimide adhesives, Cytec Fiberite™ FM-5 and LaRC™ PETI-5. Two other polyimide adhesives, Cytec Fiberite™ FM-36 and LaRC™ 8515, were used for comparative purposes. FM-5 and FM-36 were used as received from Cytec Fiberite Inc.™, Havre de Grace, MD, and consisted of polyimide adhesives supported by a glass scrim cloth arranged in a 0º/90º plain weave. As received, FM-5 contained approximately 4% NMP by weight. FM-36 contained approximately 40% volatiles by weight. Upon cure, FM-5 and FM-36 are amorphous thermosets with a T_g of 250°C. PETI-5 and 8515 were received from Imitec,™ Schenectady, NY, as amic acid solutions at 35% (PETI-5) or 30% (8515) solids (w/w) in NMP. The calculated molecular weights of PETI-5 and 8515 were 5,000 g/mol and 9,200 g/mol, respectively. Upon cure, PETI-5 is a thermoset with a T_g of 260°C. 8515 is a thermoplastic with the same backbone structure as PETI-5. At the molecular weight used here, the reported T_g is 235°C.[97]

3.1.2 Substrates

The titanium alloy substrates of all adhesive specimens were Ti-6Al-4V, an alloy consisting of 6% aluminum and 4% vanadium. Substrates were received from President Titanium Co., Hanson, MA. The substrates used with the FM-5 adhesive measured 121 × 12.7 × 1.78 mm, those used with the FM-36 adhesive were 203 × 12.7 × 1.59 mm, and those used with the PETI-5 and 8515 adhesives were 203 × 12.7 × 1.78 mm.

3.1.3 Titanium Dioxide Filler

Amorphous titanium dioxide powder, 99.9% pure and with a unit surface area of 150 to 250 m^2/g, was obtained from Alfa Aesar,® Ward Hill, MA. It was stored in a desiccator and used as received.

3.2 Sample Preparation

3.1.1 Adhesive Specimens

3.2.1.1 Surface Treatments

All titanium substrates were surface treated prior to bonding. The FM-5, PETI-5, and 8515 specimens were fabricated using chromic acid anodized (CAA) substrates. This choice of surface treatment is discussed in Chapter 2. Specimens of FM-36 adhesive were fabricated using base/acid treated titanium substrates.

3.2.1.1.1 Chromic Acid Anodization

The CAA procedure developed by Boeing was used to pretreat titanium substrates bonded with FM-5, PETI-5, and 8515. Substrates were degreased using acetone and abrasive pads until they appeared shiny. Substrates were then buffed using Crocus Cloth (Al_2O_3 paper #800), cleaned with acetone, and rinsed with water until a film of water evenly coated the surface. This ensured that the titanium surface was uniform and free of dirt and grease. Substrates were then stirred for ten minutes in Allied Kelite's Isoprep cleaning solution and rinsed with deionized water. Substrates were immersed in boiling

deionized water for five minutes, then stirred in a nitric acid solution for two minutes (114 mL deionized water, 151 mL fuming HNO_3, 10.9 mL 50% HF). After rinsing with deionized water, the substrates were anodized in chromic acid (45 g/L) at 5.0 volts and 1.25 amps/ft^2 for 20 minutes using identical Ti-6Al-4V substrates as the cathode. When necessary, the current was adjusted by dropwise addition of HF to the chromic acid while stirring. The substrates were then rinsed with deionized water for several minutes. Following drying in a 60°C oven for a minimum of one hour, substrates were stored in a desiccator until they were either primed (within 12 hours of anodization) or bonded (within 48 hours of anodization).

3.2.1.1.2 Base/Acid Etch

The as-received Ti-6Al-4V substrates were cleaned with acetone and abrasive pads before an acetone rinse. The substrates were then exposed to an agitated 10% sodium hydroxide (NaOH) bath for 15 minutes, maintained at 70°C. The substrates were removed from the NaOH, rinsed with deionized water, and placed in room temperature 3M sulfuric acid (H_2SO_4) for 5 minutes. Following the sulfuric acid bath, the substrates were again rinsed with deionized water and placed in an oven at 50°C for a minimum of 30 minutes. Upon removal from the oven, the substrates were placed in a desiccator until bonding, which was done within 72 hours of the surface treatment. The resulting titanium surfaces were covered with a uniform oxide layer since titanium oxidizes easily under typical atmospheric conditions.

3.2.1.2 Preparation of Adhesive Tape

FM-5 and FM-36 adhesive tape, supported by a glass scrim cloth, was used as received in the fabrication of adhesive specimens. PETI-5 and 8515 adhesive tapes were fabricated and subsequently used in the preparation of adhesive specimens. An E-glass scrim cloth, 0.08 mm thick with A1100 finish arranged in a 0º/90º plain weave, was stretched onto a frame and dried at 150°C for one hour prior to application of the adhesive. The cloth was impregnated with adhesive by applying PETI-5 or 8515 as a poly(amic acid) solution in NMP using a natural bristle paintbrush. Application and drying procedures were

optimized so that adhesive tape with minimal bubbles and inhomogeneities, as judged visually, was formed. The first two coats were applied at 10% solids; all subsequent coats were applied from a 20% solids solution. The following drying cycle was performed after each coat was applied: ramp from room temperature to 100ºC in 30 minutes, hold at 100ºC for one hour, ramp from 100ºC to 175ºC in 30 minutes, hold at 175ºC for one hour, cool from 175ºC to room temperature in one hour. Twelve to fifteen coats were applied to the glass cloth until the desired thickness of 0.30 mm was obtained. A final drying cycle, 30 minutes at 250ºC, was performed to reduce the volatile content of the tape to less than 2.5%.

3.2.1.3 Manufacture of NCA Specimens

NCA specimens were manufactured for two segments of the current study. First, the bondline thickness was varied from 0.152 to 0.762 mm to investigate the effect of substrate plastic deformation on the NCA test. For this section, samples were manufactured using FM-5 and FM-36 adhesives. Second, the effect of elevated temperature aging was investigated. For these specimens, a constant bondline thickness was used for each adhesive studied, including FM-5, PETI-5, and 8515. The bondline thickness of FM-5 specimens was 0.76, while that of PETI-5 and 8515 specimens was 0.25. The general manufacturing procedure is illustrated in Figure 3.1, and details are given in the following sections.

3.2.1.3.1 Specimens with Varied Bondline Thickness

3.2.1.3.1.1 FM-5 NCA Specimens

Ten pieces of anodized titanium were arranged side-by-side on a Wabash hot press so that one sheet of adhesive would cover the necessary area. The adhesive sheet was centered on the substrates so that the scrim cloth orientation was parallel to the substrate dimensions. A sheet of Kapton film was placed between the adhesive sheet and the upper plate of the hot press. Steel shims were used to control the adhesive thickness. NCA test specimens with five different adhesive thicknesses, 0.152 to 0.762 mm, were prepared. For the larger adhesive thicknesses, multiple sheets of film adhesive were stacked to

attain the desired thickness. Five NCA test specimens of each adhesive thickness were fabricated. Table 3.1 describes the sample populations analyzed.

The following cure cycle was used for the FM-5 NCA specimens: 90 minute ramp to 250ºC, hold 1 hour, apply bonding pressure of 350 kPa, 45 minute ramp to 350ºC, hold 1 hour, cool to room temperature.

Once the sample plaques cooled to room temperature, the plaques were separated into individual test specimens. The edges of the individual samples were sanded to eliminate any anomalous effects arising from polymer bonded to these surfaces. A pre-crack was made between the adhesive and substrate by notching the center of the specimen with a hacksaw. The residual stresses in the adhesive created an area of localized debonding around the notch.

3.2.1.3.1.2 FM-36 NCA Specimens

The fabrication procedure was similar to that of the FM-5 specimens. The following modifications were used when making the FM-36 samples. The titanium substrates were base-acid etched rather than anodized. A Tetrahedron Model P-400 hot press was used to perform the bonding press cycle. A thin strip of Teflon film (5 mm wide) was placed across the titanium pieces, bisecting their lengths. The Teflon strip facilitated the initiation of uniform pre-cracks, which are required for the NCA test to be valid. A cardboard tube was used to apply pressure to the adhesive, which is tacky and pliable at room temperature, removing any air pockets and initializing the bond between adhesive and substrate. The prepared sample plaques were placed between two sheets of Teflon-coated release paper. Ten NCA test specimens of each adhesive thickness were fabricated. Table 3.1 describes the sample populations analyzed.

The following cure cycle was used for the FM-36 NCA specimens:

Hot press cycle: Ramp to 93°C, apply bonding pressure of 280 kPa, ramp to 177°C in 10 minutes, hold at 177°C for 90 minutes, release bonding pressure and air cool to room temperature.

Post-cure in oven: Pre-heat oven to 260°C, hold at 260°C for 3 hours, air cool to room temperature.

Once the sample plaques cooled to room temperature, the plaques were separated into individual test specimens. The edges of the individual samples were sanded to eliminate any anomalous effects arising from polymer bonded to these surfaces. A pre-crack was made between the adhesive and substrate by notching the center of the specimen with a hacksaw in the area where the Teflon strip was placed. The notch created an area of localized debonding.

3.2.1.3.2 Specimens with Constant Bondline Thickness

3.2.1.3.2.1 FM-5 NCA Specimens

FM-5 NCA specimens of constant bondline thickness were fabricated in a manner identical to those of varied bondline thickness. Two plies of FM-5 adhesive in glass scrim cloth were used, and steel shims controlled the adhesive thickness to 0.76 mm.

3.2.1.3.2.2 PETI-5 and 8515 NCA Specimens

The PETI-5 and 8515 NCA samples were manufactured using anodized Ti-6Al-4V substrates that had been primed within 12 hours of anodization. This allowed the treated substrates to be stored in a desiccator for several months without any changes in the surface morphology. The primer consisted of a 16% solids solution of the same poly(amic acid) from which adhesive bonds would be made (e.g. PETI-5 primer was used with the PETI-5 NCA specimens, 8515 primer was used with the 8515 NCA specimens). Following application of the primer with a natural bristle paintbrush, the substrates were dried in an oven under the following conditions: ramp from room temperature to 100ºC in 30 minutes, hold at 100ºC for one hour, ramp from 100ºC to 175ºC in 30 minutes, hold at 175ºC for one hour, ramp to 250°C in 30 minutes, hold at 250°C for 30 minutes. Thus, the primer had experienced a thermal history comparable to that of the poly(amic acid) applied to the adhesive tape to which the substrates would be bonded.

The PETI-5 and 8515 NCA specimens were manufactured in an autoclave rather than a hot press. This allowed a more uniform application of pressure, leading to improved consistency in bondline thickness. Two plies of PETI-5 or 8515 adhesive in glass scrim cloth were used. A Kapton sheet coated with Zyvax release coating was placed between the upper surface of the adhesive and a steel plate. Steel shims controlled the bondline to 0.25 mm. The following cure cycle was used: apply vacuum, ramp to 250ºC, hold one hour, apply bonding pressure of 690 kPa (PETI-5) or 345 kPa (8515), ramp to 350ºC, hold 30 minutes, ramp to 371°C, hold 30 minutes, cool to ambient temperature, release pressure and vacuum. The higher bonding pressure used with the PETI-5 specimens was necessary to achieve sufficient flow to obtain the desired bondline thickness.

The modifications between the FM-5 and the PETI-5/8515 cure cycles, application of a vacuum and a higher final cure temperature, were necessary to eliminate residual volatiles and crystallinity that were observed in the FM-5 NCA specimens. The use of primer on the PETI-5 and 8515 titanium coupons was recommended to protect the chromic acid anodized titanium surface. These modifications more accurately mimic the processing conditions that would be used commercially. While these changes prevent one from making a direct quantitative comparison between the FM-5 and PETI-5 or 8515 adhesive systems, a qualitative assessment of trends in adhesive durability for all systems is possible.

3.2.2 Bulk and Titanium Dioxide-Filled Moldings

3.2.2.1 Neat PETI-5 Powder

PETI-5 amic acid solution at 35% solids in NMP was cast onto a glass plate and dried under the following conditions: 30 minute ramp to 100°C, hold one hour, 30 minute ramp to 175°C, hold one hour, one hour ramp to 225°C, hold 30 minutes. The resulting brittle material was ground to a powder with a mortar and pestle. The drying cycle used here is intended to mimic those used when drying adhesive tape or primer. Note, however, the final drying temperature of 225°C rather than 250°C. This was modified to prevent reaction of the phenylethynyl end groups, which impart toughness to the material. This would prevent it from being ground to a fine powder, which was necessary for

manufacture of the moldings. To reduce the volatiles to a level comparable to that of the adhesive tape, the ground powder was dried under vacuum for 30 minutes at 225°C.

3.2.2.2 PETI-5 Powder with TiO_2 Filler

Titanium dioxide filler was mixed with the amic acid solution, rather than with the dry PETI-5 powder, to most closely mimic the formation of the PETI-5/TiO_2 interface in a bonded joint. In the bonded joint, the PETI-5/TiO_2 interface is formed when the primer, as an amic acid solution, is applied to the titanium substrate surface. Due to the high viscosity of the amic acid solution, titanium dioxide powder was first stirred with NMP to wet the surface of the particles. Amic acid solution was slowly added to the mixture while stirring. This procedure minimized the agglomeration of the TiO_2 particles.

To make 10 grams of PETI-5 powder containing 10% TiO_2 by volume, 1.87 grams of amorphous titanium dioxide powder was stirred with 7 mL of NMP. 23 grams of PETI-5 amic acid solution at 35% solids in NMP was slowly added to the mixture while stirring. This solution was cast onto a glass plate and dried, then ground to a powder, as described for the PETI-5 powder above. The ground powder was dried under vacuum for 30 minutes at 225°C.

3.2.2.3 PETI-5 and PETI-5/TiO_2 Moldings

Neat PETI-5 plaques and PETI-5 plaques with TiO_2 filler were molded in a vacuum hot press. The moldings measured 76 × 76 × 0.7 mm. Neat PETI-5 moldings were made from 6 grams of PETI-5 powder. PETI-5/TiO_2 moldings were made from 6 grams of PETI-5/TiO_2 powder blended with 1 gram of PETI-5 powder, forming a plaque with 8.4% TiO_2 by volume (16.0% w/w). The neat PETI-5 powder acted as a binder and allowed the manufacture of a molding with improved mechanical integrity compared to a molding from the PETI-5/TiO2 powder alone. (Note: a higher total mass was used to make the same size PETI-5/TiO_2 moldings due to its higher density.) To ensure a constant thickness, a 76 × 76 mm area was cut from a stainless steel plate at a depth of 0.7 mm, as illustrated in Figure 3.2. The mold was filled with PETI-5 or PETI-5/TiO_2 powder, and a stainless steel plunger was placed on the powder. The assembly was then

placed in a vacuum hot press and cured under the following conditions: apply vacuum, ramp to 250°C, hold 1 hour, apply 1380 kPa pressure, ramp to 371°C, hold 1 hour, cool to room temperature, release vacuum and pressure.

The volume fraction of polymer that is expected to behave as an interphase (i.e. the fraction that is directly affected by the TiO_2 filler particle surface) can be estimated using the following equation

$$Volume\ fraction\ interphase = \frac{Volume\ of\ adhesive\ interphase}{Total\ adhesive\ volume} \qquad \text{Equation 3.1}$$

$$= \frac{Filler\ surface\ area \times Thickness\ of\ adhesive\ interphase}{Total\ adhesive\ volume}$$

This requires the assumption that each filler particle is surrounded by polymer, that is, there is no agglomeration of the filler particles. While this is not expected to be entirely true on a microscopic scale, no large-scale clumping of the TiO_2 filler was observed upon mixing with the polymer. Therefore, using a conservative estimate of the interphase thickness, 10 nm, and the low end of the reported surface area range, 150 m^2/g, a reasonable estimate of 35% of the polymer behaving as an interphase is obtained.

3.3 Aging Conditions

FM-5 adhesive specimens were aged for 1 to 90 days in an air aging oven at 177°C. PETI-5 and 8515 adhesive specimens were aged for 30 days at 177°C in either an air or a nitrogen aging oven. PETI-5 and PETI-5/TiO_2 moldings were aged for 2 to 90 days in an air aging oven at 177° or 204°C. Atmospheric pressure was maintained in all ovens. Unaged specimens were stored in a vacuum desiccator at room temperature until testing was performed.

3.4 Characterization

3.4.1 Notched Coating Adhesion Test

3.4.1.1 FM-5 and FM-36 Specimens

The NCA specimens were tested on an Instron 4505 machine under control of a Lab View program. A 100 kN load cell was used. A 25.4 mm gage length extensometer was used to monitor strain. The strain rate used was 10 mm/min. Five replicates were tested for each thickness of FM-5 specimens, and ten replicates per thickness were tested for FM-36 specimens.

The debonding can be observed from the side of the specimen during testing. The critical strain is defined as the strain where the initial debond begins to propagate. The primary concern when performing the NCA test is consistently determining the initial debonding stage. This determination is a source of experimental error since it depends on the reactions and discretion of the experimenter.

To help eliminate the subjectivity involved in a NCA test, all FM-36 tests were video-recorded and timed using a stopwatch superimposed on the video image. The individual test time associated with catastrophic debonding could be accurately determined by video analysis. Knowing the strain rate of the tensile test, the critical strain could be easily determined. Using the critical strain, ε_c, as the tensile strain in Equation 3.2 outputs the critical strain energy release rate, G_c of the adhesive/substrate system.[55]

$$G_c = \frac{h}{E}\left\{\left[\sigma_o^2 + \sigma_o E\varepsilon_c\right](1-\nu) + \frac{1}{2}(\varepsilon_c E)^2\right\} \qquad \textit{Equation 3.2}$$

3.4.1.2 PETI-5 and 8515 Specimens

Because the hacksaw used to initiate the debond between adhesive and substrate in the FM-5 and FM-36 tests may not have caused a sufficiently sharp crack-tip for the NCA analysis to be valid, an improved method was used for the PETI-5 and 8515 specimens.

An initial debond was made between the adhesive and substrate by driving a razor blade into the interface. Specimens were then placed in a hand-held three-point-bend fixture and bent so that the adhesive coating was in tension. A photograph of this setup is shown in Figure 3.3. The razor-induced debond propagated to form a sharp-tipped debond between the adhesive and the substrate. Following initiation of the pre-crack, specimens were fully debonded by gripping the substrate in an Instron test frame, as shown in Figure 3.4, and pulling the specimens in tension at a strain rate of 2.5 mm/min. This slower strain rate was used to improve the precision of the experimentally determined critical strain, ε_c. Testing was accomplished on a 9 kN Instron test frame equipped with a System 4000 data acquisition system. Ten replicates were tested for each aging condition.

3.4.2 Surface Analysis

3.4.2.1 X-Ray Photoelectron Spectroscopy

To determine the atomic concentration of elements on the failure surfaces of NCA specimens, x-ray photoelectron spectroscopy (XPS) was performed using a Perkin Elmer model 5400 spectrometer. A Mg Kα x-ray source operated at 14 kV (300 watts) of power was used to analyze a spot size of 1.0 × 3.0 mm on the specimen surfaces. Typical sampling depths are 5 to 10 nm, and the detection limits of the instrument reflect an average atomic concentration of approximately 0.2%. Both failure surfaces of two specimens were analyzed for each aging condition of FM-5, PETI-5, and 8515 specimens.

For all reported binding energies, spectra were standardized to the hydrocarbon portion of the spectrum at 285.0 eV. The curve fitting procedure for resolution of individual peaks assumed peaks of Gaussian shape. A full-width-at-half-maximum (FWHM) of 1.7 ± 0.1 eV was used to fit the C 1s photopeak.

3.4.2.2 Field Emission Scanning Electron Microscopy

FE-SEM was performed on a LEO model 1550 Field Emission Scanning Electron Microscope at 0.25 to 2.0 kV. The adhesive and titanium failure surfaces of PETI-5 NCA specimens were analyzed. One specimen was analyzed for each aging condition. Samples were not sputter-coated, and no charging was observed.

3.4.2.3 Optical Microscopy

Optical micrographs of failure surfaces were obtained using an Olympus BH-2 optical microscope. All failure surfaces of FM-5 and PETI-5 NCA specimens used in the aging study, adhesive and metal failure sides, were analyzed.

3.4.2.4 Auger Electron Spectroscopy

Depth profiling was performed on a Perkin-Elmer model 610 scanning Auger system using a single pass cylindrical mirror analyzer with electron excitation from a coaxial electron gun. The minimum electron beam diameter is less than 100 nm. The sputter rate was calibrated using a tantalum standard. AES was performed on the metal failure surface of one PETI-5 NCA specimen for each aging condition.

3.4.2.5 Atomic Force Microscopy

A Digital Instruments Dimension 3000 Atomic Force Microscope using the Nanoscope IIIa controller was used in tapping mode to obtain height and phase AFM images. The adhesive and metal failure surface of one PETI-5 NCA specimen for each aging condition was analyzed.

3.4.3 Bulk Adhesive Analysis

3.4.3.1 Adhesive Modulus

The moduli of FM-5 and FM-36 adhesives were determined using a Polymer Laboratories Minimat miniature materials tester. Dogbone samples were made from the adhesive film that debonded during the NCA test using a Dewes-Gumbs Die Company

manual press. The dimensions of the narrow section of the dogbone sample were 8 mm by 2.8 mm. These were pulled at a constant strain rate of 10 mm/min until failure. The strain rate was chosen to be the same rate used in the NCA test. The slope of the linear portion of the stress-strain curve was taken as the adhesive's modulus. Two to three samples of each thickness were tested.

3.4.3.2 Poisson's Ratio

The Poisson's ratio of the adhesive was estimated to be 0.35, based on typical values for similar polymers.[98]

3.4.3.3 Coefficient of Thermal Expansion

The linear coefficient of thermal expansion, α, was determined for FM-5 and FM-36 adhesives using a Netzsch DIL 402C linear dilatometer. Rectangular samples, approximately 5 mm × 25 mm, were cut from the adhesive film that debonded during the NCA test. The dilatometer required samples with structural rigidity, limiting the adhesive thicknesses that could be analyzed to populations B through E (see Table 3.1). The dilatometer samples were scanned from 35°C to 350°C at a heating rate of 5°C per minute. Two replicates were tested for each adhesive thickness.

3.4.3.4 Differential Scanning Calorimetry

DSC was performed on several different instruments over the course of this study. In all cases, a heating rate of 10°C per minute was used. Typically, initial scans were made from room temperature to 300°C. Samples were then quenched and scanned to 450°C. Any deviations from this procedure are noted in the appropriate discussions. The T_g was taken at the half-height of the change in slope of the baseline. Whenever possible, groups of samples for which a direct comparison was made were performed on a single instrument. The instruments used include the DuPont Instruments 910 DSC, Perkin-Elmer Pyris 1 DSC, Perkin-Elmer DSC 7, and Shimadzu DSC-50. One to three replicates were tested in all cases.

3.4.3.5 Solvent Uptake

The weight uptake of FM-5 adhesive upon exposure to NMP at room temperature was measured. Pieces of debonded adhesive from the FM-5 NCA specimens in the aging study were cut using a Dewes-Gumbs Die Company manual press. They were weighed on an analytical balance, immersed in NMP, and re-weighed periodically. Excess solvent was removed from the samples with a Kimwipe prior to weighing. The error in the technique is estimated to be ± 0.2 mg, with a typical sample mass of 150 mg. Five replicates were tested for each aging condition.

3.4.3.6 Solvent Uptake and Extraction

Samples of neat PETI-5 moldings and PETI-5/TiO_2 moldings of all aging conditions were cut to approximately 5 mm × 25 mm. Samples were weighed on an analytical balance and placed in individual test tubes with 4.0 mL of NMP. Test tubes were stoppered and placed in a 50°C oil bath for 7 days. During these 7 days, samples were periodically removed from the NMP, blotted dry, and weighed. After 7 days, the samples were removed from the NMP, dried for 2 days at 100°C under vacuum, and weighed. They were then dried for 3 hours at 250°C under vacuum and re-weighed. The error in the technique is estimated to be ± 0.2 mg, with a typical sample mass of 100 mg. Six samples of unaged neat PETI-5 and PETI-5/TiO_2 were analyzed, and three replicates were tested for all other aging conditions. The NMP containing extracted material from these samples was retained for further analysis.

3.4.3.7 Dynamic Mechanical Thermal Analysis

DMTA was performed on neat PETI-5 and PETI-5/TiO_2 moldings using a Rheometrics Mark IV DMTA under control of Rheometric Scientific's RSI Orchestrator operating software. Samples were tested in single cantilever bending mode with temperature steps from 30 to 400°C at 3°C increments and frequencies from 0.1 to 30 Hz. A strain of 0.03% was applied, which was in the linear region of the material, and a typical sample measured 5 mm × 5 mm × 0.75 mm. One to three replicates were analyzed for each aging condition.

3.4.3.8 Thermogravimetric Analysis

Thermogravimetric analysis was performed on a Seiko TG/DTA 220 instrument using 10 to 15 mg samples. A heating rate of 2.5°C/min was used when dynamic tests were performed.

3.4.3.9 Infrared Spectroscopy

Diffuse reflectance infrared spectra were obtained using a Nicolet Magna-750 Infrared Spectrometer equipped with a KBr beamsplitter. Polymer samples were ground with a metal file and mixed with ground KBr. Spectra were collected against a KBr background. Prior to collection of spectra, the chamber was purged with dry nitrogen. 128 sample scans were collected at a spectral resolution of 1 cm^{-1}. Spectra were analyzed with Nicolet's OMNIC software package. Three replicates were analyzed for each cure time of neat PETI-5 and PETI-5/TiO_2 in the cure study. One specimen was analyzed for each aging time of fully cured neat PETI-5 and PETI-5/TiO_2.

3.4.3.10 Gel Permeation Chromatography

Molecular weight determination was performed on a Waters 150C Gel Permeation Chromatograph equipped with a model 150R differential viscosity detector and a differential refractive index detector. Poly(amic acid) solutions of PETI-5 and 8515 were prepared in distilled NMP/0.02M LiBr a few minutes before injection into the chromatograph. The solutions were filtered through a 0.2 μm filter prior to the test.

NMP solutions of extracted material from solvent uptake and extraction studies were filtered through a 0.2 μm filter prior to the analysis. Concentrations used for the molecular weight calculation were obtained by weighing the insoluble portion of the sample after all NMP was removed. It must be noted that the accuracy of the calculated molecular weights is highly dependent on the concentration used for the calculation.

Chromatography was performed at 60°C in filtered and degassed, freshly distilled NMP/0.02 M LiBr on a three column bank consisting of a linear Waters Styragel HT 6E column, which covers a molecular weight range from 10^3 to 10^7 g/mol in series with a

Styragel HT 3 column, which covers a range from 5×10^2 to 3×10^4 g/mol and a Styragel HT 2 column which covers the range from 10^2 to 10^4. The universal calibration curve used was generated with narrow molecular weight distribution polystyrene standards having molecular weights ranging from 472 to 2.89×10^6 g/mol.

Table 3.1: The range of sample adhesive thicknesses used in the NCA test analysis.

Sample Designation	Shim Thickness (mm)	FM-5 Adhesive		FM-36 Adhesive	
		layers	samples	layers	samples
A	0.152	1	5	1	10
B	0.305	1	5	1	10
C	0.457	2	5	2	10
D	0.635	2	5	3	10
E	0.762	2	5	3	10

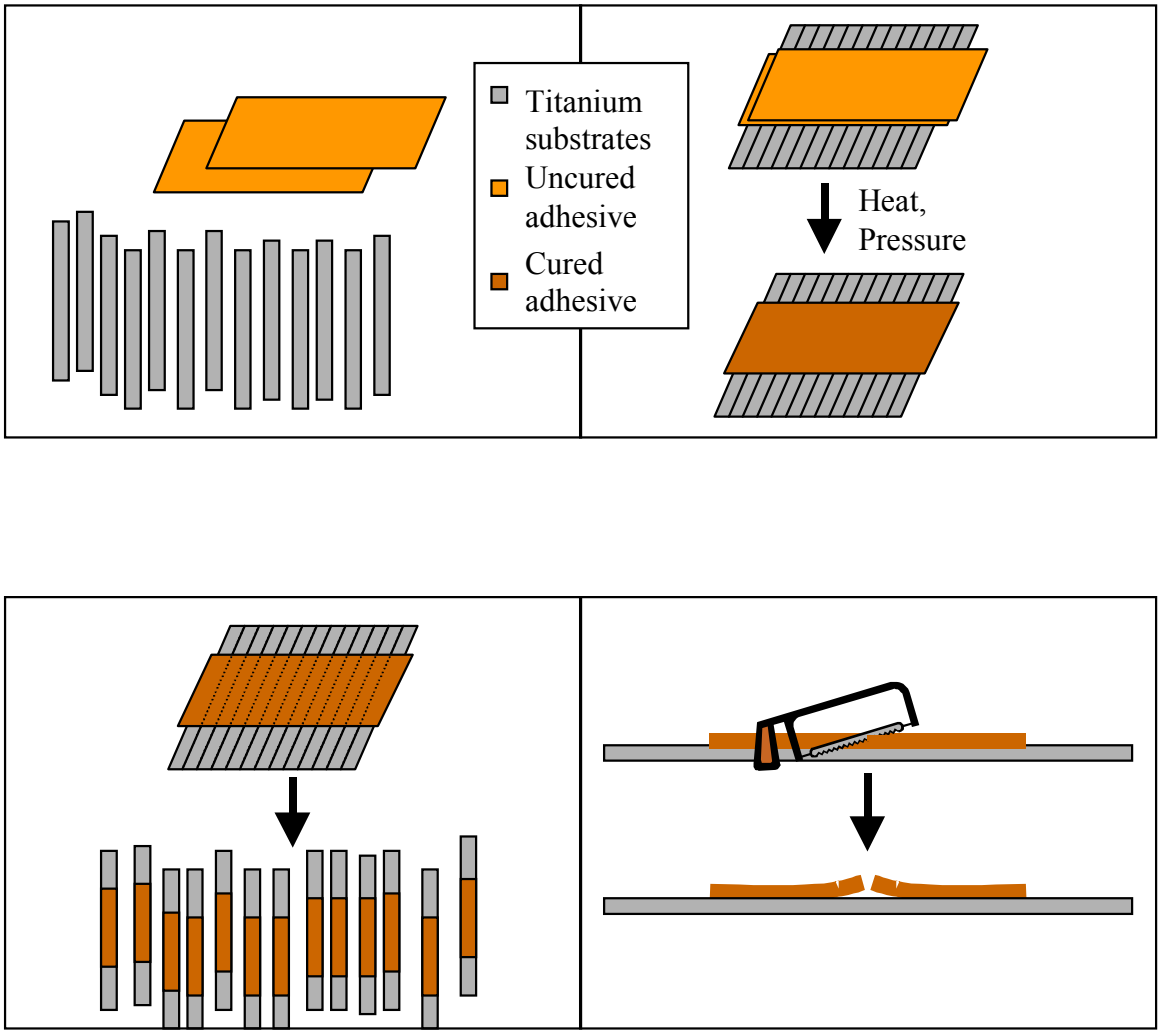

Figure 3.1: Schematic of the steps involved in the manufacture of NCA specimens.

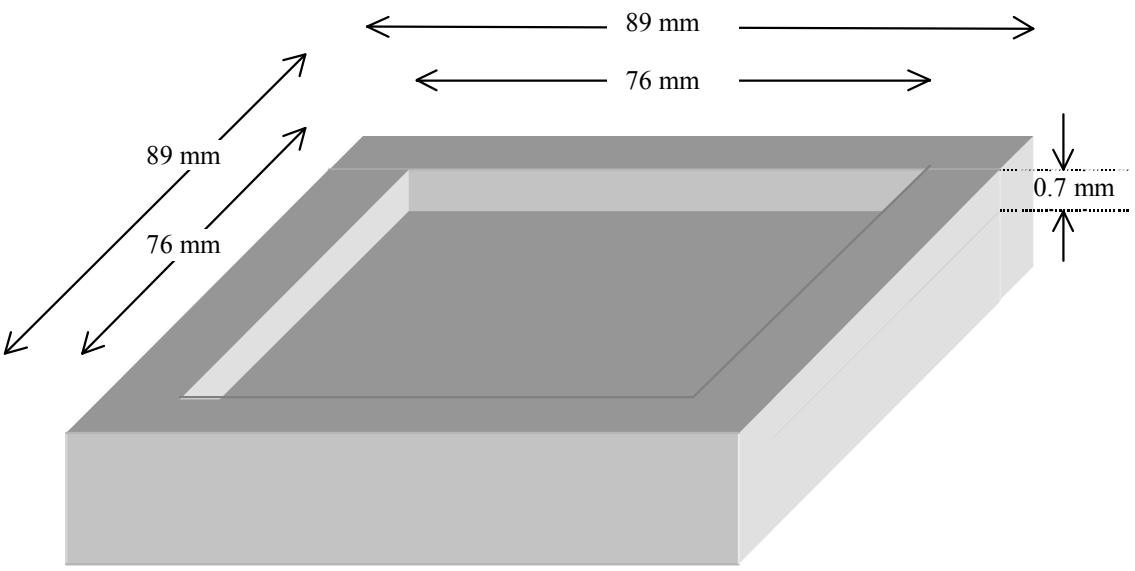

Figure 3.2: Schematic of mold used for PETI-5 and PETI-5/TiO_2 plaques.

Figure 3.3: Photograph of the three-point bend method used to initiate a debond in the PETI-5 and 8515 NCA specimens.

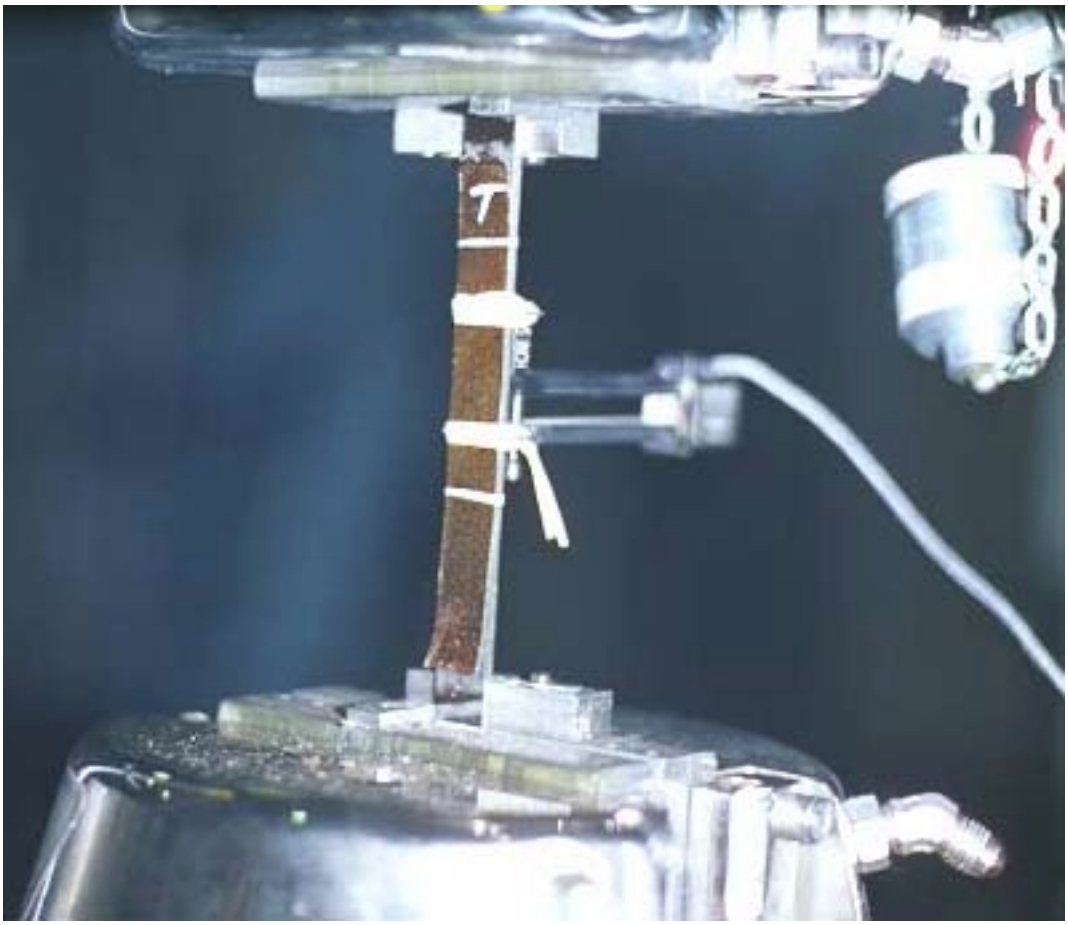

Figure 3.4: Photograph of an 8515 NCA specimen during testing.

Chapter 4: The Effect of Substrate Plastic Deformation on the NCA Test

4.1 Introduction

One of the overall objectives of the current study is to analyze the durability of adhesive systems using the notched coating adhesion test. The benefits of this test are outlined in Chapter 2. Prior to the use of this test for durability characterization, however, this relatively new technique was investigated analytically, by finite element analysis, and experimentally. Dillard *et al*.[55] have discussed the analytical and finite element analysis of the NCA specimen. The analytical expression developed for the strain energy release rate, G, of the NCA specimen allows for yielding of the substrate during testing.[55, 99] To check the validity of this assumption, a finite element analysis was performed in which the degree of plastic strain in the substrate was varied. Over the range of plastic strains considered, 0 to 2.5%, the J-integral (equivalent to G in the finite element model) was affected by less than 1%.[55] Here, the experimental analysis of the same assumption is analyzed.

In the equation used to calculate G_c for the NCA test,

$$G_c = \frac{h}{E}\left\{\left[\sigma_o^2 + \sigma_o E\varepsilon_c\right](1-\nu) + \frac{1}{2}(\varepsilon_c E)^2\right\}, \qquad \textit{Equation 4.1}$$

G_c is a function of the adhesive coating thickness, h, and the experimentally observed critical strain, ε_c. Because G_c should be independent of the adhesive coating thickness, the critical strain can be varied by changing the coating thickness. Altering the critical strain, in turn, varies the amount of plastic strain in the substrate at the critical debond moment. A thicker adhesive coating results in a lower plastic strain due to an increase in the amount of stored energy in the coating.

This variation in critical strain is illustrated in Figure 4.1. The critical strains for a hypothetical set of NCA specimens, in which h is varied from 0.1 to 1 mm, are superimposed on the force-strain curve of a titanium substrate. The parameters used in this calculation are G_c = 500 J/m^2, σ_o = 5 MPa, E = 3 GPa, and ν = 0.35. The amount of plastic strain experienced by the substrate as a function of adhesive coating thickness ranges from less than 1% to almost 5%.

Thus, the assumption that substrates may yield without significantly affecting the results of the NCA test were experimentally investigated by varying the adhesive coating thickness of two adhesive systems, FM-5 bonded to chromic acid anodized Ti-6Al-4V and FM-36 bonded to base/acid etched Ti-6Al-4V. The five adhesive coating thicknesses range from 0.152 mm, designated as sample population A, to 0.762 mm, designated as sample population E. All sample populations are described in Table 3.1.

4.2 Adhesive Modulus

As seen in Equation 3.2, several material properties must be used in the calculation of G_c. E is the modulus of the adhesive coating and σ_o is the sum of all residual stresses in the adhesive coating that are released upon debonding the adhesive from the substrate. These material properties were determined experimentally using the adhesive coating that debonded during the NCA test.

The modulus of each available adhesive thickness was measured for FM-5 and FM-36 specimens. The adhesive coating from population A of the FM-5 specimens did not debond fully during the NCA test, therefore these data represent populations B through E only. An example stress-strain plot of FM-5 adhesive is shown in Figure 4.2. The modulus was investigated as a function of adhesive thickness. For a given number of adhesive plies used, as described in Table 3.1, there was a possibility that the thinner coatings would have a higher relative content of glass fiber due to squeeze-out of resin during processing. This could lead to a higher modulus in samples with a lower thickness per ply (total coating thickness divided by number of plies used). The modulus of FM-5 is shown as a function of thickness per ply in Figure 4.3. While the linear least squares fit shows a slight dependence of modulus on thickness per ply, this dependence was not found to be statistically significant at a 95% confidence level. Therefore, the modulus used to calculate G_c is the average of all thicknesses tested. The same conclusion was reached with the FM-36 adhesive. The average moduli of FM-5 and FM-36, respectively, are 2.51 and 2.89 GPa.

4.3 Residual Stresses

The total residual stresses, σ_o, are the result of thermal stresses that form during the adhesive cure cycle due to the mismatch in the coefficient of thermal expansion, α, between the adhesive and the substrate. The equation used to determine the bulk residual stress is

$$\sigma_o = E_{adh}\left(\alpha_{adh} - \alpha_{sub}\right)\left(T_{sf} - T_{amb}\right) \qquad \textit{Equation 4.2}$$

where E_{adh} is Young's modulus of the adhesive, α_{adh} is the adhesive's coefficient of thermal expansion, α_{sub} is the substrate's coefficient of thermal expansion, T_{sf} is the stress-free temperature of the adhesive-substrate system, and T_{amb} is the ambient temperature (assumed to be 25°C).

The temperature difference in Equation 4.2 is the effective temperature range over which residual stresses can develop. Here, the stress-free temperature, T_{sf}, is assumed to be the glass transition temperature of the adhesive. Above the T_g, chain movement relaxes any residual stresses that might form on cooling the adhesive from elevated temperatures. Experimentally, Clifton[100] has found the stress-free temperature of similar systems to be as much as 50°C above the T_g. Thus, the assumption of $T_{sf} = T_g$ may be underestimating the residual stresses by up to 20%.

The α_{adh} of FM-5 and FM-36 were determined experimentally on a linear dilatometer, using the adhesive coating that debonded during the NCA test. An example of the change in length of FM-5 as a function of temperature is shown in Figure 4.4. An average α value of 24.0×10^{-6}/ºC was determined for the FM-5 adhesive and 14.0×10^{-6}/°C for the FM-36 adhesive. Again, this was determined by averaging the values obtained for the thicknesses analyzed. The α_{sub} for Ti-6Al-4V[101] is 9.6×10^{-6}/°C and the T_gs of both adhesives are 250ºC. Using Equation 4.2, the residual stress of FM-5 bonded to titanium is calculated to be 8.64 MPa, and the residual stress of FM-36 bonded to titanium is 3.45 MPa.

4.4 NCA Test

Critical strain energy release rate values determined from the FM-5 NCA test specimens are plotted against adhesive thickness in Figure 4.5. Each data point represents the average G_c value obtained for the corresponding sample population, and the error bars indicate the 95% confidence intervals. A corresponding plot of the FM-36 NCA data is given in Figure 4.6. In each plot, the solid line represents the average G_c for all coating thicknesses, with the width of the shaded bar signifying the 95% confidence interval for all samples. It is apparent from these plots that the critical strain energy release rate for sample populations B through E are consistent, as expected. However, sample population A, the thinnest adhesive coating, appears to be an outlier in both adhesive systems.

Theoretically, the values of G_c should not vary with adhesive thickness. Observing the FM-5 data in Figure 4.5, the average G_c of sample population A is higher than that of populations B through E, and the data has considerably more scatter. Several factors could be influencing this phenomenon. Chang[99] states that the adhesive coating may not yield during the NCA test. In some cases, this could be a concern with relatively thin adhesive coatings because the critical strain could be greater than the yield strain of the coating. With the FM-5 and FM-36 adhesive systems, however, the glass scrim cloth prevents yielding of the adhesive coating. This behavior can be seen in the stress-strain plot of an FM-5 debonded coating, Figure 4.2.

The explanation of the anomalous experimental data observed for sample population A, therefore, requires investigation of the validity of the assumptions that are made. First, it is assumed that, after cutting through the adhesive with a hacksaw, the residual stresses in the adhesive will be sufficient to cause a sharp-tipped debond between the adhesive and substrate in the region of the notch. While this appears to be valid for sample populations B through E, it may not be valid for population A. The total debond force is proportional to the thickness of the adhesive coating. For population A, the adhesive coating thickness is half that of population B. Thus, the debond force of population A may have been insufficient to cause a uniform, sharp-tipped initial debond. Without this geometric requirement, the NCA test analysis becomes invalid.

A second experimental assumption is that the strain measured by the extensometer is equal to the strain where the debond begins to propagate. For this to be correct requires affine deformation of the substrate. While this is expected to be the case prior to substrate yielding, there is no guarantee of affine deformation in a metal beyond its yield point. Critical strains for all thicknesses were beyond the yield point of the titanium substrate; however, the plastic strain was much higher for population A than for the thicker coatings. This is illustrated in Figure 4.7, where the average critical strain observed for the FM-5 NCA specimens of each thickness are superimposed on the force-strain curve of a typical specimen. (Note: the force-strain data was obtained for an FM-5 NCA specimen while performing the NCA test.) Here, the substantially higher plastic strain at the critical point of population A, compared to the thicker adhesive coatings, is

readily apparent. The analytical and finite element analysis of the NCA test did not indicate a dependence on substrate plastic deformation.[55] However, those analyses could not consider the ability of the experimenter to identify the critical strain accurately and precisely. The inability to correctly identify the critical strain after considerable plastic deformation of the substrate has taken place may limit the accuracy of the NCA test in this situation.

The FM-36 data support this conclusion. Although the scatter of the FM-36 population A data is not exceptionally high, as was seen in the FM-5 data, the average clearly deviates from that of populations B through E. Therefore, it is concluded that while small amounts of plastic deformation (here, less than 1%) do not appear to adversely affect the accuracy of the test, considerable plastic deformation in the substrate should be avoided. The contribution of population A in each adhesive system is therefore excluded from the averages, and the G_c values of populations B through E of FM-5 and FM-36 are presented in Figure 4.8 and Figure 4.9, respectively.

A comparison may now be made between the G_c of FM-5 and FM-36 samples. The average G_c of the FM-36 specimens is unexpectedly higher than that of FM-5. As discussed in Chapter 2, adhesive bonds made with Class III surface treatments, such as the CAA treatment used with the FM-5 specimens, consistently out-perform specimens made with Class I surface treatments, such as base/acid etching, used with the FM-36 specimens. A potential source of this discrepancy could be related to the ability of the adhesive to wet the substrate surface during processing. Without intimate molecular contact between the adhesive and substrate, a strong interface cannot be produced. Prior to processing, the FM-36 adhesive is tacky and contains approximately 40% volatiles. The FM-5 adhesive, in contrast, is boardy and contains only 4% volatiles. While the FM-36 can wet the substrate during application, the FM-5 processing relies on heat and pressure to provide the necessary interfacial contact to produce an effective bond.

Another factor leading to the increase in the experimentally determined G_c of the FM-36 specimens could be the shape of the interfacial pre-crack. A Teflon strip was placed between the FM-36 adhesive and the substrates prior to bonding to facilitate the initiation

of a uniform pre-crack. While this certainly led to pre-cracks that were uniform, it is unlikely that they were infinitely sharp-tipped, which would have been optimal. The critical strain required to propagate a blunt-tipped debond would lead to an artificially high G_c.

In addition to a higher average G_c, the FM-36 specimens had lower scatter than the FM-5 specimens. This is primarily a result of modifications applied to the FM-36 testing procedure after the FM-5 tests were performed. As discussed in Chapter 3, all FM-36 tests were video-recorded and timed using a stopwatch superimposed on the video image. This is believed to have slightly improved the precision with which the critical strain can be determined. However, it may not be a practical means of improving the precision of the test since it is quite time consuming to review each test and determine the critical debond moment. To further reduce the amount of scatter in the test, the number of samples of each adhesive thickness was increased from five to ten. Since each NCA test specimen has the opportunity to debond at two different critical strains (the notch initiates two areas of debonding), the plotted values represent a maximum of 20 data points. In actuality, these points represent between 10 and 17 data points due to inconclusive debonding behavior and elimination of outlying data points.

4.5 Conclusions

After thorough analysis of the effect of substrate plastic deformation on the NCA test, it is concluded that a small amount of plastic deformation does not appear to affect the results of the NCA test. When large amounts of plastic deformation occur (approximately 3% or more in the current example), the loss of affine deformation may make it difficult to accurately determine the actual critical strain using an extensometer. Additionally, the importance of initiating a uniform, sharp-tipped debond prior to specimen testing has been illustrated.

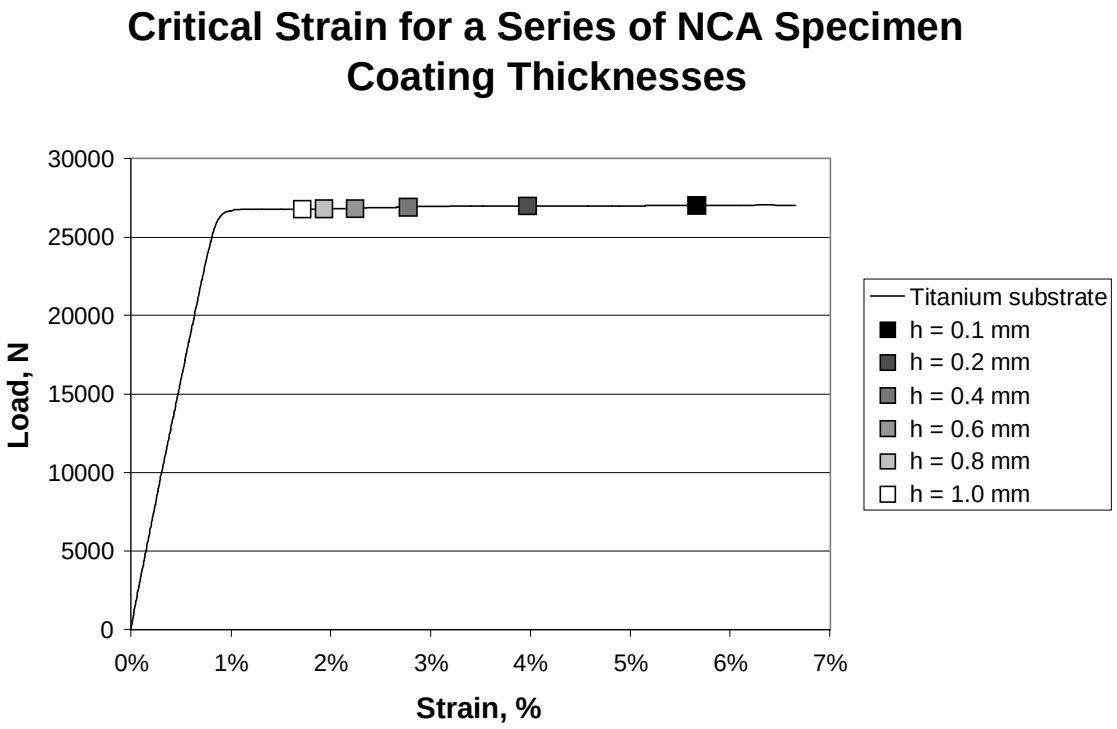

Figure 4.1: Calculated critical strain values for a hypothetical set of NCA specimens with varying coating thickness, h*, superimposed on a force-strain curve of titanium substrate.* G_c *= 500 J/m*^{2}*,* σ_o *= 5 MPa,* E *= 3 GPa,* ν *= 0.35.*

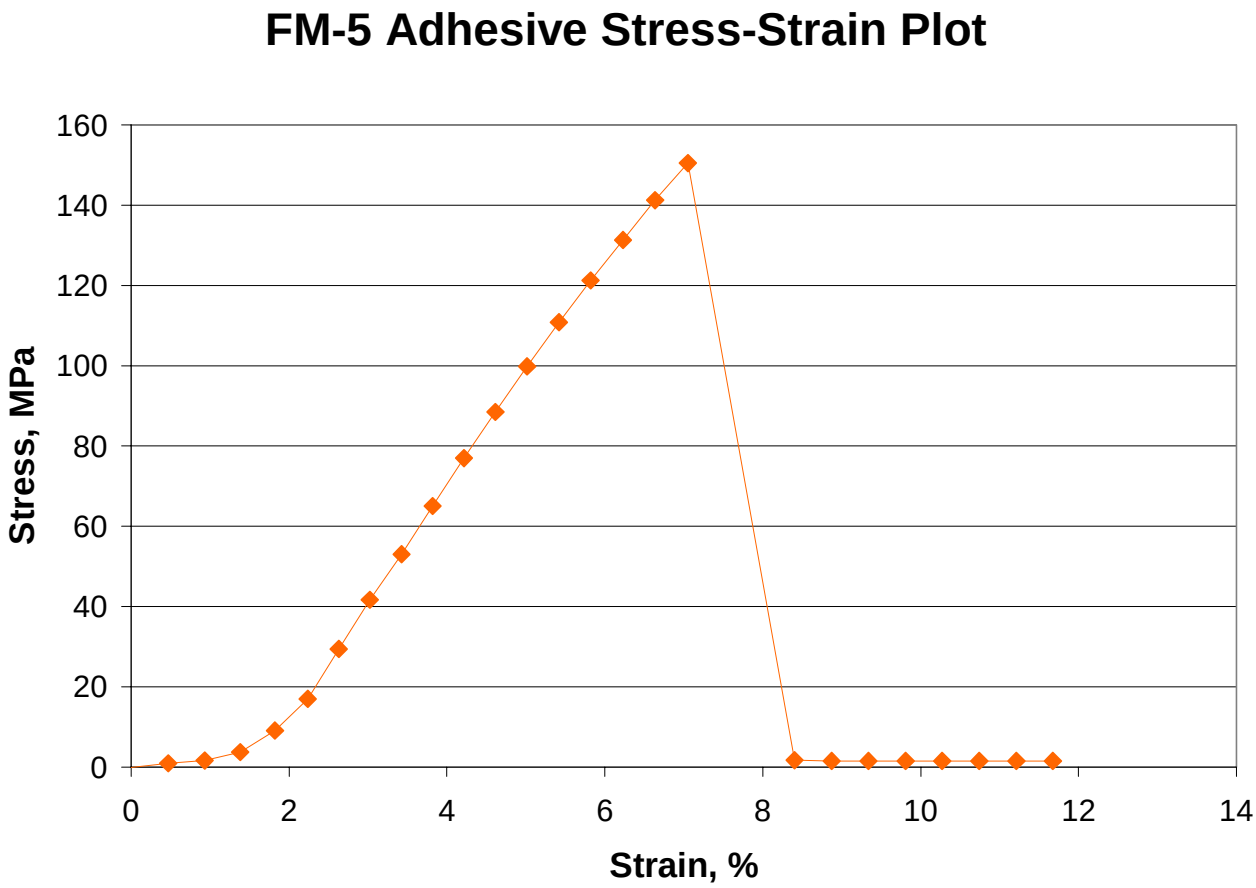

Figure 4.2: Stress-strain curve of FM-5 adhesive debonded from a NCA specimen. The modulus was calculated from the linear portion of this curve.

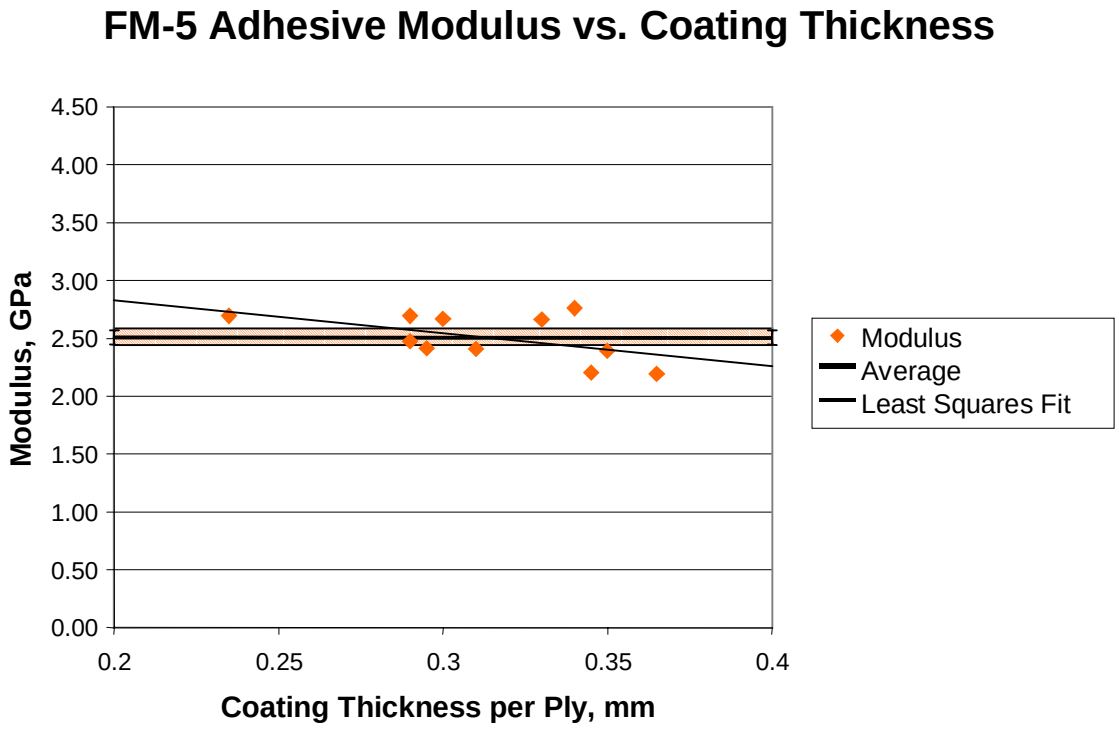

Figure 4.3: FM-5 adhesive modulus as a function of the coating thickness per ply of adhesive tape. The solid line indicates the average modulus, with the width of the shaded bar signifying the 95% confidence interval.

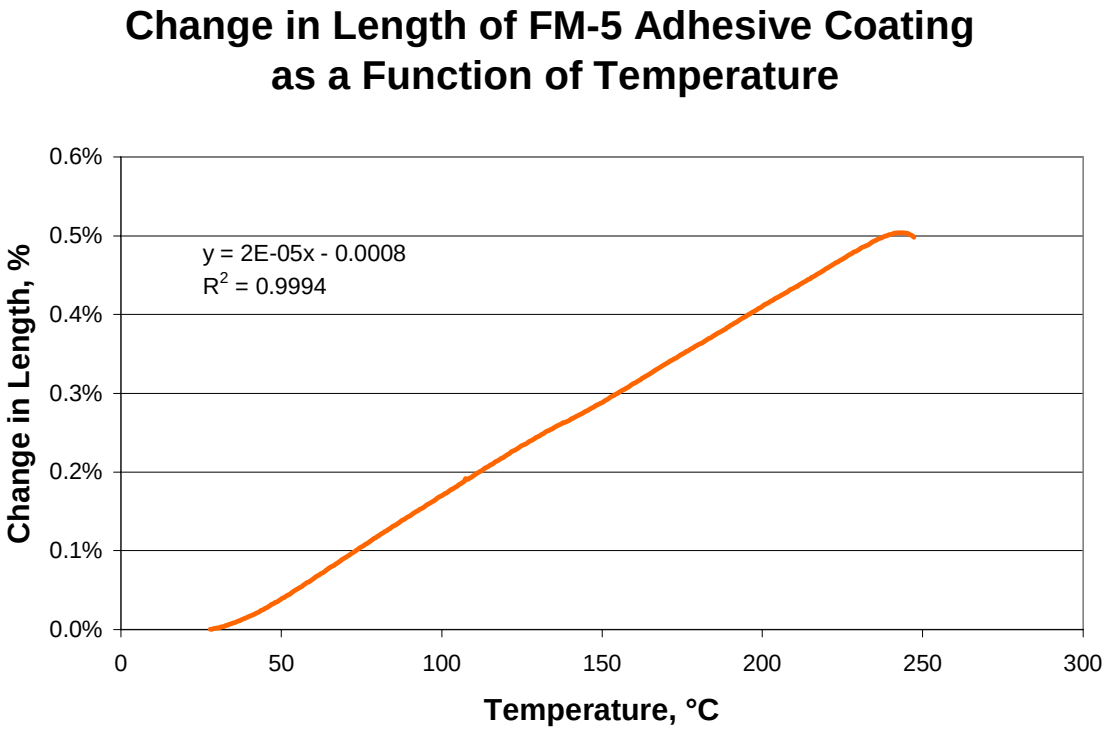

Figure 4.4: Change in length of FM-5 adhesive coating as a function of temperature, from linear dilatometer data. A straight-line fit through the linear portion was used to calculate the coefficient of thermal expansion, α.

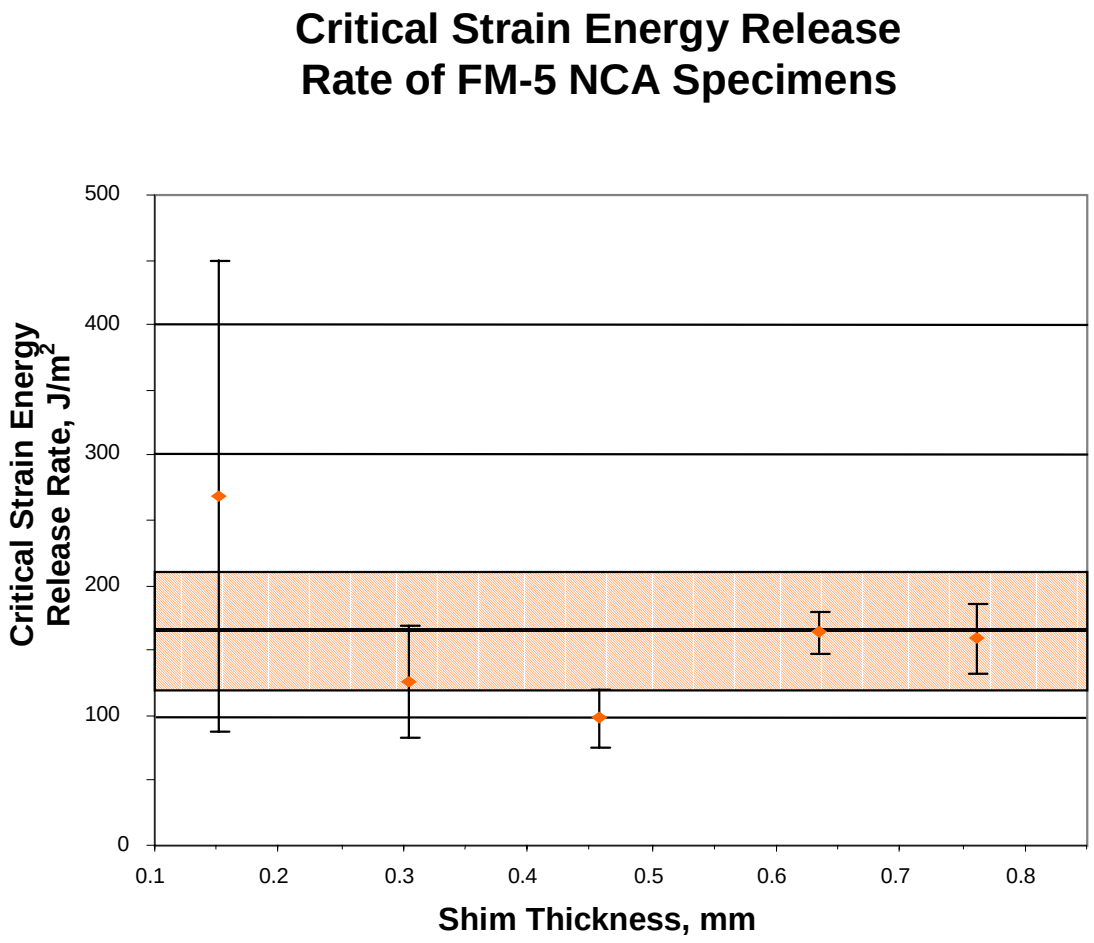

Figure 4.5: Calculated critical strain energy release rates for all FM-5 NCA test samples analyzed (populations A through E). The solid line represents the ensemble average, with the width of the shaded bar signifying the 95% confidence interval.

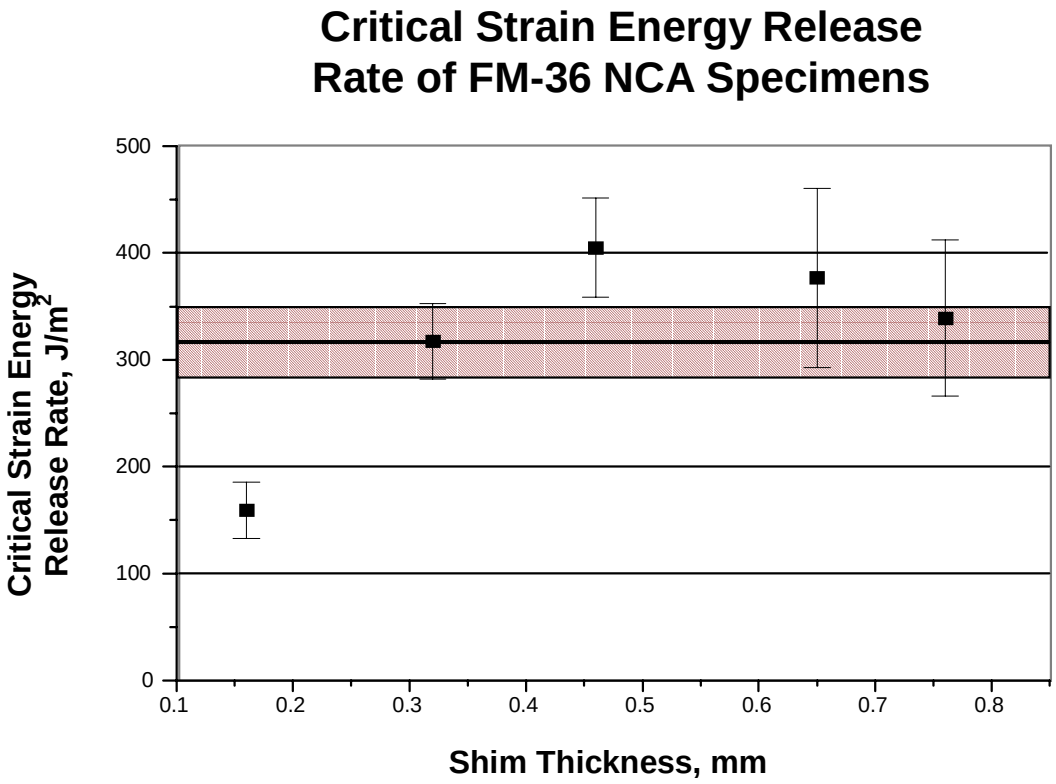

Figure 4.6: Calculated critical strain energy release rates for all FM-36 NCA test samples analyzed (populations A through E). The solid line represents the ensemble average, with the width of the shaded bar signifying the 95% confidence interval.

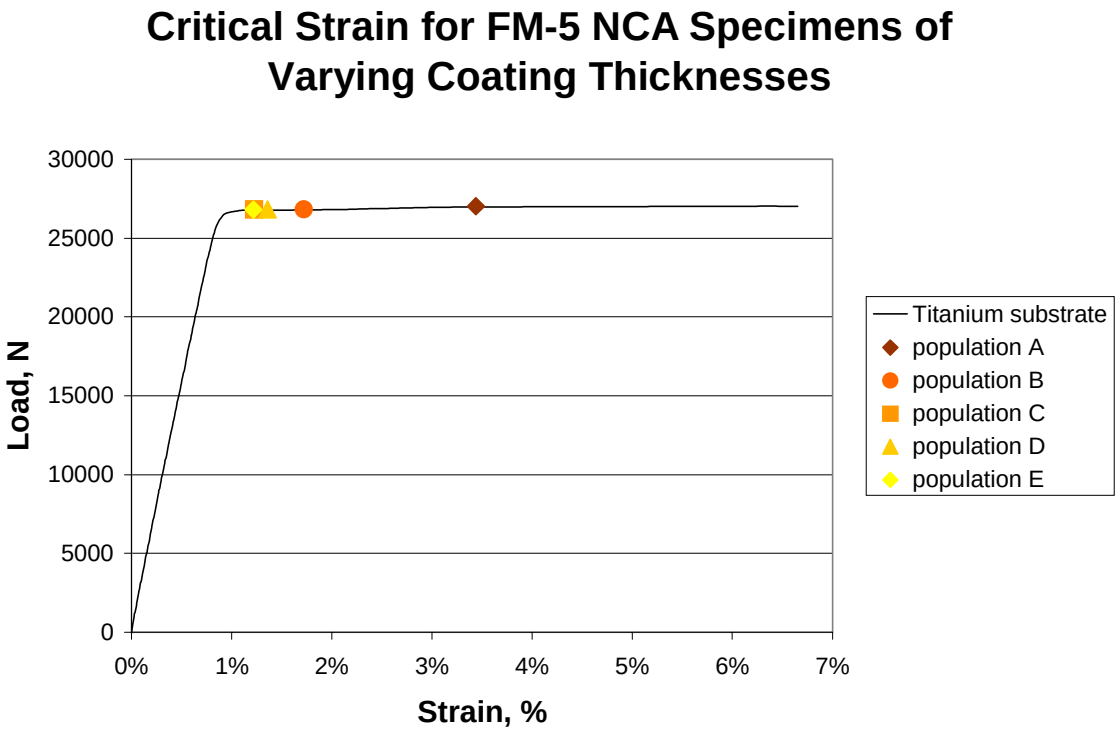

Figure 4.7: Critical strains of FM-5 NCA specimens, populations A through E, superimposed on the load-strain plot of a titanium substrate.

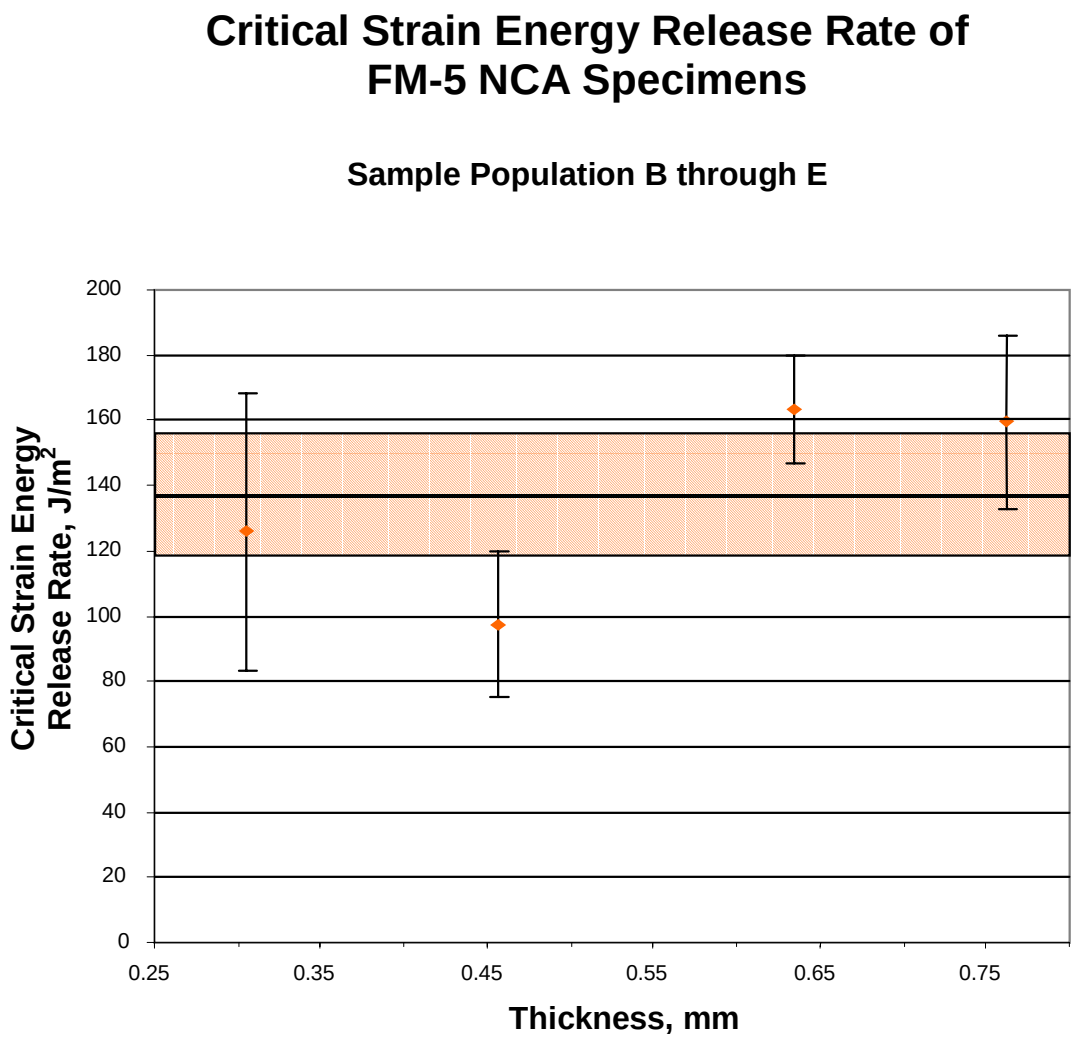

Figure 4.8: Calculated critical strain energy release rates for FM-5 NCA test sample populations B through E. The solid line represents the ensemble average of the shown data points, with the width of the shaded bar signifying the 95% confidence interval.

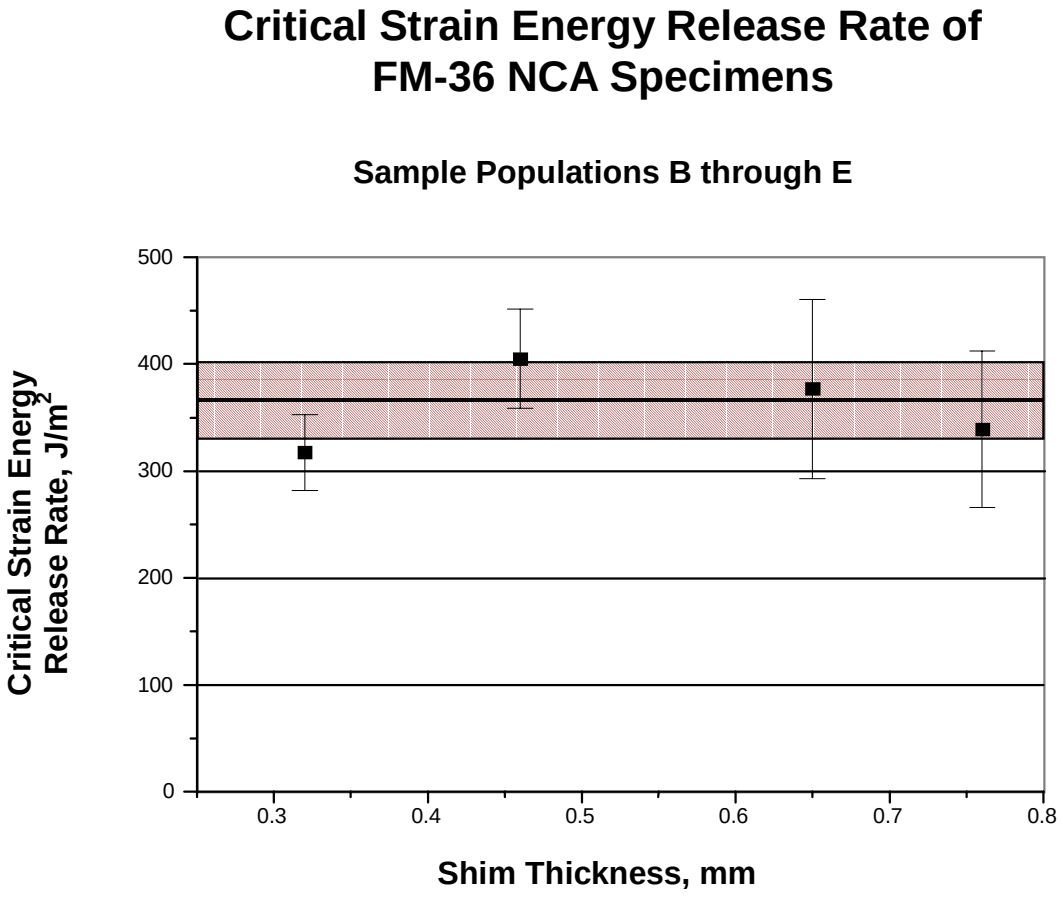

Figure 4.9: Calculated critical strain energy release rates for FM-36 NCA test sample populations B through E. The solid line represents the ensemble average of the shown data points, with the width of the shaded bar signifying the 95% confidence interval.

Chapter 5: Aging of Polyimide/Titanium Adhesive Systems

5.1 Introduction

NCA specimens fabricated with FM-5, PETI-5, or 8515 adhesive bonded to CAA Ti-6Al-4V were aged at elevated temperatures. As discussed in Chapter 2, the "open-faced" geometry of the NCA specimen allows diffusion-related aging to occur much more quickly than in comparable "sandwiched" bonded joints. Therefore, aging times considered in this study are relatively short compared to the 60,000 hour (approximately 7 year) or more intended product life of these materials. While an exact time correspondence between the NCA geometry and other bond geometries has not been established, estimates of the distances penetrated by diffusing species can be compared. If the degradation rate is assumed to be controlled by Fickian diffusion, then the diffusion time is proportional to the diffusion distance squared. Burcham *et al.*[53] found diffusion to be the controlling mechanism in the degradation of a bismaleimide, similar in structure and properties to the polyimides of interest here, when aged in air at 177°C. In the current study, we would like to study the effect of the degradation front that caused Parvatareddy's FM-5 DCB specimens to fail in the region of the interphase after aging at elevated temperature.[20] In his specimens aged at 177°C for one year, this degradation front had penetrated approximately 2 mm into the DCB specimen. Using the assumption

that Fickian diffusion is controlling the rate of degradation, an approximate time required for an equivalent level of degradation to reach the adhesive/substrate interface of an NCA specimen can be estimated using Equation 5.1,

$$t_{equiv} = h^2 \frac{t_{age}}{d^2}, \qquad \text{Equation 5.1}$$

where t_{equiv} is the equivalent time required for degradation to reach the interface of an open-faced adhesive specimen, h is the thickness of the coating in the open-faced specimen, t_{age} is the aging time of the sandwiched adhesive specimen, and d is the distance into the sandwiched specimen that the degradation front has penetrated.

With an adhesive coating of 0.76 mm, as was used with the current FM-5 NCA specimens, this equivalent level is calculated to be 53 days. Here, aging times of one, seven, thirty, and ninety days at 177°C were selected for the FM-5 NCA specimens. Following these tests, PETI-5 and 8515 NCA specimens were studied as a function of aging atmosphere, air or nitrogen, at 177°C.

5.2 Adhesive Specimens

5.2.1 NCA Test

Average critical strain energy release rates for FM-5 specimens as a function of aging time at 177°C are presented in Figure 5.1. At a 95% confidence level, the G_c values are the same for the unaged samples and those aged for one or seven days. However, the 50% to 70% drop in G_c of samples aged for 30 or 90 days is statistically significant compared to the unaged value. In Parvatareddy's study of the same adhesive, substrate, and surface treatment, a 25% drop in adhesive performance was seen in double cantilever beam (DCB) samples that had been aged for one year at the same conditions.[20] This illustrates the acceleration in aging that is associated with the decreased diffusion distance of the NCA specimens. The implication here is that degradation of bond strength is due in part to diffusion of species, presumably oxygen, to the adhesive/substrate interface. This does not eliminate the contribution of non-diffusion

related degradation mechanisms, such as physical aging, however it is apparent that diffusion contributes significantly to the aging process.

It must be noted that the G_c values obtained here for unaged specimens are significantly higher than those tested at varying adhesive thicknesses in Chapter 4. For the previous samples, an average G_c of 140 J/m^2 was reported, while a value of 390 J/m^2 is reported in the current section. Furthermore, all G_c values reported in the current work are considerably lower than those reported by Parvatareddy and Dillard[102] for FM-5/CAA Ti-6Al-4V specimens of varying mode mixities. DCB specimens with pure mode I loading had fracture energies of 2500 J/m^2, while end-notched flexure (ENF) specimens with pure mode II loading had fracture energies of 1300 J/m^2. Mixed mode I and II tests, asymmetric DCB and mixed-mode flexure, gave intermediate values. The NCA test, a mixed mode I and II test, would be expected to also give values between 1300 and 2500 J/m^2. The large discrepancy in G_c between samples made for the tests discussed in Chapter 4 and those in the current chapter indicates a strong sensitivity of G_c to manufacturing conditions. While the samples were made using the same procedure, samples made in different batches had different average G_c values. For example, the samples made for the aging study were manufactured in three batches. One gave an average G_c of 790 J/m^2 for unaged specimens, while the others gave average G_c values of 350 and 500 J/m^2. The source of this inconsistency is unknown, but regardless of the source, it should be kept in mind that the absolute G_c values reported here are much lower than expected. The relative change in G_c as a function of aging time, however, is believed to be accurate. A possible reason for the lower than expected G_c values is the calculation of residual stresses. As mentioned in Chapter 4, the residual stresses calculated from the coefficient of thermal expansion could be underestimated by approximately 20%. Adding 20% to the calculated residual stresses, however, only increases the G_c by approximately 7%. In an extreme case, if the calculated residual stresses were only half what they should be, the G_c is increased by 40%, still lower than the expected value. Experiments to determine the source of this discrepancy are suggested in the Future Work section.

PETI-5 and 8515 NCA specimens were aged for 30 days in either air or nitrogen at 177°C. This aging time was selected based on the FM-5 data, in which a significant drop in the critical strain energy release rate occurred after 30 days. Quantitative strain energy release rates were not obtained for these NCA samples due to difficulties in obtaining accurate critical strain values. This will be discussed further in the Future Work section. However, a qualitative assessment of bond strength was made by initiating a debond between the adhesive and substrate. The relative difficulty in initiating this debond indicates that PETI-5 samples are much stronger than 8515 samples. The 8515 samples were unexpectedly weak, based on previous data by Jensen *et al.*[97] who report thermal and mechanical properties of 8515 at several molecular weights. The molecular weight chosen for the current study, 9,200 g/mol, was determined to be above the critical molecular weight where increases in properties begin to plateau. To investigate the unexpectedly weak samples, gel permeation chromatography (GPC) was performed on the amic acid solutions of 8515 and PETI-5, as received from Imitec™, the starting materials for the NCA specimens. The experimentally determined number average molecular weight of 8515, 5,170 g/mol, is considerably lower than the calculated 9,200 g/mol. The PETI-5 amic acid, however, closely matched its target molecular weight of 5,000 g/mol with an experimental value of 5,083 g/mol.

Although the starting molecular weights were the same, the difference in strength originates from the elevated temperature cure of PETI-5's phenylethynyl end groups. A combination of chain extension and crosslinking during cure gives PETI-5 a cured molecular weight that can be considered essentially infinite (i.e. a network structure). 8515 does not undergo a cure reaction and thus retains a finite molecular weight. Since the actual molecular weight is much lower than that intended for this study, the data obtained here should not be considered representative of typical 8515 adhesive properties. Additionally, a higher molecular weight would be required to evaluate the effect of PETI-5's phenylethynyl end groups on its durability. The use of 8515 as a comparison for PETI-5's durability, therefore, is deemed to be inconclusive.

While no differences in strength were noted between aged and unaged samples of 8515, PETI-5 samples aged in air at 177°C appeared to have significantly lower bond strengths

than unaged samples. In contrast, strengths of PETI-5 samples aged in nitrogen at 177°C were not noticeably different from unaged samples. The effect of aging in air versus nitrogen is consistent with the observation by Parvatareddy[20] that adhesive strength is much more affected by aging at elevated temperatures in air at atmospheric pressure, compared to aging at the same temperature in a reduced air pressure environment. This is discussed in Chapter 2.

5.2.2 Failure Surface Analysis

5.2.2.1 Differential Charging

Through XPS analysis of the failure surfaces of FM-5 NCA specimens, titanium was detected on the metal and adhesive failure surfaces. The Ti $2p_{3/2}$ XPS photopeak of the metal failure surface at 459.1 eV is shown in Figure 5.2 (a). This binding energy is consistent with the literature value of titanium as TiO_2,[103] 458.7 eV, and with the Ti $2p_{3/2}$ peak position measured on the surface of a freshly anodized Ti-6Al-4V substrate, 458.8 eV, used as a reference standard. The Ti $2p_{3/2}$ peak on the adhesive failure surface, Figure 5.2 (b), is shifted to 1.7 eV higher binding energy. The shift in peak position on the adhesive failure surface is believed to be the result of differential charging. This is analogous to the example of platinum clusters on a polymer film discussed in Chapter 2. The assumption that this shift is caused by differential charging rather than a true chemical shift is confirmed by noting that the same shift in peak position, 1.9 ± 0.2 eV, is observed for all components of the substrate surface (Ti, Al, and F) that were detected on the adhesive failure surface. Aluminum is present as an oxide, Al_2O_3, and is a component of the Ti-6Al-4V alloy. Fluoride ion is adsorbed onto the surface of CAA Ti-6Al-4V during the anodization procedure, described in Chapter 3. XPS peak positions for adhesive and metal failure surfaces of FM-5 NCA specimens are presented in Table 5.1, along with those of the reference CAA Ti-6Al-4V substrate and literature values.

After accounting for the 1.9 eV shift in binding energies of titanium, aluminum, and fluorine on the adhesive failure surface, it is also noted that the binding energies of these elements on the adhesive and metal failure surfaces do not differ from those of non-bonded anodized titanium. Thus, there is no evidence for the formation of new molecular

species from the reaction of titanium, aluminum, or fluorine with one another, or with the polyimide adhesive, as a result of processing at 350°C or aging for up to 90 days at 177°C.

Further evidence of differential charging of the adhesive failure surface is observed in Figure 5.3. Figure 5.3 (a), the O 1s photopeak of the metal failure surface, clearly shows a low binding energy component at 530.3 eV that is attributed to TiO_2. The literature value of O 1s as TiO_2 is reported as 530.0 eV[103] and the reference CAA Ti-6Al-4V substrate has an O 1s photopeak at 530.3 eV. In contrast, the corresponding photopeak of the adhesive failure surface, Figure 5.3 (b), shows a very broad peak, with the TiO_2 portion of the spectrum shifted to a binding energy close to that of the organic oxygen components. This would require a shift on the order of the 1.9 eV shift observed in the Ti, Al, and F detected on the adhesive failure surface. With the multiple sources of oxygen present in a small window of binding energies (TiO_2, Al_2O_3, C=O, C-O-C, SiO_2) peak resolution to isolate the shifted TiO_2 portion of the O 1s peak could not be performed on the adhesive failure surfaces in a reliable manner. Regardless, the O 1s photopeak data support the previously presented evidence of differential charging of the adhesive failure surface during analysis by XPS.

5.2.2.2 Effect of Aging on Failure Mode

By visual inspection, all debonds of NCA specimens appeared be interfacial. That is, only the titanium substrate was visible to the naked eye on the metal failure side of the bond, and only polymer was visible on the adhesive failure side. However, when the failure surfaces of unaged NCA specimens were analyzed using XPS or optical microscopy, titanium dioxide and polyimide adhesive were detected on the adhesive and metal failure surfaces.

Evidence of titanium dioxide on the adhesive failure surface was discussed in the previous section; evidence of polyimide adhesive on the metal failure surface is displayed in Figure 5.4, the C 1s XPS photopeak, resolved into C-H, C-O, C=O, and $\pi \rightarrow \pi^*$ shake-up peaks. In addition, a N 1s peak at 400.4 eV and the organic (high binding energy) component of the O 1s peak, Figure 5.3 (a), give evidence of polyimide on the adhesive

failure surface. The specific structures to which these peaks are attributed are seen in the chemical structure of the PETI-5 backbone, Figure 1.2.

After aging the FM-5 specimens for 30 days or longer at 177°C in air, no titanium is detected on the adhesive failure surfaces by XPS; neither are the other elements associated with the substrate surface, Al and F. The atomic concentrations of these elements on the adhesive failure surfaces are presented in Figure 5.5 as a function of aging time.

Observing the FM-5 adhesive failure surfaces with optical microscopy, the same trend is seen. Representative optical micrographs for each aging time are presented in Figure 5.6. In the micrographs, the dark colored regions are adhesive and the lighter regions are titanium oxide. Essentially no titanium is observed on the failure surface of the sample aged for 90 days, and very little on the sample aged for 30 days. (Note: the 30-day sample displayed in Figure 5.6 is the only 30-day sample on which TiO_2 was observed by optical microscopy; no TiO_2 was observed on the 30-day samples analyzed by XPS.) It is apparent from these micrographs that the failure propagated alternately through two distinct regions. Where titanium is visible on the adhesive failure surface, the failure propagated through the titanium oxide layer of the substrate. Where adhesive is visible, failure occurred in the adhesive layer adjacent to the substrate, or the adhesive interphase. After aging the FM-5 specimens for 30 days or longer at 177°C in air, there is little or no titanium on the adhesive failure surfaces. Thus, as the aging time increases, failure through the adhesive interphase dominates failure through the titanium oxide layer.

A similar trend is observed on the adhesive failure surfaces of PETI-5 NCA specimens. High titanium concentrations were detected on failure surfaces of unaged specimens, by XPS and optical microscopy. This is illustrated in Figure 5.7 and Figure 5.8, respectively. No differences from the unaged samples are observed after aging for 30 days in nitrogen at 177°C. After aging in air rather than nitrogen, however, the titanium concentration by XPS has dropped by almost 50% on average and coverage, as detected by optical microscopy, has visibly decreased.

Failure through the oxide layer of the FM-5 and PETI-5 specimens, indicated by high concentrations of titanium on the adhesive failure surface, corresponds to strong adhesive specimens. The FM-5 adhesive specimens lost approximately 50% of their original adhesive strength at the same aging time, 30 days, at which the titanium coverage on the adhesive failure surface decreases substantially. In addition, the air-aged PETI-5 NCA specimens were qualitatively determined to be weaker than the unaged and nitrogen-aged specimens, which had correspondingly higher proportion of failure through the titanium oxide layer.

This indicates that, prior to aging, the strength of the adhesive is comparable to that of the titanium oxide layer, with failure propagating through both regions of the interphase. As the overall bond strength decreases during elevated temperature aging, failure through the adhesive in the interphase dominates failure in the titanium oxide. Weakened adhesive at the interphase, therefore, appears to be responsible for the overall loss of bond strength during elevated temperature aging in air.

Degradation of the adhesive in the interphase could be occurring concurrently with changes in the bulk adhesive. Alternatively, degradation in the interphase may be enhanced by interaction with the surface of the titanium substrate. To determine the source of degradation, the bulk properties of the debonded adhesive films were investigated.

5.3 Bulk Adhesive Characterization

It is clear that the adhesive in the interphase region is affected by elevated temperature aging in air. To determine whether aging is also affecting the bulk adhesive, the debonded adhesive from the NCA specimens was analyzed using DSC, infrared analysis, and a solvent uptake study.

5.3.1 Differential Scanning Calorimetry

DSC was performed on the debonded adhesive films from NCA specimens. Glass transition temperatures of FM-5 films are presented as a function of aging time in Table

5.2, and corresponding PETI-5 and 8515 data are given in Table 5.3 as a function of aging atmosphere. No significant change in glass transition temperatures of FM-5 or PETI-5 was observed after aging the specimens. In addition, there was no evidence of physical aging of FM-5 or PETI-5, as observed by the lack of a characteristic physical aging endothermic peak at the glass transition. First heat DSC thermograms of PETI-5 are illustrated in Figure 5.9.

Physical aging was detected in the 8515 debonded films that were aged at 177°C in air or nitrogen, Figure 5.10. These films had a much lower T_g, 229°C, than the FM-5 or PETI-5 samples. Therefore, the 8515 samples were closer to their T_g than the others during aging at 177°C, increasing the extent of physical aging. In addition, 8515 is a thermoplastic, while FM-5 and PETI-5 are lightly crosslinked. The increased mobility of the thermoplastic may increase its susceptibility to physical aging. While the 8515 samples exhibited a small (3 to 5°C) increase in T_g after aging, this increase was not found to be reversible after an initial heat to 300°C. First and second heat T_gs are given in Table 5.3, and second heat DSC scans of 8515 samples are shown in Figure 5.11. The average enthalpic peak of air-aged samples was 0.65 ± 0.06 J/g while that of nitrogen-aged samples was slightly higher, 1.00 ± 0.08 J/g. Since physical aging is not a chemical phenomenon, no difference in the size of the enthalpic peak would be expected unless one of the atmospheres were causing a simultaneous chemical change in the polymer. For example, some degree of crosslinking in the air-aged specimens could be decreasing the mobility of the polymer chains, reducing the extent of physical aging in these samples.

5.3.2 Infrared Spectroscopy

Diffuse reflectance infrared spectroscopy was performed on PETI-5 adhesive films that were ground and mixed with KBr. Spectra of unaged PETI-5 and PETI-5 aged in air at 177°C for 30 days are presented in Figure 5.12. No differences were detected between the aged and unaged samples. Diffuse reflectance IR was also performed directly on the failure surface of the adhesive, in an attempt to chemically characterize the adhesive interphase region. Spectra of the failure surface indicated that there was no significant

difference between the surface and the bulk material. However, the penetration depth of IR, approximately one micron, may be much greater than the thickness of the interphase region. Therefore, the bulk material may dominate the spectra of the failure surface.

5.3.3 Solvent Uptake

Debonded adhesive films were immersed in NMP to qualitatively determine if chemical changes such as crosslinking or chain scission had occurred during aging. After 1200 hours of exposure, equilibrium had not been reached in weight uptake, as seen in Figure 5.13. However, hypotheses concerning degradation mechanisms can be made from the sorption curves.

The sorption by films from NCA specimens that were aged for one day was within 0.1% of the sorption by unaged films. After seven days of aging, there was 25% less solvent absorbed after 900 hours. This may be the result of thermally induced crosslinking. After longer aging times, however, the sorption increased. Absorbed solvent in films that were aged for 30 days is greater than that of films aged for seven days, and weight uptake in films aged for 90 days was much greater than in any other films. This increase in sorption could be a result of chain scission or microcracking; these are both related to embrittlement of the adhesive. The trend of an initial decrease in weight uptake of NMP at short aging times, followed by an increase in weight uptake at longer aging times, implies that there are two competing mechanisms, one that dominates at short aging times and one that becomes important at longer aging times.

The inference from this data, that adhesive embrittlement dominates at aging times of 30 days or longer, is consistent with the G_c data from the NCA test and the change in failure location determined by XPS and optical microscopy. Embrittlement of the adhesive at the interphase would decrease the adhesive joint's resistance to fracture. This would lower the G_c of the adhesive/substrate system and simultaneously force the failure to occur within the weakened adhesive, rather than at the adhesive/substrate interface.

5.4 Conclusions

After aging NCA specimens of FM-5 or PETI-5 with chromic acid anodized Ti-6Al-4V at 177°C for 30 days or longer in air, the adhesive bond strength decreases significantly. Simultaneously, a greater percentage of the failure is propagating through the adhesive in the interphase region. No differences were observed between unaged adhesive samples and those aged in nitrogen rather than air. Thus, weakening of adhesive at the interphase appears to be related to components of the air-aging atmosphere, presumably oxygen.

Bulk FM-5 or PETI-5 changes were not detected by DSC or IR spectroscopy, although evidence of adhesive embrittlement was observed by sorption of NMP. While this embrittlement may be responsible for the increase in failure propagating through the adhesive interphase, degradation in that region may be enhanced by interaction with the substrate surface, as discussed in Chapter 2. The interaction of PETI-5 with titanium dioxide is investigated in Chapter 7.

Table 5.1: Binding energies of XPS photopeaks on FM-5 failure surfaces, referenced to the C 1s peak at 285.0 eV, with 95% confidence intervals.

XPS Photopeak	Binding energy, eV			
	Adhesive failure surface	Metal failure surface	CAA Ti-6Al-4V reference	Literature value[103]
N 1s	400.2 ± 0.1	400.4 ± 0.1	400.3 ± 0.1	400.9[a]
O 1s	532.5 ± 0.4	530.4 ± 0.2 532.3 ± 0.1	530.3 ± 0.1	530.0[b] 531.1[c]
Ti $2p_{3/2}$	460.8 ± 0.1	459.0 ± 0.1	458.9 ± 0.1	458.7[b]
F 1s	687.5 ± 0.1	685.6 ± 0.3	685.0 ± 0.1	685.1[d]
Al $2p_{3/2}$	76.3 ± 0.1	74.1 ± 0.1	74.6 ± 0.1	74.3[c]

[a] as Kapton™ polyimide

[b] as TiO_2

[c] as Al_2O_3

[d] as CaF_2

Table 5.2: Glass transition temperatures, by DSC, of FM-5 before and after an initial heat to 300°C. Samples shown are aged for the indicated time at 177°C in air.

Aging time, days	Glass transition temperature, °C	
	First heat	Second heat
0	241	248
1	238	247
7	242	249
30	240	248
90	241	249

Table 5.3: Glass transition temperatures, by DSC, of PETI-5 and 8515 before and after an initial heat to 300°C. Samples shown are aged at 177°C at the indicated time and atmosphere.

Aging time, days	Aging atmosphere	PETI-5 T_g, °C		8515 T_g, °C	
		First heat	Second heat	First heat	Second heat
0	none	252	254	229	232
30	nitrogen	249	252	234	236
30	air	251	252	232	234

Table 5.4: PETI-5 infrared spectrum peak identification.[104]

Wavenumber, cm^{-1}	Peak identification
3066, 1604, 1507, 1488	Aromatic C-H
1777, 1720	Imide
2214	Phenylethynyl

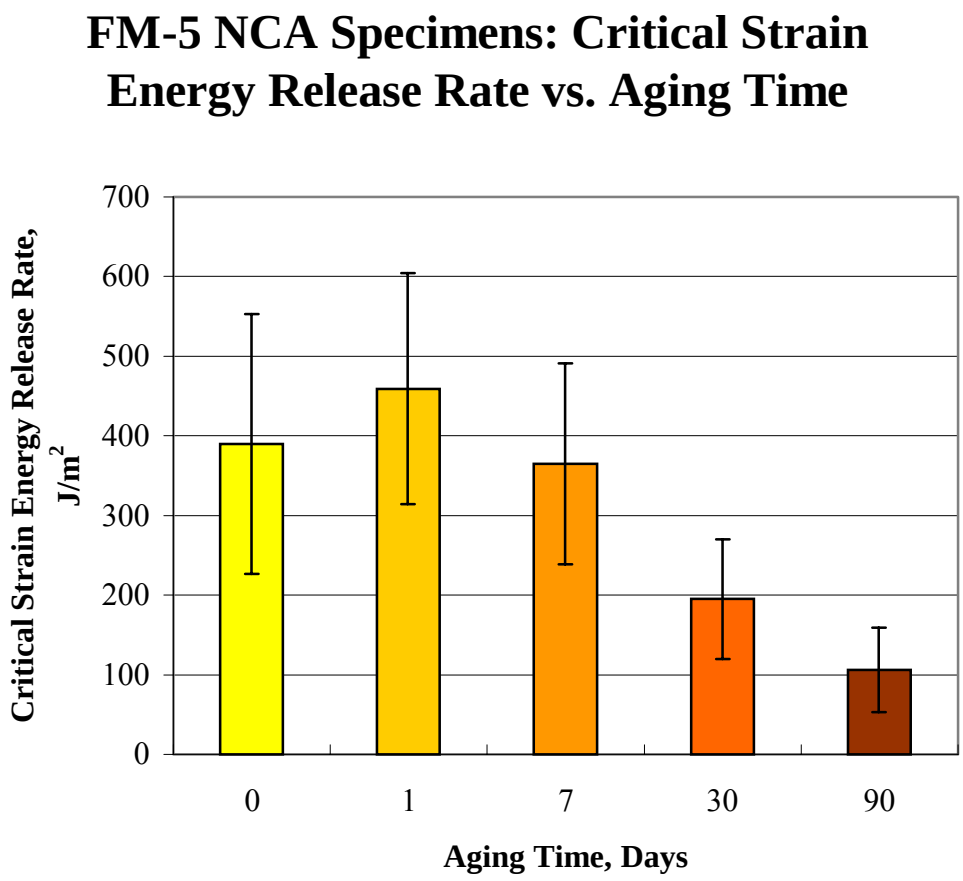

Figure 5.1: Critical strain energy release rate, G_c, for Ti/FM-5 NCA specimens aged at 177ºC in air. Error bars represent the 95% confidence intervals.

(a)

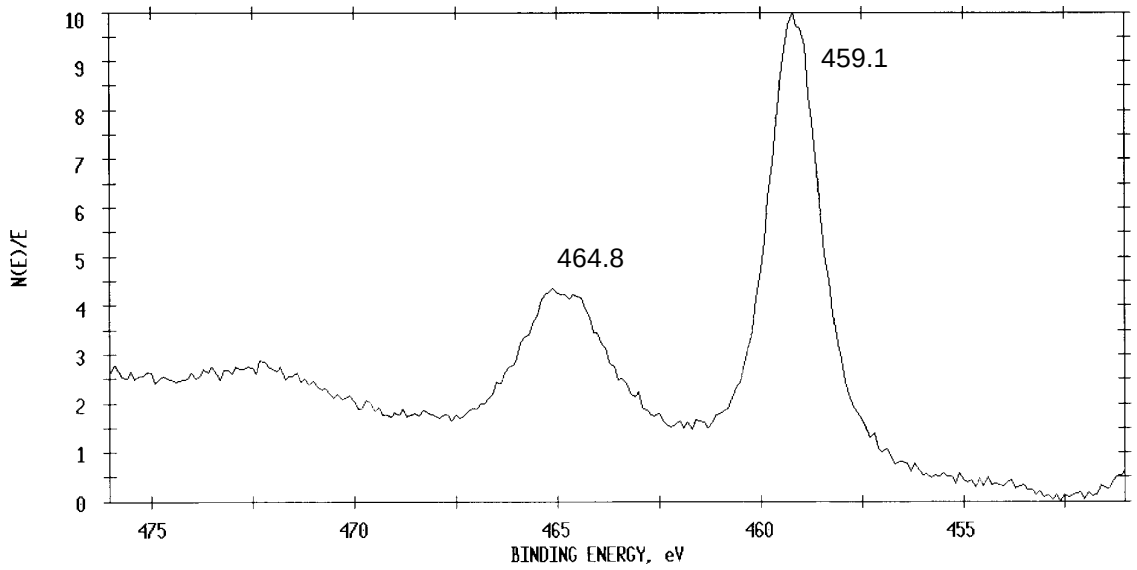

(b)

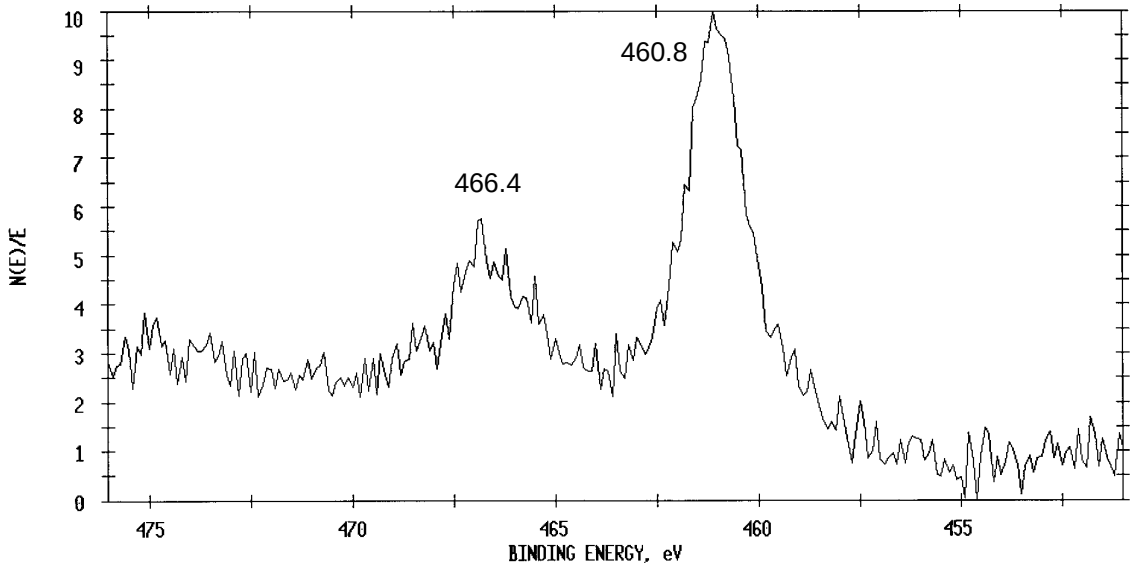

Figure 5.2: Ti $2p_{3/2}$ XPS spectra from (a) unaged FM-5 metal failure surface (b) unaged FM-5 adhesive failure surface. Note: Each spectrum is on a normalized x-axis scale; as shown, peak heights and areas cannot be compared between the two spectra.

(a)

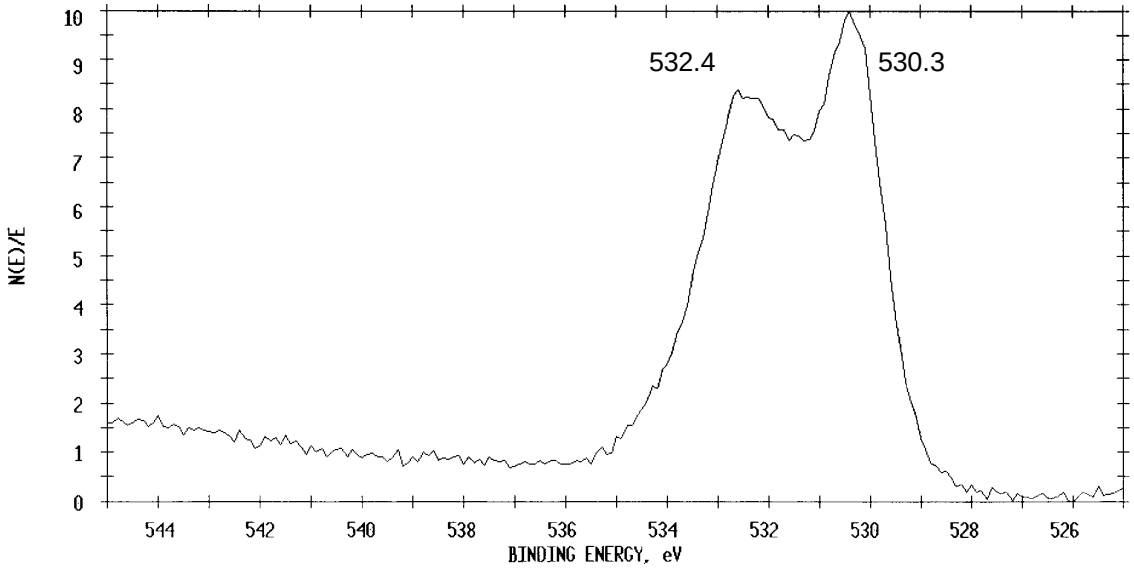

(b)

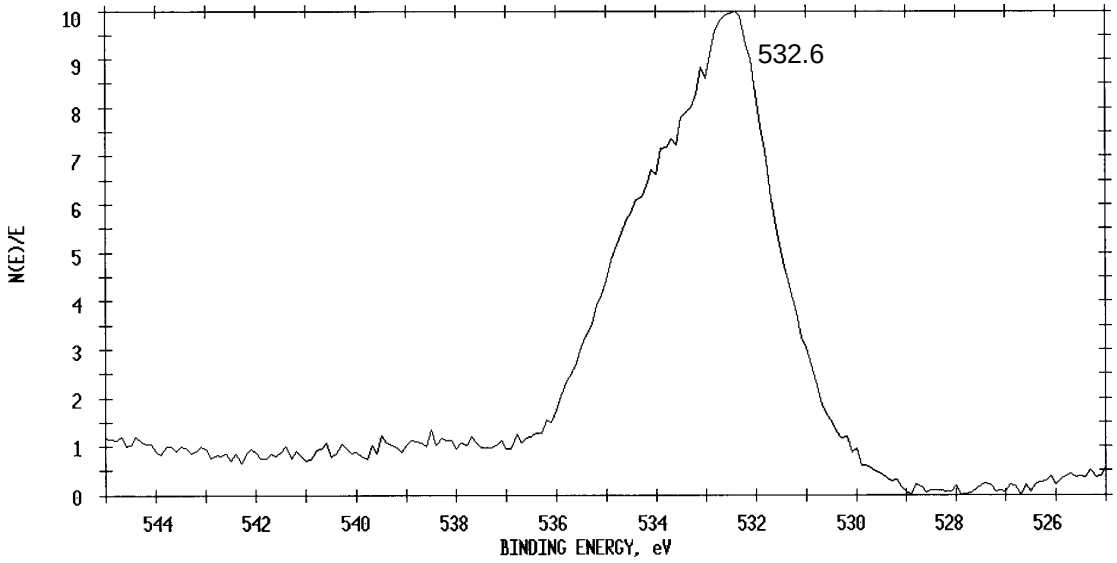

Figure 5.3: O 1s XPS spectra from (a) unaged FM-5 metal failure surface (b) unaged FM-5 adhesive failure surface. Note: Each spectrum is on a normalized x-axis scale; as shown, peak heights and areas cannot be compared between the two spectra.

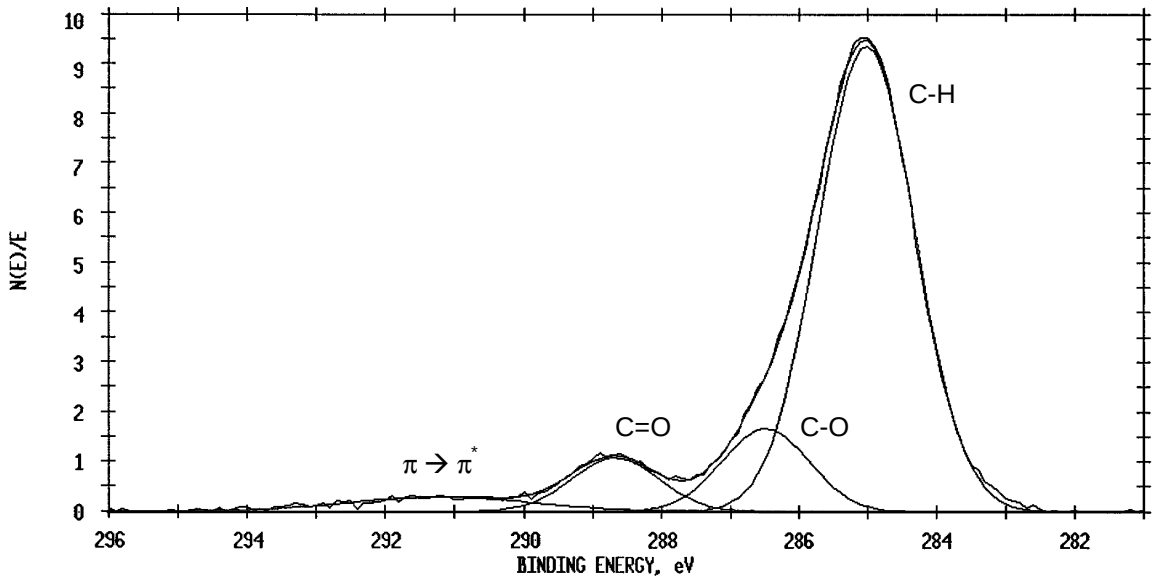

Figure 5.4: C 1s XPS spectrum from an unaged FM-5 metal failure surface, resolved into the peaks corresponding to C-H, C-O, and C=O present in the polyimide adhesive. A $\pi \rightarrow \pi^*$ *shake-up peak is also present.*

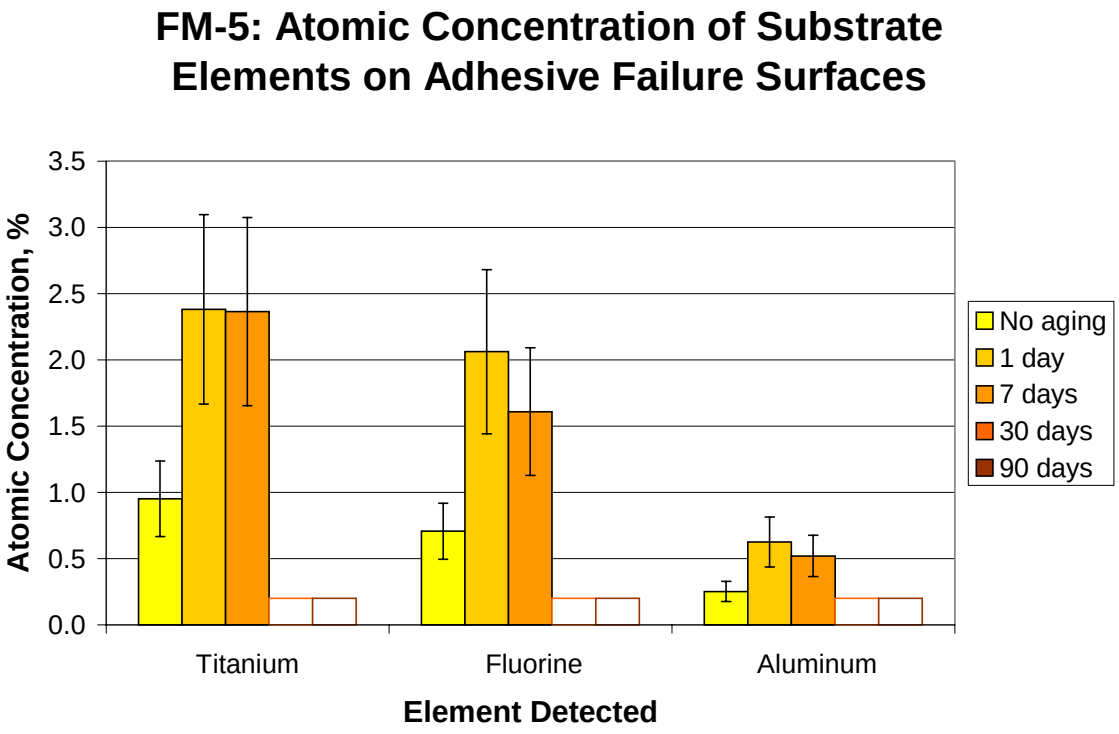

Figure 5.5: Atomic concentration of titanium, fluorine, and aluminum on FM-5 NCA adhesive failure surfaces, by XPS. Samples were aged for the indicated times at 177°C in air. White bars indicate that none was detected, with the height representing the detection limits of the XPS instrument. Error bars represent the pooled estimate of error.

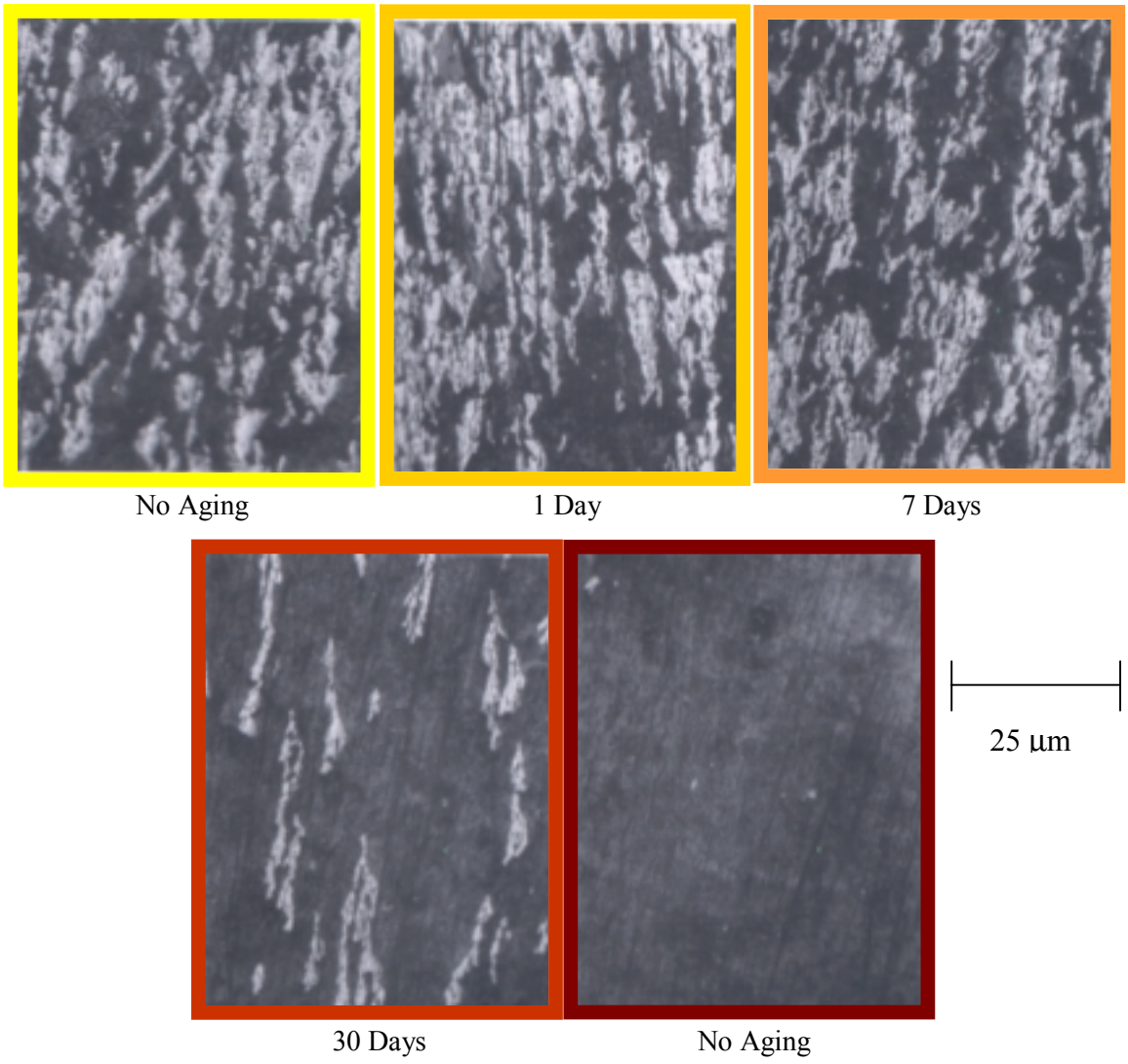

Figure 5.6: Optical micrographs of FM-5 adhesive failure surfaces from NCA specimens. Aging times at 177°C in air are indicated below each micrograph.

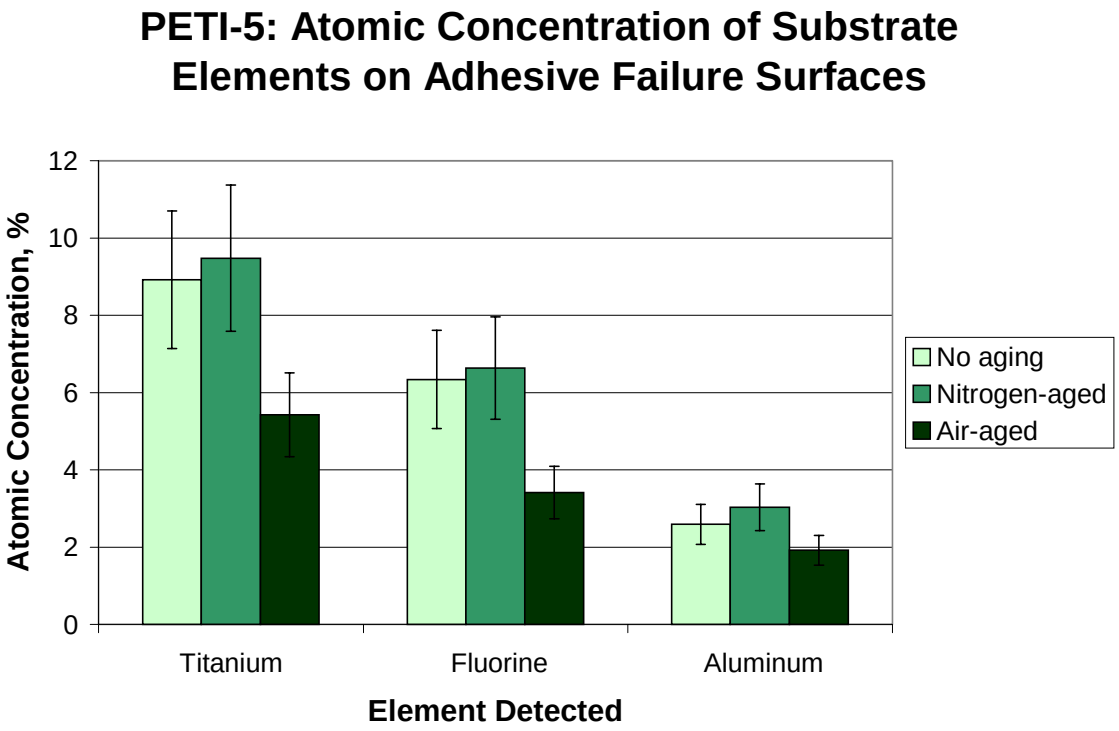

Figure 5.7: Atomic concentration of titanium, fluorine, and aluminum on PETI-5 NCA adhesive failure surfaces, by XPS. Samples were aged for 30 days at 177°C in the indicated atmosphere. Error bars represent the pooled estimate of error.

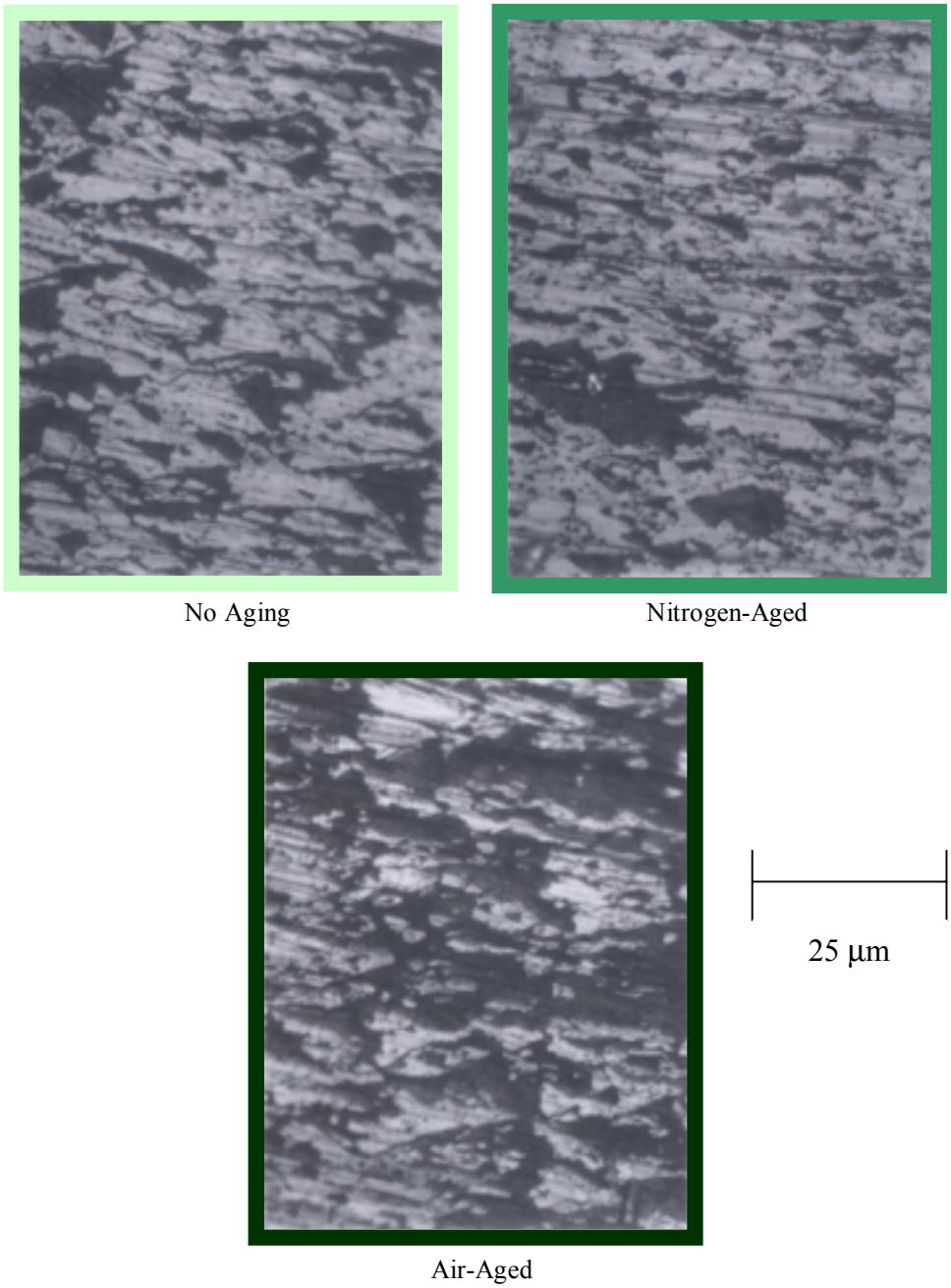

Figure 5.8: Optical micrographs of PETI-5 adhesive failure surfaces from NCA specimens. Specimens were aged for 30 days at 177°C in the indicated atmosphere.

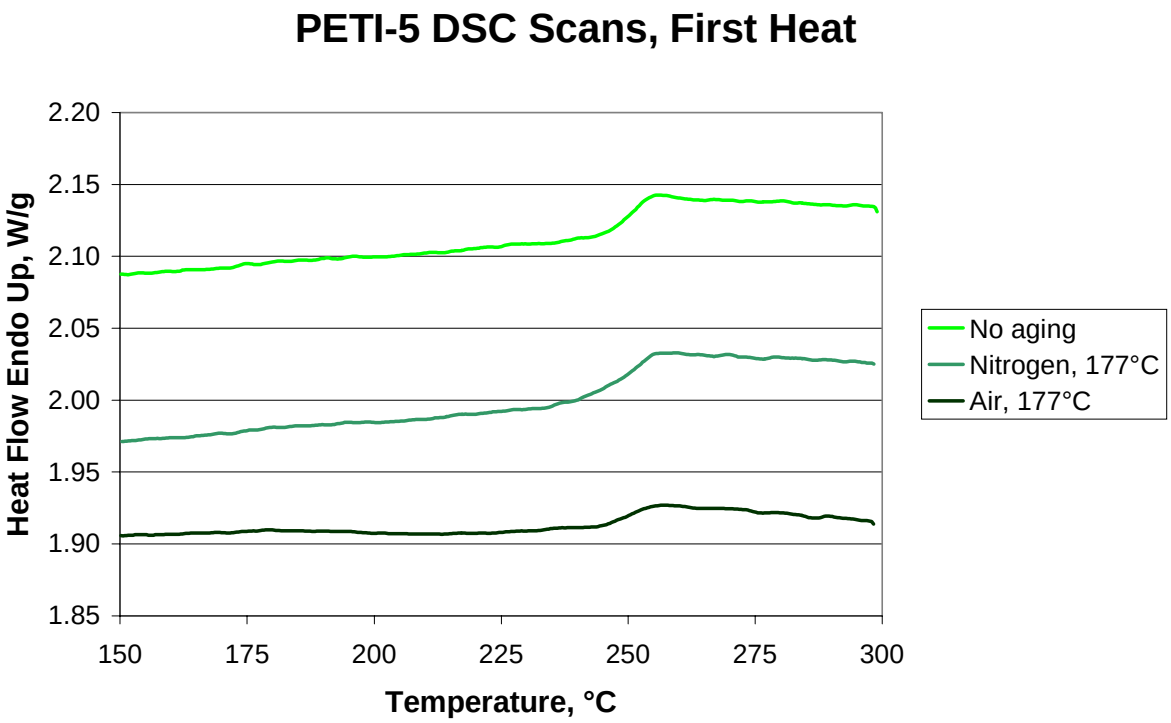

Figure 5.9: First heat DSC thermograms of PETI-5 adhesive samples removed from titanium substrates. Samples shown are unaged, aged for 30 days at 177°C in nitrogen, or aged for 30 days at 177°C in air.

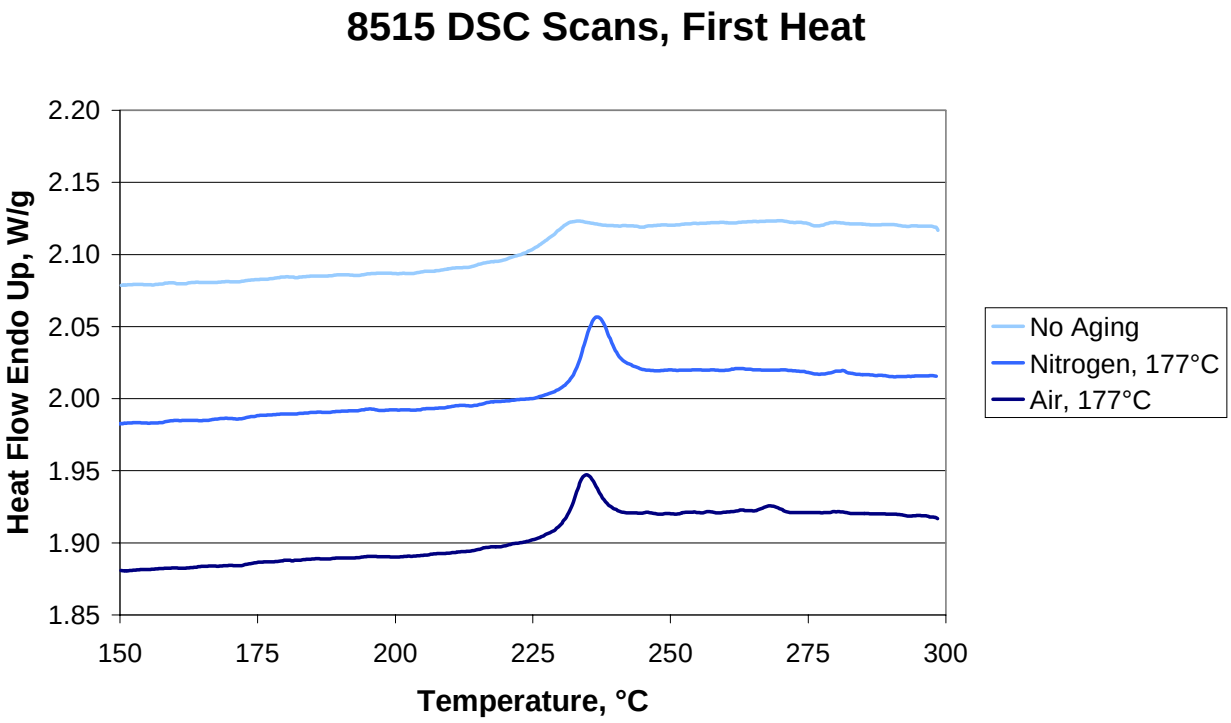

Figure 5.10: First heat DSC thermograms of 8515 adhesive samples removed from titanium substrates. Samples shown are unaged, aged for 30 days at 177°C in nitrogen, and aged for 30 days at 177°C in air.

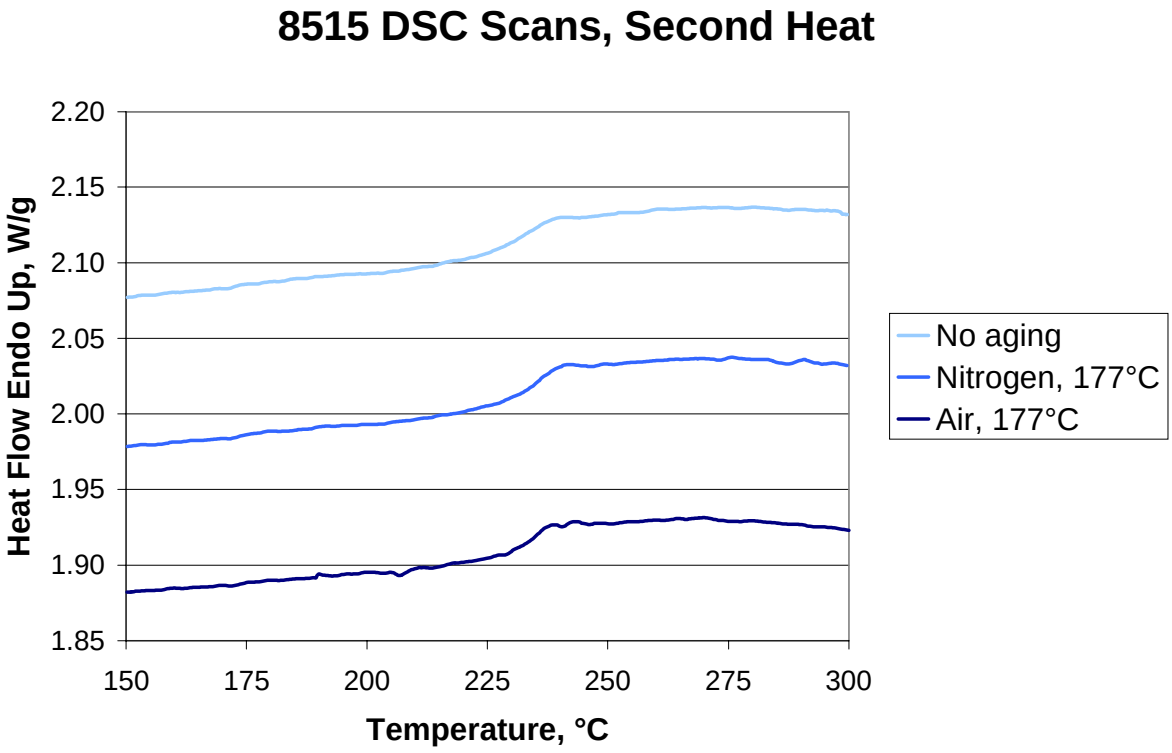

Figure 5.11: DSC thermograms of 8515 adhesive samples removed from titanium substrates, after an initial heat to 300°C. Samples shown are unaged, aged for 30 days at 177°C in nitrogen, and aged for 30 days at 177°C in air.

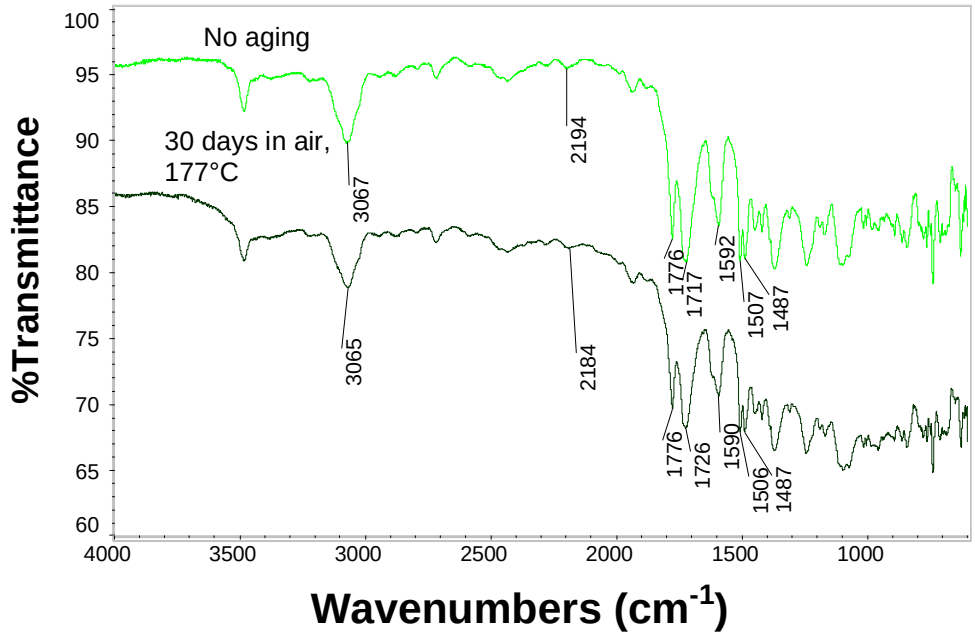

Figure 5.12: Infrared spectra of unaged PETI-5 and PETI-5 aged 30 days in air at 177°C.

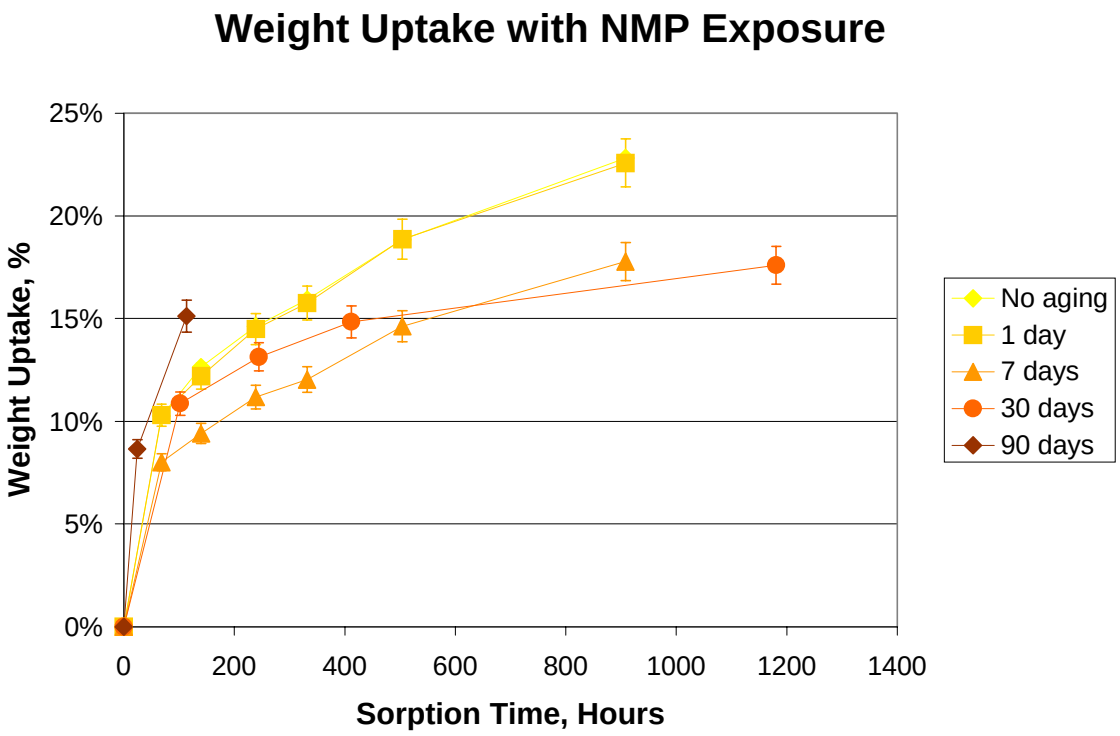

Figure 5.13: Weight uptake of debonded FM-5 adhesive films upon exposure to NMP. Samples were aged for the indicated times at 177°C in air. Error bars represent the standard error of the mean, based on the pooled error of each sample for all sorption times.

Chapter 6: Failure Surface Analysis: PETI-5 NCA Specimens

6.1 Introduction

In addition to the failure surface analysis of NCA specimens discussed in Chapter 5, several additional analysis techniques were applied to the PETI-5 NCA failure surfaces. While the analysis results discussed in Chapter 5 related to factors that were a function of aging time or atmosphere, the current chapter focuses on an in-depth understanding of the PETI-5/CAA Ti-6Al-4V interphase.

6.2 Mechanical Interlocking

As discussed in Chapter 2, mechanical interlocking between an adhesive and a substrate occurs when the liquid adhesive flows into interstices of the substrate, solidifies, and becomes locked in place. Mechanical interlocking is believed to significantly contribute to the adhesion of substrates that exhibit microroughness, such as metal surfaces treated with chromic acid anodization or sodium hydroxide anodization. Filbey and Wightman[105] found that an epoxy penetrated the pores of CAA Ti-6Al-4V, one of the limited number of pore penetration studies that have been reported.[105] Here, the

penetration of PETI-5 into the pores of CAA Ti-6Al-4V is investigated using several surface analysis techniques.

First, however, one must determine if it is possible for PETI-5 polymer molecules to penetrate the porous oxide layer of CAA titanium. FE-SEM images of CAA Ti-6Al-4V are shown in Figure 6.1. The dark circular regions are pores in the CAA oxide layer, approximately 30 nm in diameter. When PETI-5 is applied to the anodized substrate surface, it is a primer in the form of a 16% solids amic acid solution in NMP. Using gel permeation chromatography, the radius of gyration of the PETI-5 amic acid solution was determined. The number average radius of gyration was found to be 3.6 nm, with weight average and z-average radii of gyration of 4.8 and 5.7 nm, respectively. The diameter of the coiled polymer chain conformation, therefore, is less than the diameter of the substrate pores. Thus, it is reasonable to assume that PETI-5 amic acid can penetrate the pores of the CAA substrate.

6.3 Optical Microscopy

As discussed in Chapter 5, titanium was observed by optical microscopy on the adhesive failure surfaces of PETI-5 NCA specimens. In Figure 6.2, the adhesive and metal failure surfaces of a PETI-5 specimen are shown. These micrographs were taken in the same spot on corresponding adhesive and metal failure surfaces. The original black and white micrographs were colorized to reproduce the colors that were actually observed using the optical microscope. On both failure surfaces, the light gray regions correspond to metal or metal oxide. Here, failure occurred either through the metal oxide layer, between the metal and metal oxide, or through the metal itself. On the adhesive failure surface, dark brown features are observed which are mirror images of blue features on the metal failure surface. The dark brown color on the adhesive failure surface is indicative of exposed PETI-5 adhesive. The blue color on the metal failure surface is consistent with the surface of anodized titanium. Although this appears to indicate interfacial failure between adhesive and substrate, the XPS results discussed in Chapter 5 contradict this conclusion. Evidence of polyimide adhesive on the metal failure surface was consistently detected by XPS. Thus, polyimide must be either coating the blue oxide layer or

embedded within it. To further investigate this region, Auger depth profiling, field emission SEM, and atomic force microscopy were utilized.

6.4 Auger Electron Spectroscopy

From Auger depth profiling of a PETI-5 metal failure surface, Figure 6.3, carbon and titanium coexist in the top 70 to 100 nm of the failure surface. While this does imply the presence of polyimide at this depth, Auger data alone cannot be interpreted as confirmation of mechanically interlocked polymer. Auger spectroscopy cannot distinguish carbon as polyimide from carbon that may be present as a contaminant. However, if we tentatively assume that the presence of carbon represents polymer, we can construct a simple model of the interfacial region. Beyond the depth at which carbon is detected, titanium, aluminum, and oxygen (indicative of metal oxide) are present through an additional 50 nm. Deeper than this, only titanium and aluminum are detected. Thus, the polymer does not appear to penetrate the entire thickness of the titanium oxide layer. The validity of this interpretation of the Auger data can now be examined using additional surface analysis techniques. The model interphase is illustrated in Figure 6.4. The region in which adhesive and metal oxide are assumed to be present will be referred to as oxide A and the area in which there is only metal oxide is referenced as oxide B.

6.5 Scanning Electron Microscopy and Atomic Force Microscopy

Field emission SEM was performed on the adhesive and metal failure surfaces of PETI-5 NCA specimens. Figure 6.5 is a FE-SEM of the metal failure surface. The features visible at this magnification are similar to those observed by optical microscopy. Dark areas correspond to the blue regions of Figure 6.2 (b), and light areas are exposed metal or metal oxide. Enlarging the center of Figure 6.5 by a factor of five, additional features become visible in Figure 6.6. The dark region on the left is the CAA substrate surface. The pores in the anodized oxide layer, which are believed to be infiltrated with polyimide adhesive, are clearly visible in this region. The failure here occurred between the bulk adhesive and the upper surface of oxide A. The porous structure of the lighter colored region on the right side of the micrograph is also apparent. Failure here occurred within

the porous oxide layer. In the upper right corner of the micrograph, there is a circular region in which the porosity is not well defined. Here, it appears that the failure occurred at the interface of oxide B and the bulk titanium substrate.

These observations are supported by additional FE-SEM micrographs. Figure 6.7 is a metal failure surface at the same magnification as Figure 6.6. Similar features are seen here, including several small areas in which failure occurred between the oxide and bulk titanium. In the center of this micrograph, the edge of a porous oxide/polyimide region can be seen. Enlarging this area by a factor of four, this region can be viewed in Figure 6.8. This micrograph allows for the observation of the sponge-like morphology through the thickness of the oxide layer. One can also see, from the scale of this micrograph, that the thickness of the oxide/polyimide layer is on the order of 100 nm, in agreement with the Auger depth profiling data.

Additional features are observed in FE-SEMs of adhesive failure surfaces. Figure 6.9 is a FE-SEM of an adhesive failure surface. The dark region at the top of this micrograph corresponds to the dark brown adhesive observed by optical microscopy, Figure 6.2 (a), while the lighter region on the bottom corresponds to the light gray metal oxide. Across the top of this micrograph, the ductility of the polymer is evident by the drawing and fibrillation that occurred as the failure propagated from the right to the left of this micrograph. In the lower half of the micrograph, the titanium failure region is observed. On this metal oxide surface, features of two sizes can be seen. Increasing the magnification and focusing on the lower left region of the micrograph, these features are observed in Figure 6.10. The larger features are approximately 150 to 400 nm in diameter, while the smaller features are less than 50 nm. The size, shape, and spatial distribution of the smaller features are consistent with the pores on the anodized titanium surface in Figure 6.1. The larger features could be the result of the failure propagating through the walls of several pores in close proximity. The features, small and large, in Figure 6.10 appear to be raised, while the corresponding features on the micrographs of titanium failure surfaces appear to be indented (e.g. lower left corner of Figure 6.7). The directions of these features, raised versus lowered, are confirmed using atomic force microscopy. AFM images of the titanium failure surface and the adhesive failure surface

are shown in Figure 6.11 and Figure 6.12, respectively. Note that the scales are different in the two micrographs. The 30 nm pores cannot be resolved by AFM; however, the larger features (approximately 200 nm) observed in Figure 6.7 and Figure 6.10 appear in a periodic fashion in the AFM images.

In the AFM height images, on the left in each figure, lighter shades correspond to higher features. In Figure 6.11, the metal failure surface, the dark background is exposed oxide. The diagonal strip of lighter color is the anodized oxide layer (i.e. the blue region of Figure 6.2). The small features on the exposed oxide surface are darker than the background and therefore indented. On the adhesive failure surface, Figure 6.12, features of approximately the same size are raised, illustrated by the fact that they are lighter in color than the background. The matching raised features on the adhesive failure surface and indented features on the metal failure surface support the assertion that polyimide adhesive is embedded in the pores of the CAA oxide layer. From the model proposed in Figure 6.4, the failure within the oxide layer appears to be occurring at the interface of oxide A and oxide B. The raised features on the adhesive failure surface would then be attributed to polymer embedded in the oxide, and the indented features in the metal oxide layer would be holes left in the oxide layer, having been pulled out by the polymer. Had the failure occurred through porous oxide that did not contain adhesive, these features would have appeared indented on both failure surfaces.

Additional information is obtained from the AFM phase images. Darker regions of the phase image indicate a higher phase lag that, in general, means dark areas are softer than light areas. The diagonal strip on the metal failure surface, Figure 6.11, is both higher and softer than the surrounding area. If there were no polymer embedded in the metal oxide, it would not be softer than the surrounding metal oxide. This again confirms that the substrate pores contain polyimide. All surface analysis data appears to validate the model in Figure 6.4. Thus, it is concluded that PETI-5 is penetrating the pores of the CAA substrate and becoming mechanically interlocked.

6.6 X-ray Photoelectron Spectroscopy

XPS analysis of adhesive failure surfaces of PETI-5 NCA specimens supports the conclusion that the polymer is imbedded in the pores of the titanium substrate surface. As discussed in Chapter 5, differential charging causes the titanium, aluminum, and fluorine XPS photopeaks of FM-5 adhesive failure surfaces to be shifted to 1.9 eV higher binding energy than is observed on the corresponding metal failure surface. While the data presented in Chapter 5 related to differential charging of FM-5 samples, the same effect is observed in PETI-5 samples. Ti $2p_{3/2}$ XPS photopeaks from the metal and adhesive failure surfaces of PETI-5 NCA specimens are given in Figure 6.13, illustrating the 2.1 eV shift caused by differential charging on the adhesive failure surface. Table 6.1 lists the XPS photopeak binding energies for N 1s, Ti $2p_{3/2}$, F 1s, and Al $2p_{3/2}$ referenced to the C 1s photopeak at 285.0 eV. As with the FM-5 specimens, all components of the substrate surface, titanium, fluorine, and aluminum, are shifted to a higher binding energy on the adhesive failure surface. From the observed binding energies, the substrate elements are attributed to TiO_2, fluoride ion, and Al_2O_3, as was the case with the FM-5 specimens. An additional effect, believed to be caused by differential charging, is observed in the PETI-5 NCA specimens. The C 1s XPS photopeaks of the metal and adhesive failure surfaces of PETI-5 NCA specimens are shown in Figure 6.14. While both C 1s photopeaks have been resolved with four sub-peaks in approximately the same position, the peak at 287.0 eV on the adhesive failure surface is obviously much larger than the corresponding peak on the metal failure surface. The peak position on the adhesive failure surface is also shifted to a slightly higher binding energy than that observed on the metal failure surface, 286.4 eV. Average binding energies for the four C 1s sub-peaks on the adhesive and metal failure surfaces are listed in Table 6.2. In Chapter 5, the peak at 286.4 eV was assigned to carbon single bonded to oxygen. An additional feature obscures the C-O peak on the adhesive failure surface. The peak at 286.9 eV is believed to arise from the C-H component of the PETI-5 adhesive that is embedded in the porous TiO_2 substrate surface, the adhesive portion of oxide A. If the polymer is in electrical contact with the titanium, they are expected to undergo differential charging in unison.[91] The percentage of the C 1s peak that is shifted to higher binding energy is proportional to the amount of titanium detected on the surface. This is

illustrated in Figure 6.15, in which the shifted component of the C 1s photopeak is plotted as a function of atomic concentration of titanium. The shifted component has been normalized by the total carbon concentration. The R^2 value of 0.88 indicates a strong linear fit, and the p-value of 0.017 indicates a 98.3% probability that the trend is significant. The relationship between the titanium detected on the surface and the amount of shifted carbon is evidence that the shifted carbon originates from polymer embedded in the pores of the oxide. To further illustrate this point, the C 1s photopeaks of three adhesive failure surfaces are presented in Figure 6.16 along with the titanium concentration of the sample. This clearly illustrates the decrease in the shifted portion of the C-H photopeak with decreasing titanium coverage. The charging component of the C-H peak, therefore, is attributed to polymer that is embedded in the porous oxide, or oxide A from the model discussed previously.

The observation of a charging component of the adhesive in PETI-5 specimens and not FM-5 specimens may relate to differences in manufacturing techniques, as described in Chapter 3. A primer, consisting of PETI-5 amic acid solution, was applied to the substrates prior to fabrication of PETI-5 bonds. The low viscosity primer could easily penetrate the pores of the substrate surface and become mechanically interlocked. No primer was applied to the substrates when manufacturing FM-5 bonds. The FM-5 adhesive applied to the anodized substrates was in the form of an imide, rather than an amic acid, and contained less than 4% volatiles. The conversion of amic acid to imide is illustrated in Figure 6.17. The backbone of the amic acid is considerably more flexible than that of the imide due to its flexible amide groups rather than the fused imide ring. Because the imide is insoluble, its radius of gyration cannot be determined using gel permeation chromatography. Regardless, the imide is assumed to take on a more elongated conformation, making it more difficult for the imide to penetrate the 30 nm pores on the CAA surface. In addition, even under the high temperatures and pressures of processing, the viscosity of the FM-5 adhesive could not approach that of the PETI-5 primer. Thus, application of an amic acid primer to an anodized substrate is more likely to result in mechanical interlocking between the adhesive and substrate than direct application of a polyimide to the substrate. In turn, this is expected to result in higher interfacial bond strength. Figure 6.18 illustrates the relationship between bond strength

and the titanium detected on the failure surfaces of FM-5 NCA specimens. The R^2 value of 0.67 does not indicate an especially high degree of linearity, however, the p-value of 0.004 indicates that the relationship between bond strength and titanium is highly significant. As discussed in Chapter 5, a high portion of failure propagating through the oxide is indicative of a strong adhesive-substrate interface. Mechanical interlocking is expected to contribute to the strength of the interface and therefore to the portion of failure propagating through the oxide. The substantial increase in titanium detected on PETI-5 failure surfaces compared to those of FM-5, from XPS and optical microscopy data presented in Chapter 5, is consistent with the expected result of increased mechanical interlocking. Thus, the use of primer on the PETI-5 NCA specimens may be leading to increased mechanical interlocking and therefore increased failure through the oxide layer.

6.7 Conclusions

The interface of PETI-5/CAA Ti-6Al-4V bonds was studied using several surface analysis techniques. From Auger spectroscopy, field emission SEM, and AFM studies, polymer is believed to be penetrating the pores of the anodized substrate to a depth of approximately 100 nm. From XPS data, this polymer appears to be in electrical contact with the titanium oxide, leading to differential charging. These analyses confirm that the polymer is becoming mechanically interlocked within the substrate surface.

Table 6.1: Binding energies of XPS photopeaks on PETI-5 failure surfaces, referenced to the C 1s peak at 285.0 eV, with 95% confidence intervals.

XPS Photopeak	Binding energy, eV			
	Adhesive failure surface	Metal failure surface	CAA Ti-6Al-4V reference	Literature value[103]
N 1s	400.5 ± 0.1	400.5 ± 0.1	400.3 ± 0.1	400.9[a]
O 1s	532.4 ± 0.2	530.2 ± 0.1 531.7 ± 0.1	530.3 ± 0.1	530.0[b] 531.1[c]
Ti $2p_{3/2}$	461.0 ± 0.2	458.8 ± 0.1	458.9 ± 0.1	458.7[b]
F 1s	687.8 ± 0.2	685.3 ± 0.2	685.0 ± 0.1	685.1[d]
Al $2p_{3/2}$	77.0 ± 0.2	74.3 ± 0.1	74.6 ± 0.1	74.3[c]

[a] as Kapton™ polyimide

[b] as TiO_2

[c] as Al_2O_3

[d] as CaF_2

Table 6.2: Binding energies of C 1s XPS sub-peaks on PETI-5 failure surfaces, referenced to the C 1s C-H sub-peak at 285.0 eV, with 95% confidence intervals.

XPS Photopeak	Binding energy, eV	
	Adhesive failure surface	Metal failure surface
Peak 1	285.0	285.0
Peak 2	286.9 ± 0.1	286.4 ± 0.1
Peak 3	288.5 ± 0.1	288.6 ± 0.1
Peak 4	291.1 ± 0.1	291.1 ± 0.1

(a)

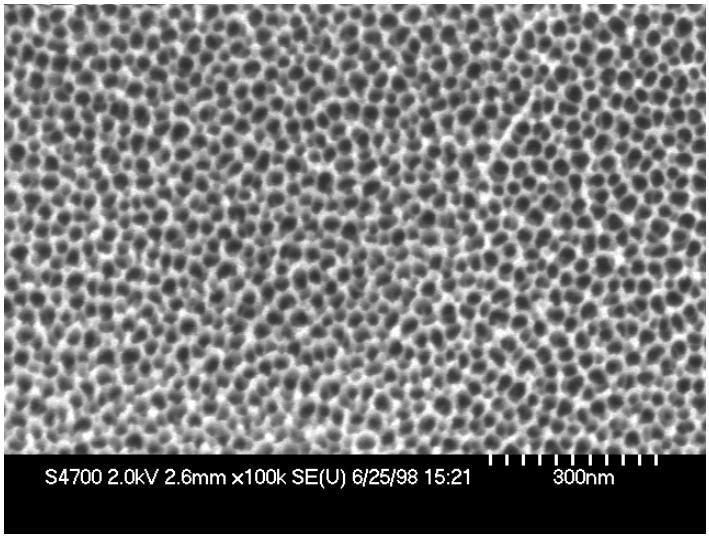

(b)

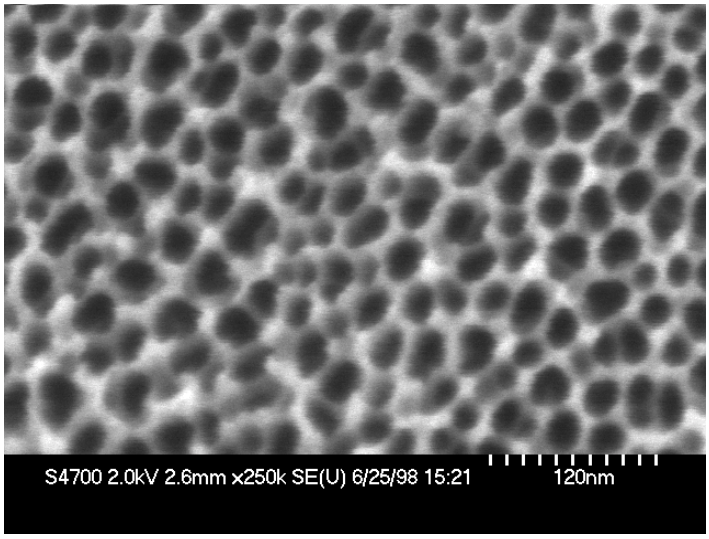

Figure 6.1: Field emission scanning electron micrographs of a chromic acid anodized Ti-6Al-4V substrate surface.

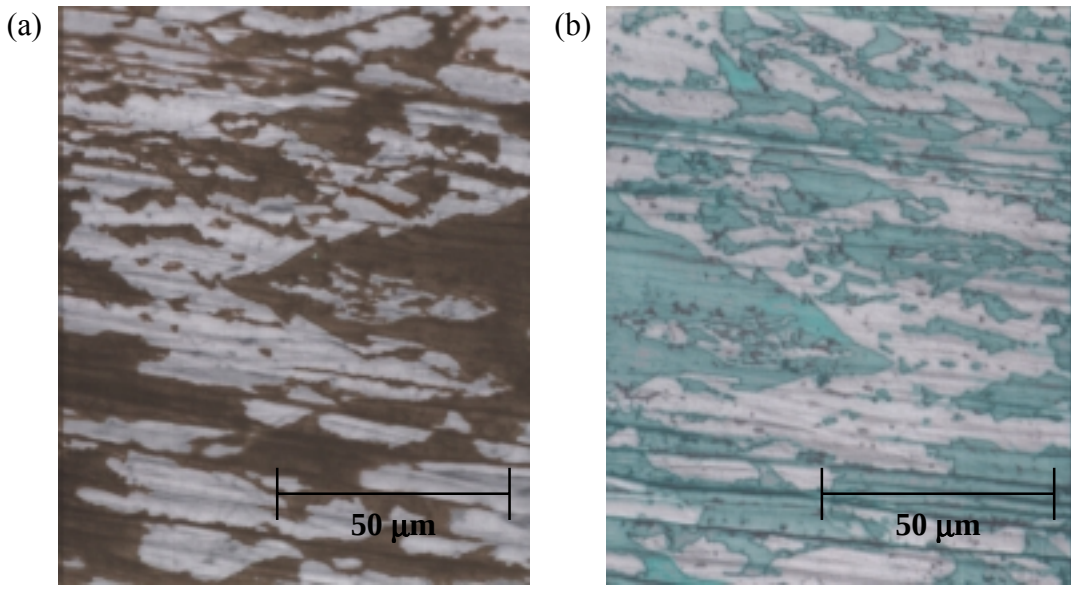

Figure 6.2: Optical micrographs of failure surfaces of a PETI-5 NCA specimen, (a) adhesive failure surface and (b) titanium failure surface. Micrographs were taken from failure surfaces in locations that were originally bonded to one another. Mirror images of features can be observed on the two failure surfaces.

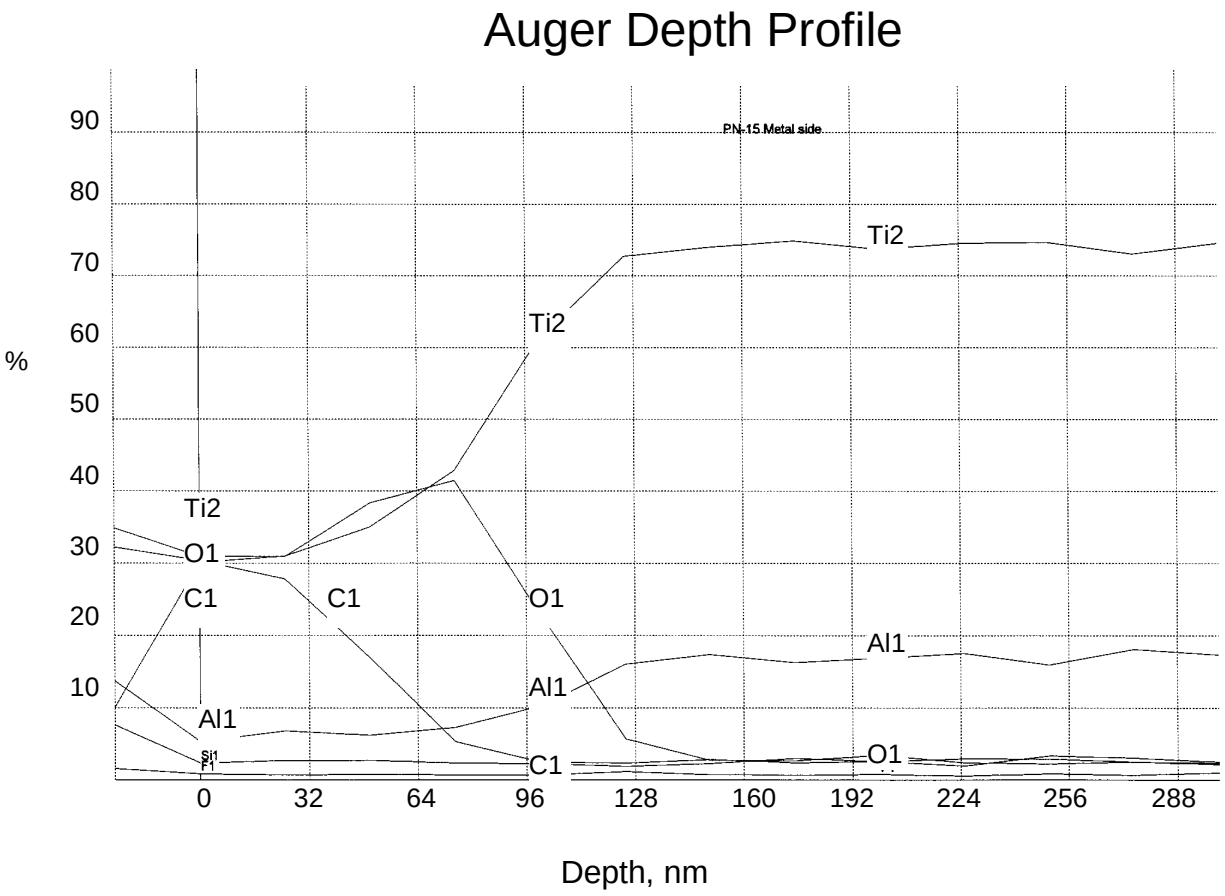

Figure 6.3: Auger electron spectroscopy depth profile of a PETI-5 metal failure surface from a NCA specimen.

Figure 6.4: Schematic model of the PETI-5/CAA Ti-6Al-4V interphase based on Auger depth profiling data. Oxide A consists of the porous oxide layer embedded with adhesive. Oxide B is the porous oxide layer that contains no adhesive.

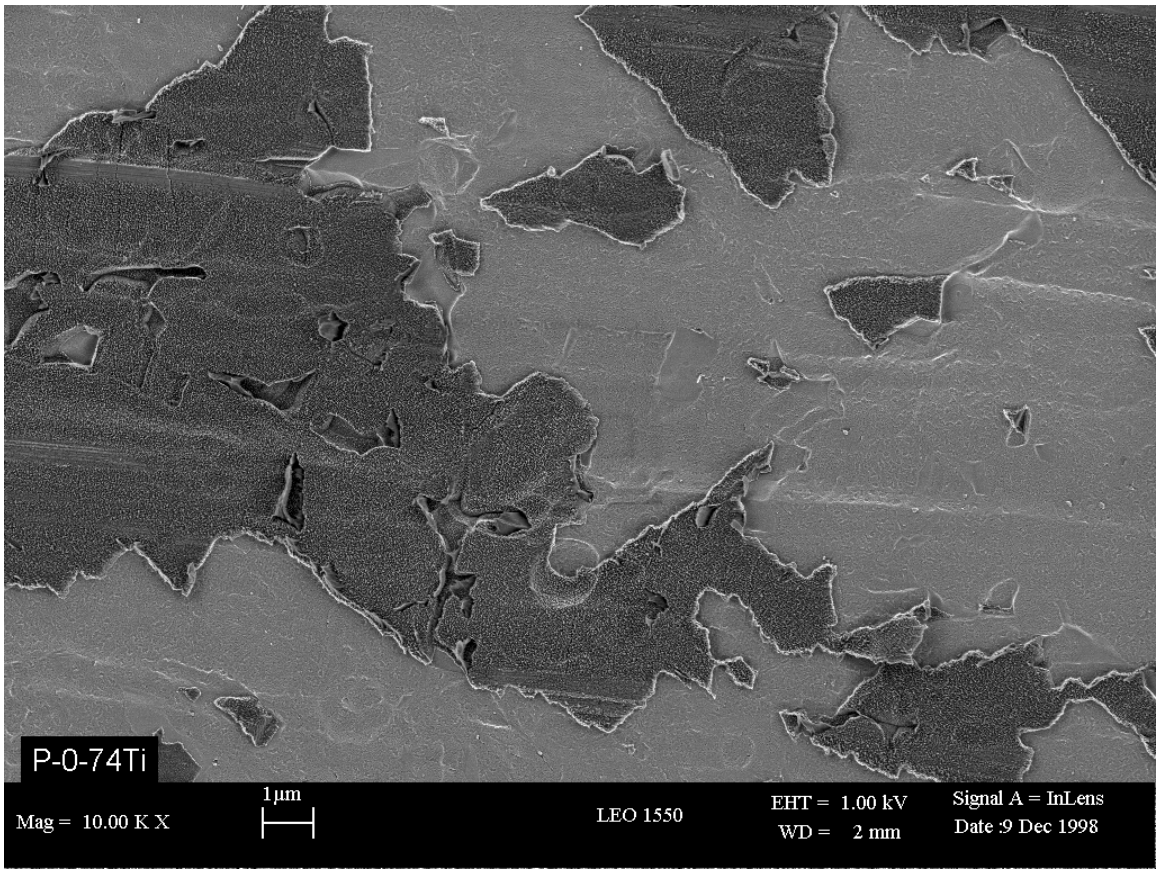

Figure 6.5: Field emission SEM of the metal failure surface of a PETI-5 NCA specimen.

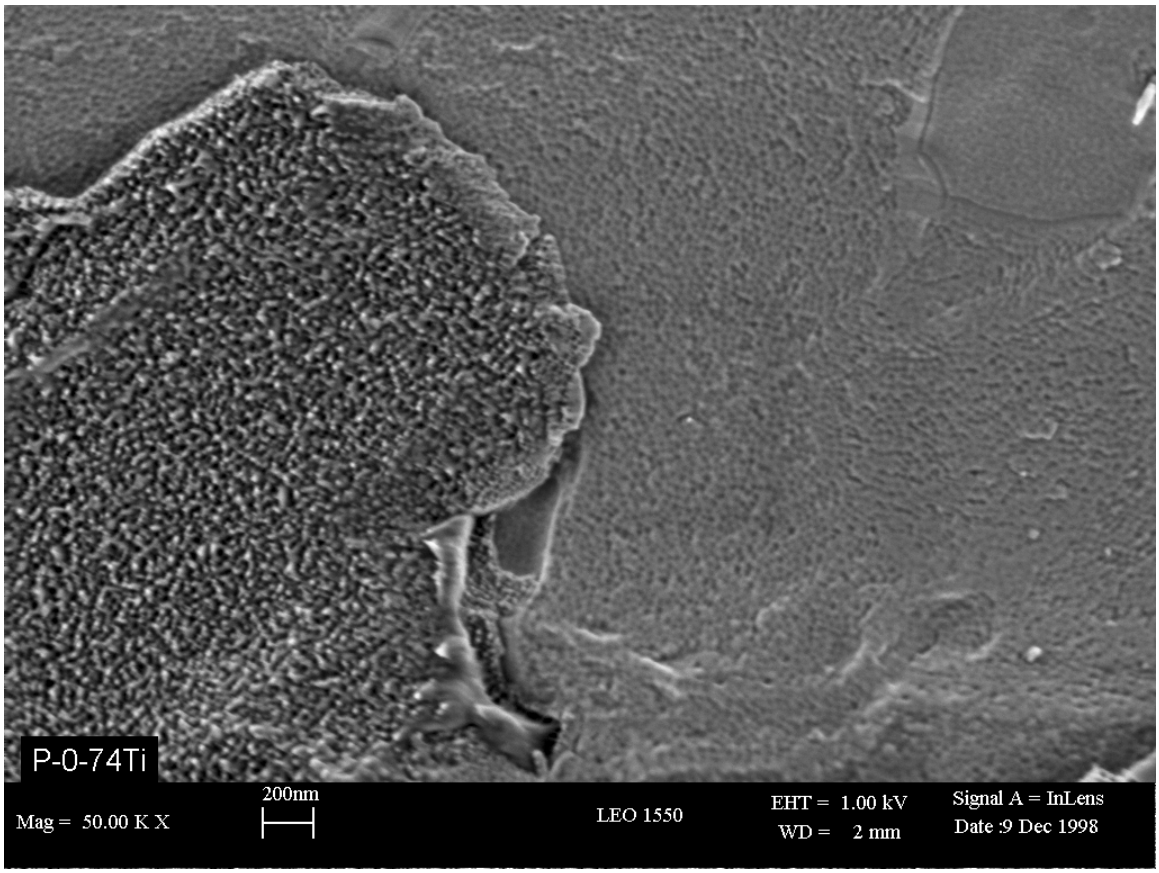

Figure 6.6: Field emission SEM of the metal failure surface of a PETI-5 NCA specimen.

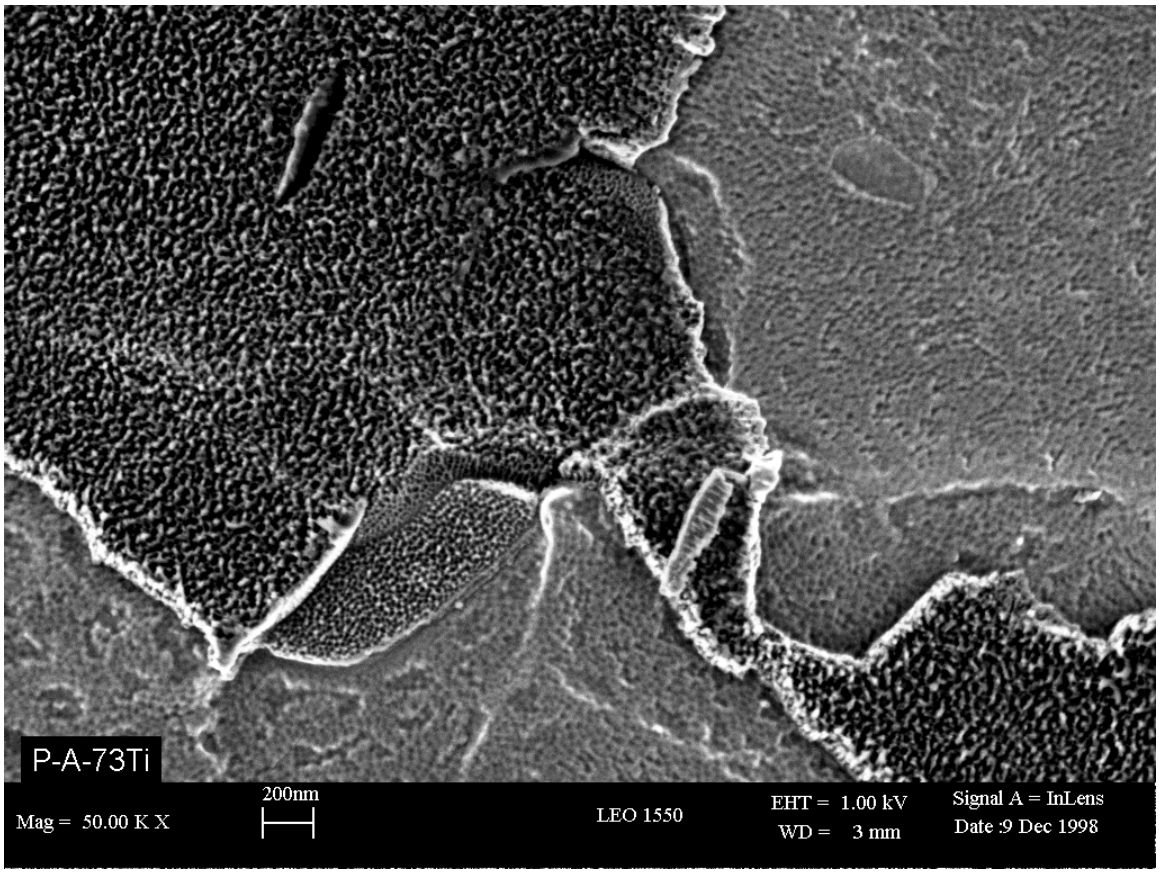

Figure 6.7: Field emission SEM of the metal failure surface of a PETI-5 NCA specimen.

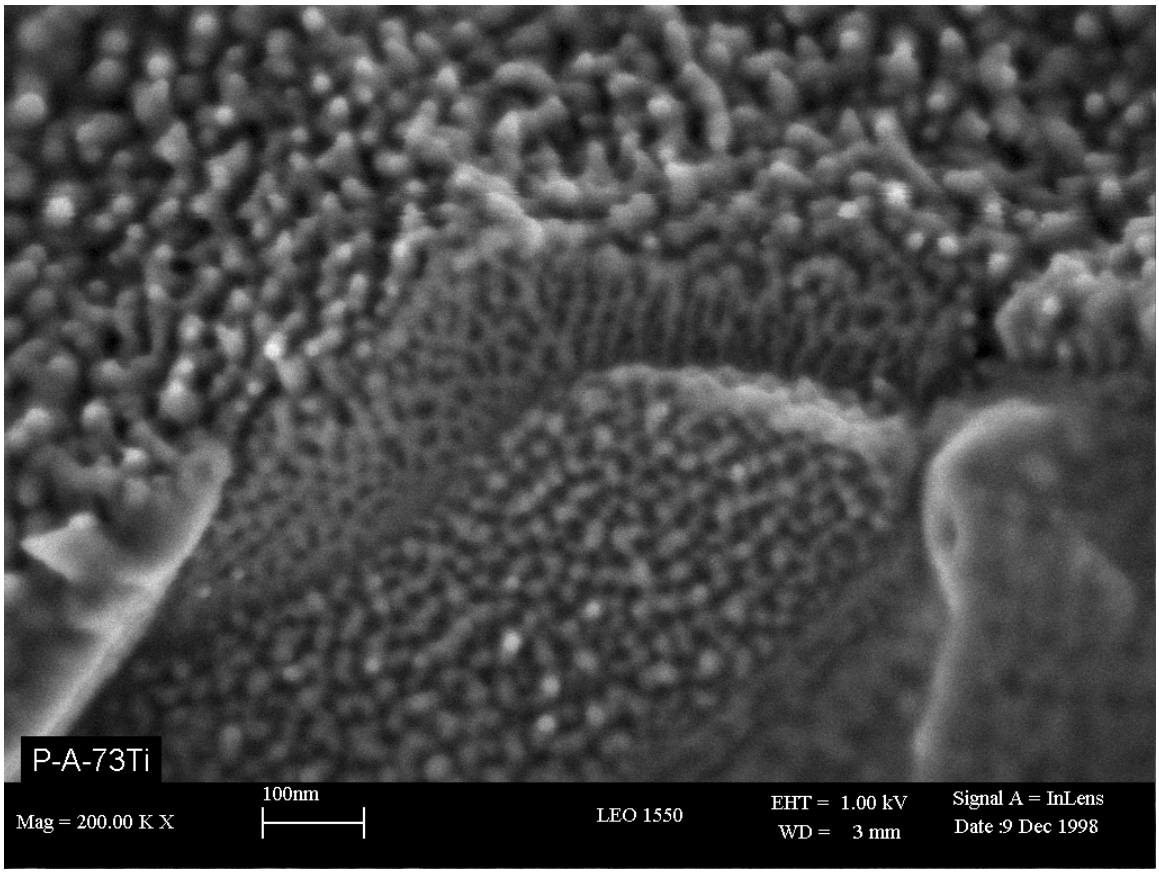

Figure 6.8: Field emission SEM of the metal failure surface of a PETI-5 NCA specimen.

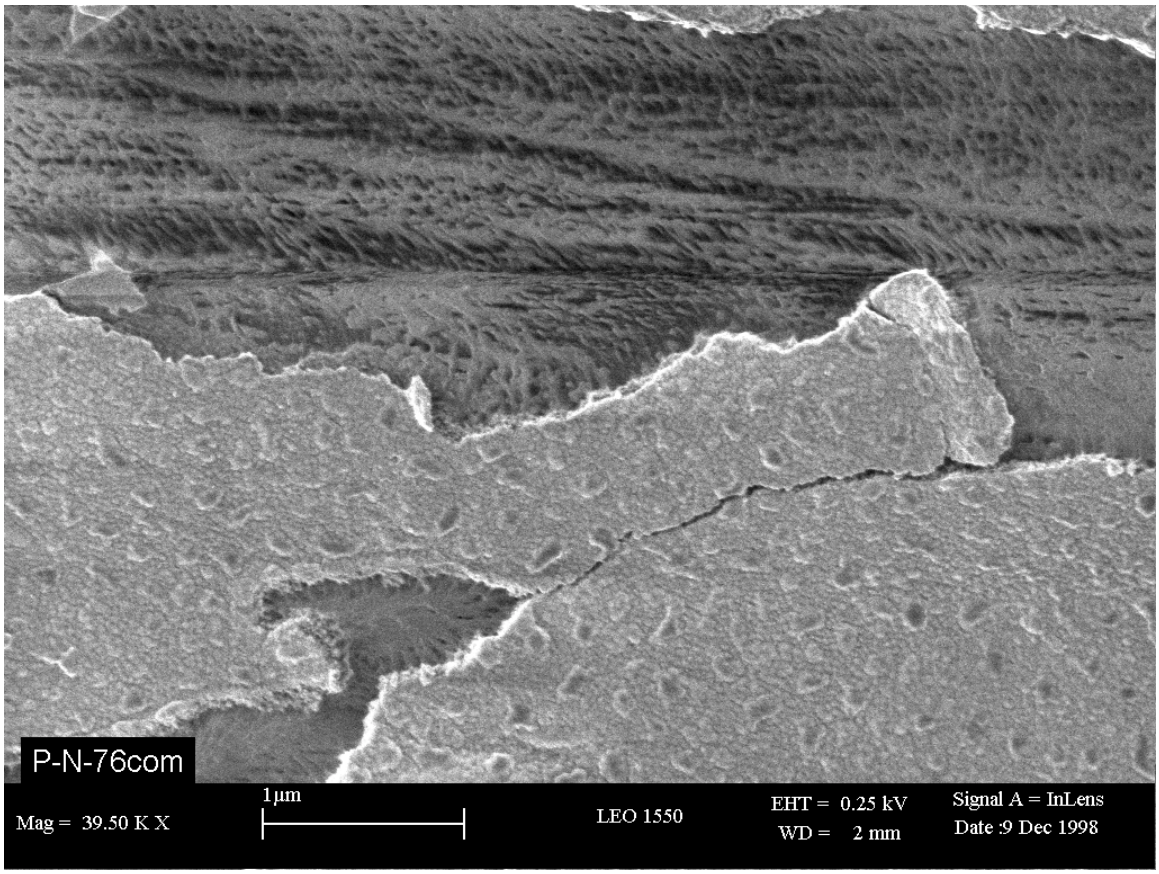

Failure direction

Figure 6.9: Field emission SEM of the adhesive failure surface of a PETI-5 NCA specimen.

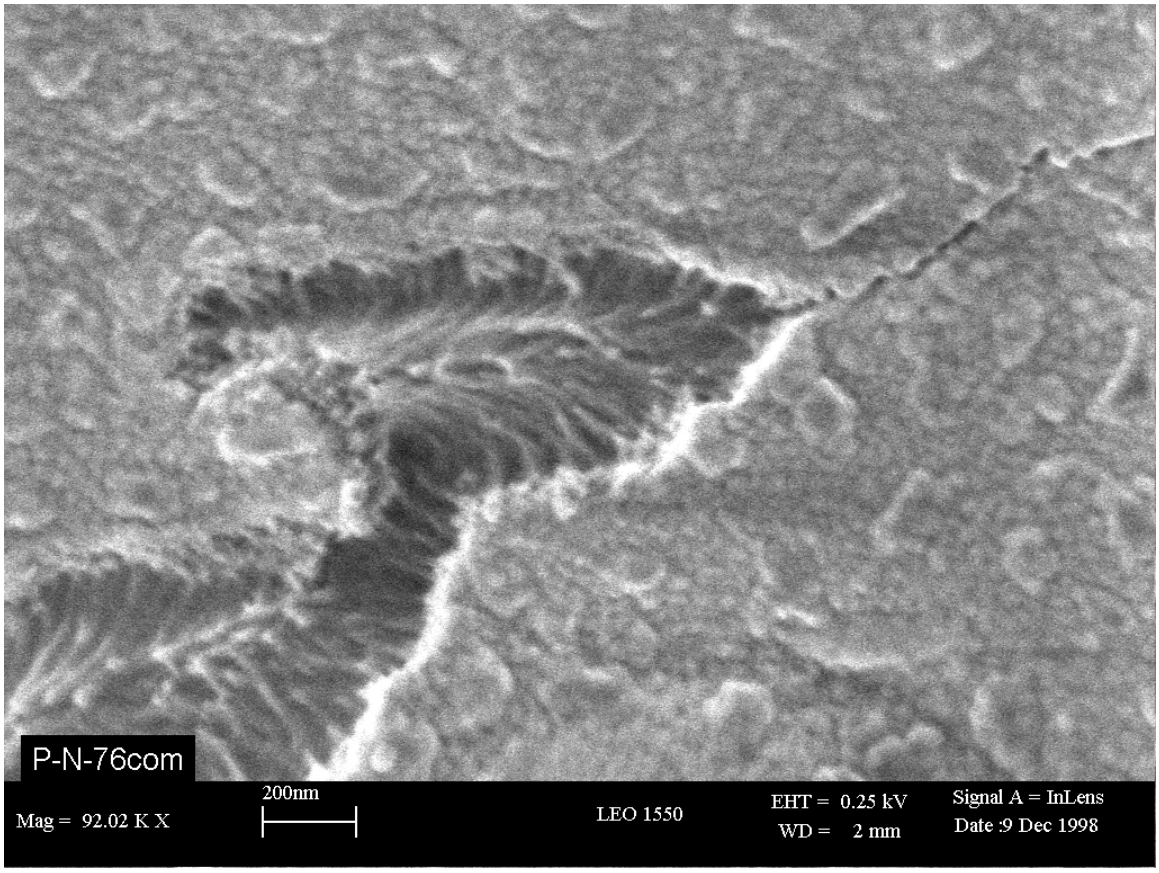

Figure 6.10: Field emission SEM of the adhesive failure surface of a PETI-5 NCA specimen.

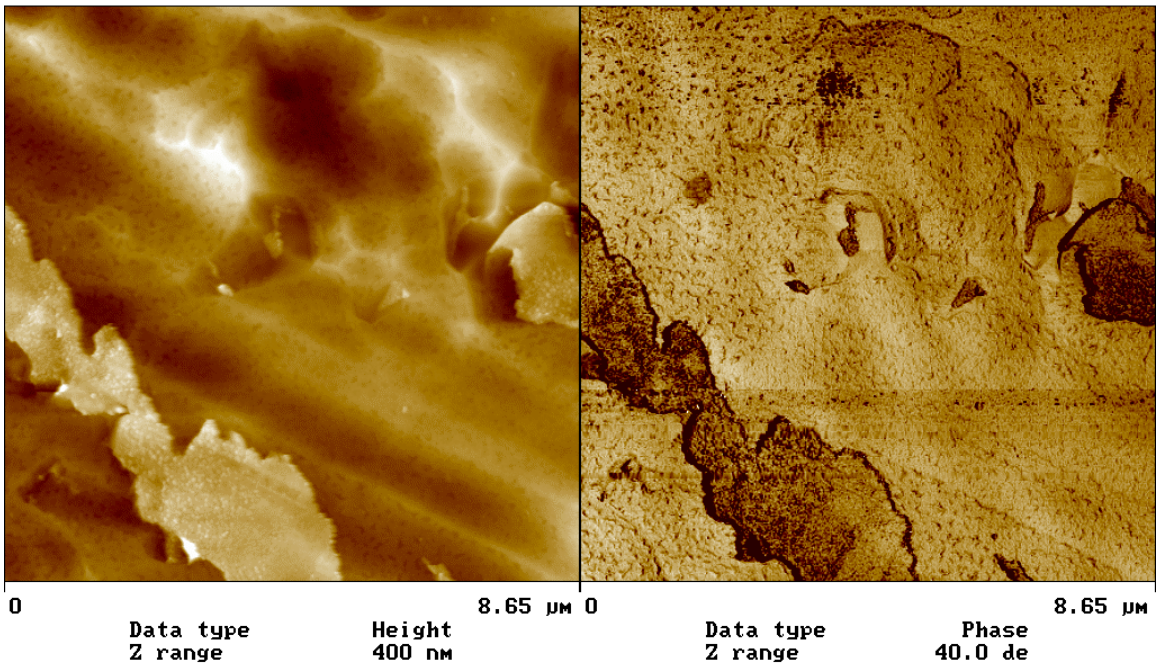

Figure 6.11: Height (left) and phase (right) atomic force microscopy images of the metal failure surface of a PETI-5 NCA specimen

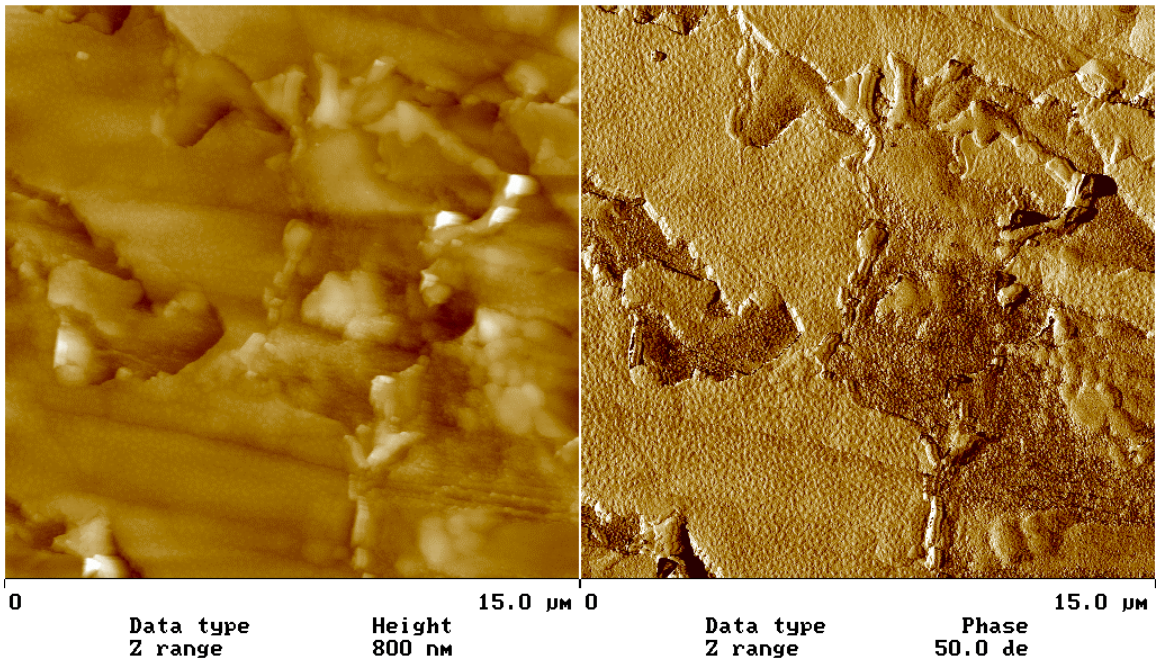

Figure 6.12: Height (left) and phase (right) atomic force microscopy images of the adhesive failure surface of a PETI-5 NCA specimen.

(a)

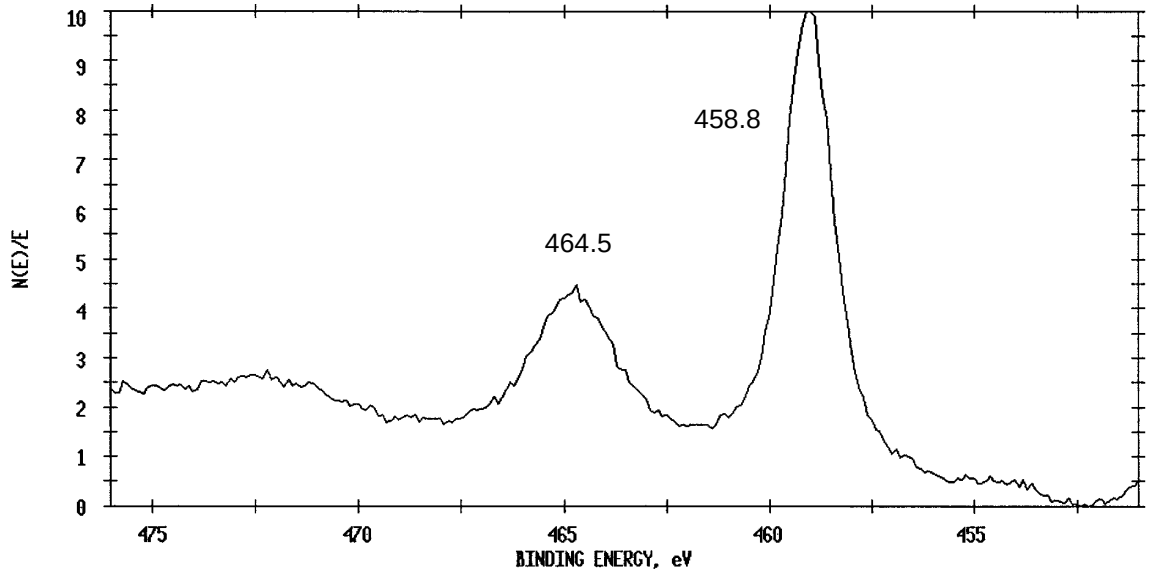

(b)

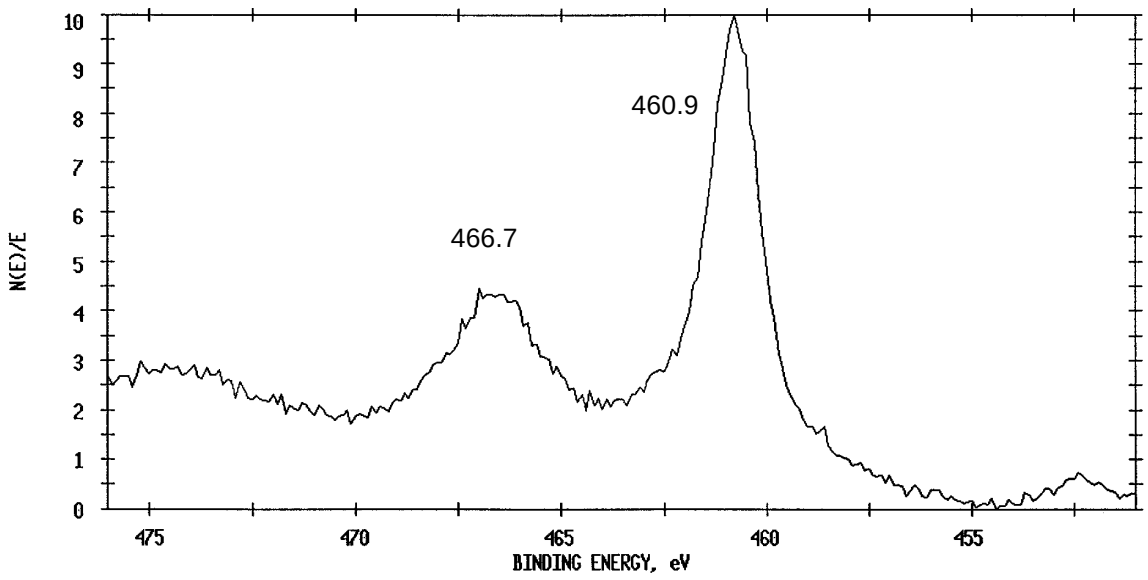

Figure 6.13: Ti $2p_{3/2}$ XPS spectra from (a) PETI-5 metal failure surface and (b) PETI-5 adhesive failure surface. Note: Each spectrum is on a normalized x-axis scale; as shown, peak heights and areas cannot be compared between the two spectra.

(a)

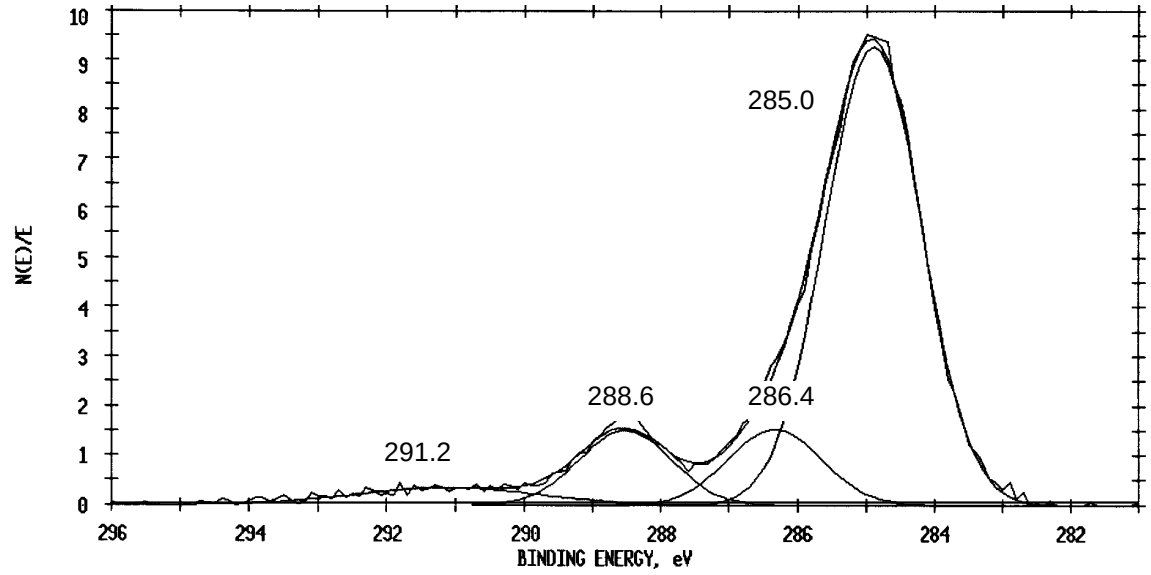

(b)

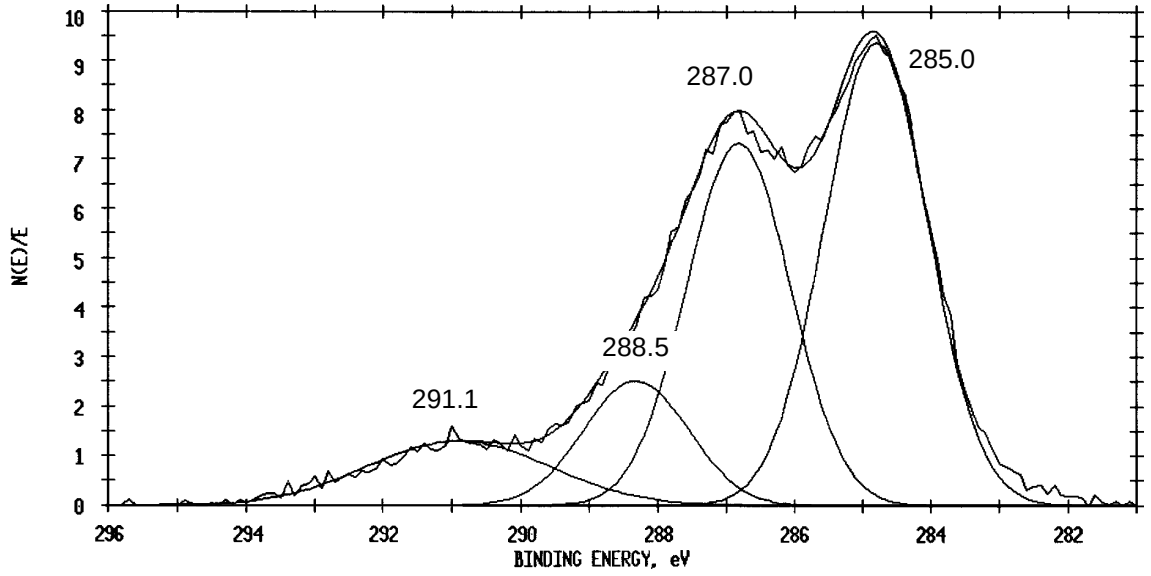

Figure 6.14: C 1s XPS spectra from (a) PETI-5 metal failure surface and (b) PETI-5 adhesive failure surface. Note: Each spectrum is on a normalized x-axis scale; as shown, peak heights and areas cannot be compared between the two spectra.

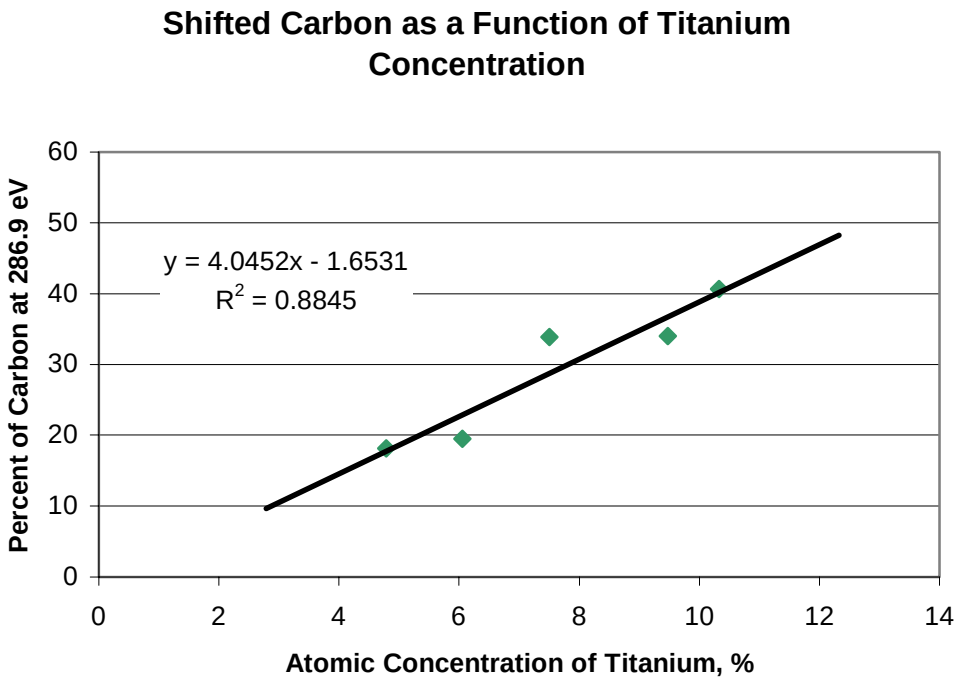

Figure 6.15: From XPS analysis of the PETI-5 adhesive failure surface, percent of the C 1s photopeak that is shifted to 286.9 eV as a function of titanium coverage.

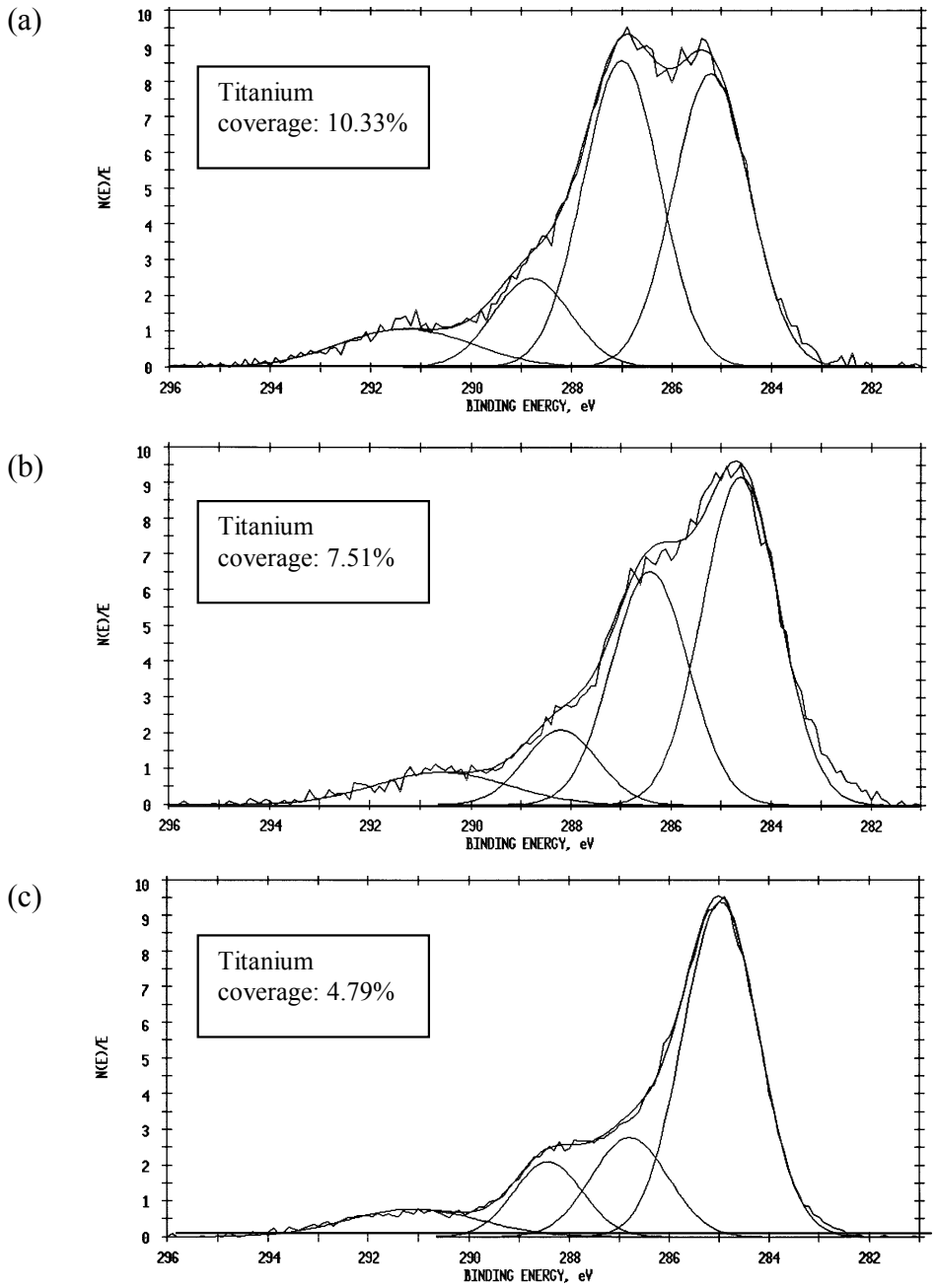

Figure 6.16: C 1s XPS spectra from PETI-5 adhesive failure surfaces with varying titanium coverage. Note: Each spectrum is on a normalized x-axis scale; as shown, peak heights and areas cannot be compared among the three spectra.

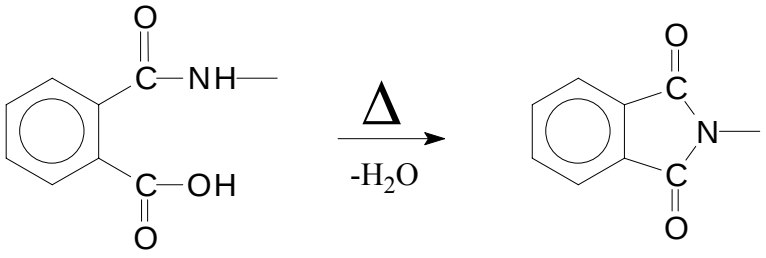

Figure 6.17: Conversion of amic acid groups to imide groups, contained in the backbone of the polyimide adhesives used in the current study.

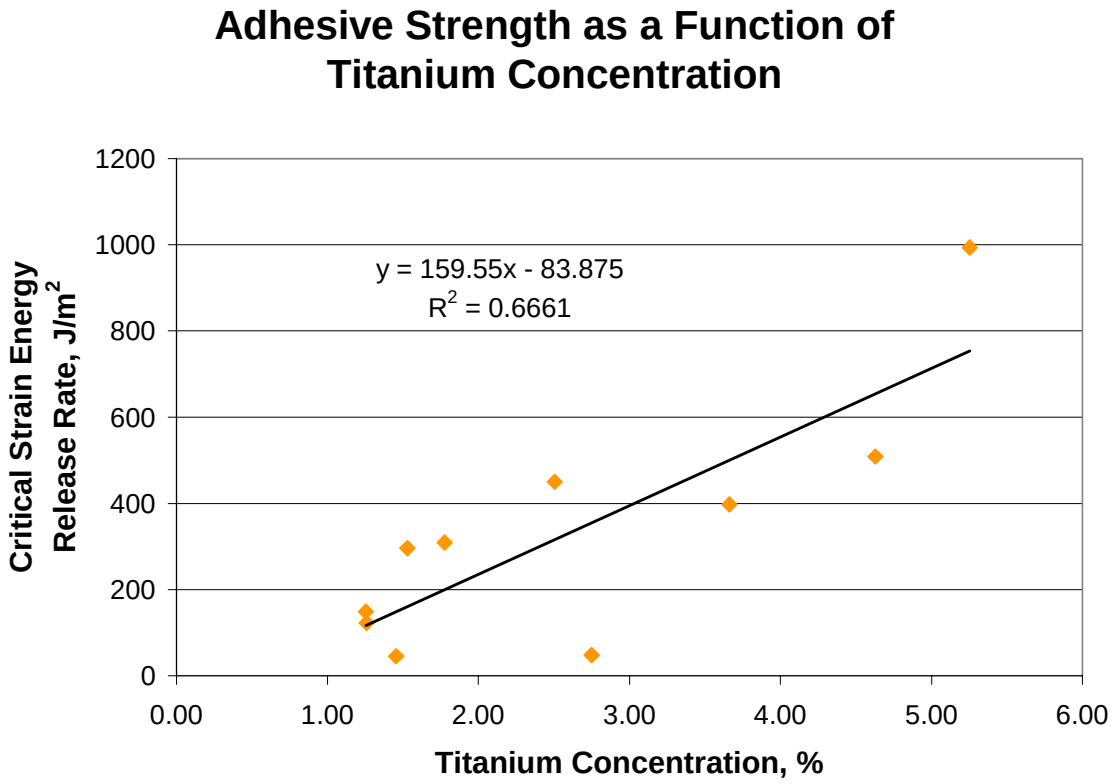

Figure 6.18: Critical strain energy release rate of FM-5 NCA specimens as a function of the average titanium concentration detected on both failure surfaces by XPS.

Chapter 7: PETI-5 Moldings Containing Titanium Dioxide Filler

7.1 Introduction

To investigate the effect of the titanium substrate surface on PETI-5 at the adhesive/substrate interphase, titanium dioxide filler particles were blended with PETI-5 and bulk molded samples were fabricated. Amorphous titanium dioxide was used to mimic the oxide found on the surface of CAA titanium, and a high surface area, 150 to 250 m^2/g, maximized the contact between polymer and titanium dioxide. The effect of titanium dioxide on the cure of PETI-5's phenylethynyl end groups was studied using IR spectroscopy and DSC. In addition, fully cured molded samples of PETI-5/TiO_2 were analyzed and compared to neat PETI-5, and the effect of elevated temperature aging on the molded samples was investigated.

An important assumption is made in the selection of this model system: that the surface of amorphous titanium dioxide filler accurately represents the surface of CAA Ti-6Al-4V. From XPS analysis of the CAA substrate surface, it is known that this is not strictly true. As mentioned in Chapter 5 and Chapter 6, aluminum oxide and fluoride ion are present on the surface of the CAA substrate surface. The aluminum and fluorine components of the CAA substrate surface are not present in the model system. It was

believed that, as a first approximation, analysis of the interaction between PETI-5 and titanium dioxide would provide valuable information regarding the interphase, without creating an overly complex system. Addition of Al_2O_3 and fluoride ion is recommended as future work in this area.

7.2 PETI-5/TiO_2 Cure Study

Plaques of neat PETI-5 and PETI-5/TiO_2 (16% TiO_2 w/w) were made by molding the respective powders at 371°C for one hour, curing the phenylethynyl end groups. The molding procedure is described in Chapter 3. To investigate the effect of TiO_2 on the cure of phenylethynyl end groups, PETI-5 and PETI-5/TiO_2 samples were studied as a function of cure time. Small quantities (10-15 mg samples) of uncured PETI-5 powder and PETI-5/TiO_2 powder, prepared as described in Chapter 3, were heated to 250°C, held for 1 hour, heated to 371°C, and held for 0, 10, 20, 40, or 60 minutes. A TGA was used as the furnace, and samples were cured in flowing nitrogen. This is a slight change from the molded samples, which were cured in a vacuum hot press. Since both atmospheres are inert, however, the cure chemistry of the PETI-5 is believed to be unaffected by this difference. The TGA samples, at various degrees of cure, were analyzed by DSC and diffuse reflectance IR spectroscopy. Previous work by Wood[88] has shown that as the T_g of PETI-5 increases with cure time, the characteristic phenylethynyl IR peak decreases in intensity. Simultaneously, the peak position is shifted to lower wavenumbers. The current study will investigate the effect of titanium dioxide filler particles on the cure of PETI-5.

7.2.1 Infrared Spectra

The carbon-carbon triple bonds present in the terminal phenylethynyl groups of uncured PETI-5 exhibit a distinct band in the 2215 – 2195 cm^{-1} region of the infrared spectrum, arising from stretching vibrations.[106] Figure 7.1 is an example infrared spectrum of uncured neat PETI-5. In general, the intensity of the carbon-carbon triple bond stretching vibrations varies considerably. The more asymmetric the substitution, the stronger the intensity. In uncured PETI-5, the asymmetric substitution of one phenyl ring offset by

the remainder of the 5,000 g/mol oligomer results in a sharp band of medium intensity. The band at 3070 cm^{-1} is associated with aromatic C-H stretches. Bands at 1590, 1508, and 1489 cm^{-1} arise from vibrations of the benzene nucleus in the PETI-5 backbone.[106] Bands characteristic of imides are seen at 1772 and 1716 cm^{-1}.[107]

Subtle differences were observed in the infrared spectra of PETI-5/TiO_2 compared to those of neat PETI-5. These differences were consistent with the addition of a spectrum of TiO_2 to that of PETI-5. A spectrum of the amorphous TiO_2 used for this experiment is shown in Figure 7.2. Typical of most inorganic compounds, few intense or distinctive bands are produced by TiO_2 in the mid-infrared region. The broad band at 3200 cm^{-1} is related to intermolecular hydrogen bonded hydroxyl groups.[106] These hydroxyl groups are assumed to be the result of adsorbed water on the titanium dioxide surface. The peaks observed in the 1000 to 1600 cm^{-1} region are likely the result of surface contamination, which may be displaced as a result of blending with PETI-5 amic acid solution. Evidence of these peaks in the blended PETI-5/TiO_2 spectrum, Figure 7.3, is not observed. However, the mixture created increased absorbances throughout the spectrum, particularly above 2500 cm^{-1} and below 1000 cm^{-1}, due to the additive nature of Beer's law concerning the absorbance of overlapping spectral bands.[108] Note: the peaks observed at 1660 to 1680 cm^{-1} in Figure 7.3, not present in Figure 7.1, are related to a small amount of residual NMP in the uncured material and should not be interpreted as a chemical difference between the two polymer systems.

The phenylethynyl peaks of neat PETI-5 and TiO_2-filled PETI-5 at various stages of cure are shown in Figure 7.4 and Figure 7.5, respectively. The aromatic peak at 1590 cm^{-1}, indicated in Figure 7.1 and Figure 7.3, is used as an internal reference when calculating quantitative ratios indicating height changes of the phenylethynyl peak of PETI-5 (2215 - 2195 cm^{-1}). The relative heights of the phenylethynyl peaks of neat and TiO_2-filled PETI-5 are given as a function of cure time at 371°C in Figure 7.6.

The band resulting from the phenylethynyl group of PETI-5 decreases in height as the polymer is cured. Though the exact molecular structure of cured PETI-5 is unknown, this decline is suspected to occur because free radical reactions transform the carbon-carbon

triple bonds of the PETI-5 terminal groups into chain extended and cross-linked conformations.

TiO_2-filled PETI-5 exhibits a similar decline in height of the weak band associated with the phenylethynyl group as does neat PETI-5, although the relative peak heights of PETI-5/TiO_2 samples are slightly higher than those of neat PETI-5 at short cure times. Despite a slight overlap in the error bars, analysis of variance fit to all data points results in a p-value of 0.03 with regard to the peak height of PETI-5 versus that of PETI-5/TiO_2. This indicates a 97% chance that the difference between peak heights at all cure times is statistically significant. This indicates that the addition of TiO_2 may have altered the reaction mechanism of the phenylethynyl end groups. This could lead to a polymer with a different molecular weight and/or crosslink density, which would have a significant impact on the properties of the polymer in the interphase region.

Further evidence of an altered cure mechanism in the presence of TiO_2 is seen when investigating the position of the phenylethynyl peak. In Figure 7.7, the phenylethynyl peak position is plotted as a function of cure time at 371°C. Although the peak positions of neat PETI-5 and PETI-5/TiO_2 are essentially the same at hold times of 0 and 60 minutes, the PETI-5/TiO_2 peak occurs at higher wavenumbers at intermediate times. In Figure 7.8, the phenylethynyl peaks of neat PETI-5 and PETI-5/TiO_2 are displayed at hold times of 10, 20, and 40 minutes. At these intermediate hold times, the shift in peak position of neat PETI-5 to a lower wavenumber is illustrated. Despite these differences, the same low-intensity peak is present in PETI-5 and PETI-5/TiO_2 after a 60 minute hold at 371°C. The differences in peak intensity and position as a function of cure time, however, indicate that PETI-5 cures by a different mechanism in the presence of TiO_2.

7.2.2 Differential Scanning Calorimetry

The glass transition temperatures of PETI-5 and PETI-5/TiO_2 samples increase as they are cured at 371°C for longer times, as illustrated in Figure 7.9. This is indicative of increased molecular weights and/or greater cross-link density of the polymer chains as the polymer becomes fully cured. T_g values for the TiO_2-filled PETI-5 samples were slightly lower than were those of the neat PETI-5 samples, 3.8 ± 0.5°C lower on average.

This is consistent with the IR data, which indicate a change in the cure mechanism of PETI-5 in the presence of TiO_2. In fact, if the polymeric component of PETI-5/TiO_2 were identical to neat PETI-5, the filled polymer would be expected to have a higher T_g than the neat material. Chain pinning and adsorption of polymer molecules on filler particles restrict the mobility of polymer chains and thus, more thermal energy is required for the glass transition to occur. Therefore, the actual depression in the T_g in the presence of TiO_2 may be higher than the 3.8°C observed here.

7.3 PETI-5 and PETI-5/TiO_2 Molded Samples

Molded plaques were made from PETI-5 and from PETI-5 blended with titanium dioxide powder. The blended samples simulated the PETI-5/TiO_2 interphase of adhesively bonded specimens, allowing bulk characterization of this region through DSC, DMTA, extraction, and IR spectroscopy.

7.3.1 Differential Scanning Calorimetry

There were significant differences between the neat and TiO_2-containing plaques. Although they were fabricated under identical conditions, the plaques made with TiO_2 contained voids and were brittle, in contrast to the neat PETI-5 plaques. The glass transition temperature of the PETI-5/TiO_2 plaques was substantially lower, 246 ± 2°C, versus 265 ± 1°C in the neat PETI-5 plaques. This is a much larger T_g discrepancy than that observed during the cure study of PETI-5 and PETI-5/TiO_2. The T_g of molded PETI-5 is the same as that of PETI-5 cured for one hour in a TGA for the cure study. In contrast, the T_g of molded PETI-5/TiO_2 is considerably lower than that of PETI-5/TiO_2 cured in the TGA for one hour, 261 ± 1°C. Thus, it appears that curing small samples in the TGA does not accurately represent the stages of cure during the molding process. An aspect of the molding process that could not be replicated in the TGA is the application of pressure following the hour hold at 250°C. The purpose of the hold is to remove volatiles before applying pressure, preventing the formation of voids in the molded samples. However, the TGA data collected during the partial cures indicates the samples are still losing weight, presumably due to solvent volatilization after completion of the hold at

250°C. In subsequent stages of the curing procedure, the PETI-5/TiO_2 samples lose an additional 2.1 ± 0.5% of their mass, while the PETI-5 samples lose only 0.5 ± 0.3%. During the molding process, this solvent would remain trapped in the curing polymer due to applied pressure, creating voids in the molded plaque. In addition, exposure to NMP vapor at 371°C (or the degradation products of NMP) could lead to degradation of the polymer backbone. For example, an oxidized form of NMP is expected to form at elevated temperatures in the presence of water or oxygen. This oxidized form of NMP could then react with any carbon-carbon double bonds that remain in the backbone of PETI-5 after the reaction of phenylethynyl groups. Oxidation of these double bonds could then lead to bond cleavage and thus, a reduction in molecular weight. A reaction of this type may be responsible for the vast differences in properties observed between the PETI-5 and PETI-5/TiO_2 molded samples.

7.3.2 Dynamic Mechanical Thermal Analysis

7.3.2.1 Glass Transition

The decreased glass transition temperature, detected by DSC, was confirmed by DMTA. The glass transition regions of neat PETI-5 and PETI-5/TiO_2 DMTA scans at 1 Hz are illustrated in Figure 7.10. The glass transition temperature, as determined by the peak of the loss modulus at 1 Hz, is 276 ± 3°C in neat PETI-5 and 258 ± 3°C in PETI-5/TiO_2. Note: data points were taken every 3°C in all DMTA scans. Therefore, all temperatures from DMTA data represent a minimum error of ± 3°C.

In addition to the difference in the glass transition temperature, two distinct differences between the tan delta spectra of neat and TiO_2-filled PETI-5 are noted, as displayed in Figure 7.11. To illustrate the reproducibility obtained, data from two samples of each type are presented. In addition to a lower T_g, the PETI-5/TiO_2 samples exhibit a suppressed beta transition magnitude (between 25 and 200°C) and a shoulder on the glass transition peak (between 300 and 400°C). The beta transition will be discussed in Section 7.3.2.2. The shoulder observed on the tan delta peak is similar to the "second T_g" observed by Tsagaropoulos and Eisenberg,[109, 110] in dynamic mechanical tan delta data of several polymers filled with 7 nm silica particles. They attribute the additional transition

to the reduced mobility of polymer chains bound to the surface of the silica. While Tsagaropoulos and Eisenberg saw two distinct peaks in their tan delta spectra, the same effect is believed to be causing the shoulder in the current study. Reduction of the transition from a distinct peak to the shoulder observed here is indicative of a smaller change in mobility between the loose and bound polymer chains. This could imply that the polymer chains do not interact as strongly with the filler in the current study. Alternatively, the stiff aromatic backbone of PETI-5 may not undergo as large of a decrease in mobility when bound to a filler particle as the relatively flexible polymers studied by Tsagaropoulos and Eisenberg, such as poly(vinyl acetate) and poly(dimethyl siloxane).

Part of the evidence presented by Tsagaropoulos and Eisenberg that the second tan delta peak is a T_g is the high activation energy of the transition, 110 to 460 kJ/mol, depending on the polymer used and the filler content. Activation energies of the main T_g and the shoulder in the current study were calculated. The tan delta data in the region from 200° to 400°C was fitted to two overlapping Gaussian peaks. Peak maxima of the main T_g and the shoulder at multiple frequencies were then used to calculate the activation energies of each transition. The main T_g had an activation energy of 660 kJ/mol, while the shoulder had an activation energy of 445 kJ/mol. This is consistent with the trend observed by Tsagaropoulos and Eisenberg, in which the second transition has a lower activation energy than the primary T_g. The detection of a T_g of the constrained phase illustrates that the polymer/filler interphase can be studied by DMTA in the PETI-5/TiO_2 molded samples, which is a primary goal of the current study.

Typical results of addition of filler to a polymer, as discussed in Chapter 2, include an increase in the height of the tan delta peak at the T_g and an increase in the breadth of the glass transition. To determine if these effects are present in addition to the shoulder on the tan delta peak, the magnitude of the tan delta peak and the KWW β parameter, which characterizes the breadth of the relaxation distribution, were evaluated. The average tan delta peak height of neat PETI-5 at 1 Hz is 0.72 ± 0.06, while that of PETI-5/TiO_2 is 0.82 ± 0.07, indicating no significant difference between the two. An average β of 0.265 ± 0.005 for PETI-5 and 0.268 ± 0.008 for PETI-5 indicate that the addition of TiO_2 does

not affect the breadth of the glass transition relaxation. Superposed loss modulus curves were used to calculate the KWW parameter, β, which characterizes the breadth of the glass transition. In the temperature region in which the shoulder appears on the tan delta peak, time-temperature superposition could not be achieved. This indicates that several different relaxation mechanisms are occurring simultaneously in this temperature region. Thus, the shoulder region could not be included in the calculation of the β parameter. The lack of dependence of β on addition of TiO_2 filler indicates that the breadth of relaxation time for the *unconstrained* phase in the filled specimens is the same as that in neat PETI-5. A β parameter could not be calculated to quantify the breadth of relaxation times for the constrained phase. However, when overlapping Gaussian peaks were fit to the main tan delta peak and the shoulder, as illustrated in Figure 7.12, it is clear that the shoulder is considerably more broad than the main tan delta peak. This is interpreted as a broader distribution of relaxation times in the constrained phase, as one would expect. The chain segments closest to sites that are bound to filler particles would have more limited mobility than segments farther from bound sites. This further confirms the interpretation that the shoulder on the tan delta peak is the glass transition of the interphase material, the polymer chains that are bound to TiO_2 filler particles.

7.3.2.1.1 Calculation of the KWW β Parameter

Multifrequency sweeps between 0.1 and 30 Hz, as seen in Figure 7.13, neat PETI-5, and Figure 7.14, PETI-5/TiO_2, allowed time-temperature superposition of the DMTA data. Master curves and shift factor plots of neat PETI-5 and PETI-5/TiO_2 are presented in Figure 7.15 and Figure 7.16. Excellent fits to the Williams-Landel-Ferry (WLF) equation were achieved, as seen in the shift factor plots. Average WLF constants of $C_1 = 14 \pm 1$ and $C_2 = 64 \pm 1$ for neat PETI-5 and $C_1 = 13 \pm 1$ and $C_2 = 70 \pm 7$ were calculated. These values are reasonably close to the "universal" values of $C_1 = 17.4$ and $C_2 = 51.6$.[111] As with the β parameters, no significant differences were seen between the neat and filled materials.

In the calculation of β, superposed loss modulus data were first fitted using the Havriliak-Negami equation,

$$\frac{E^* - E'_o}{\Delta E'} = \frac{1}{\left(1 + (i\omega\tau)^{\alpha}\right)^{\gamma}} \qquad \textit{Equation 7.1}$$

where E^* = complex modulus, E'_o = short time modulus, $\Delta E'$ = short time minus long time storage modulus, ω = frequency, radians per second, τ = characteristic relaxation time, and α and γ are fitting parameters.

Calculations of α, γ, τ, and $\Delta E'$, using Havriliak-Negami fits to neat PETI-5 and PETI-5/TiO_2 superposed loss modulus data, are illustrated in Figure 7.17 and Figure 7.18. The calculated α, γ, and τ parameters are input to the autocorrelation function,

$$\phi(t) = \int_0^{\infty} \frac{E''(\omega)}{\Delta E'} \frac{\cos \omega t}{\omega} dt \,, \qquad \textit{Equation 7.2}$$

outputting $\phi(t)$ as a function of t for times $t = 10^{-11}$ to $t = 10^{11}$ seconds. The Mathematica program used for this calculation is listed in Appendix A. The autocorrelation function is then fitted using the KWW equation,

$$\phi(t) = \exp\left(-\left(\frac{t}{\tau} \right)^{\beta} \right), \qquad \textit{Equation 7.3}$$

allowing the calculation of τ, the characteristic relaxation time, and β, the fitting parameter that characterizes the breadth of the relaxation distribution. Examples of the KWW equation fitted to PETI-5 and PETI-5/TiO_2 data are shown in Figure 7.19 and Figure 7.20.

7.3.2.2 Beta Transition

As seen in Figure 7.11, the magnitude of the beta transition is suppressed in the PETI-5/TiO_2 samples when compared to the neat PETI-5 samples. The magnitude of tan delta

at the maximum of the beta transition is 0.030 ± 0.001 for neat PETI-5, and 0.021 ± 0.002 for PETI-5/TiO_2. As discussed in Chapter 2, the magnitude of the beta transition is frequently related to the toughness. This is consistent with the current data, since the PETI-5/TiO_2 samples were qualitatively determined to be much more brittle than the neat PETI-5 specimens. For example, the PETI-5/TiO_2 samples were prone to break while individual samples were cut from the molded plaques, while the neat PETI-5 plaques were not. The suppressed beta transition could be an effect of changes in the backbone structure, crosslink density, or molecular weight of the polymeric component of PETI-5/TiO_2 molded samples, i.e. the same changes that may be contributing to the decreased glass transition temperature in these samples. Alternatively, the small-scale molecular motions that are responsible for the beta transition may be hindered by adsorption of the polymer chains to the TiO_2 filler particles. Fewer chains participating in the beta transition would readily explain the decreased magnitude of the transition.

7.3.3 Solvent Uptake and Extraction

PETI-5 and PETI-5/TiO_2 samples at all aging conditions were immersed in NMP at 50°C for 7 days, weighed periodically, and weighed again after drying in a vacuum oven. This gave two pieces of information, the amount of solvent absorbed by a sample and the percent of material that is extractable, or soluble in NMP at 50°C. Both are expected to be inversely proportional to the amount of crosslinking and/or the amount of high molecular weight material in the polymer. The amount of solvent uptake and the percent of material extracted were dramatically different for the neat versus TiO_2-filled moldings. Neat PETI-5 specimens exhibited very little swelling upon immersion in NMP, with a 1.5 ± 1% weight gain. The weight gain of PETI-5/TiO_2 samples ranged from 50 to 165% and was highly dependent on the position within the molded plaque from which the sample had been cut. In general, samples cut from the edges of the molded plaques absorbed less solvent than those from the center of the plaque. This supports the hypothesis that trapped NMP is contributing to the degradation of PETI-5 in the TiO_2-filled moldings. Diffusion would have allowed the NMP vapor around the edges of the mold to escape, while that in the center remained trapped.

Following the weight uptake study in NMP, the extracted samples were dried under vacuum at 250°C for three hours, and the total weight loss after extraction of soluble species was determined. The same trend is observed with extractable material and solvent uptake, with the samples that had absorbed the most solvent losing the most weight. 0.75 ± 0.07% of neat PETI-5 specimens was extracted, and 1.4 to 22% of PETI-5/TiO_2 specimens was extracted. This is consistent with the decreased T_g upon addition of TiO_2, since extractable material tends to be lower molecular weight species that also depress the T_g. This trend also indicates that the lower T_g in PETI-5/TiO_2 samples is not simply an effect of trapped NMP behaving as a plasticizer. The PETI-5/TiO_2 samples contain an estimated 2% NMP, and up to 22% of the mass of these samples was extracted.

Gel permeation chromatography was performed on the material extracted from the PETI-5/TiO_2 specimens. Insufficient material for GPC analysis was extracted from the neat PETI-5 samples. By GPC, the material extracted from PETI-5/TiO_2 samples has a number average molecular weight of 4,065 g/mol. Thus, the PETI-5/TiO_2 samples appear to contain a low molecular weight component, up to 22% by weight, that is not present in the neat PETI-5 specimens. The molecular weight of the extracted material is very close to that of PETI-5 before cure, approximately 5,000 g/mol. Knowing that TiO_2 may affect the cure reaction, this could imply that the extracted material consists of PETI-5 chains in which the phenylethynyl end groups did not form chain extended or crosslinked conformations, or that chain scission occurred at the double bonds remaining after the reaction of phenylethynyl groups.

7.3.4 Infrared Spectroscopy

In spite of evidence that the cure mechanism may be altered by the presence of TiO_2, along with evidence by DSC, solvent uptake, and extraction suggesting that the polymer component of PETI-5/TiO_2 is different from that of neat PETI-5, no chemical differences between the molded plaques were detected by IR spectroscopy. The only significant differences between the spectra of neat and TiO_2-filled PETI-5 arise from the increased absorbances above 2500 and below 1000 cm^{-1}. This is consistent with the addition of a

TiO_2 spectrum to that of neat PETI-5, as discussed in Section 7.2.1. Spectra of neat PETI-5 and PETI-5/TiO_2 moldings are presented in Figure 7.21.

If the differences between neat and TiO_2-filled moldings are primarily a result of a change in cure mechanism, it is not surprising that differences are not detected by IR spectroscopy. The only difference observed between uncured and fully cured PETI-5 IR spectra is the change in the phenylethynyl band at 2215 to 2195 cm^{-1}. As this band weakens with cure time, no new band is detected in the mid-IR region. Thus, the disappearance of uncured phenylethynyl end groups can be monitored by IR, but new chemical structures formed are unobservable in the mid-IR region. Another form of spectroscopy, such as Raman or NMR, may be useful in determining what chemical differences between the polymeric components of neat PETI-5 and PETI-5/TiO_2 actually exist.

7.4 Aging PETI-5 and PETI-5/TiO_2 Molded Samples

As a function of aging time at 177° and 204°C, changes in the PETI-5/TiO_2 plaques were observed in weight loss, DSC, and DMTA studies. No significant changes were detected by swelling and extraction studies or IR spectroscopy.

7.4.1 Weight Loss

The weight loss of PETI-5 and PETI-5/TiO_2 is plotted as a function of aging time at 177° and 204°C in Figure 7.22. The weight loss of PETI-5/TiO_2 samples increases as a function of aging time and aging temperature, with more weight lost as a result of aging at 204°C than 177°C. After 90 days at 177°C, PETI-5/TiO_2 samples have lost 0.75 ± 0.09% of their original weight, and 1.75 ± 0.07% after 90 days at 204°C. It is likely that the weight loss represents the loss of trapped NMP in the PETI-5/TiO_2 molded samples. As discussed in Section 7.3.1, trapped NMP is estimated to be up to 2% of the sample weight prior to aging. In addition to loss of NMP, the evolution of volatiles as a result of polymer degradation could be contributing to the weight loss. In contrast, there was little or no weight loss of neat PETI-5 specimens as a result of elevated temperature aging.

After 90 days, an average weight loss of 0.1 ± 0.1% (i.e. no significant weight loss) after aging at 177°C and 0.09 ± 0.1% after aging at 204°C was observed.

7.4.2 Differential Scanning Calorimetry

From DSC data, two significant pieces of information were obtained: the glass transition temperatures of the samples and the endothermic peak superimposed on the T_g. A small endotherm was observed at the T_g of unaged samples of PETI-5 and PETI-5/TiO_2, as illustrated in Figure 7.23. While the endotherm appears similar to a physical aging enthalpic peak, observing the peak area as a function of aging time leads to the conclusion that the peak is a result of solvent loss as the material undergoes the glass transition. As the mobility of the polymer molecules increases, trapped solvent is released and an endothermic peak results. In Figure 7.24, the areas of the endothermic peaks at the T_g are plotted as a function of aging time. For the neat PETI-5 specimens, the enthalpic peak decreases as a function of aging time. As trapped NMP diffuses out of the samples during aging at 177 or 204°C, the enthalpic peak represents the vaporization of a smaller volume of solvent. After aging the neat PETI-5 specimens for 60 days at 204°C, a physical aging peak begins to form in the low-temperature portion of the glass transition. An example of the first and second heats of PETI-5 at various aging times is shown in Figure 7.25.

The PETI-5/TiO_2 samples have glass transition temperatures approximately 20°C below those of the neat PETI-5 specimens. Thus, they are much closer to their T_g during aging at 177 and 204°C, with an undercooling of 69°C and 42°C, respectively. With a lower undercooling, the PETI-5/TiO_2 samples are expected to undergo physical aging to a greater extent than neat PETI-5. After aging PETI-5/TiO_2 at 204°C for 2 days or longer, the enthalpic peak at the T_g is larger than that of the unaged samples. This enthalpic peak is believed to result from the addition of NMP volatilization and a physical aging endotherm. Between aging times of 2 and 90 days, the endotherm remains approximately constant. This is consistent with the expected trends, with a higher contribution from physical aging and, simultaneously, a lower contribution from NMP volatilization as aging time increases.

Glass transition temperatures (second heat) of all samples are presented as a function of aging time in Figure 7.26. While the T_g of neat PETI-5 remains constant during aging at 177° or 204°C, the T_g of PETI-5/TiO_2 increases significantly in the first 30 days at 204°C. A slight increase in T_g is observed after aging PETI-5/TiO_2 at 177°C.

As a function of aging time, glass transition temperatures would be expected to increase as a result of solvent loss and physical aging. To distinguish between these phenomena, first and second heat T_gs are investigated. First and second heat T_gs of PETI-5/TiO_2 samples aged at 204°C are presented as a function of aging time in Figure 7.27. Samples were first heated to 300°C, quenched, and heated through the T_g a second time. The T_gs from both heats show a clear increase as a function of aging time. While a T_g increase from loss of residual NMP during aging would be detected in both heats, a T_g increase as a result of physical aging is recoverable upon heating above the T_g. Thus, the higher T_g would only be detected in the first DSC scan. From Figure 7.27, it is clear that the T_g increase in PETI-5/TiO_2 aged at 204°C is irreversible, although the enthalpic peak at the T_g is reversed on the second heat. A difference in the calculated T_g from the first and second scan can arise from the difference in the shape of the T_g region due to the enthalpic peak in the first heat. Figure 7.28, which displays the first and second DSC scans of PETI-5/TiO_2 samples after various aging times at 204°C, demonstrates that the T_g remains relatively constant after an initial heat to 300°C. Thus, it can be concluded that the increase in T_g of PETI-5/TiO_2 as a function of aging time is irreversible, probably due to solvent loss. Although there is evidence of physical aging from the enthalpic peak superimposed on the glass transition, physical aging has not caused a significant increase in T_g at these aging times.

7.4.3 Dynamic Mechanical Thermal Analysis

7.4.3.1 Glass Transition

The increase in glass transition temperature of PETI-5/TiO_2 as a function of aging time at 204°C, as detected by DSC, is confirmed by DMTA. DMTA loss moduli of these samples at 1 Hz is presented in Figure 7.29 at aging times up to 90 days. After 90 days of

aging at 204°C, the T_g has increased from 258 ± 3°C to 267 ± 3°C, as measured by the maximum of the loss modulus peak.

As with the unaged samples, no significant differences were detected in the height of the tan delta peak or KWW β parameter as a function of aging time. However, the shoulder that appears on the high temperature side of the tan delta T_g peak has undergone significant changes as a function of aging. In Figure 7.30, the tan delta spectra of unaged neat PETI-5 and PETI-5/TiO_2 are contrasted with those aged for 7, 30, and 90 days. After 30 days of aging at 204°C, the shoulder of PETI-5/TiO_2 has decreased to the point that it is almost indistinguishable from that of neat PETI-5. Since tan delta is a ratio of the loss modulus to the storage modulus, it is instructive to look at these spectra as well. In Figure 7.31, the storage and loss moduli of neat PETI-5 and PETI-5/TiO_2, unaged and aged for 90 days at 204°C, are presented. From this figure, it is clear that the shoulder on the tan delta peak originates from the loss modulus, which plateaus at a higher level than that of neat PETI-5. This is consistent with the assignment of the shoulder to the glass transition of the constrained phase.

A decrease in the magnitude of the shoulder is seen, to a slightly lesser extent, after aging at 177°C rather than 204°C. In Figure 7.32, the corresponding tan delta spectra of samples aged at 177°C are illustrated. After 90 days of aging at 177°C, the shoulder is still present, although the magnitude has decreased considerably. The same changes are observed at the two aging temperatures, however they are occurring more slowly at 177°C, as expected for any thermally activated process. Tsagaropoulos and Eisenberg[109, 110] observe a similar decrease in the magnitude of the second transition after annealing above the T_g. They attribute this effect to the polymer chains loosely bound to the filler particles rearranging and becoming more tightly bound, so that the T_g is suppressed altogether. While this is a reasonable explanation in the case of annealing above the T_g (particularly annealing above the T_g of the constrained phase), it is doubtful that sufficient mobility exists in the bound polymer chains for substantial rearrangement to occur at the aging temperatures used in the current study. The extent of physical aging can be used to gauge the mobility of the PETI-5 polymer backbone while aging. Physical aging is detected by DSC in the PETI-5/TiO_2 samples aged at 204°C for times comparable to

those in which the shoulder on the tan delta peak is observed to decrease. However, this reflects the mobility of the non-bound polymer. Significantly higher aging temperatures (or longer aging times) would be required for the bound polymer to reach the same level of mobility. Further, little or no physical aging is detected by DSC in the PETI-5/TiO_2 samples aged at 177°C, while the shoulder on the tan delta peak is observed to decrease in these samples. Thus, it is concluded that, in the current example, a rearrangement of polymer chains from loosely bound to tightly bound is not a likely cause of the depression in the tan delta shoulder.

On the other hand, loss of residual NMP may decrease the mobility of the loosely bound polymer. Weight loss and an increase in the glass transition temperature as a function of aging time suggest that the PETI-5/TiO_2 samples lose a significant amount of residual solvent during aging. If NMP is plasticizing the bound polymer, the loss of NMP could restrict the mobility of the PETI-5 backbone to the point that the T_g of the constrained phase is suppressed. Alternatively, the decrease in the prominence of the shoulder as a function of aging time could be interpreted as the presence of fewer bound chains. This would imply that the quality of adhesion between polymer and filler has degraded as a result of elevated temperature aging. If this is found to be the case, it would establish an important relationship between the model filled system and the NCA specimens which, as discussed in Chapter 5, exhibit a decrease in adhesive strength as a result of aging at 177°C. Further work in this area is required to determine the cause of the decrease in the magnitude of the tan delta shoulder as a function of elevated temperature aging. Regardless of the cause, the effect has the potential to provide valuable information regarding the effect of aging on the matrix/filler and adhesive/substrate interphase regions.

7.4.3.2 Beta Transition

While the magnitude of the PETI-5/TiO_2 beta transition remains smaller than that of neat PETI-5, its magnitude does not change significantly as a function of aging time. While the shape of the beta transition does change somewhat from sample to sample, no systematic changes are observed as a function of aging time. This may indicate that the

beta transition is not sensitive to loss of residual solvent, the accompanying increase in T_g, physical aging or polymer/filler interactions, all of which are varying systematically with aging time. Alternatively, the transition could be sensitive to two or more of these factors, which have opposing impacts on the beta transition magnitude. For example, fewer bound polymer chains could increase the magnitude of the beta transition, while physical aging simultaneously depressed the magnitude. Multiple events affecting the beta transition would explain the variation in the shape of the tan delta peak at the beta transition.

In contrast, the beta transition of the neat PETI-5 samples is systematically decreasing as a function of aging time at 204°C. This effect can be observed in Figure 7.30, in which the neat PETI-5 beta transition is getting closer to that of PETI-5/TiO_2 as aging time increases. A suppression of the neat PETI-5 beta transition is not observed during aging at 177°C. Physical aging is a likely cause for the observed decrease in the beta transition magnitude. As discussed in Section 7.4.2, a physical aging enthalpic peak is observed by DSC on neat PETI-5 samples after aging at 204°C for 90 days, but not after aging for the same period of time at 177°C. Previous researchers[80, 85] have seen suppressed beta transitions after aging polyimides below their glass transition temperatures. Another possible reason for the observed depression in the beta transition is additional crosslinking during aging at 204°C. Increased crosslink density has also been shown to cause suppression of the beta transition.[74]

7.4.4 Solvent Uptake and Extraction

While the weight uptake and extracted material were consistently much higher in PETI-5/TiO_2 samples compared to neat PETI-5 samples, no trends were observed as a function of aging time for any samples. The variation in weight uptake and extraction as a function of plaque position, as mentioned in Section 7.3.3, continued to be observed in aged specimens. The percent of extractable material in samples of all aging conditions is plotted versus the position in the plaque from which the sample was cut in Figure 7.33. It is apparent that the samples cut from the center of the plaque contained more low molecular weight extractable material, particularly the samples cut from plaque 1 or

plaque 3. As stated previously, this may be the result of trapped NMP leading to a degradation reaction in the polymer backbone during processing, since NMP would have been able to escape from the edges of the mold more easily than from the center. The range of weight uptake and extraction of neat PETI-5 and PETI-5/TiO_2 are presented in Table 7.1 for all sample conditions. Samples aged at 177 and 204°C are combined in the table data for simplicity; no differences were observed as a function of aging temperature. It is apparent from these data that there is a significantly higher weight uptake and percent of extracted material in PETI-5/TiO_2 samples compared to neat PETI-5. This supports the previous discussion of solvent uptake and extraction. As a function of aging time, however, no change in weight uptake or extraction is detected. This is partially a result of the variation among replicate samples, although changes with aging time are still not detected when plaque position is considered.

7.4.5 Infrared Spectroscopy

As with the solvent uptake and extraction data, no changes were detected in the IR spectra of neat PETI-5 and PETI-5/TiO_2 as a function of aging time. Spectra of PETI-5 and PETI-5/TiO_2, unaged and aged for 30 days at 204°C, are presented in Figure 7.34 and Figure 7.35. Considering the changes that were detected as a function of aging time, weight loss and an increase in the glass transition temperature of PETI-5/TiO_2 samples aged at 204°C, the lack of changes detected by IR spectroscopy are not surprising. The weight loss and increase in T_g of PETI-5/TiO_2 are believed to be primarily the result of NMP volatilization during aging at 204°C. Prior to aging, the residual NMP in the cured moldings is at a level too low to be detected by IR. (Note: peaks indicative of residual NMP are observed at 1680-1660 cm^{-1} in Figure 7.3, uncured PETI-5/TiO_2, but not observed in any spectra of cured PETI-5 or PETI-5/TiO_2.) Thus, loss of NMP at the levels at which it exists in molded PETI-5/TiO_2 samples cannot by monitored by IR spectroscopy.

7.5 Conclusions

A cure study of neat PETI-5 and PETI-5 with titanium dioxide filler indicates that the filler affects the cure mechanism of PETI-5. In addition, weight loss due to solvent volatilization indicates that, in the presence of TiO_2 filler, a small amount of residual NMP remains trapped in the PETI-5/TiO_2 plaques during the molding process. The difference in cure mechanism and trapped NMP have a significant impact on the properties of PETI-5/TiO_2 moldings, which exhibit a much lower T_g, absorb more solvent during exposure to NMP, and contain a significant amount of extractable material. In contrast, neat PETI-5 moldings have a higher T_g, absorb very little solvent, and contain very little extractable material.

DMTA reveals information regarding the PETI-5/TiO_2 interphase of the filled samples. Polymer chains bound to TiO_2 filler particles cause a shoulder to appear on the tan delta glass transition peak. This shoulder is significantly reduced after aging at elevated temperatures, and almost eliminated after aging for 90 days at 204°C. A possible interpretation of the reduction in the shoulder is that there are fewer polymer chains bound to the filler particles and thus, a loss of polymer-filler adhesion as a function of aging time.

The influence of titanium dioxide filler on PETI-5 has significant implications regarding adhesive specimens manufactured from PETI-5 and CAA Ti-6Al-4V. The major component of the CAA substrate surface is amorphous titanium dioxide, the same material as the filler used in the current study. The contact between adhesive and substrate is generally in the form of an amic acid primer in NMP applied to the substrate surface. The same amic acid solution in NMP is blended with TiO_2 when manufacturing the current moldings. Thus, if titanium dioxide influences the cure mechanism of PETI-5 and causes residual NMP to remain in the molded samples during cure, the same effects may be seen at the interphase of PETI-5/titanium adhesively bonded specimens. This verifies the importance of considering the effect of the interphase in the analysis of multi-component systems.

The changes in the DMTA data as a function of aging time also have important implications regarding adhesive/substrate systems. Changes in the shoulder on the tan delta peak, which may be related to a decrease in adhesive strength, occur under the same aging conditions as decreases in the strength of adhesively bonded samples were observed, as discussed in Chapter 5. This supports the idea that the interphase region of adhesively bonded samples can be investigated using a model system of an adhesive matrix with filler particles that reproduce the substrate surface.

Table 7.1: Weight uptake of neat PETI-5 and PETI-5/TiO_2 samples after exposure to NMP at 50°C for 7 days, and weight loss after drying the same samples.

Aging time, days	Solvent Uptake, % (w/w)		Extractable Material, % (w/w)	
	Neat PETI-5	PETI-5/TiO_2	Neat PETI-5	PETI-5/TiO_2
0	-0.35 to 1.98%	50 to 166%	0.79 to 0.82%	1.4 to 22%
2	-0.75 to 0.95%	21 to 280%	1.3 to 1.5%	1.9 to 35%
7	-0.54 to 2.0%	12 to 241%	0.46 to 0.72%	0.60 to 32%
30	0.0 to 2.0%	93 to 239%	0.27 to 0.48%	5.3 to 30%
60	1.0 to 3.8%	15 to 112%	0.49 to 1.1%	1.3 to 17%

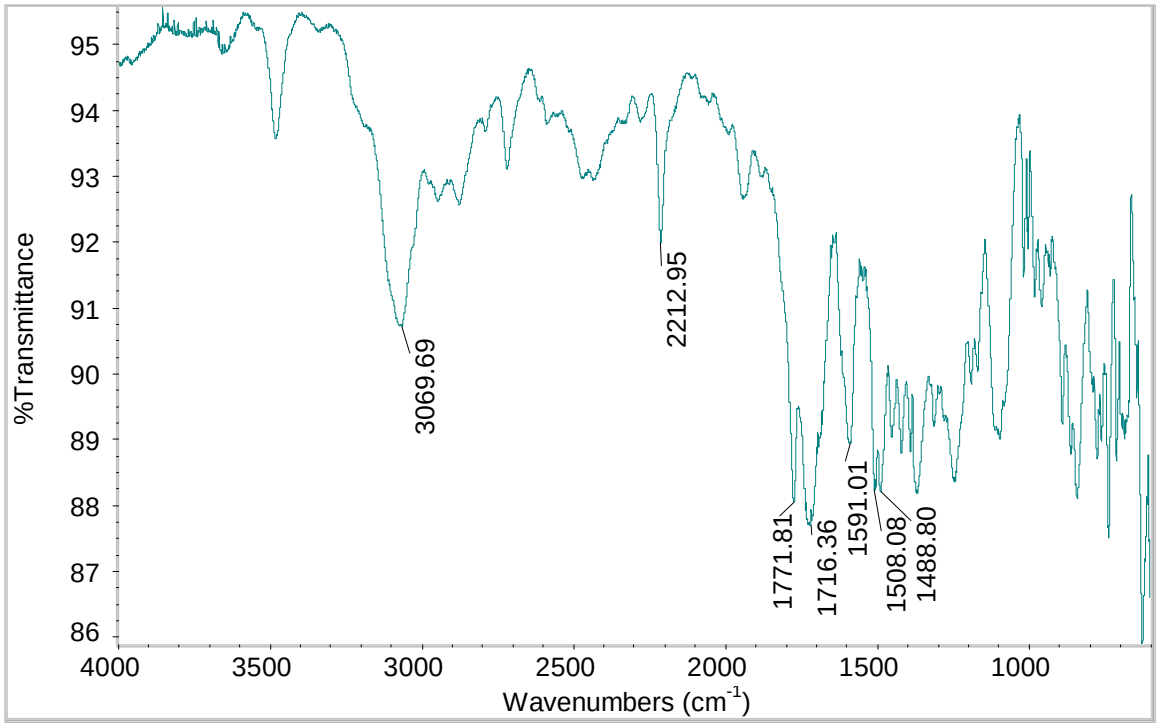

Figure 7.1: Infrared spectrum of uncured neat PETI-5.

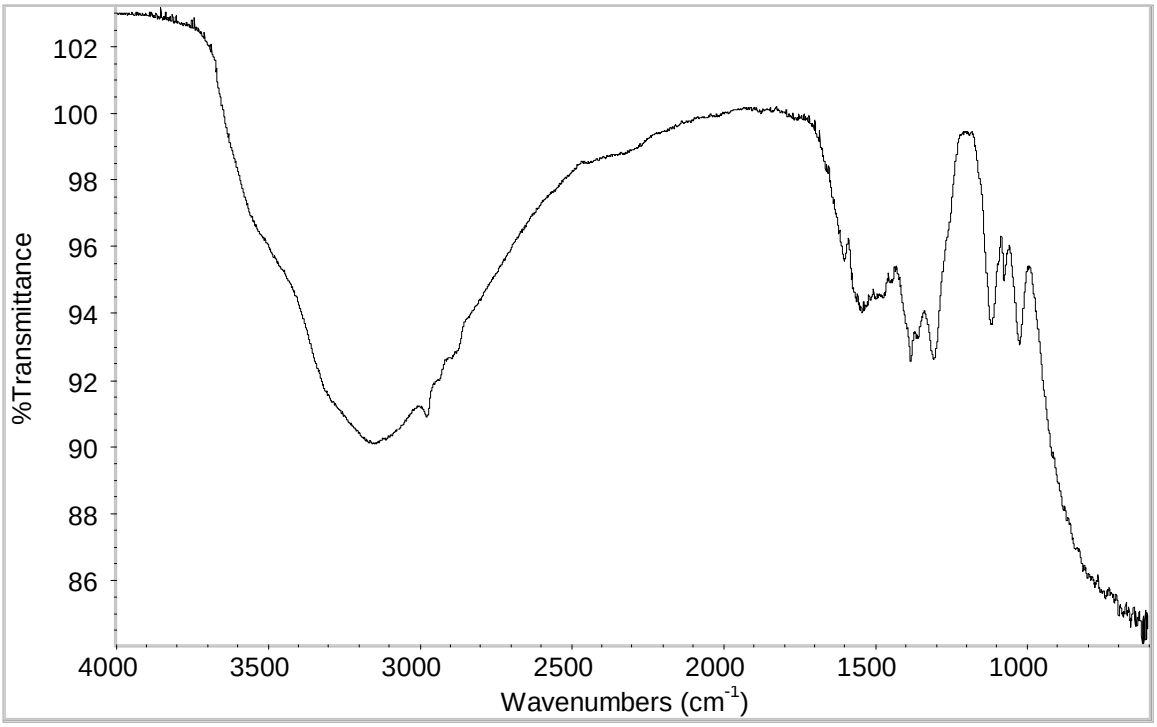

Figure 7.2: Infrared spectrum of amorphous titanium dioxide.

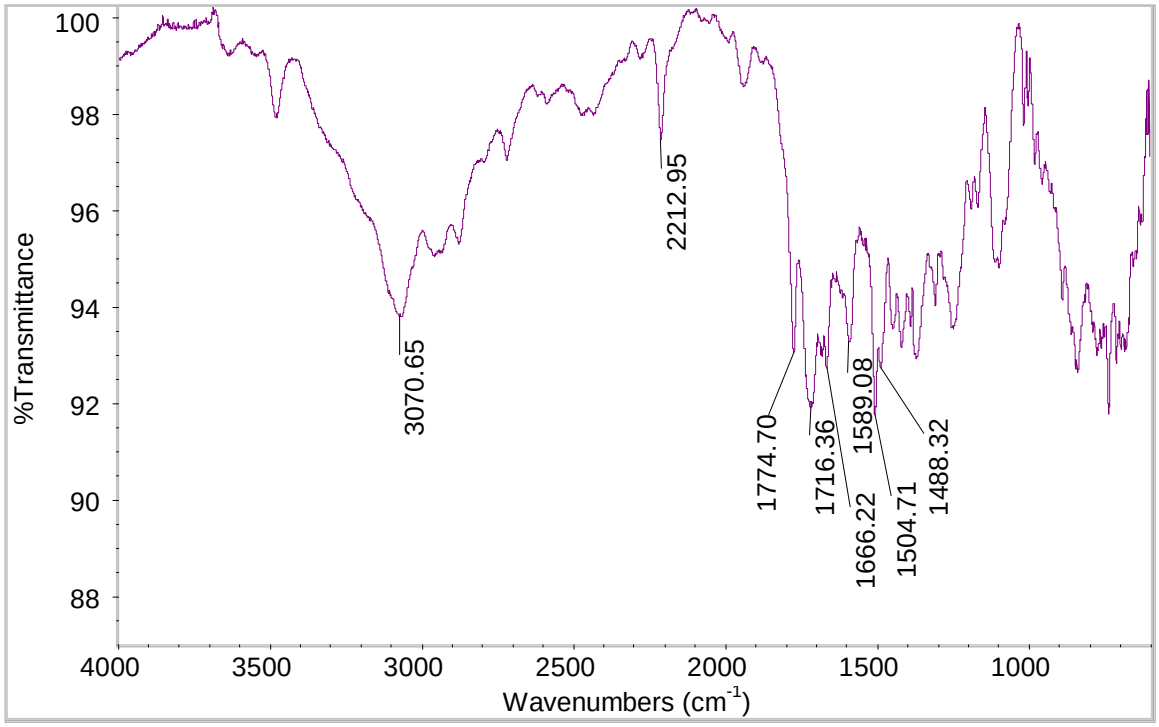

Figure 7.3: Infrared spectrum of PETI-5 blended with titanium dioxide prior to cure.

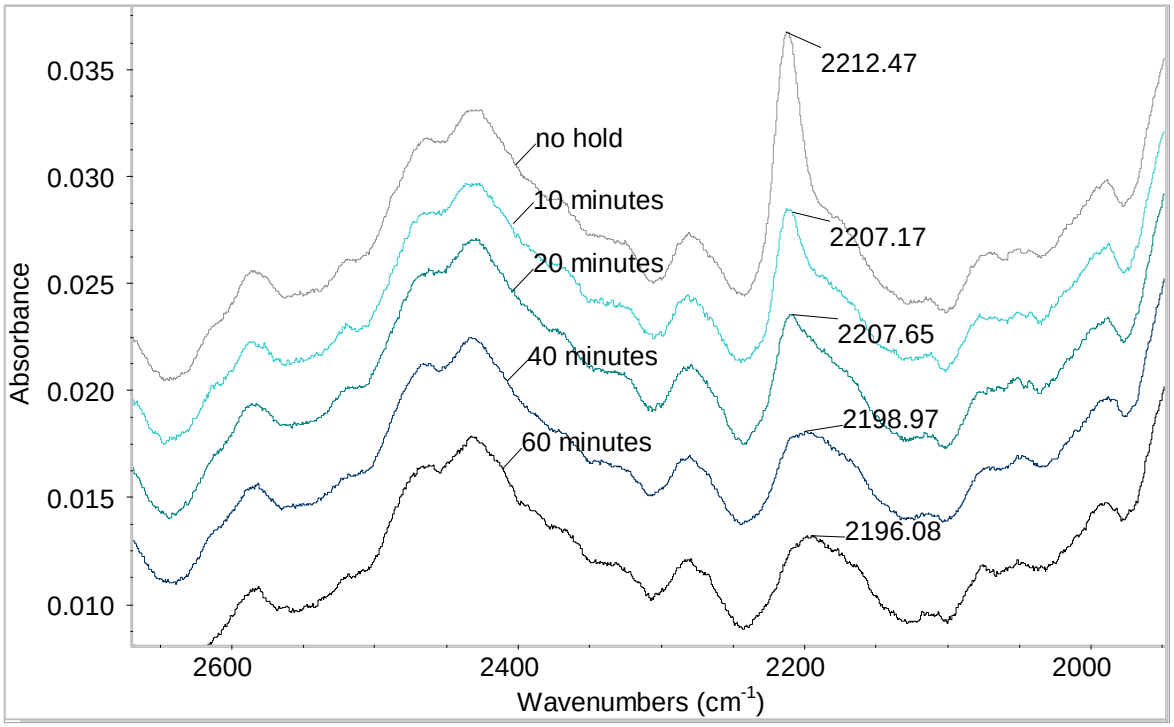

Figure 7.4: Infrared spectrum of PETI-5 at various stages of cure. Note the decrease in peak wavenumber and intensity of the band at 2200 – 2220 cm^{-1} as a function of cure time.

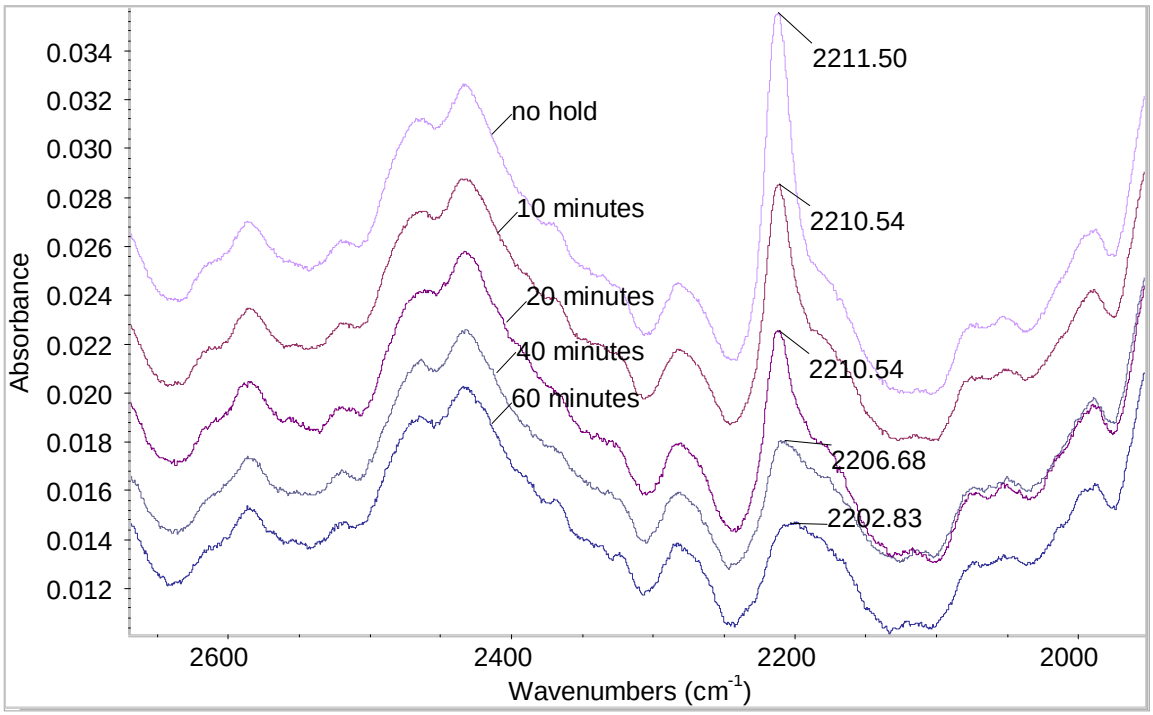

Figure 7.5: Infrared spectrum of PETI-5/TiO_2 at various stages of cure. Note the decrease in peak wavenumber and intensity of the band at 2200 – 2220 cm^{-1} as a function of cure time.

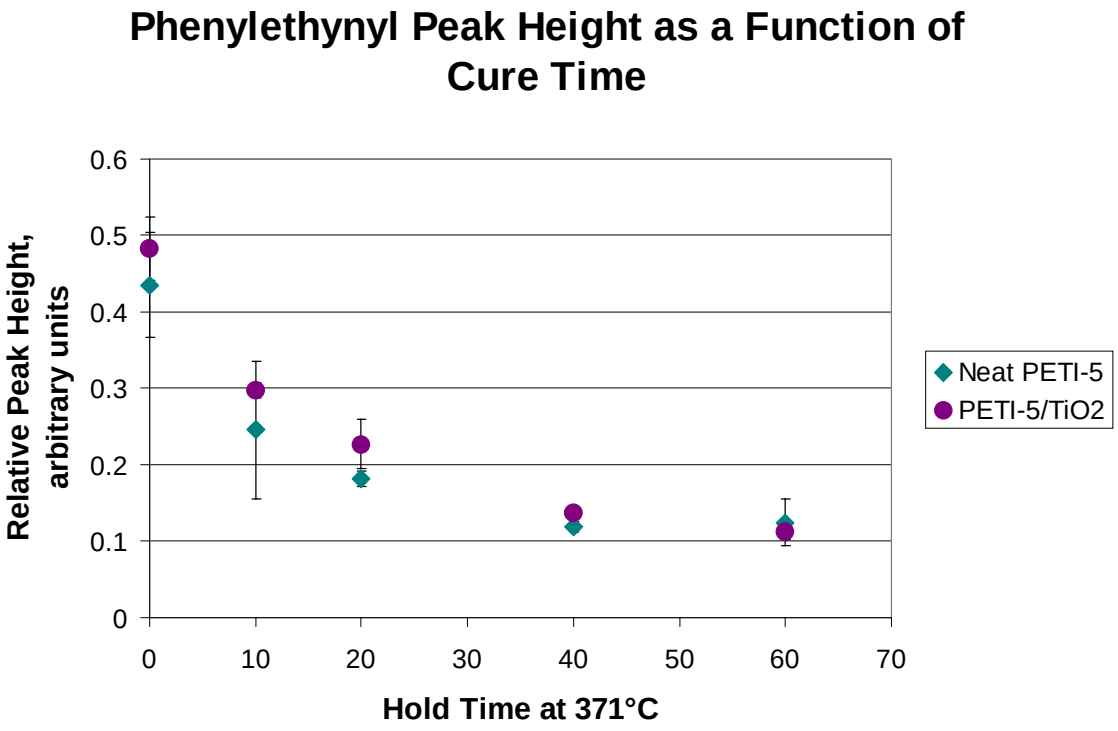

Figure 7.6: Relative height of the carbon-carbon triple bond band in IR spectra of neat and TiO_2-filled PETI-5 as a function of cure time at 371°C. Error bars indicate 95% confidence intervals.

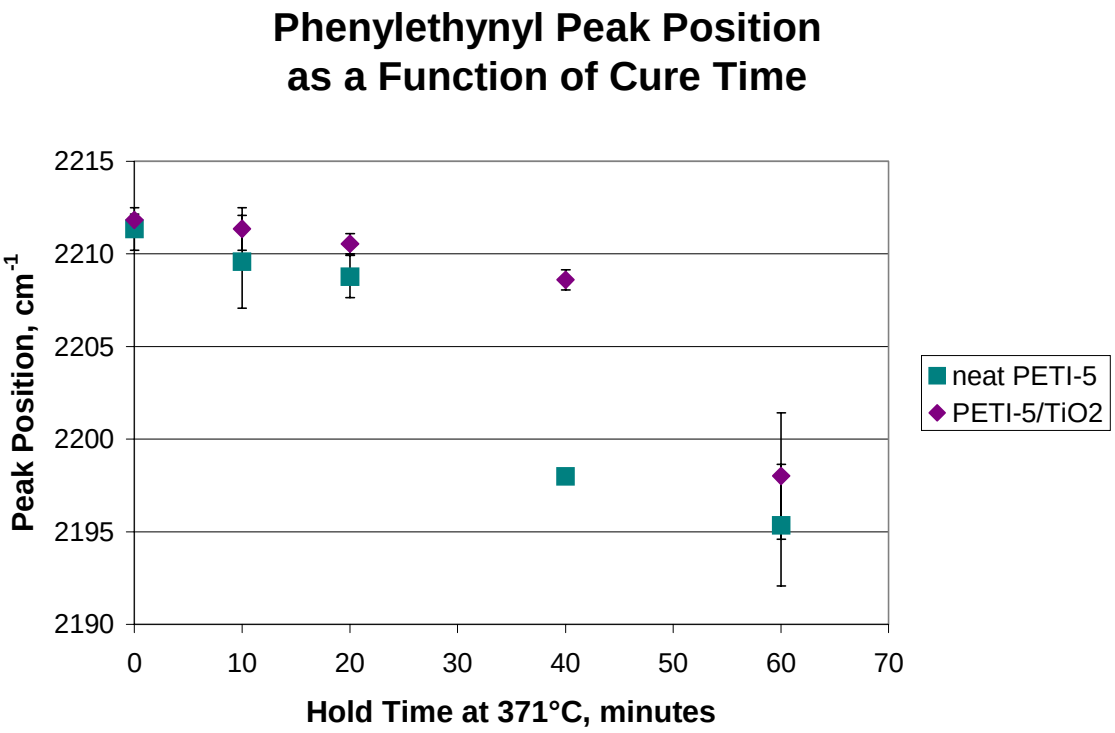

Figure 7.7: Position of the carbon-carbon triple bond band in IR spectra of neat and TiO_2-filled PETI-5 as a function of cure time at 371°C. Error bars indicate 95% confidence intervals.

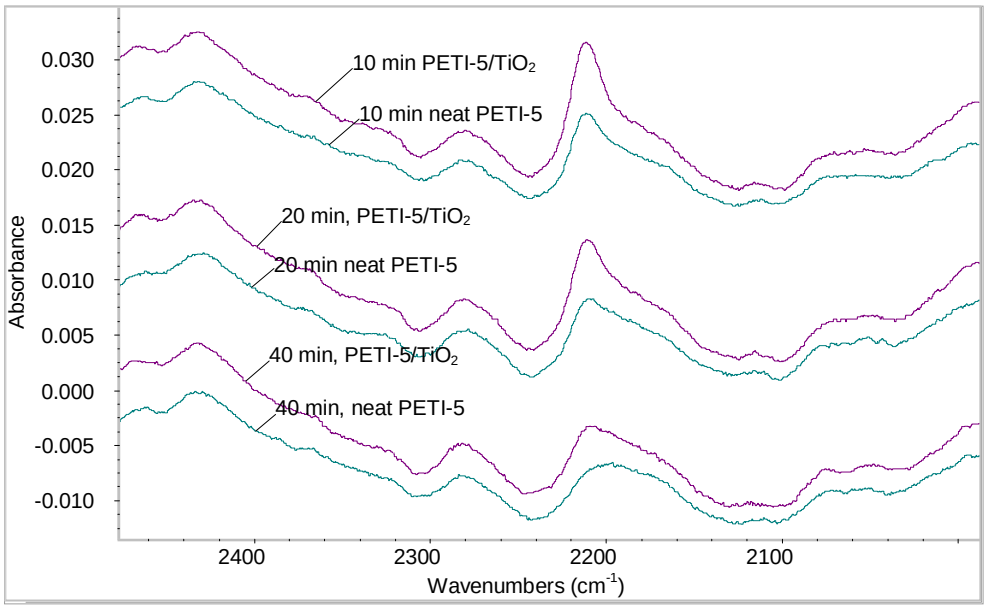

Figure 7.8: Phenylethynyl peaks of PETI-5/TiO_2 and neat PETI-5 IR spectra after 10, 20, or 40 minute cures at 371°C.

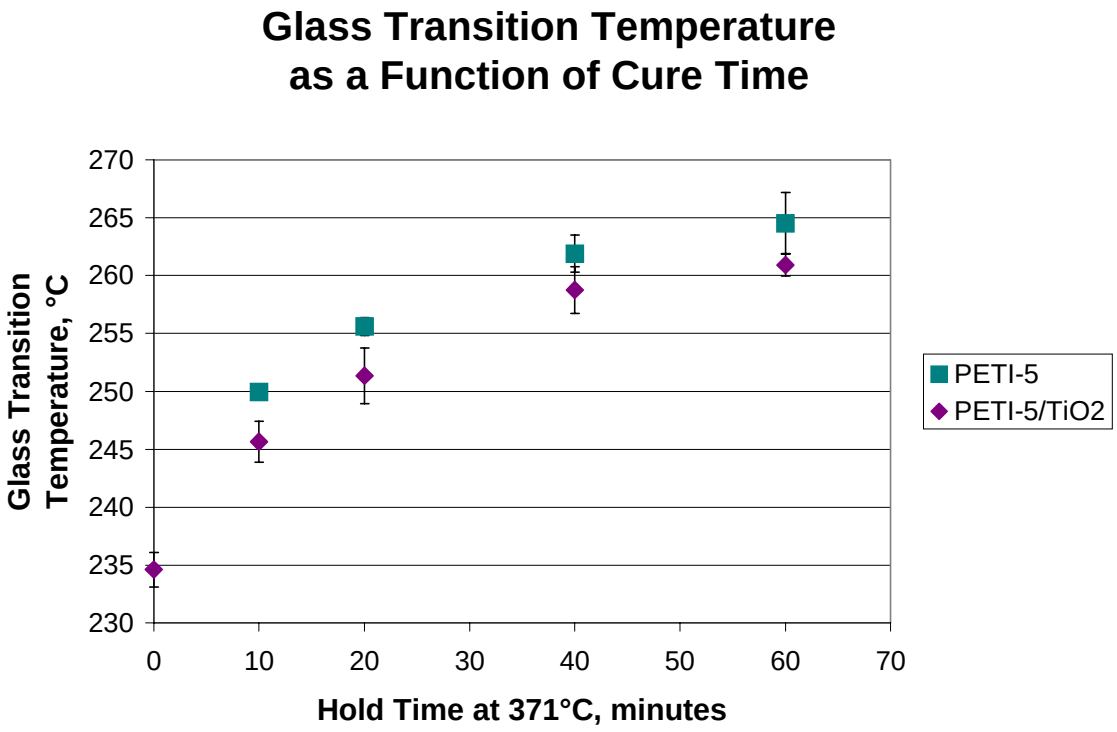

Figure 7.9: Glass transition temperatures of neat and TiO_2-filled PETI-5 as a function of cure time at 371°C. Error bars represent 95% confidence intervals.

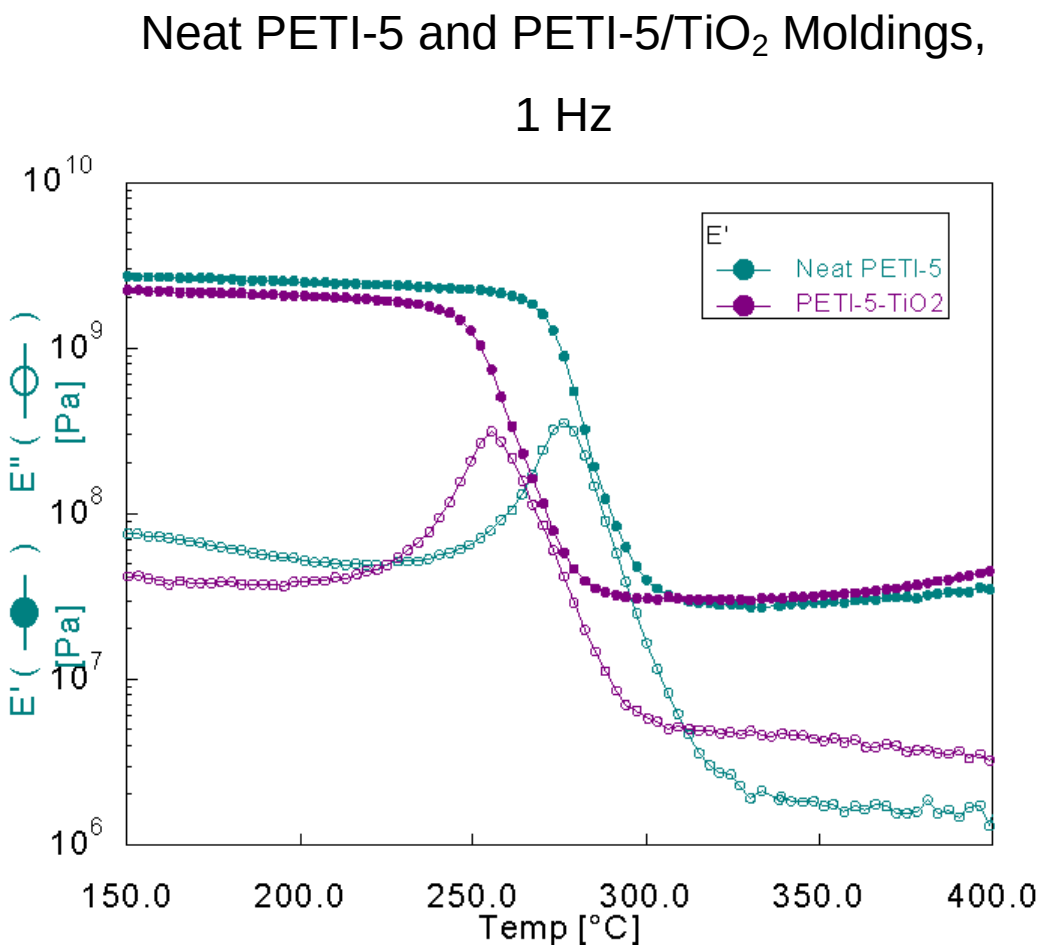

Figure 7.10: Dynamic mechanical spectra of neat PETI-5 and PETI-5/TiO_2 moldings.

Neat PETI-5 and PETI-5/TiO_2 Moldings,

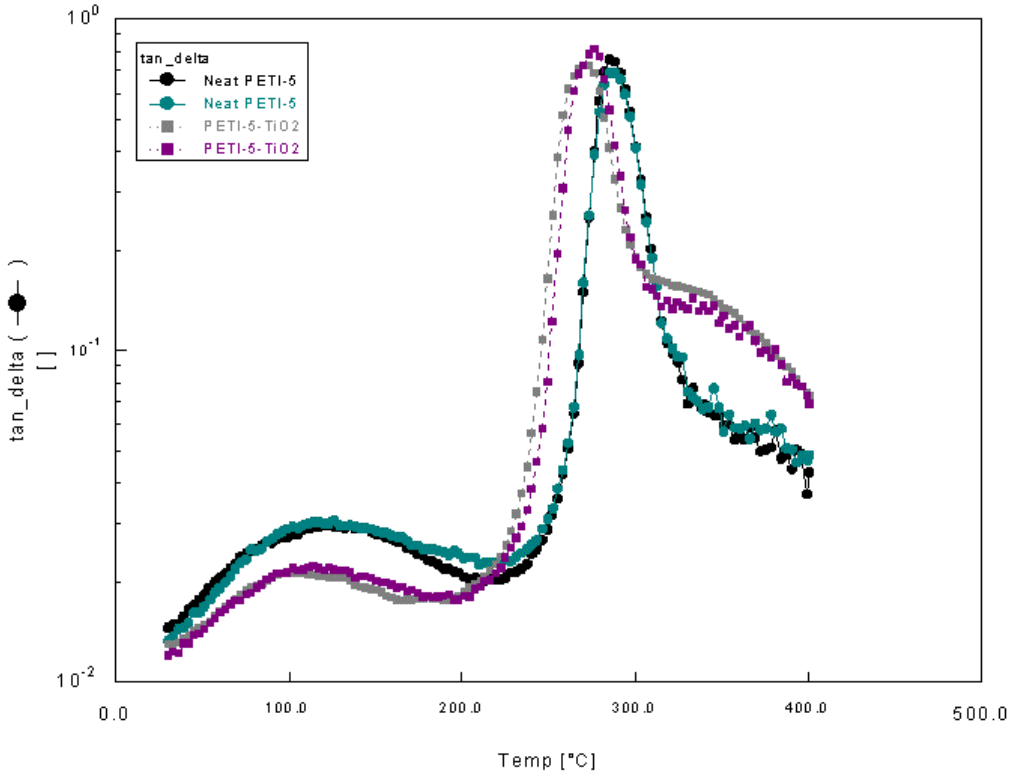

Figure 7.11: DMTA tan delta curves of neat PETI-5 and PETI-5/TiO_2 moldings, at 1 Hz. Duplicate samples of each material are presented to illustrate the reproducibility obtained.

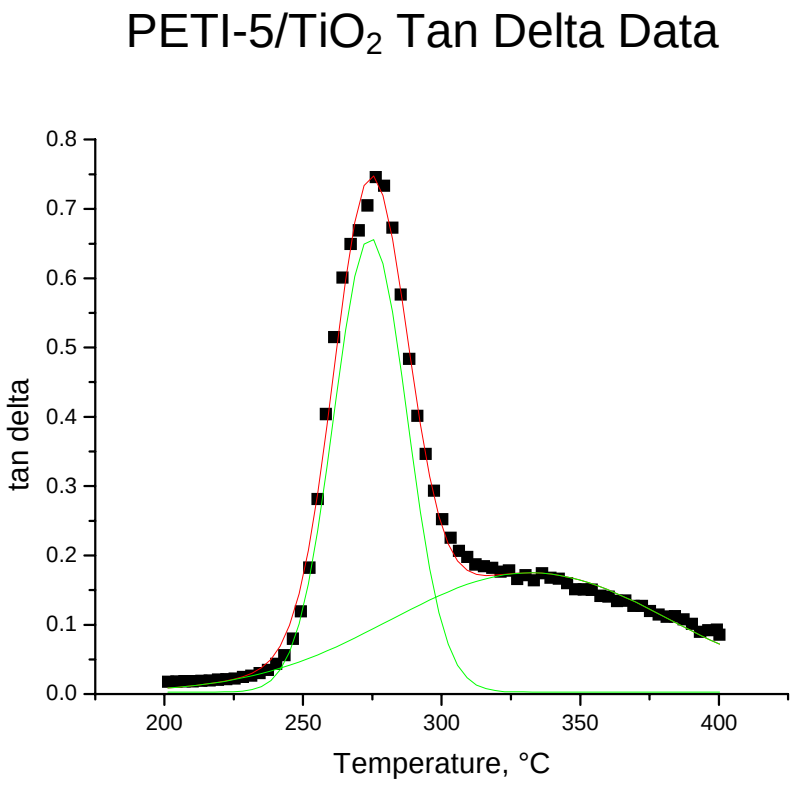

Figure 7.12: Tan delta spectrum of a PETI-5/TiO_2 molding, fit with overlapping Gaussian peaks.

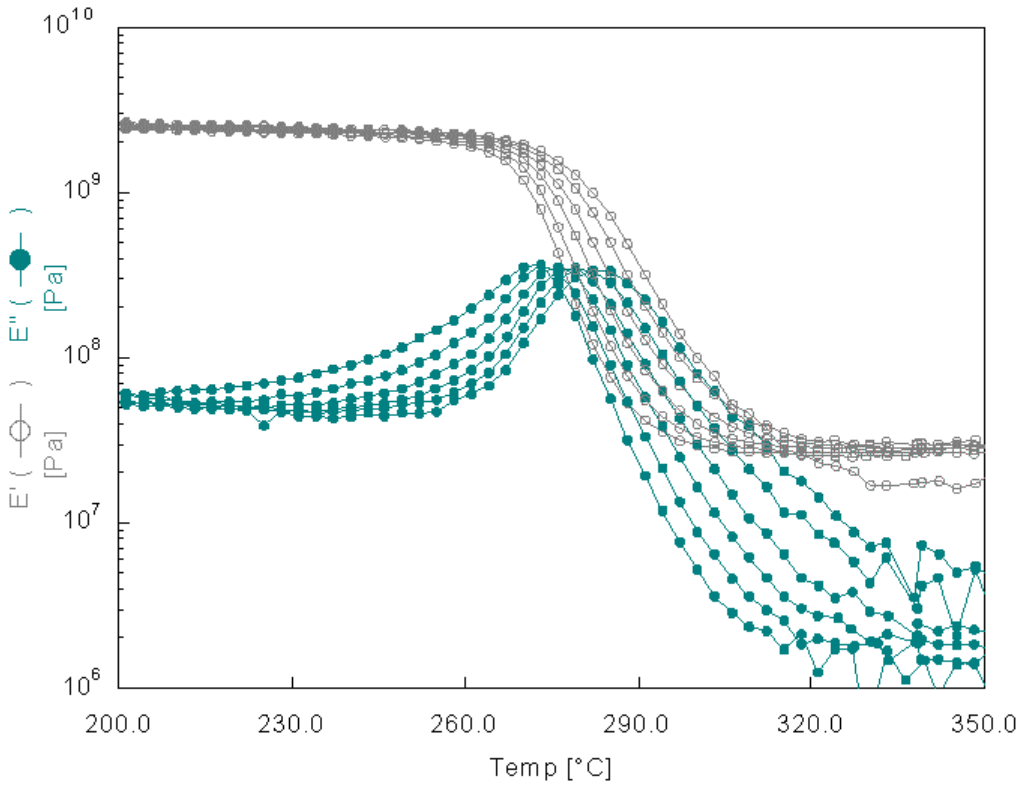

Figure 7.13: Multifrequency DMTA data of PETI-5 molding. Data represent 0.1, 0.3, 1.0, 3.0, 10, and 30 Hz.

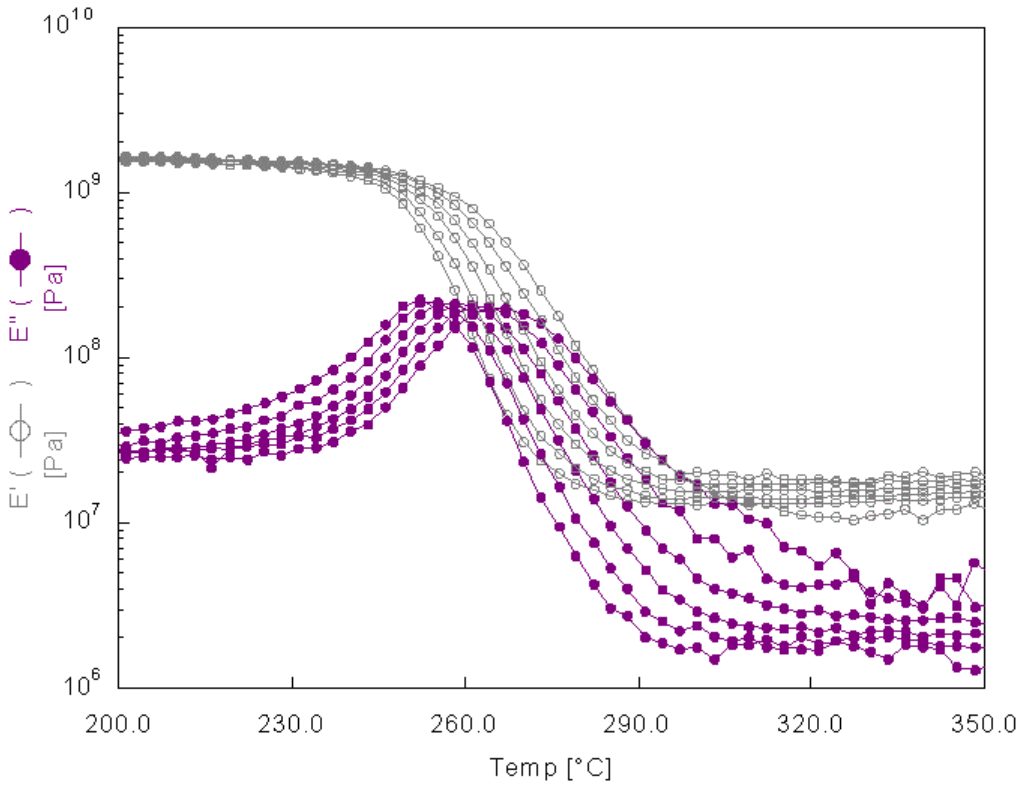

Figure 7.14: Multifrequency DMTA data of PETI-5/TiO_2 molding. Data represent 0.1, 0.3, 1.0, 3.0, 10, and 30 Hz.

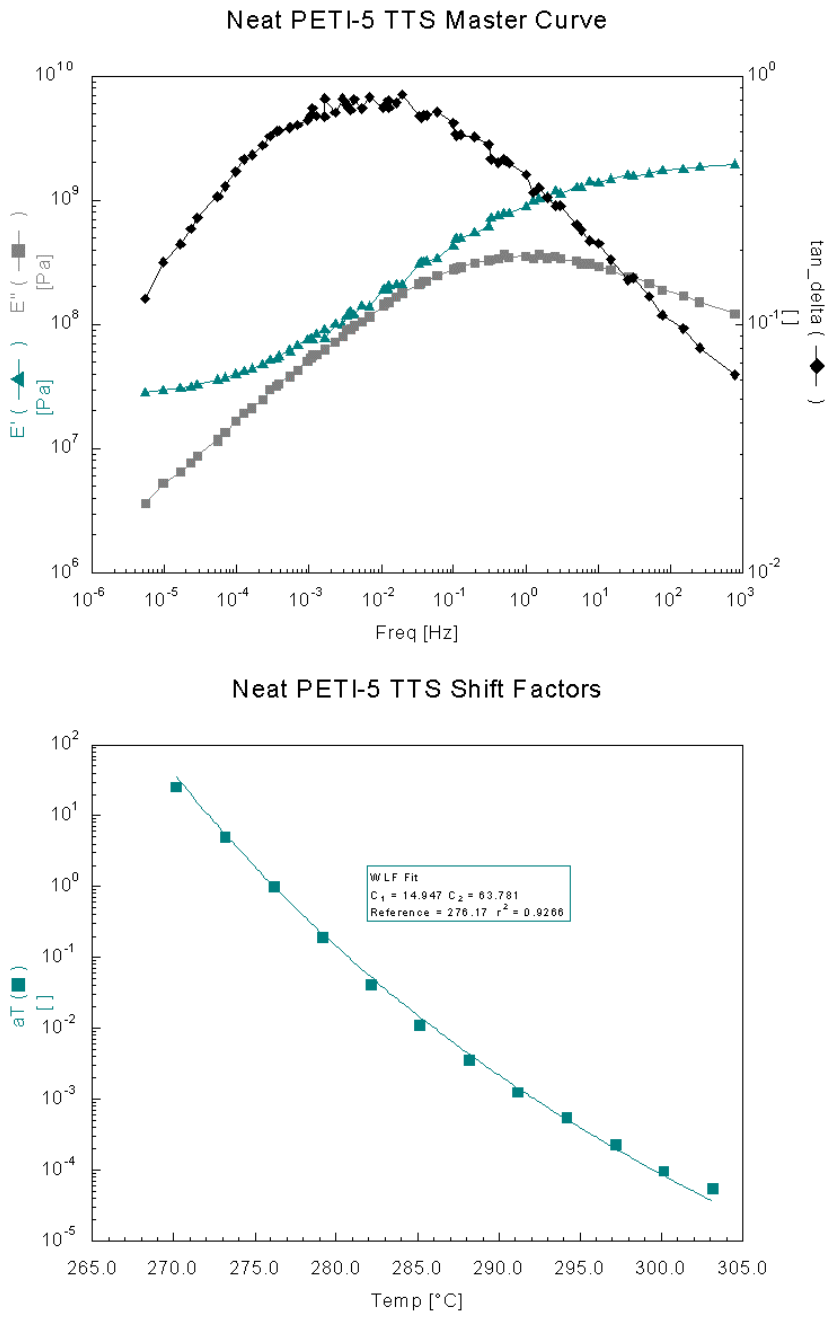

Figure 7.15: Neat PETI-5 master curve and shift factor plot, from time-temperature superposition of DMTA multifrequency sweeps. The line through the shift factor data points represents the WLF fit.

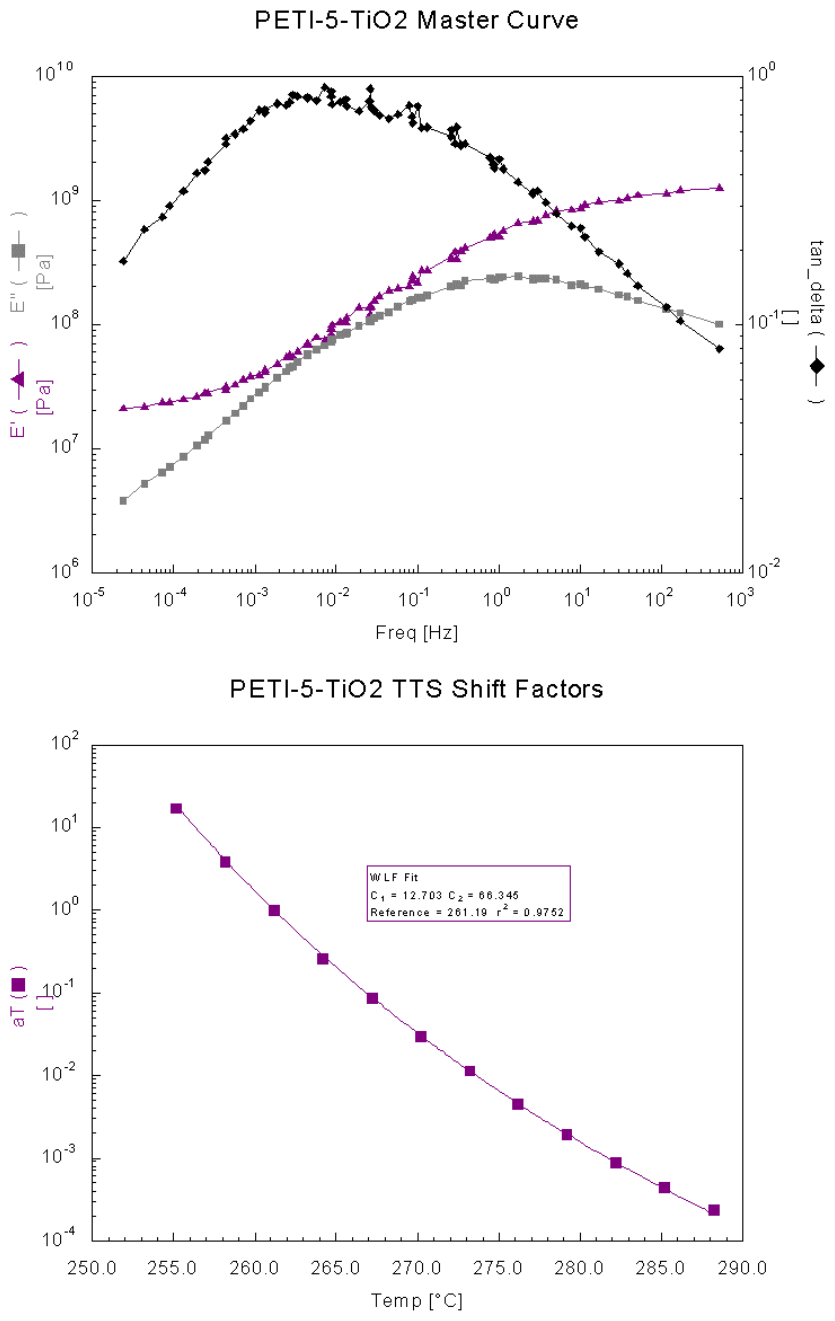

Figure 7.16: PETI-5/TiO_2 master curve and shift factor plot, from time-temperature superposition of DMTA multifrequency sweeps. The line through the shift factor data points represents the WLF fit.

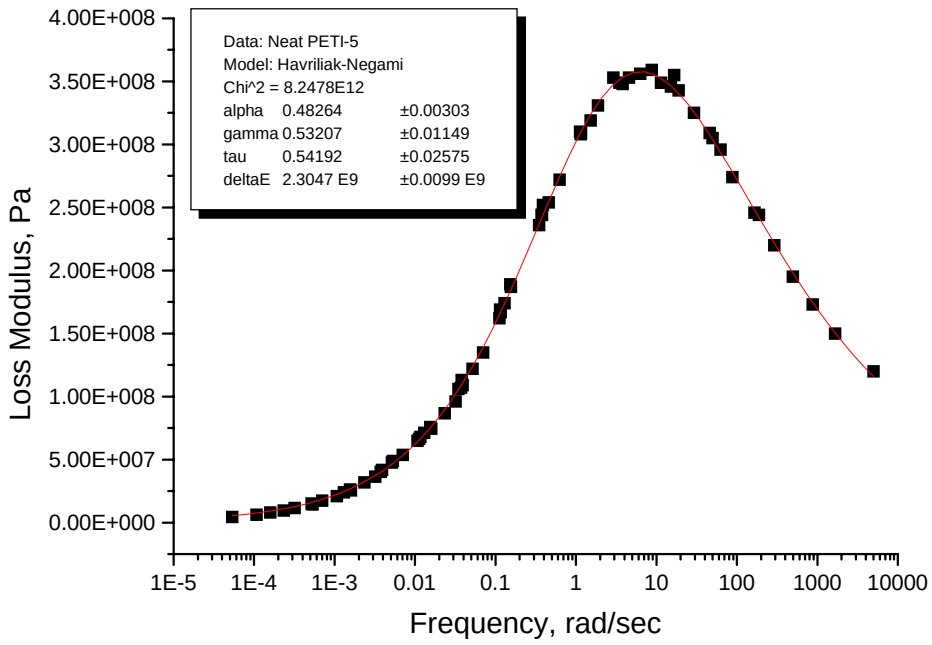

Figure 7.17: Havriliak-Negami fit to neat PETI-5 superposed loss modulus data. The line through the data points indicates the fit of the model.

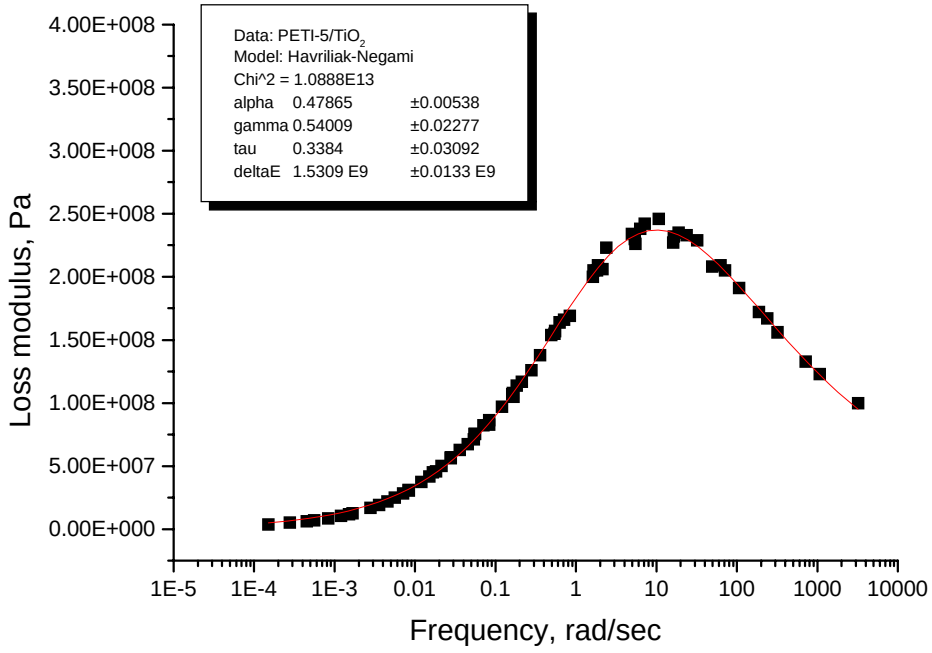

Figure 7.18: Havriliak-Negami fit to PETI-5/TiO_2 superposed loss modulus data. The line through the data points indicates the fit of the model.

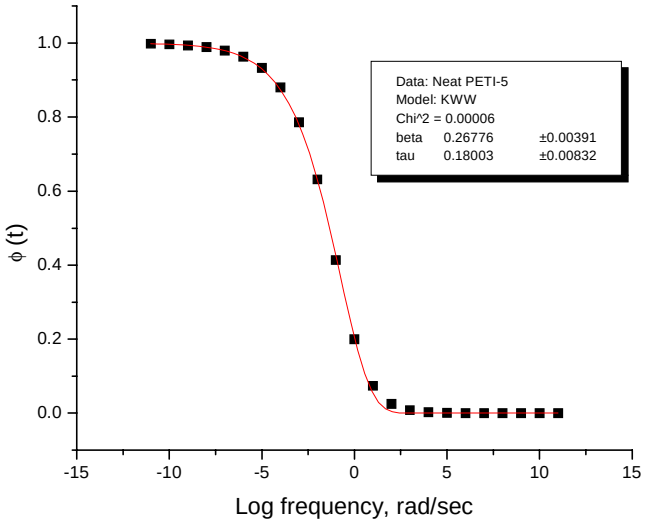

Figure 7.19: KWW fit to neat PETI-5 autocorrelation function.

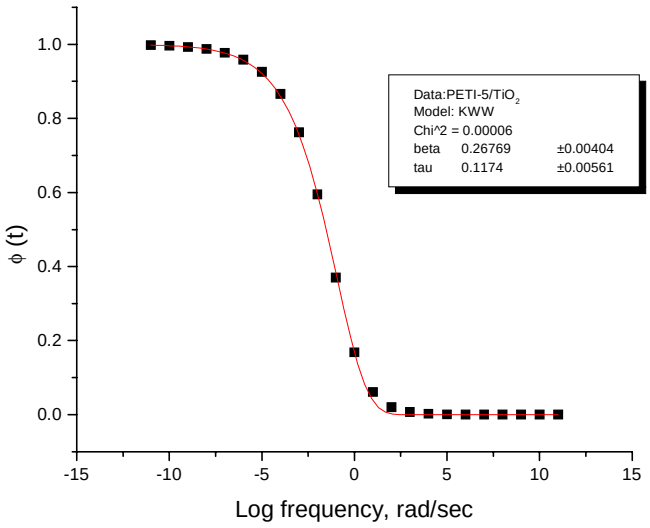

Figure 7.20: KWW fit to PETI-5/TiO_2 autocorrelation function.

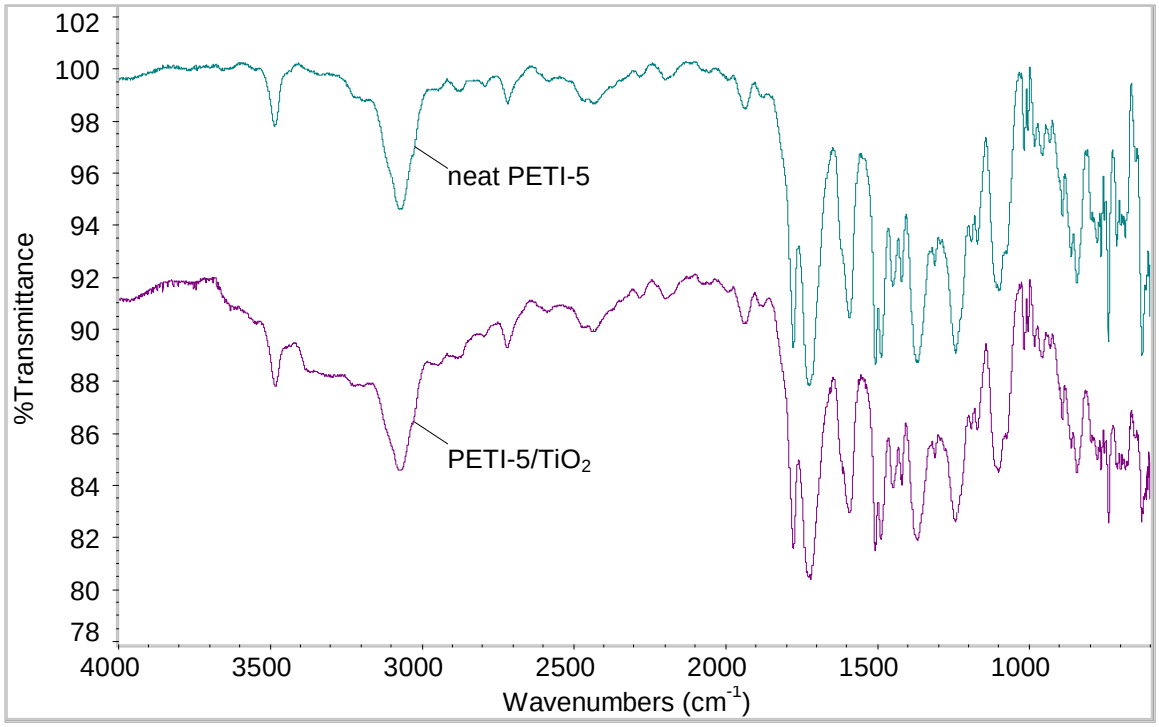

Figure 7.21: Infrared spectra of cured neat PETI-5 and PETI-5/TiO_2 moldings.

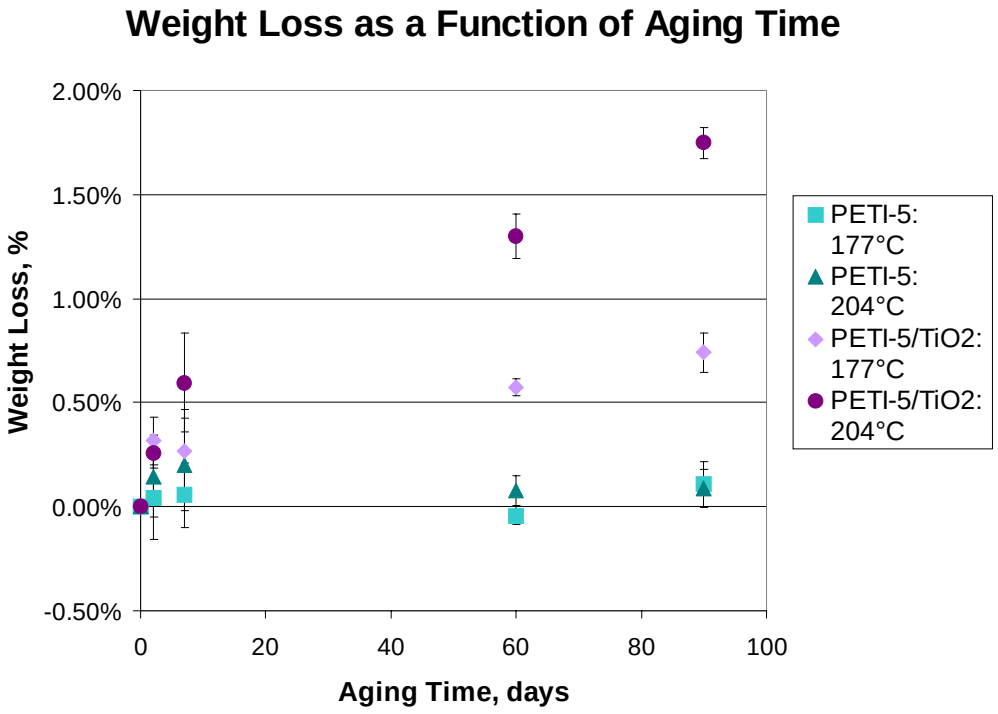

Figure 7.22: Weight loss of PETI-5 and PETI-5/TiO_2 samples as a function of aging time at 177° and 204°C in air. Error bars represent the 95% confidence intervals.

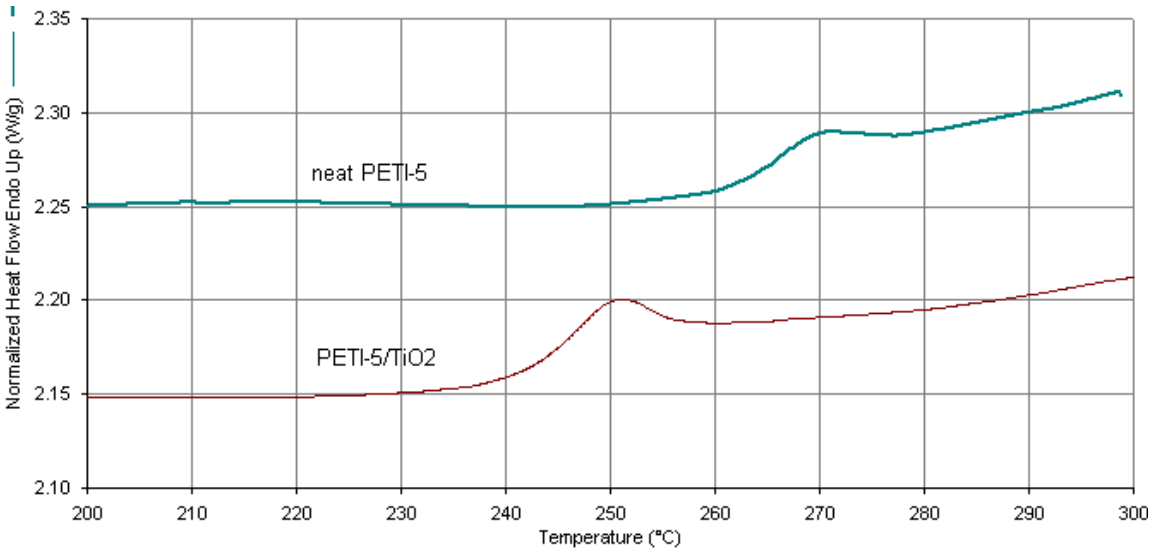

Figure 7.23: First heat DSC scans of fully cured neat PETI-5 and PETI-5/TiO_2 moldings.

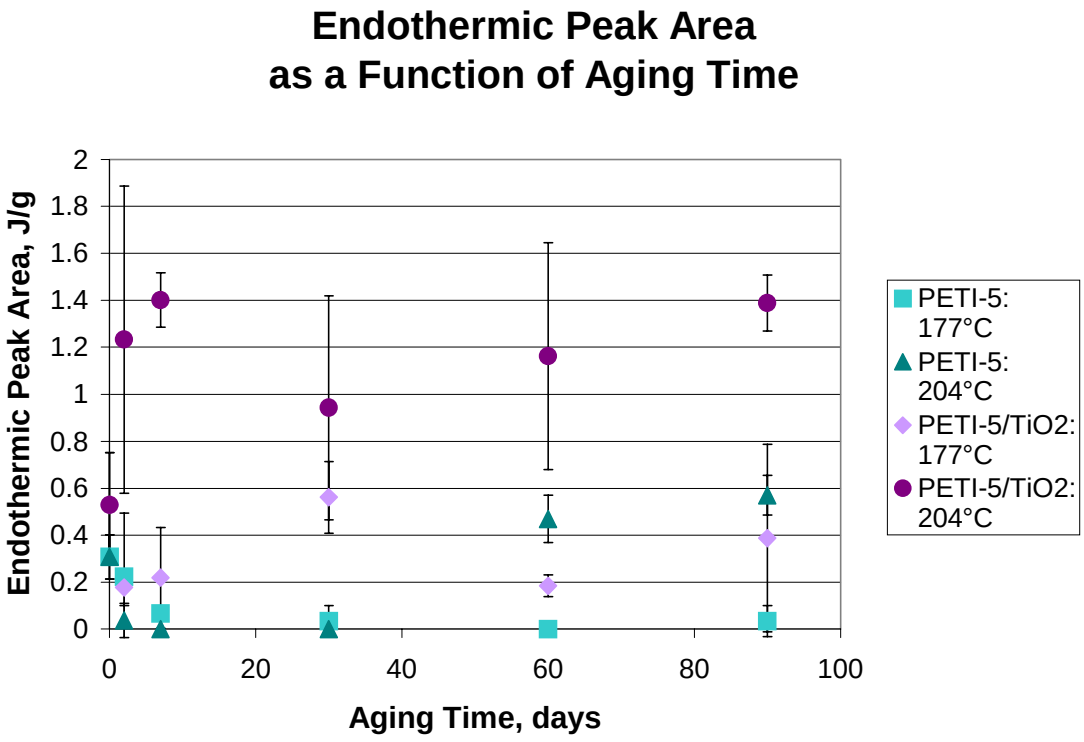

Figure 7.24: Endothermic peak area at the T_g *of PETI-5 and PETI-5/*TiO_2 *samples as a function of aging time at 177° and 204°C in air. Error bars represent the 95% confidence intervals.*

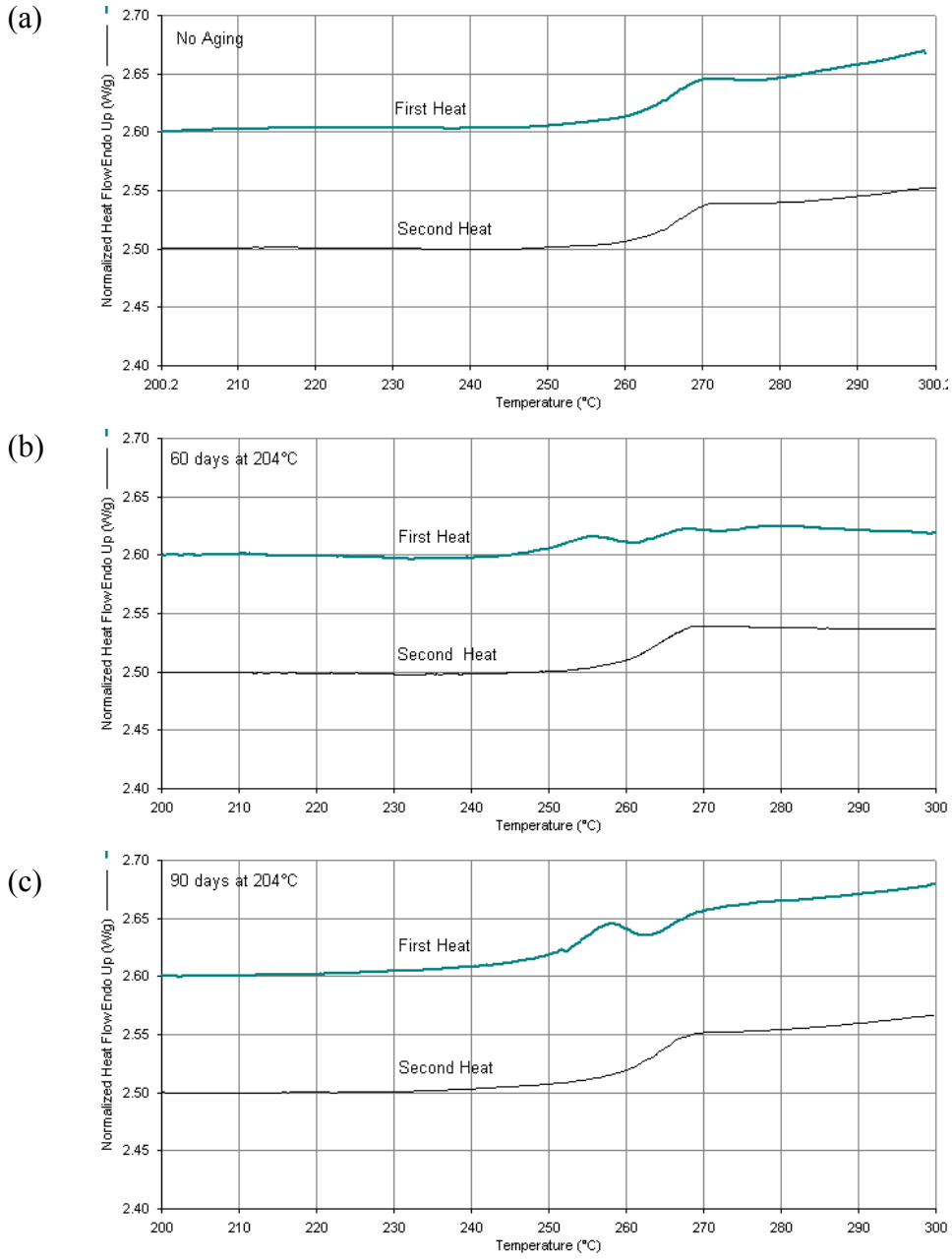

Figure 7.25: First and second heat DSC scans of neat PETI-5 moldings (a) no aging (b) aged 60 days at 204°C in air (c) aged 90 days at 204°C in air. For the second heat, samples were quenched after an initial heat to 300°C.

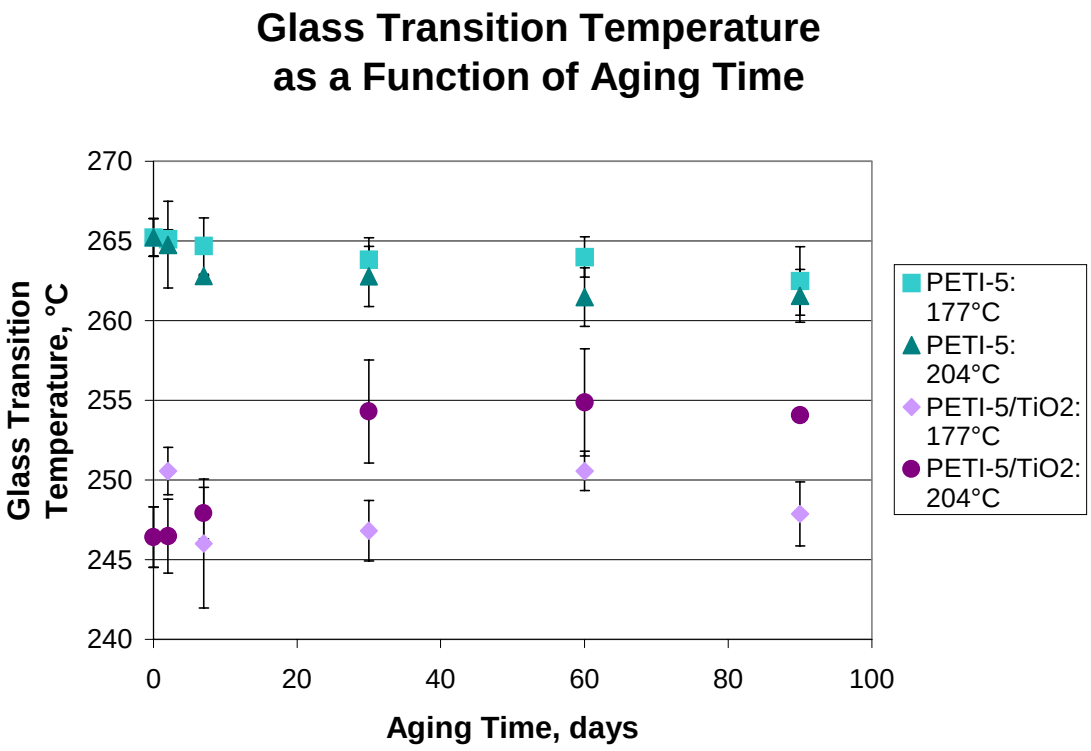

Figure 7.26: Glass transition temperatures of PETI-5 and PETI-5/TiO_2 samples as a function of aging time at 177° and 204°C in air, after an initial heat to 300°C. Error bars represent the 95% confidence intervals.

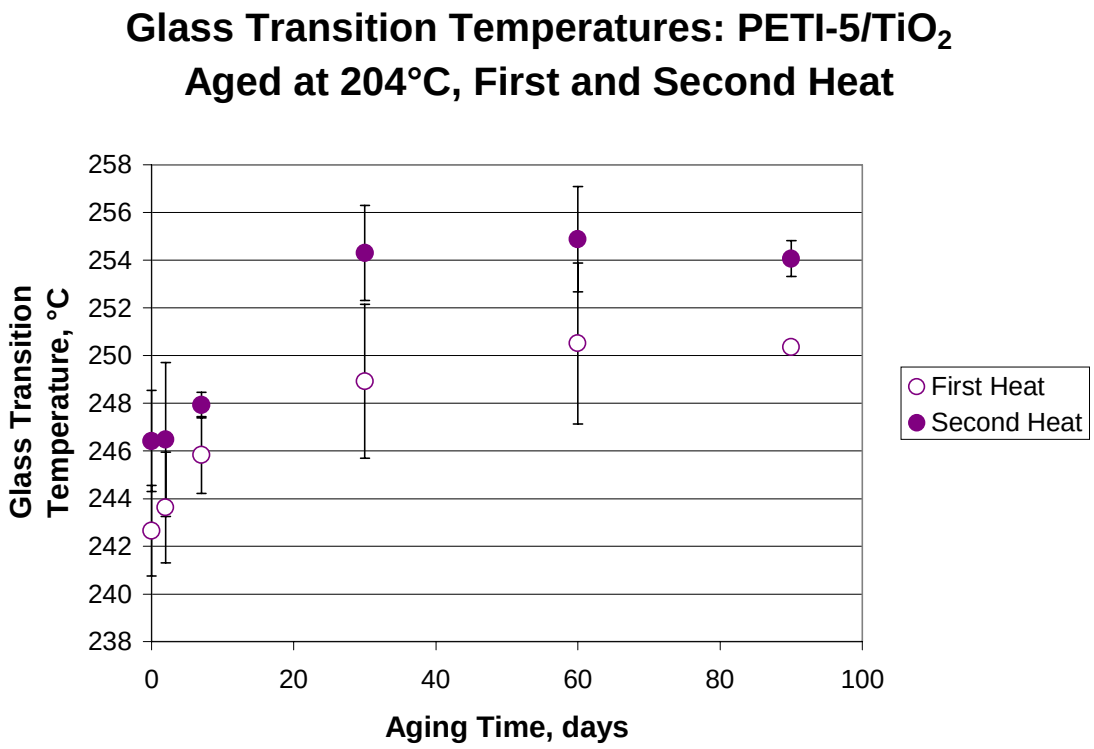

Figure 7.27: Glass transition temperatures of PETI-5/TiO_2 samples as a function of aging time at 204°C in air. For the second heat, samples were quenched after an initial heat to 300°C. Error bars represent the 95% confidence intervals.

(a)

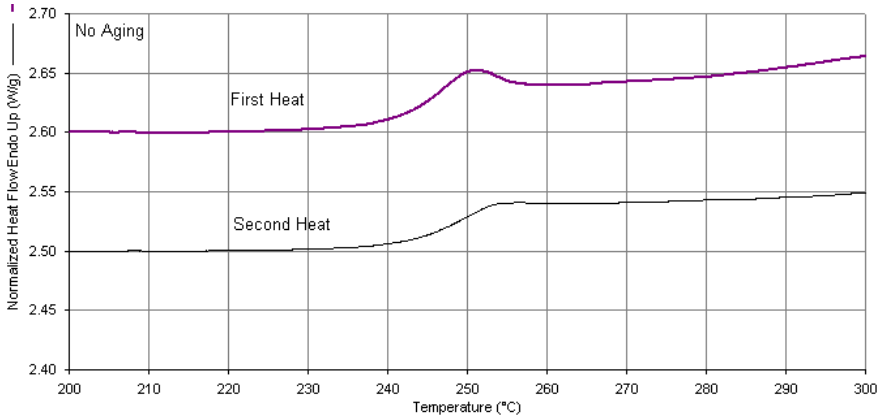

(b)

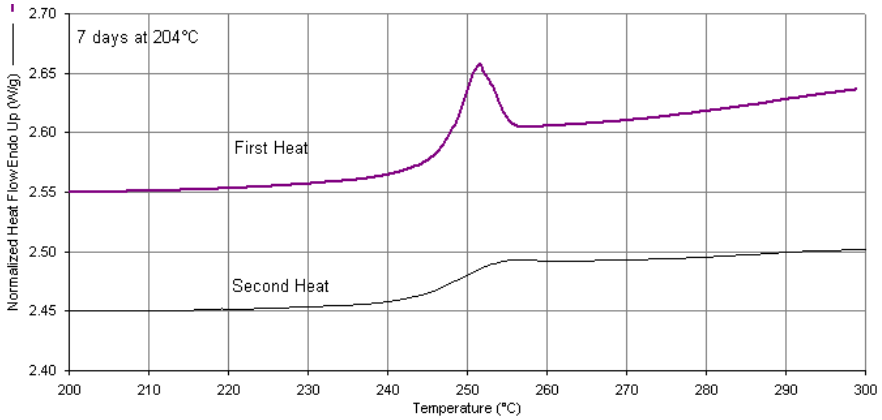

(c)

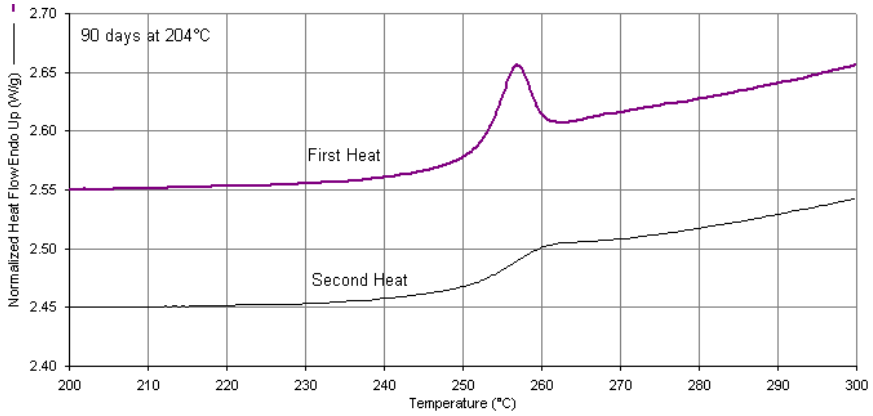

Figure 7.28: First and second heat DSC scans of PETI-5/TiO_2 moldings (a) no aging (b) aged 7 days at 204°C in air (c) aged 90 days at 204°C in air. For the second heat, samples were quenched after an initial heat to 300°C.

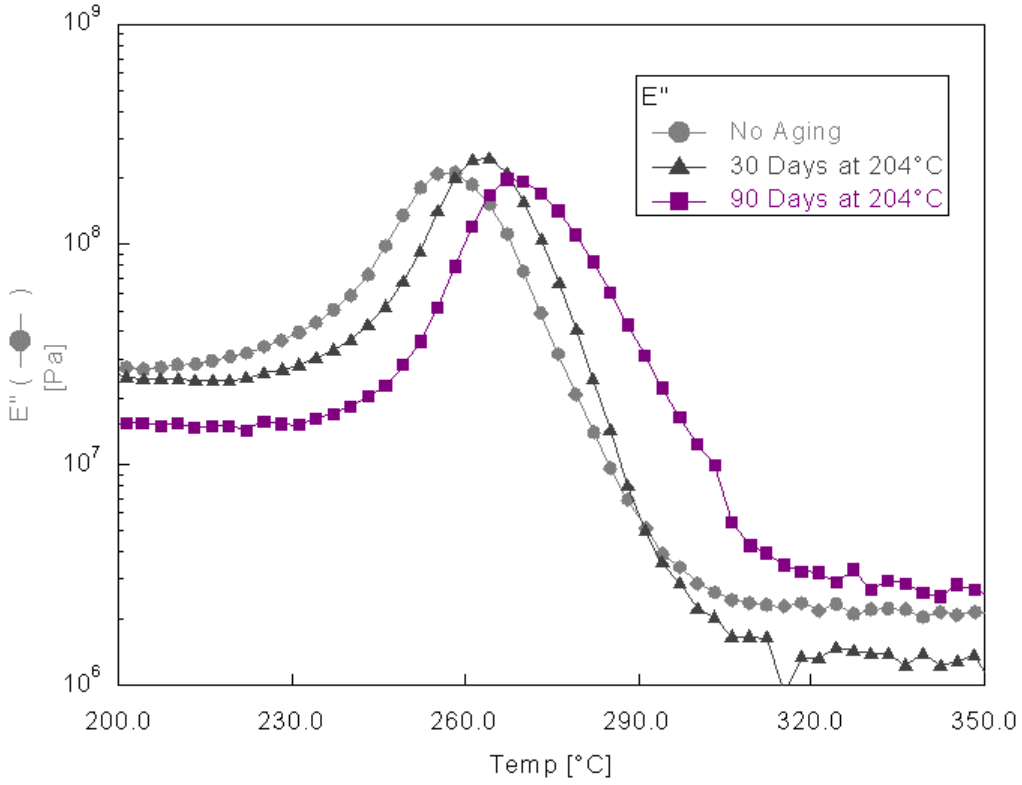

Figure 7.29: Loss modulus DMTA data of PETI-5/TiO_2 moldings, unaged, aged at 204°C for 30 days in air, and aged at 204°C for 90 days in air, taken at 1 Hz.

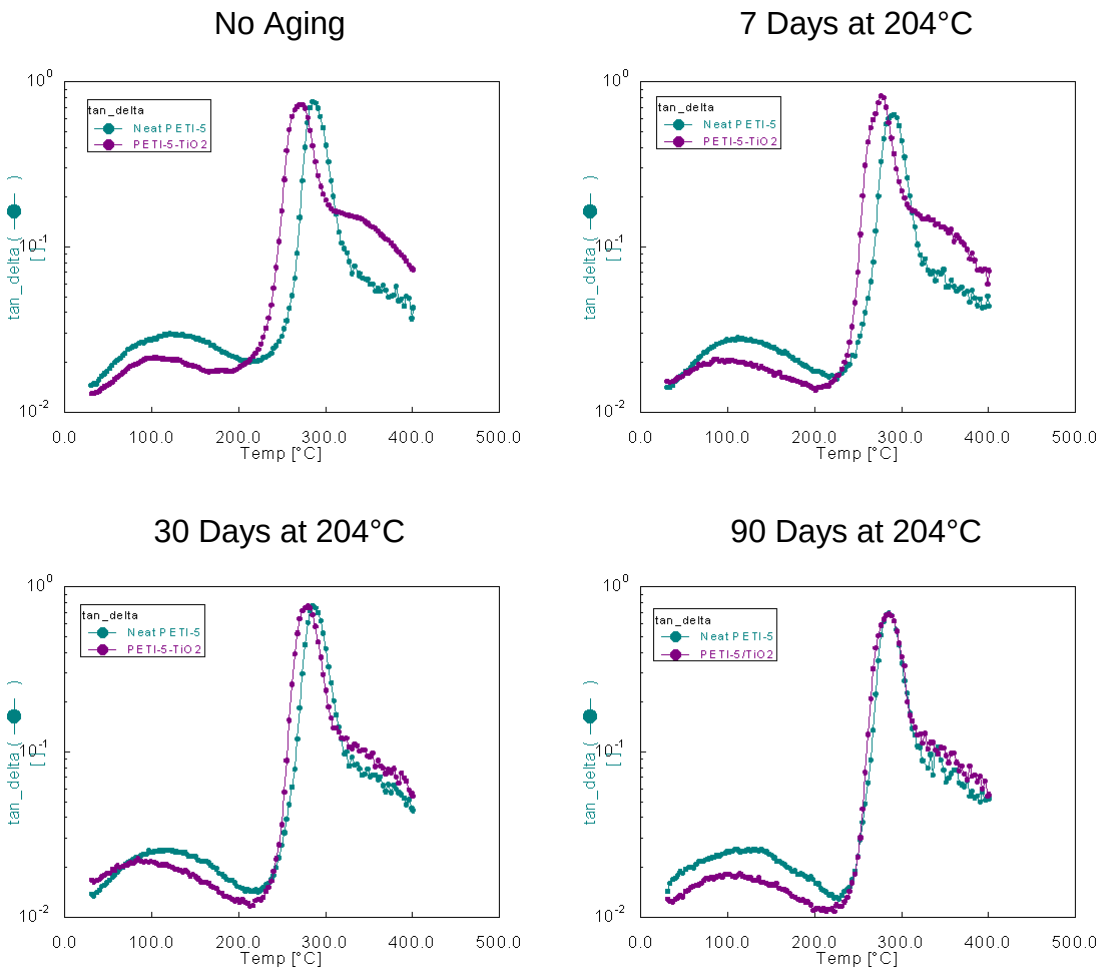

Figure 7.30: Tan delta of neat PETI-5 and PETI-5/TiO_2 as a function of aging time at 204°C in air. Note the decrease in the magnitude of the shoulder at 300° to 400°C as aging time increases.

a)

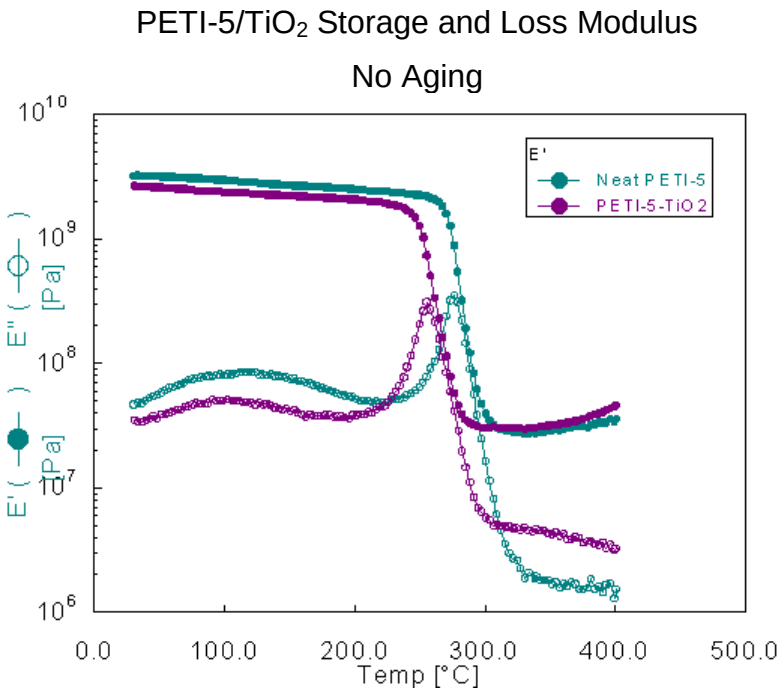

b)

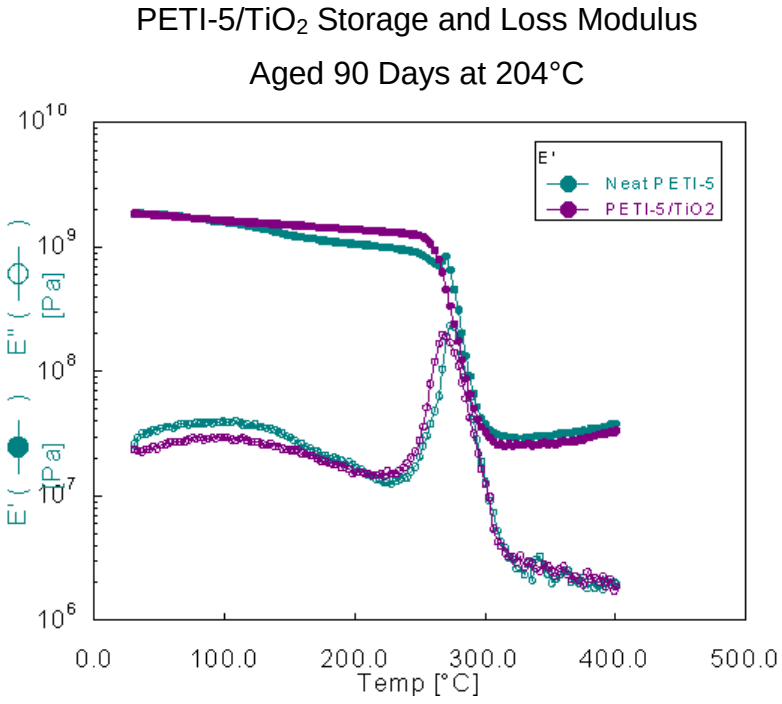

Figure 7.31: Storage and loss modulus of PETI-5/TiO_2 molded samples, a) unaged and b) aged at 204°C for 90 days.

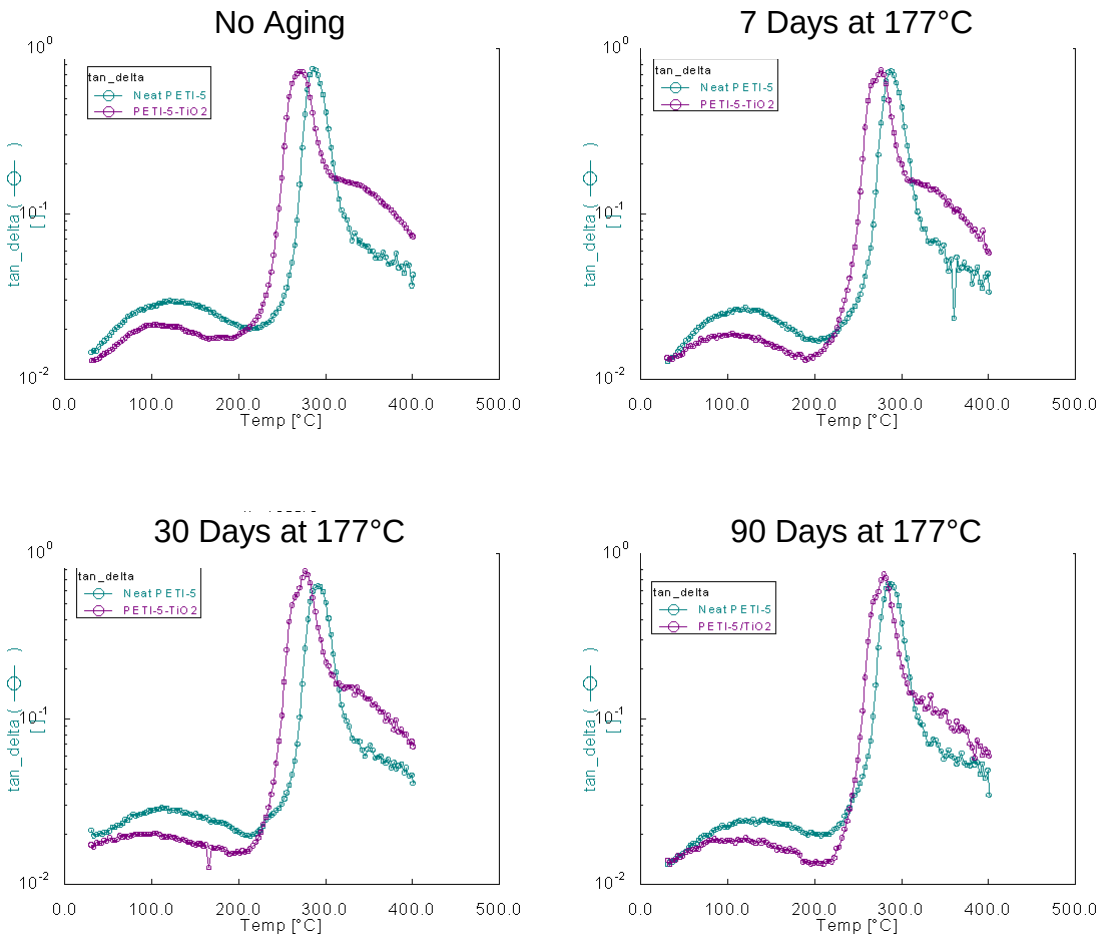

Figure 7.32: Tan delta of neat PETI-5 and PETI-5/TiO_2 as a function of aging time at 177°C in air. Note the decrease in the magnitude of the shoulder at 300° to 400°C as aging time increases.

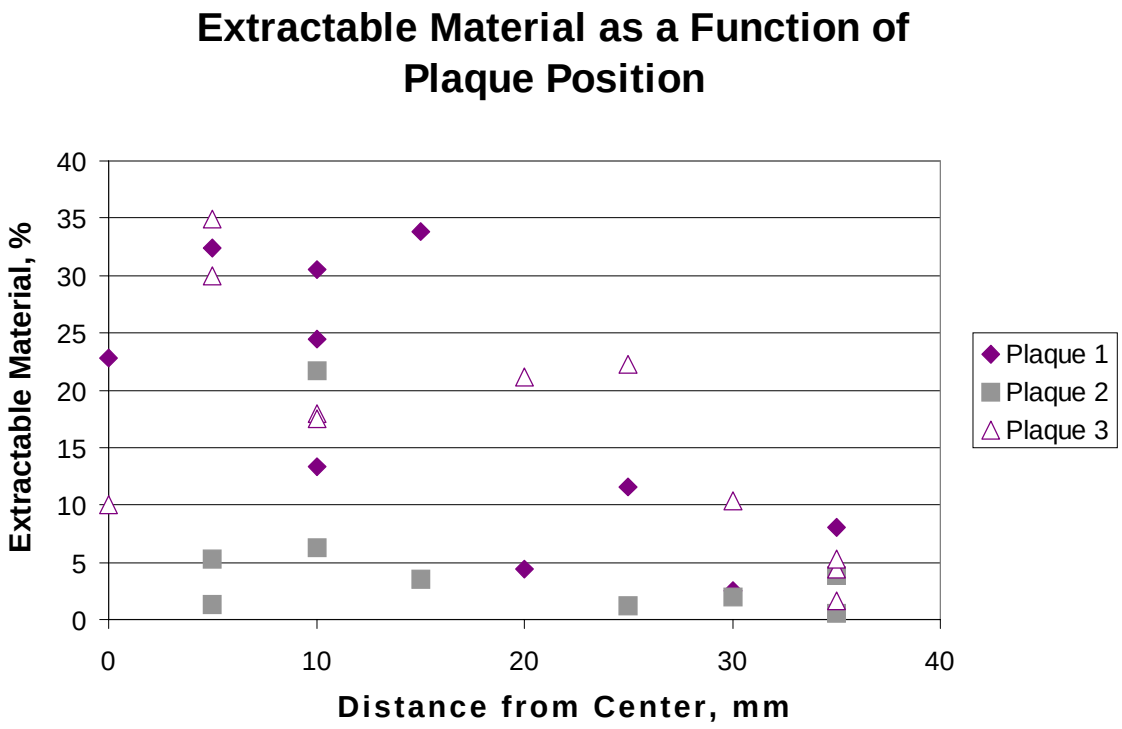

Figure 7.33: Percent of extractable material from three PETI-5/TiO_2 molded plaques as a function of the distance from the center of the plaque that the sample was cut.

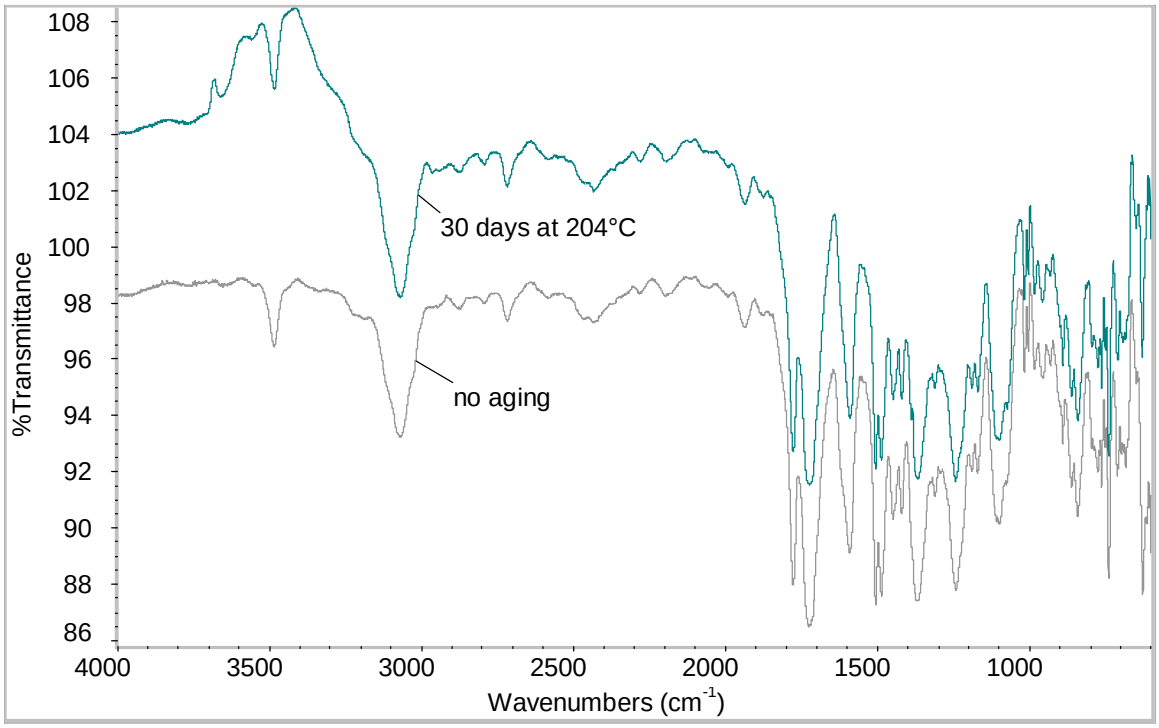

Figure 7.34: IR spectra of neat PETI-5 moldings, unaged and aged for 30 days at 204°C in air.

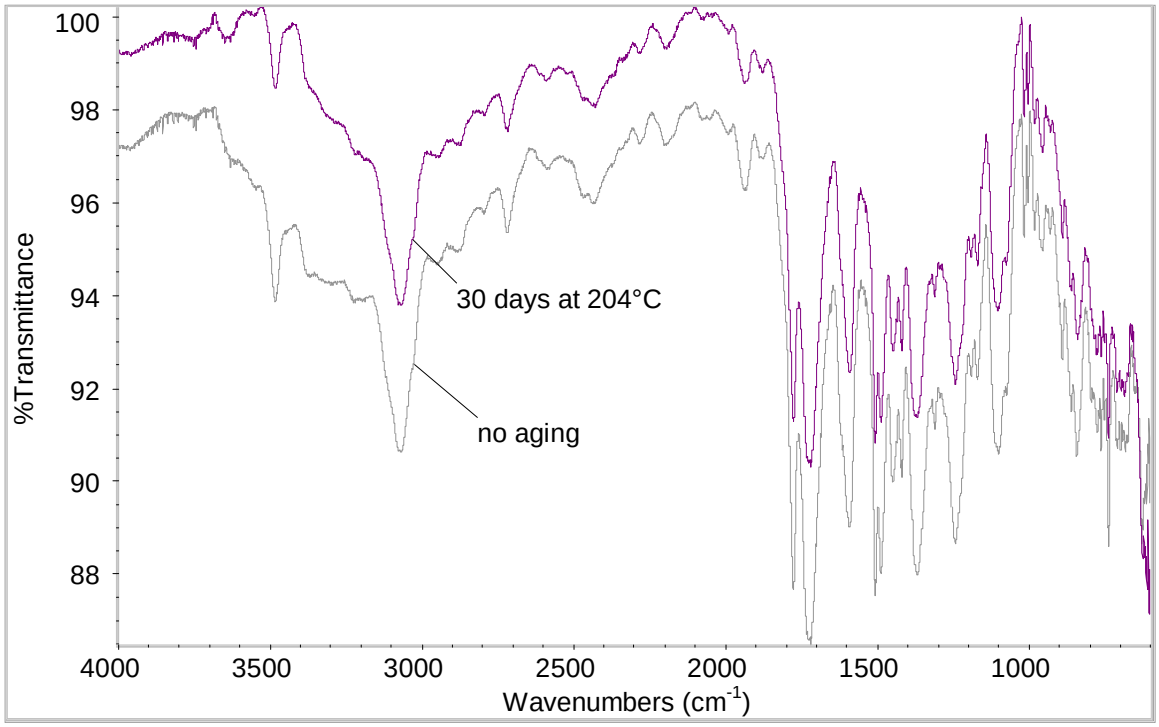

Figure 7.35: IR spectra of PETI-5/TiO_2 moldings, unaged and aged for 30 days at 204°C in air.

Chapter 8: Conclusions

This study has investigated the adhesive/substrate interphase of a phenylethynyl-terminated polyimide adhesive bonded to chromic acid anodized Ti-6Al-4V. Previous work determined that, upon aging in air at elevated temperatures, double cantilever beam specimens of FM-5 bonded to CAA Ti-6Al-4V exhibited a change in failure location. While unaged samples failed cohesively through the centerline of the adhesive, aged specimens exhibited failure in the region of the adhesive/substrate interphase. The current work investigated the effect of aging on the interfacial strength of adhesively bonded specimens, the mechanism of adhesion at the interface, and the effect of titanium dioxide on the adhesive in a model filled system.

Notched coating adhesion specimens of FM-5 and PETI-5 bonded to CAA Ti-6Al-4V aged in air at 177°C for 30 days or longer exhibited a decrease in overall adhesive strength. At the same aging time, a significant portion of the failure shifts from propagating through the substrate oxide layer to propagating through the adhesive at the interphase. Thus, it is concluded that the strength of the adhesive is reduced in the region very close to the CAA oxide surface as a result of aging in air at elevated temperatures.

To understand why the adhesive in the interphase is weakening, the mechanism of adhesion between PETI-5 and CAA Ti-6Al-4V was investigated using surface analysis techniques to analyze the interphase of NCA specimens after failure. It was confirmed

that PETI-5 primer is penetrating the pores of the CAA oxide layer of the substrate, leading to mechanical interlocking between adhesive and substrate.

To investigate further the effect of the titanium substrate surface on the chemical and thermal properties of PETI-5, a model system was studied, which consisted of fine titanium dioxide particles dispersed in a PETI-5 matrix. The filled specimens contained a significant amount of low molecular weight extractable material, leading to a lower glass transition temperature and a more brittle material. This is believed to be a result of an altered cure mechanism in the presence of TiO_2 in addition to the presence of residual solvent, possibly adsorbed to the filler surface, during processing. Analysis of the model system points to possible reasons that the adhesive adjacent to the substrate surface is more prone to degradation than the bulk adhesive. This emphasizes the importance of analyzing an entire adhesive/substrate system rather than isolating the constituent parts, and it presents a means of analysis in which bulk properties of the interphase can be assessed using a model system.

Dynamic mechanical thermal analysis of the TiO_2-filled samples reveals a shoulder on the tan delta peak that is attributed to the higher glass transition of polymer molecules bound to the surface of the filler particles. This shoulder decreases in magnitude as a function of aging time at elevated temperatures. This decrease coincides with the aging conditions at which the NCA specimens decreased in strength. Loss of adhesive strength between the polymer chains and the filler particle surface is a possible explanation of the observed behavior. This is consistent with the observed change in failure location after aging NCA specimens.

With the ability to detect interphase properties of filled systems, DMTA provides a valuable link between bulk analysis of the interphase using a model filled system and analysis of actual adhesive bonds. Here, considerable insight was gained regarding the interphase of PETI-5/CAA Ti-6Al-4V adhesive bonds, as well as the analysis of adhesively bonded systems in general, through the use of an interfacially debonding adhesive test and a model filled system.

Chapter 9: Future Work

As is frequently the case in a research endeavor, this work has answered many questions and has caused many more questions to arise. Some suggested future avenues of research in these areas are outlined below.

While the NCA test proved to be an efficient means of assessing the durability of adhesively bonded systems and of studying failure in the interphase region, there is some question as to the accuracy of the fracture energies obtained from these specimens. To determine if the low G_c values obtained here are related to specimen preparation, NCA specimens could be fabricated and tested, and the fracture energies compared to double cantilever beam, end-notched flexure, and mixed-mode flexure tests in which a second substrate is bonded to the upper surface of a NCA specimen. Furthermore, it is recommended that when the NCA test is used in the analysis of relatively stiff adhesives, such as the polyimide adhesives supported by glass scrim cloth that were analyzed here, the test be performed in bending rather than tension. This can be accomplished in either three- or four-point bending with appropriate modifications to the to the calculation of G_c. When testing in tension with a stiff adhesive, the ability to determine the exact moment at which the adhesive debonds is severely hindered, since there is no significant movement of the adhesive to indicate that debonding has occurred. In bending, however, the adhesive would continue to bend along with the substrate until the moment the

debond propagates, at which point the stiff adhesive would straighten and separate from the substrate.

An additional area of future work relates the conclusion that primer is penetrating the pores of the CAA substrate surface. Since the concentration of titanium on the adhesive failure surface was found to be related to the strength of the bond, maximizing penetration of primer in the pores of the CAA substrate would be expected to maximize bond strength. On the other hand, the PETI-5 primer may be prone to degradation in the presence of titanium dioxide, as was observed in the model filled system. Explorations in this area include drying the PETI-5 primer to a higher temperature to remove the potentially damaging NMP solvent (at the risk of initiating premature reactions of the phenylethynyl end groups) or investigation of other polymers as primers, such a thermoplastic polyimides (eliminating the ability for chemical bonds to form between adhesive and primer.) A simple assessment of primer quality could be made by performing the NCA test and analyzing the failure surfaces using optical microscopy, by which evidence of the CAA oxide layer was easily viewed on the adhesive failure surfaces.

Further work in the use of a model filled system to analyze the interphase region of adhesive/substrate systems will be of great interest. By varying the molding conditions used with the current system, the influence of NMP solvent on the thermal and mechanical properties of the cured molded samples can be analyzed. Previous researchers[109, 110] have shown that the T_g of the constrained phase can be observed in the tan delta spectrum of several filled polymers. By investigating similar systems, it can be determined if a decrease in the magnitude of the T_g of the constrained phase typically corresponds to loss of adhesive strength. SEM may prove to be a valuable technique by which adhesive strength can be assessed in filled specimens. By analyzing the fracture surfaces of filled specimens, polymer-filler adhesion quality may be related to the quantity of polymer observed on the filler particle surface.

Appendix A: Autocorrelation Function

The following Mathematica program was used to calculate the autocorrelation function, Equation 7.2, as function of time. Values of alpha, gamma, and tau were input from Havriliak-Negami fits to dynamic mechanical data.

```
Clear["Global`@"];
SetDirectory["c:\Rachel's files\Mathematica\Time decay output"];
a = Input["Input alpha of H-N model"];
Print["alpha ", a];
g = Input["Input gamma of H-N model"];
Print["gamma ", g];
tau = Input["input tau of H-N model"];
Print["tau ", tau];
k = ((1-a) Pi/2);
theta=ArcTan[(w tau)^a Cos[k]/(1+(w tau)^a Sin[k])];
r= (1 + (w tau)^a Sin[k])^2 + ((w tau)^a Cos[k])^2;
amp = 2/Pi Sin[theta g]/r^(g/2);
obj = amp Cos[w t]/w;
fname = InputString["Name of file to store data:"];
OpenWrite[fname];
Write[fname, "alpha = ", a] ;
```

```
Write[fname, "gamma = ", g] ;
Write[fname, "tau = ", tau] ;
Do[t = 10^lt; hp = N[Pi/t];
                Print["----------------------"];
                Print["half period ", hp]; m = 0; s = 0; l1 = 0; l2 = l1 + hp;
                Print[" "];(Label[again]);
                m = NIntegrate[obj, {w, l1,l2}, MaxRecursion \[Rule] 40 ];
                (*Print["m = ", m, "     s = ", s];*)
                s = s + m; l1 += hp; l2 += hp;
                If[Abs[m]>10^(-6), Goto[again]];
                 Print["ACF at t = ", t, " is ", s, " up to w = ", l2];
                Write[fname, lt," ",s],
                {lt, -11, 11, 1}];
Close[fname]
```

References

1 P. A. Fay, A. Madison, *International J. Adhesion Adhesives,* **10**, 179 (1990).

2 J. F. Watts, J. E. Castle, T. J. Hall, *J. Mater. Sci. Lett.,* **7**, 176 (1988).

3 A. J. Kinloch, *J. Adhesion,* **10**, 193 (1979).

4 A. J. Kinloch, S. J. Shaw, D. L. Hunston, *Polymer*, **24**, 1355 (1983).

5 A. Raveh, D. Marouani, R. Yolgar, J. E. Klemberg-Saphieha, A. Bettelheim, *J. Adhesion*, **36**, 109 (1991).

6 F. J. Boerio, D. J. Ondrus, and R. G. Dillingham in *Adhesion Science Review* (H. F. Brinson, J. P. Wightman, T. C. Ward, eds.), Commonwealth Press, Radford, Virginia (1987).

7 L. T. Drzal, M. J. Rich, P. F. Lloyd, *J. Adhesion,* **16**, 1 (1982).

8 T. K. Kwei, *J. Polym. Sci:,Part A,* **3**, 3229 (1965).

9 P. M. Hergenrother, M. E. Rogalski, *Polym. Prepr.* **33**(1), 354 (1992).

10 J. G. Smith, P. M. Hergenrother, *Polym. Prepr.*, **35**(1), 353 (1994).

11 P. M. Hergenrother, J. G. Smith, *Polymer* **35**, 4857 (1994).

12 P. M. Hergenrother, R. G. Bryant, B. J. Jensen, S. J. Havens, *J. Polym. Sci. Poly. Chem. Ed.*, **32**, 3061 (1994).

13 J. A. Hinkley and B. J. Jensen, *High Perform. Polym.* **7**(1), 1 (1995).

14 B. J. Jensen, R. G. Bryant, J. G. Smith, and P. M. Hergenrother, *J. Adhesion*, **54**(1), 57 (1995).

15 T. H. Hou, B. J. Jensen, and P. M. Hergenrother, *J. of Composite Materials,* **30**(1), 109 (1996).

16 J. A. Hinkley and B. J. Jensen, *High Perform. Polym.* **8**, 599 (1996).

17 R. J. Cano, M. Rommel, J. A. Hinkley, E. D. Estes, *Proceedings of the 41st International SAMPE Symposium,* (G. Schmitt, J. Bauer, C. J. Magurany, C. Hurley, H. Kliger, eds.), 1047 (1996).

18 R. J. Cano and B. J. Jensen, *J. Adhesion,* **60**, 113 (1997).

19 H. Parvatareddy, J. G. Dillard, J. E. McGrath, D. A. Dillard, *J. Adhesion Sci. Technol.,* **12**, 615 (1998).

20 H. Parvatareddy, *Durability of Polyimide Adhesives and their Bonded Joints for High Temperature Applications*, Ph.D. Dissertation, Virginia Polytechnic Institute and State University (1997).

21 T. Chang, E. A. Sproat, Y. Lai, N. E. Shephard, and D. A. Dillard, *J. Adhesion,* **60**, 153 (1997).

22 A. J. Kinloch in *Durability of Structural Adhesives* (A. J. Kinloch, ed.), Applied Science, New York (1983).

23 D. A. Dillard, ESM 5654: Adhesion Science, course notes, Virginia Polytechnic Institute and State University, (1996).

24 D. J. Shaw, *Introduction to Colloid and Surface Chemistry, 4th Ed.,* Butterworth-Heinemann, Boston (1992).

25 W. C. Wake, *Polymer*, **19**, 291 (1978).

26 A. J. Kinloch, *J. Mat. Sci.*, **15**, 2141 (1980).

27 J. D. Venables, *J. Mat. Sci.*, **19**, 2431 (1984).

28 L. H. Sharpe, *J. Adhesion*, **4**, 51 (1972).

29 E. Sancaktar, *Appl. Mech. Rev.*, **49**(10) part 2, S129 (1996).

30 R. F. Landel, *Trans. Soc. Rheology*, **II**, 53 (1958).

31 R. G. Dillingham, F. J. Boerio, *J. Adhesion*, **24**, 315 (1987).

32 A. Mahoon in *Durability of Structural Adhesives* (A. J. Kinloch, ed.), Applied Science, New York (1983).

33 G. D. Davis, *Surface and Interface Analysis,* **17**, 439 (1991).

34 R. F. Wagman, W. C. Hamilton, M. J. Bodnar, *Proceedings of the 4th National SAMPE Technical Conference*, 425 (1972).

35 M. T. Jones, P. D. Pitcher, P. Poole, M. H. Stone in *I. Mech. E. Conference Publications: International Conference on Structural Adhesives in Engineering*, Mechanical Engineering Publishers, London (1986).

36 R. E. Day, *Poly. Deg. and Stab.,* **29**, 73 (1990).

37 B. Ohtani, S. Adzuma, S. Nishimoto, T. Kagiya, *Poly. Deg. and Stab.,* **35**, 53 (1992).

38 N. S. Allen, M. Ledward, G. W. Follows, *Poly. Deg. and Stab.,* **38**, 95 (1992).

39 H. Hidaka, Y. Suzuki, K. Nohara, S. Horikoshi, Y. Hisamatsu, E. Pelizzetti, N. Serpone, *J. Polymer Sci. Part A: Polym. Chem.,* **34**, 1311 (1996).

40 S. A. Visser, *J. Appl. Polym. Sci.,* **63**, 1805 (1997).

41 P. R. McDaniel, T. L. St. Clair, *Mat. Res. Soc. Symp. Proc.,* **405**, 535 (1996).

42 G. Ya. Gordon *Stabilization of Synthetic High Polymers,* Israel Program for Scientific Translations, Jerusalem, 1964, p. vii.

43 R. K. Eby, Ed. *Durability of Macromolecular Materials*, American Chemical Society, Washington, D. C., 1979, p. xi.

44 T. H. Hou, S. P. Wilkinson, and B. J. Jensen, *Proceedings of the Fifth International Conference on Polyimides*, C. Ferger, M. M. Khojasteh, S. E. Molis, Eds., Ellenville, NY, November, 1994.

45 A. C. Chang, T. H. Hou, T. L. St.Clair, *Polyimides: Trends in Materials and Applications* (C. Ferger, M. M. Khojasteh, and S. E. Molis, eds.), Soc. Plast. Eng., Mid-Hudson Section, Hopewell Jct., NY (1996).

46 G. W. Meyer, B. Tan, J. E. McGrath, *High Perform. Polym.,* **6**, 423 (1994).

47 H. Parvatareddy, A. Pasricha, D. A. Dillard, B. Holmes, and J. G. Dillard, *High Temperature and Environmental Effects on Polymeric Composites, 2nd Volume, ASTM STP 1302* (T. S. Gates and A.-H. Zureick, eds.), American Society for Testing and Materials, 149 (1997).

48 R. J. Morgan, E. Shin, C. Dunn, E. Fouch, B. Jurek, A. Jurek, *Proceedings of the 39th International SAMPE Symposium*, (K. Drake, J. Bauer, T. Serafini, P. Cheng eds.), 1564 (1994).

49 J. A. Hinkley and J. J. Yue, *J. Appl. Polym. Sci.* **57**, 1539 (1995).

50 W. M. Lee and S. A. Laman, *Proceedings of the 38th International SAMPE Symposium* (V. Bailey, G. C. Janicki, T. Haulik, eds.), 1978 (1993).

51 M. D. Brunner and T. Cebeci, *Proceedings of the 39th International SAMPE Symposium* (K. Drake, J. Bauer, T. Serafini, P. Cheng, eds.), 1554 (1994).

52 R. Kiefer, J. J. Yue, J. A. Hinkley, *J. Adv. Mater.* **26**(3), 55 (1995).

53 L. J. Burcham, R. F. Eduljee, and J. W. Gillespie, Jr, *Polymer Composites*, **16**(6), 507 (1995).

54 S. Xu, H. Parvatareddy, D. A. Dillard, *Proceedings of the 22nd Annual Meeting of the Adhesion Society* (D. R. Speth, ed.), 221 (1999).

55 D. A. Dillard, B. Chen, T. Chang, and Y.-H. Lai, *J. Adhesion*, **69**, 99 (1999).

56 R. J. Farris and C. L. Bauer, *J. Adhesion,* **26**, 293 (1988).

57 C. A. Kumins, J. Roteman, C. J. Rolle, *J. Polym. Sci.: Part A,* **1**, 541 (1963).

58 R. H. Bott in *CASS Review Series Volume 1, Polyimides: Synthesis, Characterization, and Adhesion* (J. E. McGrath, L. T. Taylor, T. C. Ward, J. P. Wightman, eds.) Christiansburg Printing Company, Christiansburg, Virginia (1992).

59 R. H. Bott, L. T. Taylor, and T. C. Ward in *Adhesion Science Review* (H. F. Brinson, J. P. Wightman, T. C. Ward, eds.), Commonwealth Press, Radford, Virginia, (1987).

60 S. A. Paipetis, G. Papanicolaou, P. S. Theocaris, *Fibre Sci. Tech.*, **8**, 221 (1975).

61 K. L. Ngai, C. M. Roland, *Macromolecules,* **26**, 2688 (1993).

62 M. Connolly, F. Karasz, M. Trimmer, *Macromolecules,* **28**, 1872 (1995).

63 V. J. Nagpal and R. M. Davis, *J. Mater. Res.,* **10**, 3068 (1995).

64 K. A. Mauritz, C. K. Jones, *J. Applied Polymer Sci.*, **40**, 1401 (1990).

65 N. G. McCrum, B. E. Read, and G. Williams, *Anelastic and Dielectric Effects in Polymeric Solids*, Dover Publications, New York (1967).

66 J. J. Aklonis, W. J. MacKnight, *Introduction to Polymer Viscoelasticity, 2nd Ed.*, John Wiley and Sons, New York (1983).

67 I. M. Ward, D. W. Hadley, *An Introduction to the Mechanical Properties of Solid Polymers*, John Wiley and Sons, New York (1996).

68 S. A. Paipetis, G. Papanicolaou, P. S. Theocaris, *Fibre Sci. Tech.,* **8**, 221 (1975).

69 G. Perault, G. Duchesne, *J. Appl. Polymer Sci.,* **21**, 3153 (1977).

70 R. H. Bott, in *Polyimides: Synthesis, Characterization, and Adhesion* (J. E. McGrath, L. T. Taylor, T. C. Ward, J. P. Wightman, eds.) pp. 168-187, Virginia Tech Center for Adhesive and Sealant Science, Blacksburg, VA (1992).

71 J. J. Fitzgerald, C. J. T. Landry, J. M. Pochan, *Macromolecules*, **25**, 3715 (1992).

72 R. F. Boyer, *Polymer Eng. Sci.,* **8**(3), 161 (1968).

73 R. Y. Ting, R. L. Cottington, *J. Adhesion*, **12**, 243 (1981).

74 J. A. Hinkley, *J. Polymer Sci., Polymer Lett. Ed.,* **22**, 497 (1984).

75 R. F. Boyer, *Polymer*, **17**, 996 (1976).

76 B. Hartman, G. F. Lee, *J. Appl. Polymer Sci*., **23** 3639 (1979).

77 A. M. Kotukhova, S. G. Novikova, P. P. Chegodayev, L. V. Yudina, S. A. Dolmatov, *Polym. Sci. U.S.S.R.*, **30**(7), 1473 (1988).

78 Y. Y. Gotlib, N. N. Kozlovich, I. S. Milevskaya, *Polym. Sci. U.S.S.R.,* **32**(7), 1340 (1990).

79 A. Fukami, K. Iisaka, S. Kubota, S. Etoh, *J. Applied Polym. Sci.,* **42**, 3065 (1991).

80 R. A. Venditti, J. K. Gillham, *J. Applied Polym. Sci.,* **45**, 1501 (1992).

81 F. E. Arnold, Jr., K. R. Bruno, D. Shen, M. Eashoo, C. Lee, F. Harris, S. Z. D. Cheng, *Polym. Eng. Sci.*, **33**(21), 1373 (1993).

82 J. P. Habas, M. F. Grenier-Loustalot, J. Peyrelasse, *High Perform. Polym.*, **8**, 407 (1996).

83 G. Hougham, T. Jackman, *Polym. Prepr.*, **37**(1), 162 (1996).

84 H. Tang, L. Dong, J. Zhang, M. Ding, Z. Feng, *European Polymer Journal*, **32**(10), 1221 (1996).

85 A. B. Brennan, F. Feller III, *J. Rheol.* **32**, 453 (1995).

86 G. Hougham, G. Tesoro, and J. Shaw, *Macromolecules,* **27**, 3642 (1994).

87 R. G. Bryant, B. J. Jensen, P. M. Hergenrother, *Polymer Prepr.,* **34**(1), 566 (1993).

88 K. H. Wood, *The Thermal Cure of Phenylethynyl-Terminated Polyimides and Selected Model Compounds*, Ph.D. Dissertation, The College of William and Mary in Virginia (1997).

89 C. R. Brundle *Applied Spectroscopy* **25**, 8 (1971).

90 D. T. Clark and H. R. Thomas *J. Polym. Sci.: Polym. Chem. Ed.*, **16**, 791 (1978).

91 A. J. Pertsin and Y. M. Pashunin, *Appl. Surf. Sci.,* **44**, 171 (1990).

92 G. Polzonetti, M. V. Russo, G. Iucci, A. Furlani, *Appl. Surf. Sci.*, **72**, 227 (1993).

93 M. C. Davies, K. M. Shakesheff, A. G. Shard, A. Domb, C. J. Roberts, S. J. B. Tendler, and P. M. Williams, *Macromolecules*, **29**, 2205 (1996).

94 R. A. Haring, S. L. Nunes, R. P. McGouey, E. A. Galligan, W. Volksen, J. L. Hedrick, J. Labadie, *J. Mater. Res.* **10**, 1028 (1995).

95 N. V. Glefond, I. K. Igumenov, *Surf. Sci.*, **275**, 323 (1992).

96 W. Grunert, R. Schlogl, H. G. Karge, *J. Phys. Chem.*, **97**, 8638 (1993).

97 B. J. Jensen, T. H. Hou, S. P. Wilkinson, *High Perform Polym*, **7**, 11 (1995).

98 N. E. Dowling, *Mechanical Behavior of Materials*, Prentice Hall, Englewood Cliffs, New Jersey, 1993, p. 100.

99 T. Chang, *The Notched Coating Adhesion Specimen: A Fracture Test for Coatings and Accelerated Screening Test for Adhesion,* Master's Thesis, Virginia Polytechnic Institute and State University (1996).

100 A. P. Clifton, *Solvent Induced Microcracking in High Performance Polymeric Composites*, Master's Thesis, Virginia Polytechnic Institute and State University (1996).

101 F. P. Beer, E. R. Johnston, Jr., *Mechanics of Materials, 2nd Ed.*, McGraw-Hill, New York, 1992, p. 703.

102 H. Parvatareddy and D. A. Dillard, *International J. of Fracture*, **96**, 215 (1999).

103 XPS International, Inc., http://www.xpsdata.com

104 R. G. Bryant, B. J. Jensen, P. M. Hergenrother, *Polymer Prepr.,* **34**(1), 566 (1993).

105 J. A. Filbey, J. P. Wightman, *J. Adhesion,* **28**, 1 (1989).

106 D. Dolphin and A. Wick, *Tabulation of Infrared Spectral Data*, John Wiley and Sons, New York (1977).

107 R. G. Bryant, B. J. Jensen, P. M. Hergenrother, *Polym. Prepr.* **34**(1), 566 (1993).

108 N. B. Colthup, L. H. Daly, S. E. Wiberly, *Introduction to Infrared and Raman Spectroscopy*, 3rd Edition, Academic Press, San Diego (1990).

109 G. Tsagaropoulos, A. Eisenberg, *Macromolecules,* **28**, 396 (1995).

110 G. Tsagaropoulos, A. Eisenberg, *Macromolecules,* **28**, 6067 (1995).

111 T. C. Ward, Chem/ESM 5174: Polymer Viscoelasticity, course notes, Virginia Polytechnic Institute and State University (1997).

Vita

Rachel Knudsen Giunta was born Rachel Louise Knudsen on February 14, 1971 to Dennis and Bonnie Knudsen in Fredericksburg, Virginia. After graduating from Stafford High School in Fredericksburg, Virginia, in 1989, she attended Virginia Tech. She received her Bachelor of Science degree in Chemistry from Virginia Tech in 1993 and her Master of Arts degree in Applied Science from the College of William and Mary, Williamsburg, Virginia, in 1995. She then returned to Virginia Tech to pursue her doctorate in Materials Science and Engineering. In 1997, she married Dr. Anthony Andrew Giunta and they moved to Hampton, Virginia, where she continued to work on her doctorate through Virginia Tech while performing her thesis research at NASA Langley Research Center. Following the completion of her Ph.D. in 1999, she will begin a postdoctoral research position at Sandia National Laboratories in Albuquerque, New Mexico.